MODELING LAND SURFACE HETEROGENEITY IN LAND SURFACE AND REGIONAL CLIMATE MODELS

A Thesis Submitted to the
College of Graduate and Postdoctoral Studies
In Partial Fulfillment of the Requirements
For the Degree of Doctor of Philosophy
In the School of Environment and Sustainability
University of Saskatchewan
Saskatoon

By

Zhe Zhang

PERMISSION TO USE

In presenting this thesis/dissertation in partial fulfillment of the requirements for a Postgraduate degree from the University of Saskatchewan, I agree that the Libraries of this University may make it freely available for inspection. I further agree that permission for copying of this thesis/dissertation in any manner, in whole or in part, for scholarly purposes may be granted by the professor or professors who supervised my thesis/dissertation work or, in their absence, by the Head of the Department or the Dean of the College in which my thesis work was done. It is understood that any copying or publication or use of this thesis/dissertation or parts thereof for financial gain shall not be allowed without my written permission. It is also understood that due recognition shall be given to me and to the University of Saskatchewan in any scholarly use which may be made of any material in my thesis/dissertation.

Requests for permission to copy or to make other uses of materials in this thesis/dissertation in whole or part should be addressed to:

Executive Director
School of Environment and Sustainability
Room 323, Kirk Hall, 117 Science Place
University of Saskatchewan
Saskatoon, Saskatchewan, S7N 5C8, Canada.
Phone: (306) 966-1985 Fax: (306) 966-2298 Email: sens.info@usask.ca

OR

Dean
College of Graduate and Postdoctoral Studies
University of Saskatchewan
116 Thorvaldson Building, 110 Science Place
Saskatoon, Saskatchewan, S7N 5C9 Canada

Abstract

We all live on Earth's land surface. The state of and changes to land surface conditions can strongly alter surface energy and water balance, eventually affecting the weather and climate. An essential component in regional climate models and Earth system models, the land surface provides lower boundary conditions, which are critical both for weather forecasting and projecting the future climate. This research advances knowledge in representing land surface heterogeneity, including the energy-water-carbon cycle and land surface feedback to the regional climate in Central North America, where land use and hydrological conditions are complex. An extensive area of fine-scale surface heterogeneity, this region includes the U.S. corn belt agricultural land and wetlands that dominate the landscape in the Prairie Pothole Region (PPR) across the Northern Great Plains and Canadian Prairies. This study highlights two distinct landscapes—wetlands and croplands—for their dominance in the region, important roles in land-atmosphere interaction, and unique characteristics impacted by human activities. In addition, advances in high-resolution convection-permitting models provide a unique opportunity to investigate these interactions, especially to explicitly resolve land surface heterogeneity.

This thesis first investigates the soil moisture conditions of the land and their feedback to extreme temperatures during heatwave events in a long-term high-resolution convection-permitting simulation. Second, a joint crop-irrigation simulation is conducted, which shows the capability of land surface models (LSMs) to estimate crop phenology and biomass and irrigation, the key impacts of human decisions. Third, the thesis explores the shallow groundwater dynamics and the hydrological cycle in the PPR under current and future climate change scenarios; fourth, the soil moisture conditions from the current and future climate are used to statistically estimate the future distribution of the prairie wetlands. Finally, a surface wetland scheme is developed to represent spatial wetland extents and dynamic wetland storage in the PPR. This scheme is incorporated into an LSM (Noah-MP) and regional climate model (Weather Research & Forecasting model) to study its impacts on energy-water balance and feedback to the regional climate. This research allows potential future research on the wetland-climate feedback at a local/regional scale and on the potential on-farm benefits of wetland retention and restoration. This research has critical implications for understanding the land and climate interactions in this unique and complex terrain and has potential to help human beings to develop a sustainable lifestyle.

ACKNOWLEDGEMENTS

I would like to thank my supervisor, Dr. Yanping Li, for being an empathic and generous guide, who is always available to discuss research ideas and give me space to pursue my research in a collaborative environment. Thanks to the advisory committee members, especially to those I have taken lessons from and collaborated with, Dr. Andrew Ireson, Dr. Michael Barlage, Dr. Warren Helgason, and Dr. James Famiglietti, for their valuable revisions in this thesis. Thank you to the Hydrometeorological Application Program at the National Center for Atmospheric Research, who provided critical tools and resources to conduct my research. Thanks to Dr. Fei Chen and Dr. Changhai Liu for their kind hosting and endless support during my visits to NCAR, where many brilliant research ideas incubated. Thank you to Dr. Lauren Botorlotti in the Institute for Wetlands and Waterfowl Research in Ducks Unlimited Canada, who introduced me to ecological and sustainable studies of prairie wetlands, where my research can be applied.

Thank you to the supporting agencies that made this Ph.D. possible. To Mitacs student internship program partnering with Ducks Unlimited Canada. To the Global Institute for Water Security and to the Global Water Futures.

I am especially grateful to my parents and family in China, who have undoubtedly supported my study in all these years and taught me most of what I am today. This family binding is a supportive strength that helps me through difficult time, especially through this pandemic, and in the future.

Finally, I want to share a quote from Laozi in Tao Te Ching about water – “The highest goodness is like water. Water benefits all things and does not compete. It stays in the lowly places with others despise. Therefore, it is near the Eternal.” It is hoped that I can hold this belief through pursuing goals and achievements in my lifetime.

TABLE OF CONTENT

LIST OF TABLES

LIST OF FIGURES

LIST OF ABBREVIATIONS

BATS	Biosphere-Atmosphere Transfer Scheme
CAPE	Convective Available Potential Energy
CLASS	Canadian LAnd Surface Scheme
CLM	Community Land Model
CLSM	Catchment Land Surface Model
CMIP5	Climate Model Inter-comparison Phase 5
CONUS	CONtituous U.S.
CPM	Convection-Permitting Model
CRHM	Cold Region Hydrological Model
CTRL	Control simulation
CWI	Canadian Wetland Inventory
DEM	Digital Elevation Model
DUC	Ducks Unlimited Canada
ESM	Earth System Model
ET	Evapotranspiration
GAM	Generalized Additive Model
GCM	Global Climate Model/General Circulation Model
GDD	Growing Degree Day
GEWEX	Global Energy Water Exchange
GHCN	Global Historical Climate Network
GIEMS-2	Global Inundation Extent from Multiple Satellite – version 2
GRACE	Gravity Recovery And Climate Experiment
GSWE	Global Surface Water Explorer
HW	Heatwave
HWF	Heatwave Freqency
HWM	Heatwave Magnitude
LAI	Leaf Area Index
LH	Latent Heat
LMA	Leaf Mass per Area
LMRB	Lower Mississippi River Basin
LSM	Land Surface Model
MMF-GW	Miguez-Macho & Fan – Groundwater model
MW	Midwest
NASH	North Atlantic Subtropic High
NCAR	National Center for Atmospheric Research
NEE	Net Ecosystem Exchange
Noah-MP	Noah LSM with Multi-Parameterization
NWM	National Water Model
OBS	Observation
PAR	Photosynthesis Active Radiation
PBLH	Planetary Boundary Layer Height
PET	Potential Evapotranspiration

PGW	Pseudo Global Warming
PILPS	Project for Intercomparison of Land-Surface Parameterization Schemes
PPR	Prairie Pothole Region
PR	Precipitation
PSN	Photosynthesis
RCM	Regional Climate Model
RCP8.5	Representative Concentration Pathway 8.5
REP	REPlace soil texture simulation
RMSE	Root Mean Square Error
S2S	Seasonal to Sub-seasonal
SCAN	Soil Climate Analysis Network
SDNWA	St. Denis National Wildlife Area
SFCRUN	Surface runoff
SGP	South Great Plain
SH	Sensible Heat
SIMGM	Simple Groundwater Model
SM	Soil Moisture
SMA	Soil Moisture Anomaly
SMC	Soil Moisture Content
SPEI	Standardized Precipitation Evapotranspiration Index
SPI	Standardized Precipitation Index
SVAT	Soil Vegetation Atmosphere Transfer
SWE	Snow Water Equivalent
TOPMODEL	TOPography-based hydrological MODEL
TX90	The 90^{th} percentile of maximum daily temperature
UDGRUN	Underground runoff
USDA	U.S. Department of Agriculture
USGS	U.S. Geological Survey
VIC	Variable Infiltration Capacity
WETCHIMP	Wetland CH4 Inter-comparison Modeling Project
WRF	Weather Research & Forecasting model
WS	Wetland Scheme
WTD	Water Table Depth

Chapter 1 – Introduction

1.1 Motivation and Relevance

Covering about 30% of Earth's surface, land has important interactions with Earth's climate system (Yang 2004). Several hydrological, biogeophysical, and biogeochemical processes occurring on or within the land's surface can interact with the atmosphere, hydrosphere, and biosphere, through an exchange of energy, water, and carbon fluxes. These processes are referred to as land surface processes. For example, various forms of available water (snow, soil moisture, open water surfaces) on the land surface play key roles in altering surface energy balance. Through changing the albedo, they influence the absorbed solar radiation and control the partition to sensible or latent heat, further inducing feedback to air temperature and humidity. This feedback may affect cloud formation, boundary layer height, or even trigger convective precipitation. These land-atmosphere interactions are most active in dry-to-wet transitional climate regions (Koster et al., 2004, 2006). Plant growth, through the development of leaves and stems, alters surface albedo, the leaf area index (LAI), surface roughness length, and aerodynamic and stomatal resistance, all of which are significant in affecting the energy and water exchange between plants and the atmosphere. Moreover, the photosynthesis occurring in plant canopies can assimilate inorganic carbon (CO_2) from the atmosphere and store it as organic matter (CH_2O). Through its control of leaf stomata and intake of CO_2 and O_2, soil moisture is also a limiting factor for photosynthesis and transpiration. Therefore, land surface processes have a profound influence on shaping Earth's climate system.

Land surface models (LSMs) are numerical descriptions of these processes, particularly focusing on the exchange of momentum, energy, moisture, and carbon between land and Earth's other components (Niu and Zeng, 2012). LSMs are also a key link that bridges the atmospheric models above and hydrological models below the Earth's surface. Originally designed to provide the atmospheric models with lower boundary conditions, such as upwards shortwave, longwave radiation and sensible and latent heat fluxes, LSMs can also supply upper boundary conditions to sub-surface and surface hydrological models, which focus on simulating water movements. Therefore, correctly representing these land surface processes in LSMs is of great importance to the comprehensive understanding of the Earth's systems.

In this thesis research, I provide a broad understanding of modeling the land surface processes in the North American Great Plains and explore their feedback to the regional climate. An extensive and strongly heterogeneous region across the Canadian Prairies and the U.S. Great Plains, the North American Great Plains consist of important ecosystems, such as forests, grasslands, mountains, wetlands, croplands, and urban areas. Two important ecosystems are of particular interest: the prairie pothole wetlands and croplands. These two ecosystems provide important services, such as flood control, wildlife habitat, and food security. At the same time, through strong exchanges of energy and water between land and the atmosphere, they also play key roles in regulating the regional climate, especially in influencing extreme heat and precipitation events.

To investigate land surface modeling and feedback to the regional climate, it is essential to improve the representation of hydrological processes in these two ecosystems in current land surface models. An advanced land surface model, the Noah land surface model with multiple-parameterization (Noah-MP, Niu et al., 2011; Yang et al., 2011), is applied as the major tool in this study. The Noah-MP LSM provides multiple options in simulating surface energy balance, snow physics, dynamic

vegetation phenology, groundwater, frozen soil parameterization, etc. Noah-MP is also has been used as the land component of the Weather Research & Forecasting model (WRF, Skamarock et al., 2008) for coupled regional climate simulations (Barlage et al., 2015; Liu et al., 2017; Li et al., 2020). Several advances in Noah-MP parameterizations, such as shallow groundwater dynamics, crop growth, irrigation, and wetland hydrology are applied and further developed in the course of this thesis. These advances add value to improving land surface heterogeneity and precipitation forecasting, especially in applications of the high-resolution convection-permitting WRF regional climate model.

The outcome of this research will have great importance for scientists' understanding of land-atmosphere interactions, especially heterogeneous land characteristics. It will also have strong implications for wetland habitat conservation organizations, agricultural industries, government agencies, and sustainable development for the people living in the North American Great Plains.

1.2 Theoretical background

1.2.1 Land-atmosphere interaction

The land surface is the key control of Earth's surface energy and water balance. On the land surface, the weather and climate are more variable and changeable than they are above the ocean. The storage and transformation of water on the land surface induce significant feedbacks to the climate system. Earth's surface energy and water balance is coupled through, most commonly, evapotranspiration, i.e., water from its liquid phase to gas phase (Seneviratne et al., 2010). The energy and water balance equations directly show the coupling between energy and water through evapotranspiration:

$$\frac{dS}{dt} = P - E - R_s - R_g \quad (1.1)$$

$$\frac{dH}{dt} = R_n - G - SH - \lambda E \quad (1.2)$$

On the water balance, the change of surface water storage with time ($\frac{dS}{dt}$) is the net result of precipitation (P, mm) minus total evapotranspiration (E, mm), surface runoff (R_s, mm) and underground runoff (R_g, mm). On the energy balance, the change of surface energy with time ($\frac{dH}{dt}, W/m^2$) is the result of net radiation ($R_n, W/m^2$), ground heat flux ($G, W/m^2$), sensible heat fluxes ($SH, W/m^2$) and latent heat fluxes ($\lambda E, W/m^2$).

Soil moisture is the most common form of surface water storage occurring in the unsaturated soil at the land surface. Evapotranspiration's dependence on soil moisture can be categorized into two main regimes: the soil moisture-limited regime and the energy-limited regime, as in Budyko's conceptual framework (Budyko, 1974). Figure 1.1 introduces Budyko's framework, showing the evapotranspiration regime represented as the evaporative fraction ($EF = \lambda E/R_n$) dependent on the volumetric soil moisture (θ, m^3/m^3). In the energy-limited evapotranspiration regime, soil moisture is above a critical value, θ_{crit}, beyond which evapotranspiration has a constant value and is no longer impacted by soil moisture but by insufficient energy input. In the soil moisture-limited evapotranspiration regime, soil moisture is below the critical value and provides a first-order constraint to evapotranspiration. Another important threshold is the wilting point, under which transpiration from plants ceases to take place. Between these two thresholds, soil moisture provides a linear positive control on evapotranspiration. Consequently, three soil moisture regimes can be identified (Koster et al., 2004; Seneviratne et al., 2006): 1) dry ($\theta < \theta_{wlt}$), 2) wet ($\theta > \theta_{crit}$), where soil moisture does not impact evapotranspiration and 3) transitional ($\theta_{wlt} < \theta < \theta_{crit}$), where soil moisture strongly constrains evapotranspiration and thus resulting feedback to the atmosphere. In Figure 1.1, this strong dependence is depicted as a linear relationship between soil moisture and evapotranspiration. In the first-generation bucket style LSMs (Section 1.2.2), this dependence is used as a linear limiting factor, β.

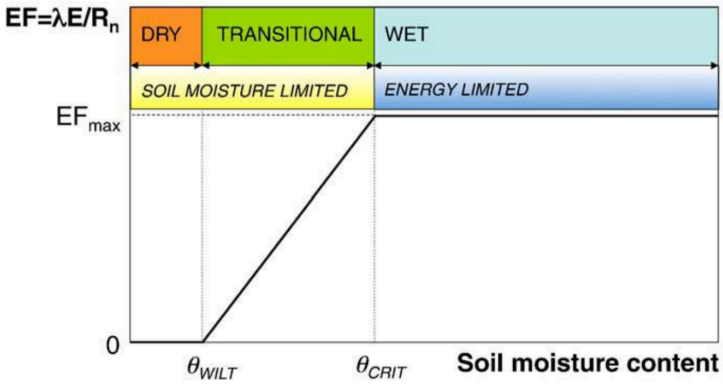

Figure 1.1. Evapotranspiration regime and soil moisture regime according to Budyko's framework. EF is the evaporative fraction, defined as evaporation energy divided by net radiation. Adapted from Fig. 5 in Seneviratne et al. (2010).

1.2.2 Soil moisture-temperature and soil moisture-precipitation feedback

An important impact of soil moisture on the near surface climate is its influence on air temperature. Whenever latent heat fluxes are limited by soil moisture, energy partition produces more sensible heat fluxes, increasing the air temperature. This impact in turn affects soil moisture availability due to an increase in the water vapor deficit, forming the soil moisture-temperature feedback. Related to the occurrence of extreme heatwaves, this feedback can significantly modulate temperatures near the surface climate (Perkins et al., 2015).

Figure 1.2 depicts a conceptual framework of the soil moisture-temperature feedback processes—soil moisture anomalies impact temperature mediated by evapotranspiration changes. The positive red arrow indicates positive feedback processes leading to warming/drying, while the blue arrow represents potential negative feedback. Thus, the whole process can be described as: (A) a low soil moisture anomaly induces a positive impact on a low evapotranspiration anomaly; (B) the decreased evapotranspiration produces a shift in surface energy balance components, increasing sensible heat and temperature; (C) the warmer temperature leads to a higher water vapor deficit, further decreasing soil moisture. Thus, the entire process forms a positive feedback loop—low soil moisture suppresses evapotranspiration but increases sensible heat flux, increasing temperature, which, in turn, increases evaporative demand and dries out soil moisture even more. This feedback loop can go on until the soil moisture is completely dry, for example, in the case of deserts or extreme droughts.

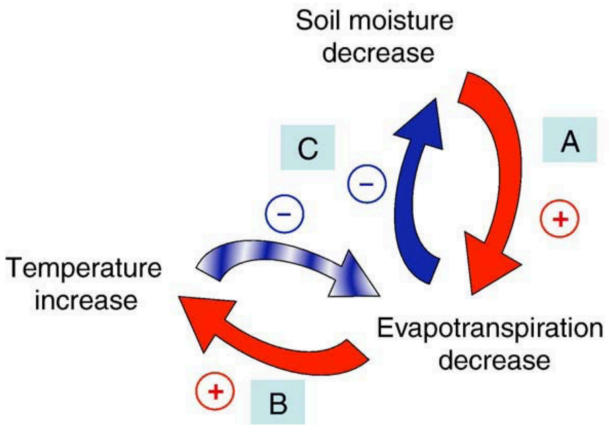

Figure 1.2. Processes contributing to the soil moisture-temperature feedback Adapted from Fig. 9 in Seneviratne et al. (2010).

This soil moisture-temperature feedback is well documented in and highlighted for its significant role in extreme heatwaves (Perkins, 2015; Whan et al., 2015). This direct and strong link between soil moisture and temperature is of interest in this thesis because the mechanism is better understood. In particular, this feedback is prominently linked to global climate change: As temperatures rise and the soil becomes drier, extreme heatwave events occur more frequently.

However, the soil moisture-precipitation feedback involves highly complex processes, and the feedback's potential impacts can be uncertain, with either positive or negative influences. This uncertainty occurs because the formation of precipitation is less directly impacted by surface evaporation than by larger scale atmospheric conditions. On the other hand, precipitation is

indirectly influenced by the boundary layer stability and the available precipitable water in the troposphere.

Figure 1.3 shows a conceptual framework of the soil moisture-precipitation feedback processes. The blue positive arrow represents an increasing impact while the red negative arrow represents a decreasing impact. The feedback loop starts with (A) increased wet soil on the surface leads to enhanced evapotranspiration (the blue arrow) when energy is not limited, while a potential red and negative arrow may exist if increasing evapotranspiration reduces the available soil moisture; (B) the increased surface evapotranspiration input to the atmosphere may trigger either positive or negative impacts on precipitation, noted by the mixed red/blue arrow. This process occurs because an increase in local evapotranspiration input in the atmosphere may directly increase the atmosphere's precipitable water, hence, increasing the humidity in the atmosphere and leading to a higher likelihood of precipitation. However, higher humidity is not a sufficient condition for precipitation formation because the moisture source might not be a local region via moisture transport. Precipitation formation also requires an unstable atmosphere condition, possibly aerodynamic lifting, i.e., air flow across mountains or thermodynamic lifting, characterized by the convective available potential energy (CAPE). A dry and warm surface produces strong sensible heat fluxes, and turbulent conditions push up the unstable boundary layer height. In the latter case, additional evapotranspiration input may actually suppress precipitation because a higher unstable boundary layer may favor cloud formation and reduce the available radiation received on the land surface. Therefore, the link between soil moisture and precipitation is complicated and uncertain. (C) The additional rainfall on the land surface naturally increases soil moisture availability through infiltration.

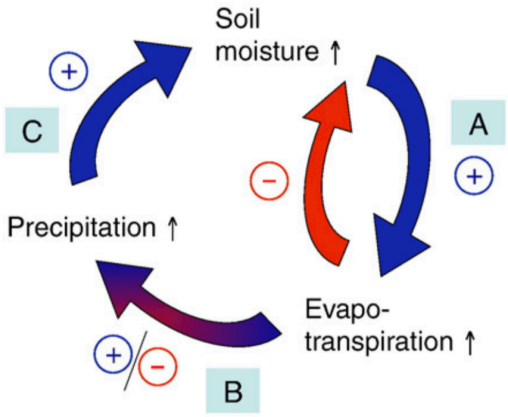

Figure 1.3. Processes contributing to the soil moisture-precipitation feedback. Adapted from Fig. 10 in Seneviratne et al. (2010).

Given the importance of soil moisture-precipitation feedback, atmospheric scientists and the hydrology community have been particularly attentive to this mechanism. However, as the mechanism is poorly understood and the processes embedded in it can be complex, this section briefly introduces soil moisture-precipitation feedback, although it is not the focus of this thesis.

1.2.3 Land surface model development

Land surface models (LSMs) also known as "soil-vegetation-atmosphere transfer schemes" (SVATs) are tools representing land surface processes and biophysical responses on Earth's land surface (Yang, 2004; Seneviratne et al., 2010; Zeng and Niu, 2011). Land surface models were originally used as a module in climate models, such as general circulation models (GCMs), to provide lower boundary conditions, i.e., sensible and latent heat fluxes and momentum and carbon flux exchanges with Earth's other components. In addition, LSMs provide hydrological models with surface storage conditions, such as soil moisture and the snowpack, both of which are important to simulating surface runoff and baseflow. In all, LSMs play a key role in bridging the overlaying atmospheric model and underlying hydrological model in the Earth System model (ESM).

LSMs have evolved for three generations and more than five decades (Clark et al., 2015; Fisher and Koven, 2020). The first generation LSM was the "bucket model" in Manabe (1969), which has a fixed water holding capacity of 15 cm. The water balance of the bucket is described as being filled by precipitation and emptied by evaporation. The surface runoff is represented as the excess bucket capacity. The sensible and latent heat flux is calculated using the aerodynamic bulk transfer equation with prescribed uniform surface properties, such as bucket holding capacity, surface albedo, and roughness length. Moreover, the evaporation (E) is a product of the potential evaporation (E_{pot}) and a β coefficient, commonly known as "soil wetness" or "moisture availability," and is a linear function of soil moisture content. Thus, the bucket model simulates no evaporation when the soil is dry ($\beta = 0$) and has a potential evaporation when the soil is wet ($\beta = 1$).

$$E = \beta E_{pot} \quad (1.3)$$

$$\beta = \frac{\theta - \theta_{wlt}}{\theta_{crit} - \theta_{wlt}} \quad (1.4)$$

There was no explicit representation of ecological processes, such as transpiration, photosynthesis, stomatal control, or detailed hydrological process infiltration, frozen soil, and groundwater. Despite their simplicity, the bucket models represent a key step in describing land surface processes in climate models, and their simulated soil moisture and evapotranspiration (ET) are comparable to more complex models at longer timescales.

Deardorff (1978) proposed an advanced LSM with one-layer vegetation and two-layer soil, which was suitable for use in GCMs. More complex hydrological processes are considered within the vegetation canopy, including evaporation from the soil as well as the wet canopy, canopy interception, and transpiration. This model later came to be known as the "big-leaf" model, as the structure of the one-layer vegetation canopy is analogous to a big leaf covering the model grid cell. This advanced structure opened paths for the future development of more complex structures for the second-generation LSMs.

From the 1980s to early 1990s, a second generation of LSMs emerged with explicit representation of vegetation effects and more complex soil hydrology, improving the realization of surface energy and water balance. Two representatives of the second generation LSMs are the Biosphere-Atmosphere Transfer Scheme (BATS, Dickinson, 1983, 1993) and the Simple Biosphere Model (SiB, Sellers et al., 1986, 1996a, b). These models usually have more than two soil layers, a single canopy layer, and a bulk snow layer. One noteworthy advance in the second generation LSMs is

the inclusion of explicit representation of stomatal resistance and its impacts on transpiration. Transpiration through plants' stomata was first represented with the Jarvis-type stomatal conductance scheme, a simple empirical equation as a function of radiation (photosynthetically active radiation, PAR), water (leaf water potential), and other environmental conditions (temperature and humidity).

In the early 1990s, third generation LSMs were developed with distinct features of dynamic vegetation and the incorporation of the carbon cycle using the Ball-Berry type of stomatal conductance scheme (Ball et al., 1987):

$$g_s = m\left(\frac{A_n}{C_s}\right)\beta P + b \quad (1.5)$$

where g_s is the stomatal conductance, A_n is the net carbon assimilation, C_s is the CO_2 partial pressure adjacent to the leaf, P is atmosphere pressure, and β is the soil moisture availability representing a humidity stress factor, and b is the minimum stomatal conductance. This change reflected in the above equation appeared in a later version of BATS (Dickinson et al., 1993) and a revised version of SiB2 (Sellers et al., 1996a) and even distinguished the photosynthesis pathway between C3 and C4 plants. This change opened a path for explicit modeling of plant photosynthesis and transpiration, as well as for linking CO2 assimilation in the coupling of water and the carbon cycle. Dickinson et al. (2002) included the effect of nitrogen cycling in the stomatal resistance equation. Furthermore, the BATS model has become the foundation of the Community Land Model (CLM, Dai et al., 2003), with other processes in development.

In the early 2000s, more complex representations of the hydrological cycle were developed into third generation LSMs, for example the frozen soil scheme in Niu and Yang (2006), surface runoff scheme (Niu et al., 2005) and simple groundwater scheme (Niu et al., 2007). These processes were included as multiple physics options in the community Noah-MP (multi-parameterization) LSM in 2011 (Niu et al., 2011; Yang et al., 2011).

1.2.4 Major issues with land-surface models at this stage

So far, this literature review has discussed the development of three generations of LSMs. Although these models have been successful, their application has also encountered outstanding issues, some of which are presented in here. First, these models are all designed to be one-dimensional soil column models. In other words, the models focus on representing the vertical soil and vegetation structures while neglecting the spatial heterogeneity of the surrounding environment. For example, many of these models only include a simple description of the runoff process by water balance excessing the soil capacity, which do not consider the surface heterogeneity of precipitation and soil moisture. This issue has been addressed with a TOPMODEL-based runoff and evaporation scheme (Famiglietti and Wood, 1994), which is reviewed in the next section. Second, vegetation is treated as a "big leaf" as in Deardorff (1978), scaling linearly from a leaf's typical size to 10 km x 10 km or 100 km x 100 km, referring to the size of the model's grid cell, which is unrealistic as one single leaf and stomata. Third, these abovementioned models explicitly account for only three land types (bare ground, snow, and vegetation) while they neglect lakes and open water. Fourth, although carbon cycles and dynamic plant growth are included, the spatial extent of vegetation types within a grid are prescribed.

1.2.5 The application of TOPMODEL in LSMs

The previously introduced LSMs focused on the vertical structure of the soil column as the basic hydrological unit, while effectively ignoring the spatial heterogeneity of soil moisture over a small watershed or large regions. The complex vertical structure, i.e., multiple layers of soil, snowpack, and vegetation canopy, is effective in simulating the evolution of ground temperature and snowpack accumulation/ablation. However, the one-dimensional soil column structure is not adequate for addressing the runoff generation mechanism, which is naturally controlled by the spatial heterogeneity of precipitation and surface conditions, especially topography and soil moisture. Given the complexity of the modeling hydrological cycle, the traditional one-dimensional soil column LSM cannot capture the main physical mechanism that controls runoff production.

The motivation for improving surface runoff simulation in LSM comes from the work of Koster and Milly (1997). These authors found that one common shortcoming of the Project for Intercomparison of Land-Surface Parameterization Schemes (PILPS) LSMs is that the representation of LSM's runoff processes also strongly controls the annual evaporation rates, as much as the evaporation process itself. Therefore, the logical improvement to this problem is to apply a sub-grid horizonal structure of the land surface hydrological process. This is where the application of the TOPMODEL statistical treatment enables the representation of soil moisture heterogeneity, which is important for runoff and also improves the representation of evaporation.

Developed more than 40 years ago, TOPMODEL (TOPography-based hydrological MODEL) is a rainfall-runoff model that uses topography data to reflect its dynamic processes responses in downslope hydrology, especially in runoff generation in a variable contributing area (Beven and Kirkby, 1979; Beven et al., 2020). The TOPMODEL makes three necessary assumptions, which are summarized in Stieglitz et al. (1997): (1) The water table gradient is close to the terrain gradient so that the local hydraulic gradient can be represented by the terrain slope angle, ($tanb$); (2) the saturated hydraulic conductivity, K_s, declines exponentially with depth with a decaying factor *f*:

$$K_s(z) = K_s(z=0)e^{-fz} \quad (1.6)$$

and z is the depth; (3) at the water table depth, recharge occurs at a steady and spatially homogeneous rate so that the recharge and water table are at the equilibrium state. Thus, the runoff generation responses to a steady state rainfall are proportional to the spatial variation of moisture contents in a drainage basin and can be characterized by its topography variation by digital topography analysis. Therefore, the local water table depth (z_i) can be defined as:

$$z_i = \bar{z} - \frac{1}{f\left[\ln\left(\frac{a}{tanb}\right) - \overline{\Lambda}\right]} \quad (1.7)$$

where $\bar{z}$ is the mean water table depth of the grid cell, $\ln\left(\frac{a}{tanb}\right)$ is defined to be a topographic index, and a is the unit contour of the drainage contributing area at the location and $tanb$ is the local slope at that point, f is a decaying function for saturated conductivity in depth, and $\overline{\Lambda}$ is the average of topographic index of the grid cell. High index values are likely to saturate first, thus indicating potential subsurface or surface contributing areas (Beven, 1997).

From the knowledge of grid-cell mean water table depth ($\bar{z}$) and the cumulative distribution of the topographic index (analyzed from DEM data), the saturated fraction of the watershed and its control on baseflow can be calculated. In a steady state, a critical threshold value for the local

topographic index (Λ_{cri}) can be obtained when the local water table depth is at the surface, compared to the grid-cell mean water table depth. Setting the local water table depth to 0 in the equation 1.7 ensures that all locations associated with values of the topographic index greater the critical threshold (Λ_{cri}) are within the saturated region. So, a sub-grid fraction F_{sat} can be defined by integrating the topographic index interval from this critical value to the maximum, following its probability distribution function:

$$F_{sat} = \int_{\Lambda_{cri}}^{\infty} pdf(\Lambda)\, d\Lambda \quad (1.8)$$

This probability distribution function can be obtained from DEM data and was assumed to be a three-parameter gamma distribution by Sivapalan et al. (1987).

This saturated fraction of a watershed is a key control of the surface water as well as energy balance (Famiglietti and Wood, 1994 a, b). In the hydrological community, F_{sat} refers to the partial contributing area, and the direct overland flow from precipitation over this saturated region is a major component of surface runoff (Dunne runoff or saturation excess runoff). Moreover, energy and water balance are strongly coupled in the distribution of heterogeneous soil moisture in the watershed: Evapotranspiration will therefore be near the potential rate in the lowland saturated portion, and it will fall rapidly off into vegetation and soil moisture-controlled drier uplands.

The application of TOPMODEL in aggregated watershed and macroscale hydrological modeling allows simplified calculation of surface energy and water balance, combining the vertically complex single soil column LSMs with a spatial heterogenous model that considers topographic effect. One essential assumption is that all the points of the same value of the index respond similarly in the catchment. It is therefore not necessary to calculate all the points in a catchment, but it is necessary to integrate each interval of index values through the distribution function (Famiglietti and Wood, 1994a&b). In Famiglietti (1994a&b), this TOPMODEL concept is used in a local site, aggregated watershed, and macroscale model in a FIFE experiment.

Hereafter, the discretized soil column grid cell can be separated into a saturated fraction (F_{sat}) and unsaturated fraction (1-F_{sat}). Surface energy and water balance, such as latent heat fluxes, evapotranspiration, and runoff can be obtained separately for these two fractions of the watershed. The subsequent fluxes are then combined by the weighted average function, given their fractions, to update the mean state of the single column model. This efficient approach is further incorporated into LSMs in the NASA GISS LSM (Stieglitz et al., 1997) and the NASA Catchment Land Surface Model (CLSM, Koster et al., 2000) among others.

In 2000, Koster et al. described a catchment strategy to improve the horizontal heterogeneous sub-grid soil moisture variability and its impact on runoff generation in LSMs. This approach is different from traditional SVAT strategy in two ways: First, the boundaries of the basic land surface unit is a hydrological catchment, based on topography data, rather than a quasi-rectangle grid derived from an atmospheric model grid. Atmospheric forcings are disaggregated to several catchments in each grid for independent calculation of surface fluxes, ET, runoff, etc., and the resultant fluxes are aggregated and returned to the larger grid. Second, the sub-catchment distribution of root zone soil moisture is diagnosed from bulk moisture variables and topographic characteristics, using the TOPMODEL concept. The distributions are used to separate the catchment area into three sections, each representing a distinct moisture regime. Evaporation and

runoff processes are modeled separately in each regime, thereby producing more reliable catchment mean rates.

In 2005, the three-parameter gamma distribution used for F_{sat} parameterization in Sivapalan et al. (1987) was simplified by an exponential function in Niu and Yang et al. (2005): $F_{sat} = F_{satmx}e^{-Cfz_{\nabla}}$. F_{satmx} is the maximum saturated fraction given in a grid cell, defined as the cumulative density function of the topographic index when the grid cell mean water table is at the surface and *C* is a coefficient that can be derived by fitting the exponential function to the discrete cumulative distribution function to the topographic index. These two parameters can be estimated by terrain analysis using the digital elevation model (DEM) data from the studied watershed. The newly simplified equation shows an improved representation of the F_{sat} parameter, especially in mountainous regions. This modification was incorporated into the National Center for Atmospheric Research (NCAR) Community Land Model version 2.0 (CLM 2.0) and afterwards in Noah-MP LSM in 2011 (Niu and Yang et al., 2011).

1.2.6 Noah-MP LSM and some advanced physics options

This study will focus on the application and development of the community Noah LSM with Multiple-Parameterizations scheme (hereafter Noah-MP). A candidate for the third-generation LSM, the Noah-MP LSM is an enhancement of the Noah LSM (Chen & Dudhia, 2001; Niu et al., 2011, Yang et al., 2011). The multiple parameterizations imply that different physical options are available to select many key land surface processes, such as vegetation canopy energy, stomatal conductance, plant transpiration factor, layered snowpack, surface runoff, and groundwater hydrology.

Noah-MP has been comprehensively evaluated in various climate regimes, especially in the contiguous U.S. (Cai et al., 2014a & 2014b; Chen et al., 2018). This model is widely applied in several modeling centers as a land component for climate models and data assimilation. Noah- MP is a primary model employed in the NASA Land Information System (Kumar et al., 2006), the next phase North American Land Data Assimilation System (Xia et al., 2012), the Weather Research and Forecasting model (Skamarock et al., 2019), and the National Water Model (Cosgrove et al., 2016).

Since the initial development of Noah-MP in 2011, several new physical schemes have progressed to address newly emerged needs for representing land surface processes that were neglected or oversimplified in previous models. Four specific processes are included in this thesis for detailed study: dynamic crop growth (Liu et al., 2016), dynamic irrigation scheme (Xu et al., 2019), shallow groundwater scheme (Miguez-Macho et al., 2007), and dynamic surface wetland scheme (Zhang et al., 2021 under review). The description of these new schemes is provided in Chapters 3, 4, and 6, respectively.

1.2.7 Convection-permitting model (CPM) and Pseudo Global Warming (PGW) method

Global climate models (GCMs; 60-300 km spatial resolution) are the primary tools for understanding climate change under increasing greenhouse gases (Taylor et al., 2012). Higher resolution regional climate models (RCMs; 12-50 km spatial resolution) are often used to provide regional details. At these typical model resolutions (10-100 km), many important processes, such as convection that occur on a smaller scale, cannot be resolved explicitly and, instead, are parameterized. However, convection parameterization may lead to deficiencies in the precipitation diurnal cycle, frequency, and extremes (Dai, 2006; Ban et al., 2014; Prein et al., 2015; Kendon et al., 2017; Liu et al., 2017). Several studies have recognized that convection parameterization is a major source of uncertainties and errors in the simulation of the precipitation diurnal cycle.

There is an emerging trend to using convection-permitting models (CPMs, spatial resolution < 5-km) in regional climate studies. Previous research (Weisman 1997) has suggested that 4-km spatial resolution is sufficient for atmospheric models to explicitly represent convections. Thus, convection parameterizations can be switched off. A review provided by Prein et al. (2015) on this topic concludes that the largest added values of CPM are found in regions dominated by convective precipitation, a heterogeneous land surface, and complex topography. A recent study by Zhang et al. (2018) of extreme heatwaves in the U.S. (Chapter 2) also found added values of CPM. The feedback from antecedent soil moisture to summer heatwaves reveals a much higher agreement with the observational dataset than do other coarser resolution studies.

The land surface state and land-atmosphere exchange of energy and moisture fluxes exert a strong control on the climate system over land. A previous CPM study of the snowpack in the western U.S. has shown that model results are sensitive to the choice of LSM (Chen et al., 2014). Nonetheless, even with the same LSM, perturbations in the initial soil moisture state and multiple LSM parameterizations may also induce uncertainties in simulating both precipitation and temperature in regional climates (Trier et al., 2008; Zheng et al., 2015). These results suggest that, even though a CPM model can constrain the major source of precipitation uncertainties from convection parameterizations, the deficiencies from other model physics parameterizations, such as the LSMs, may emerge.

Most recently, two long-term RCM studies have been conducted in the continental U.S. and Western Canada (Liu et al., 2017; Li et al., 2019). These studies are powerful tools to investigate the impacts of climate change on the water cycle and important data source for this thesis. The two sets of CPM simulations have two distinctive advantages for the current study: (1) High-resolution forcing and grid spacing allow a detailed representation of the land surface heterogeneity (Prein et al., 2015); (2) Switching off the convection parameterization allows improved forecasting for precipitation diurnal cycle, intensity, and frequency (Kendon et al., 2017). Figure 1.4 shows the domain coverage and terrain height of the CONUS WRF study.

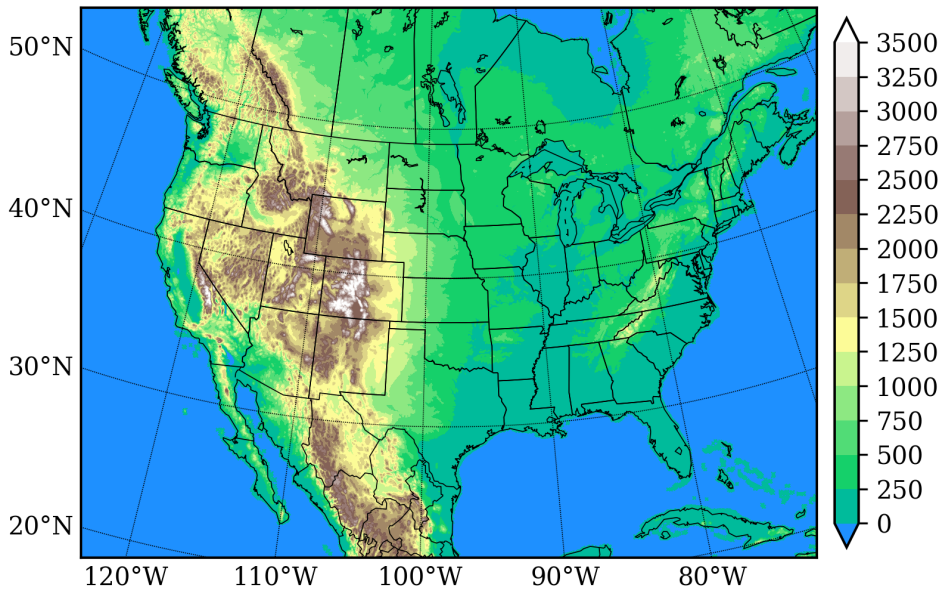

Figure 1.4. Model domain and terrain height (m) for the CONUS WRF simulations.

The CONUS WRF simulations adapt a method called "pseudo global warming" (PGW), a hypothetical warming scenario by the end of 2100 downscaled by an ensemble of GCMs. These GCMs provide a surrogate climate change scenario for investigating climate change impacts on hydrological and land surface characteristics. The PGW method consists of two paralleled climate simulations: the control simulation (CTRL), which is a realization of the contemporary climate, and the future simulation (PGW), which adds a delta climate change signal from GCM projections upon the CTRL. For the CTRL simulation, the initial and boundary conditions are from the 6-hr ERA-Interim re-analysis dataset. For the PGW simulation, the initial and boundary conditions are created by adding a climate change perturbation by the end of the 21st century, derived from an ensemble of GCMs in an RCP8.5 emission scenario upon the ERA-Interim reanalysis.

The climate change perturbation includes wind, geopotential height, temperature, specific humidity, sea surface temperature, soil temperature, sea level pressure, and sea ice (Liu et al., 2017). The perturbation in these fields impact large-scale planetary waves and associated thermal dynamics, while the synoptic scale weather events remain structurally constrained by the boundary conditions in terms of frequency and intensity (Schär et al., 1996; Rasmussen et al., 2011). The PGW method has gained popularity in the climate science and hydrology communities, as it concomitantly allows certain processes to be examined in isolation, such as snowfall and snowpack (Rasmussen et al., 2011; Musselmen et al., 2018), meso-scale convection systems (Prein et al., 2017), land-atmosphere interactions (Zhang et al., 2018), and groundwater responses to climate change (Zhang et al., 2020).

$$\text{CTRL: } \mathrm{WRF}_{\mathrm{input}} = \text{ERA–Interim} \quad (1.9)$$

$$\text{PGW: } \mathrm{WRF}_{\mathrm{input}} = \text{ERA–Interim} + \Delta\mathrm{CMIP5}_{\mathrm{RCP8.5}} \quad (1.10)$$

$$\Delta\mathrm{CMIP5}_{\mathrm{RCP8.5}} = \mathrm{CMIP5}_{2071-2100} - \mathrm{CMIP5}_{1976-2005} \quad (1.11)$$

Both CTRL and PGW simulations were dynamically downscaled using the WRF model at convection-permitting resolution (4-km) from 2000-10-01 to 2013-10-01 (Liu et al., 2017). A flow chart of the PGW method used in the CONUS WRF simulations is included in Appendix A.

1.3 Research design

1.3.1 Research purpose

The purpose of this research is to provide a better understanding and improve the representation of two major land ecosystems in the North American Great Plains—the prairie pothole wetlands and croplands—and study their interactions with the regional climate. These two ecosystems provide important services to the surrounding environment, such as flood regulation, wildlife habitats and food security. At the same time, they play a key role in interacting with the regional climate through strong exchanges of energy, moisture and carbon. Their impacts on the regional climate, such as influencing temperature and precipitation, are critical to understanding and mitigating climate change impacts and are essential to sustainable development.

1.3.2 Study region

Figure 1.5 shows the land use map for the North American Great Plains, with the black contour depicting the Prairie Pothole region (PPR). The yellow color covers the U.S. corn belt, soybean fields in the Lower Mississippi River Basin, and the massive wheat field across the U.S. and Canada, which are also referred to as one of the world's food baskets. The Prairie Pothole wetlands are small features co-located between the grasslands and croplands in the PPR region. Key hydrological processes and land-atmosphere interactions occur in these two land types. For example, the crop growth may alter the surface albedo, LAI, hence, surface energy partitioning. Human management, such as irrigation, adds an additional water supply to the fields, effectively changing the water balance as well. Shallow groundwater acts as a buffer for the land surface and soil moisture, absorbing excessive water during wet times and supplying uplands during dry times. Wetlands are also open water features that can significantly cool the surrounding environment through partitioning available surface energy to latent heat fluxes. Therefore, it is essential to study these processes and their impacts on the regional climate through improving their representation in LSMs.

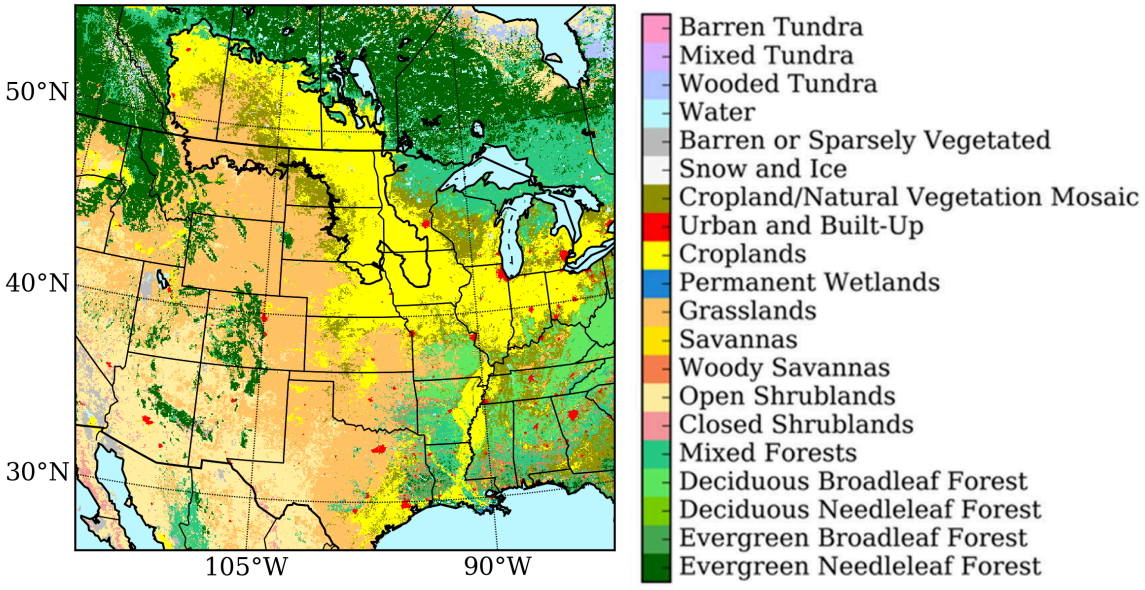

Figure 1.5. Land use map for the North American Great Plains region. The yellow color covers a massive area of cropland. The black contour depicts the Prairie Pothole Region across Canada and the U.S.

1.3.3 Objectives

Objective 1

Understand the land-atmosphere interactions during extreme heatwaves. To achieve this objective, the following steps were taken:

- Define heatwaves and soil moisture anomalies using historical statistics.
- Understand the statistical relationship between heatwaves and soil moisture.
- Study the responses of heatwaves to soil moisture, given different quantiles of heatwave frequency and magnitude.

Objective 2

Assess the interactions between crop growth and irrigation in cropland ecosystems. To achieve this objective, the following steps were taken:

- Assess Noah-MP's performance in the joint modeling of crop yields and irrigation amounts.
- Investigate the impacts of irrigation on crop yields, from field to regional scale.
- Study the impacts of climate change on crop yields and irrigation amounts.

Objective 3

Study the shallow groundwater dynamics in the Prairie Pothole Region (PPR) under the current and future climate. The following steps were taken:

- Simulate and evaluate the modeled water table depth using well observations in the PPR.
- Understand the contribution of climate change to the surface, subsurface, and groundwater hydrological cycle.
- Assess the uncertainties of soil texture in modeling water table depth

Objective 4

Explore the wetland distribution in the Canadian Prairies under future climate change. The following steps were taken:

- Develop a generalized additive model from soil moisture and ecoregion factors in the Canadian Prairies.
- Understand the wetland extent changes associated different hydrological components.
- Combine the future wetland extent with historical drainage conditions and design diversified conservation strategies over this region.

Objective 5

Represent the dynamics of the prairie pothole wetlands and study their hydrological cycle, spatial distribution and their feedback to the regional climate. The following steps were taken:

- Develop a sub-grid wetland parameterization.
- Test this sub-grid wetland scheme at a single-point site and offline regional simulations.
- Investigate the impacts of wetland hydrology on the regional climate in a coupled WRF model.

1.4 Outline

Chapter 2 of this thesis presents a study that quantifies the relationship between summertime extreme heatwaves and antecedent springtime soil moisture anomalies in the U.S. from station observations and a long-term high-resolution convection-permitting model. Both heatwaves and soil moisture anomalies from the CONUS WRF simulations are evaluated against station observations. A quantile regression method is used to analyze the asymmetric responses of various quantiles of heatwave frequency and magnitude against springtime soil moisture. Strong negative correlation coefficients are found over two regions in the U.S. Midwest and South Great Plains. This study adds predictability to seasonal-to-sub-seasonal (S2S) forecasting of summertime extreme heatwave events. The manuscript, entitled "Evaluation of convection-permitting WRF CONUS simulation on the relationship between soil moisture and heatwaves", was published in the journal *Climate Dynamics* in 2018: https://link.springer.com/article/10.1007/s00382-018-4508-5.

Chapter 3 presents joint crop-irrigation simulations in the central U.S. for corn and soybean in the Noah-MP LSM. The purpose of these simulations is to investigate the impacts of soil water stress and the improvement modeled irrigation has on simulating crop photosynthesis and carbon allocation in a semi-arid region. This study also assesses the uncertainties associated with crop physiology, planting/harvesting and irrigation management. The results show that irrigation has a stronger impact on corn in the semi-arid region of Nebraska than for soybeans in the Lower Mississippi River Basin. Updating the state-level planting/harvesting dates generally reduces crop yields, mostly due to shortening the growing seasons. Finally, modeling uncertainties are assessed and associated with crop physiology parameters, crop yield records, yield gaps, human management such as planting/harvesting, irrigation, and fertilization. This manuscript, entitled "Joint modeling of crop and irrigation in the Central United States using the Noah-MP land surface model", was published in *the Journal of Advances in Modeling Earth Systems* in 2020: https://agupubs.onlinelibrary.wiley.com/doi/full/10.1029/2020MS002159.

Chapter 4 presents a modeling study of the shallow groundwater dynamics in the PPR across Southern Canada and the U.S. Midwest. The purpose of this study is to explore the exchange of water between soil moisture and shallow groundwater in this region with seasonal frozen soil, under the current and future climate. A shallow groundwater dynamic scheme is coupled in the Noah-MP LSM. The land surface model and groundwater scheme are driven by two sets of parallel climate forcings from CONUS WRF, one for the current and the other for the future climate. The model-simulated water table depths are evaluated against well observations. The water balance for groundwater aquifers, soil moisture, and snowpack are investigated under the current and future climate. This study manifests the potential for modeling shallow groundwater and its interaction with soil moisture in the PPR and has great implications for studying the region's hydrological cycle. The manuscript, entitled "Modeling groundwater responses to climate change in the Prairie Pothole Region", was published in the journal *Hydrological and Earth System Sciences* in 2020: https://hess.copernicus.org/articles/24/655/2020/.

Chapter 5 presents a ecological application of the Noah-MP LSM to investigate the future distribution of surface wetlands in the Canadian Prairies. The purpose of this study is to explore the future distribution of wetland extents in the Canadian Prairies and to understand the water balance contribution to these changes. This study uses the hydrological outputs from the shallow

groundwater study in Chapter 4 and ecoregions distribution to construct a statistical model—a general additive model (GAM)—to simulate wetland extents in the current and future climate. Under the future climate, two regions exhibit a consistent increase and decrease of wetland extents—the mixed grasslands in the west and mid-boreal uplands in the east, mainly due to the heterogeneity of future precipitation projections in the summer. The future wetland distributions are overlayed with a historical drainage map of the Canadian Prairies. These two increased/decreased wetlands suggest diversified conservation strategies of wetland retention and conservation in the western and eastern Canadian Prairies. This manuscript, entitled "Heterogeneous changes to wetlands in the Canadian Prairies under future climate", was published in *Water Resources Research* in 2021:
https://agupubs.onlinelibrary.wiley.com/doi/abs/10.1029/2020WR028727.

Chapter 6 presents a dynamic wetland modeling study using the Noah-MP LSM and coupled WRF regional climate model. The purpose of this study is to improve simulated wetland spatial extents and hydrological processes and investigate their impacts on the surface energy and water balance, as well as on feedback to the regional climate in the PPR. In this study, the default TOPMODEL-based saturated fraction F_{sat} parameterization is modified, based on the first layer of soil saturation. In addition, a bucket-style surface water storage scheme is implemented to simulate dynamic wetland hydrological processes, including inflow, evapotranspiration to atmosphere, and outflow. 13-year offline simulations are conducted over the PPR region using the CONUS WRF forcing. Finally, coupled WRF simulations are conducted for the summer months from April to August over three summers. The results show a significant cooling effect of 1~3℃ over high wetland fraction regions. This study has important implications for representing wetland hydrological processes and their impacts on the surface energy balance and feedback to the atmosphere in coupled regional climate models. This study is also important for wetland conservation agencies as the wetland cooling effects are evident for relieving heat stress during extreme heatwave events. The manuscript, entitled "Evident cooling effects of surface wetlands to mitigate climate change – a study of the Prairie Pothole Region" is under review in the *Water Resources Research* in 2021.

Chapter 7 summarizes the above studies in this thesis and provides a synthesis on three major challenges in land surface model development, including model process complexity, surface heterogeneity, and uncertainties in model parameters. A future outlook for a potential follow-up study of joint cropland-wetland simulation in the North American Great Plains is also provided.

Chapter 2 – Asymmetric responses of summertime heatwaves to antecedent soil moisture

This manuscript has been modified for inclusion in this thesis. It was originally published as:

Zhang, Z., Li, Y., Chen, F., Barlage, M. & Li, Z. Evaluation of convection-permitting WRF CONUS simulation on the relationship between soil moisture and heatwaves. *Clim. Dyn.* (2018) doi:10.1007/s00382-018-4508-5.

Author contributions: Z. Zhang, F. Chen and M. Barlage designed the study and wrote the paper. Y. Li and Z. Li contributed to the interpretation of the results and reviewed the manuscript.

Keywords

Soil moisture, heatwaves, land-atmosphere interaction, convection-permitting, regional climate model, WRF model

Abstract

Soil moisture plays an important role in modulating regional climate from sub-seasonal to seasonal timescales. Particularly important, soil moisture deficits can amplify summer heatwaves (HWs) through soil moisture-temperature feedback which has critical impacts on society, economy and human health. In this study, we evaluate decade-long convection-permitting Weather Research and Forecast (WRF) model simulations over the contiguous US on simulating heatwaves and their relationship with antecedent soil moisture using a dense observational network. We showed that the WRF model is capable of capturing the spatial patten of temperature threshold to define HWs, though the simulation shows a warm bias in the Midwest and cold bias in western mountainous regions. Two HW indices, based on frequency (HWF) and magnitude (HWM), are evaluated. Significant anti-correlations between antecedent soil moisture and both HW indices have been found in most parts of the domain except the South Pacific Coast. A detailed study has been conducted for the Midwest and South Great Plains regions, where two heatwaves had occurred in the last decade. In both regions, the high quantile of the HWF distribution shows a strong dependence on antecedent soil moisture: drier soil leads to much larger increase on the upper quantile of HWF than it does on the lower quantile. Soil moisture effects on the higher end of HWM are not as strong as on the lower end: wetter antecedent soil corresponds to a larger decrease on the lower quantile of HWM. WRF captures the heterogeneous responses to dry soil on HWF distribution in both regions but overestimates these HWM responses in the Midwest and underestimates them in the South Great Plains. Our results show confidence in WRF's ability to simulate HW characteristics and the impacts of antecedent soil moisture on HWs. These are also important implications for using high-resolution convection-permitting mode to study the coupling between land and atmosphere.

Motivation

Since the goal of this Ph.D. study is to understand the land-atmosphere interaction in convection-permitting model simulations, the first step is to explore how this relationship is simulated in current state-of-the-art CPM research. I first study one aspect of the land-atmosphere interaction—soil moisture-temperature feedback during extreme heatwave events. The CONtinuous US WRF project provides an important opportunity for long-term high-resolution results. An evaluation of the model performance in springtime soil moisture and its relationship with summertime heatwaves provides an overall understanding of this topic.

2.1 Introduction

Summer heatwaves (HWs) have significant impacts on the environment, society, and human health (Brooke Anderson and Bell 2011). Under climate change, these extreme hot events are projected to become more frequent, intense and longer (Meehl and Tebaldi 2004; Diffenbaugh and Ashfaq 2010; IPCC 2012). Thus, understanding the physical mechanisms of HWs and improving HW forecast skills is of great importance and allows a proactive approach to mitigating potential HW damages.

Although persistent synoptic high pressure induced by large scale atmospheric blocking is a necessary factor in causing persistent heatwaves (Perkins 2015), land–atmosphere interactions also play an important role in amplifying the hot extremes through a soil moisture-temperature feedback mechanism (Jaeger and Seneviratne 2011; Miralles et al. 2014). Soil moisture availability determines the evapotranspiration, a key process in exchange of water and energy between the land surface and atmosphere. During dry periods, low soil moisture limits the available surface energy converted to latent heat. More energy is partitioned as sensible heat flux, inducing an increase of near-surface temperature. Increased temperature then leads to a higher vapor pressure deficit and evaporative demand, and thus to a potential increase in evapotranspiration despite the already existing dry conditions, leading to a further soil desiccation (Seneviratne et al. 2010).

The soil moisture-temperature feedback mechanism and its impacts on heatwaves have been studied using climate models both in long-term climate simulations (Koster et al. 2004, 2006, 2009; Guo et al. 2006; Seneviratne et al. 2006; Jaeger and Seneviratne 2011) and regional events studies (Fischer et al. 2007; Whan et al. 2015; Hauser et al. 2015). Both studies contribute to our understanding of the feedback mechanism and the key role that soil moisture plays to influence near-surface temperature. However, these results, by perturbing initial soil moisture or decoupling the land from the atmosphere, could be artificial and model dependent. Substantial observational evidence is needed to further understand the soil moisture-temperature feedback.

Several observations have confirmed previous modeling studies at regional (Durre et al. 2000; Hirschi et al. 2011; Quesade et al. 2012; Meng and Shen 2014; Sun et al. 2017) and global scale (Mueller and Seneviratne 2012). These works focus on the relationship between antecedent precipitation/soil moisture and summer hot extremes, and its impacts on different distributions of hot extreme indices. Owing to the lack of extensive long-term soil moisture observations, they inferred soil moisture conditions using a precipitation-based index called the standardized precipitation index (SPI) (McKee et al. 1993). Their results showed that antecedent negative soil moisture anomalies were associated with a high frequency of summer hot day as well as longer

duration of HW. Although precipitation is a major driver for soil moisture, SPI does not consider the effect of evapotranspiration. A similar multi-scalar statistical index called the standardized precipitation evapotranspiration index (SPEI) has been proposed to account for both precipitation and evapotranspiration on soil moisture (Vicente-Serrano et al. 2009).

Although the above observational studies have shown evidence of soil moisture-temperature feedback on HWs, they mainly focused on the frequency and duration of HWs, while the HW intensity and its relationship with soil moisture has not yet been assessed. A statistical significant correlation suggests a strong connection between soil dryness and extreme heat, but does not necessarily imply causality (Mueller and Seneviratne 2012). Moreover, previous regional climate model simulations could capture the link between the soil moisture deficits and hot extremes but only for the moisture-limited regime. For wetter climates, the models tended to overestimate the strength of soil moisture-temperature feedback (Hirschi et al. 2011). Furthermore, previous studies used data from both global/regional models and gridded observational/re-analysis products at a spatial resolution of 50–100 km, which is not sufficient to capture the land–atmosphere feedback and perform HW impact studies on a local scale.

Long-term climate downscaling using convection-permitting models (CPM) provides an opportunity to fill the gaps in spatial scales (Prein et al. 2015). A 13-year (2000 October–2013 September) 4-km CPM simulation was conducted for the contiguous US (CONUS), using the Weather Research and Forecast (WRF) model (Liu et al. 2017). The CPM simulation, by explicitly resolving convection, improves summer precipitation simulations (Liu et al. 2017), which is important for assessing soil-moisture evolution and land–atmosphere feedbacks. This simulation represented realistically fine-scale land surface properties, such as topography and land-cover types which are critical in land–atmosphere coupling studies. In addition, the fine resolution dynamical downscaling allows the studies of HW impacts on local scale, which is more relevant to public health issues.

The purposes of the study in this chapter are to: (1) evaluate different temperature thresholds in defining the simulated HW for two HW indices; (2) assess the correlation between antecedent soil moisture and summer HWs in the WRF CONUS simulation; and (3) evaluate how differently the distribution of HW indices responds to observed soil moisture and how well this feature is represented in the WRF 4-km CONUS simulations. The Midwest (MW) and South Great Plains (SGP), where soil moisture-temperature feedbacks are strong and two extreme heatwaves happened in 2006 and 2011, are investigated in detail. This paper is organized as the following: Sect. 2 describes observation and WRF simulation datasets, as well as the indices used to define heatwaves and soil moisture anomaly; Sect. 3 evaluates the CPM WRF in simulating HWs and discusses their correlations with antecedent soil moisture against observation datasets; Sect. 4 provides a broad discussion of antecedent soil moisture as a physical driver of HWs, its predictive skills and WRF CONUS performance compared to observation and other studies; conclusions are provided in Sect. 5.

2.2 Data and Method

2.2.1 WRF model

Previous studies have stated the advantages of high-resolution convection-permitting modeling in studying the land surface processes, by improving the representation of fine-scale terrains, such as mountainous and urban areas, and the heterogeneity of surface fields, such as soil moisture (Prein et al 2013a, b, 2015). In this study, we use high-resolution convection-permitting regional climate simulations, conducted on the Weather Research and Forecasting (WRF) model V3.4.1 (Skamarock et al. 2008), to explore the soil moisture-temperature feedback on summer HWs. The simulations start from the October of 2000 and run to the September of 2013 on 4-km horizontal grid spacing (1360×1016 grid points), covering the contiguous US (CONUS) (Fig. 1a). The physical parameterization schemes used in these simulations are the Thompson aerosol-aware microphysics (Thompson and Eidhammer 2014), the Yonsei University (YSU) planetary boundary layer (Hong et al. 2006), the rapid radiative transfer model (RRTMG; Iacono et al. 2008) and the Noah-MP Land Surface Model (LSM). (For more detailed descriptions about the selection of physical schemes, model modifications, and simulation configuration, please see Liu et al. 2017).

In the CONUS WRF simulations, soil moisture and surface fluxes exchange to the atmosphere are simulated by the Noah-MP Land Surface Model (LSM) (Niu et al. 2011; Yang et al. 2011), a community model with multi-parameterization options to the original Noah LSM (Chen and Dudhia 2001). The Noah-MP LSM has been applied broadly, both in offline mode (Cai et al. 2014a, b) and coupled with atmospheric models (Chen et al. 2014; Barlage et al. 2015). Particularly, previous studies have shown improvement in simulating snowpack (Musselman et al. 2017) and severe storm forecast (Duda et al. 2017) by a more realistic representation of surface physics in the Noah-MP LSM coupled with high resolution CPM. In addition, Liu et al. (2017) provided several key modifications to the Noah-MP LSM, including microphysics-based snow-rain partitioning, realistic surface snow coverage representation, patchy snow in surface energy balance calculation, and heat transport by precipitation into the ground (see Liu et al. 2017). In this study, we are interested in soil moisture anomaly and how it contributes to summer HWs through soil moisture-temperature feedback. For this purpose, the WRF model simulated soil moisture anomalies are compared with an observational network (see Sect. 2.2) and the evaluation results are shown in Sect. 3.1.

2.2.2 Observations

To evaluate the WRF model temperature and soil moisture output, we used meteorological station data from the Global Historical Climatology Network-Daily dataset (GHCN-Daily) (Menne et al. 2012; Newman et al. 2015). Daily maximum temperature (Tmax) and precipitation data from a total number of 9877 stations within the WRF model domain are used to calculate heatwave indices and soil moisture proxy in this study. The locations of the GHCN-Daily station are also shown in Fig. 1a, with stations in the Midwest (MW, 41–46N, 90–105W) and the South Great Plains (SGP, 29–40N, 95–105W) are highlighted.

Soil moisture observations from the US Department of Agriculture (USDA) Soil Climate Analysis Network (SCAN) (Schaefer et al. 2007) are used to evaluate the simulations. The SCAN soil moisture data are collected by dielectric constant measuring devices at five different depths: 5 cm, 10 cm, 20 cm, 50 cm and 100 cm. The monthly top 1-m SCAN soil water content are integrated for each observation site and compared with the 1-m soil water integrated from the top three model soil layers (i.e., 5 cm, 25 cm, 70 cm) in Noah-MP. Due to measurement maintenance and data

quality control issue, data from many stations are missing in various time, thus we calculated the ratio between available data (in monthly interval) and total period of simulation (from 2000 Oct to 2013 Sep) as the data availability. Figure 1b shows the locations of SCAN soil moisture measurement and their data availability within our simulation period.

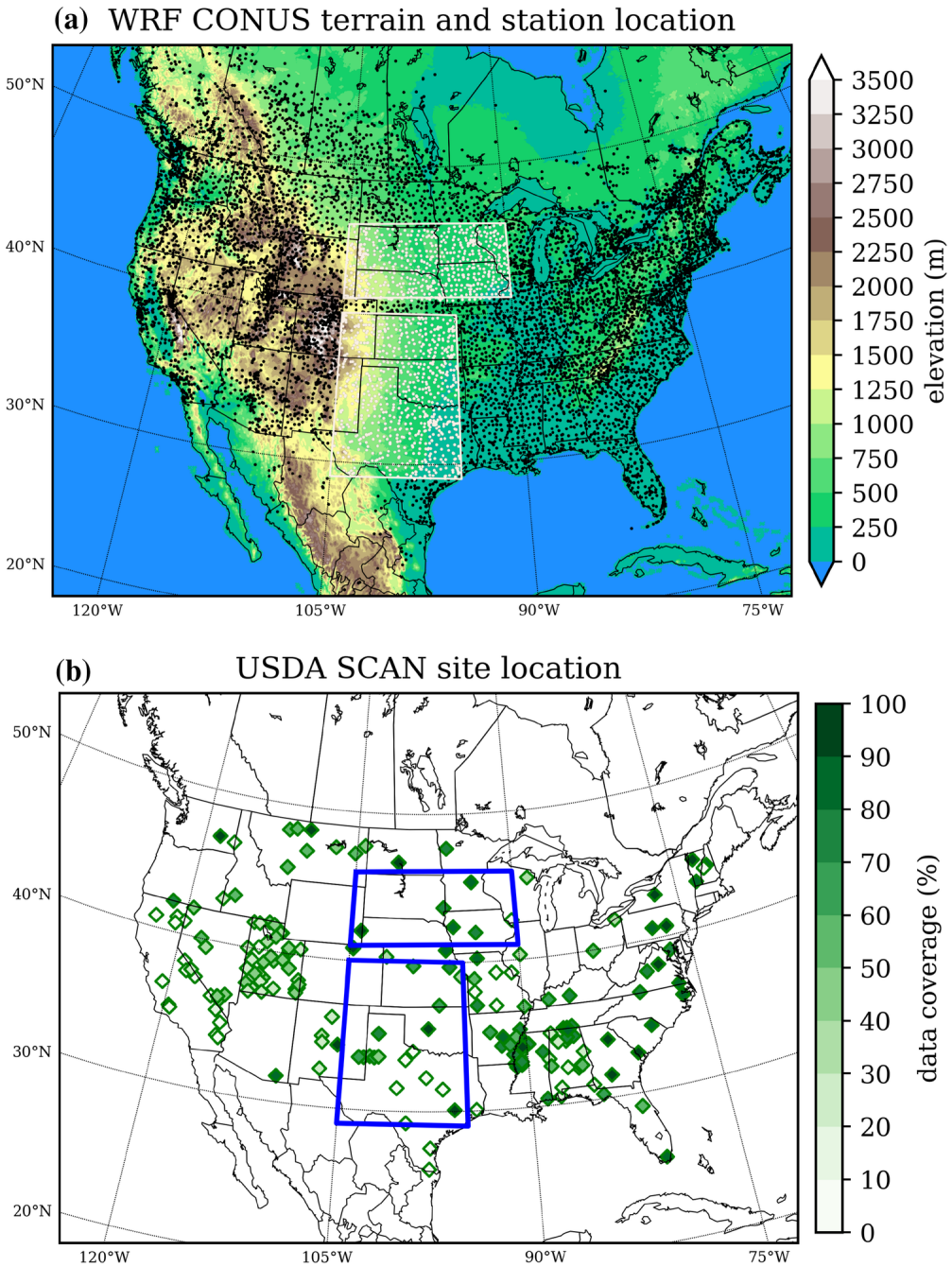

Figure 2.1. **a** WRF model domain (5440 km × 4064 km) at 4 km grid spacing showing topographic elevation in meters. Black dots are the locations of observational stations of GHCN meteorological network (9877 within model domain). Stations within the white boxes are located in Midwest and South Great Plains and are selected for the regional study. **b** Locations of soil moisture measurement from SCAN (185 within model domain) and their data availability within our simulated period.

To compare with observations from both SCAN and meteorological stations, the closest model grid points to the station locations are extracted. The fine grid spacing of the convection-permitting WRF model and the dense observational network together allow the grid-to-station comparison between WRF model grid points and observational stations. In the following text, the analysis and variables derived from observation (including SCAN soil moisture and calculated temperature and soil moisture index) and WRF model are denoted as OBS and WRF, respectively.

2.2.3 HW indices

In this study, we apply the HW definition by Perkins and Alexander (2013), in which heatwave is defined as a consecutive period of extreme high temperature upon a statistically based threshold. In their definition, the threshold is the 90th percentile of daily Tmax for each calendar day in a year, TX90. This threshold is calculated based on a 15-day moving window, which is centered on the day in question, in order to account for seasonal cycle and obtain sufficient sample size for a realistic percentile value. The HW event is defined as three or more consecutive days when daily Tmax exceeds the TX90 threshold. Based on this definition, two HW indices, frequency and magnitude, are defined: HWF (heatwave frequency) is the number of days qualified as HWs and HWM (heatwave magnitude) is the mean daily Tmax during the HWs. For assessing soil moisture impacts on summer HWs, we calculated the TX90 threshold for each day in June–July–August (JJA) for the whole 13-year simulation period (during 2000 and 2013). Therefore, the two HW indices are obtained for these three months separately, in total 39 samples in 13 years.

2.2.4 Soil moisture indices

Because of the uncertainties inherent to long-term gridded soil moisture data, many studies have used different indices to estimate soil moisture deficit (Dai 2011; Hirschi et al. 2011; Muller and; Seneviratne 2012; Quesade et al. 2012). In this study, two hydro-meteorological indices were evaluated for model simulation and observational networks, including the soil moisture anomaly (SMA) and the standardized precipitation evapotranspiration index (SPEI).

The SMA describes the deviation of soil moisture in a period of a year to the soil moisture climatology and normalized by the standard deviation of soil moisture over the same period. In this study, the monthly top 1-m SMA is calculated from both the SCAN measurements and the closest grid points in WRF model, following the method of Orlowsky and Seneviratne (2013):

$$SMA = \frac{(\bar{\theta} - \mu)}{\sigma} \qquad (2.1)$$

where θ is monthly-averaged top 1-m soil water content, μ and σ are the mean and standard deviation of top 1-m soil moisture of the same months over the 13-year study period.

As shown in Fig. 1b, there are limited number of soil moisture measurements from SCAN network within the contiguous US domain. Only 185 stations have long term soil moisture measurement, while 9877 stations have temperature and precipitation observations. In order to get better coverage of soil moisture estimate, we used the SPEI index by Vicente-Serrano et al. (2009) to estimate the soil moisture anomaly in spring. The SPEI is based on precipitation and temperature data to calculate the accumulation of water deficit/surplus, precipitation minus potential evapotranspiration (P-PET), for a selected time period. Mathematically, the SPEI is similar to the SPI, but it also includes the effect of temperature variability on soil moisture deficit. The procedure proposed by (Vicente-Serrano et al. 2009) was used to estimate potential evapotranspiration by Thornthwaite's method (Thornthwaite 1948). And the P-PET series is fitted to a 3-parameter Pearson III distribution at each station to obtain the SPEI for both station observation and the WRF model. Here, the analysis focuses on the SPEI calculated on 3-month timescale (SPEI-3) to represent the seasonal soil moisture anomalies in spring. The values of SPEI represents the standard deviation from the mean state (0), where SPEI values larger/smaller than 0.5/– 0.5 represent abnormal wet/dry conditions.

2.2.5 Methodology

The analysis was conducted locally for each individual station and model grid point. For the evaluation of WRF simulation against observation, the model grid points that are closest to station locations were extracted. In this study, the relationship between two HW indices from the three summer months (June–July–August, JJA) and the spring soil moisture from preceding months (based on the 3-month SPEI described in Sect. 2.4), for the year 2000–2013. We applied three types of analysis on the monthly HW indices and soil moisture estimate.

First, the WRF model performance on simulating summer HW indices and soil moisture proxies were evaluated against meteorological station data and SCAN soil moisture measurements. For temperature evaluation, the model simulated TX90 threshold and HWF, HWM indices are compared to those derived from observation for the summer months (JJA). For the evaluation of model simulated soil moisture indices, the monthly SMA and the SPEI-3 timeseries are calculated from model output and compared with observation data from the SCAN.

Second, the HW indices for each summer month are related to their antecedent 3 months SPEI by calculating the Pearson correlation coefficient. The purpose of calculating correlation coefficient is to identify strong and significant correlated regions, as well as to evaluate model performance across the domain. Based on the correlation coefficient results, regions with strong coupling between land and atmosphere can be identified.

Third, a quantile regression analysis was conducted to understand how soil moisture deficits impact the two HW indices. The ordinary linear regression shows the relation between the mean of the dependent variable y to the independent variable x. Quantile regression examines how different parts of the distribution of a dependent variable y respond to an independent variable x, based on the quantiles of choice. Special interests were focused on two regions, Midwest and South Great Plains, where two exceptional HWs had occurred in the last decade. The quantile regression of HW indices against antecedent SPEI are calculated for these two regions, and their regression slopes for each quantile are evaluated between the simulations and observations.

2.3 Results

2.3.1 Evaluation of WRF-simulated heatwave and soil moisture indices

The JJA seasonal averaged daily TX90 threshold from observation, WRF and their difference (model minus observation) are shown in Fig. 2. TX90 varies greatly across the contiguous US, with the hottest region in the Southwest desert area in Arizona exceeding 44 °C. Another extraordinarily hot region is located east of the Rocky Mountains in the South Great Plains, including Texas, Oklahoma, Kansas, Louisiana and Mississippi, with the threshold temperature higher than 40 °C.

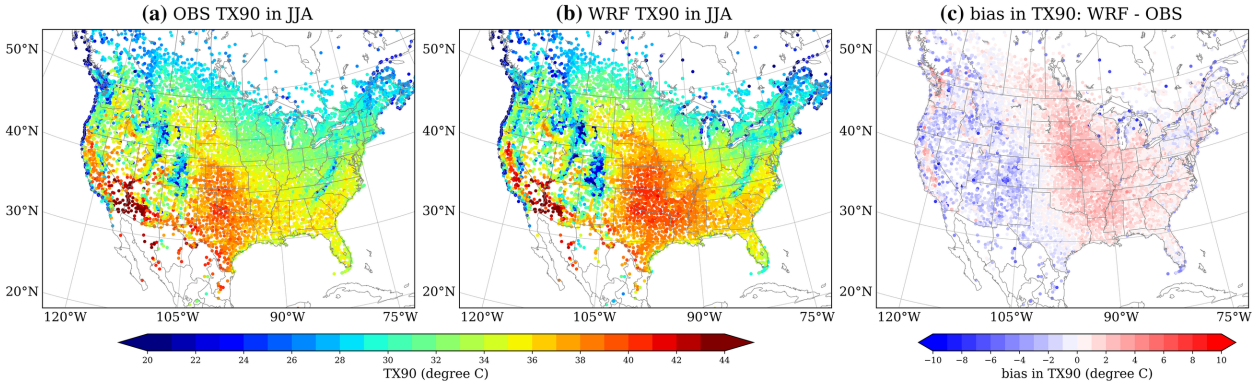

Figure 2.2. JJA-averaged daily TX90 threshold temperature calculated for **a** station, **b** WRF model, and **c** model bias (WRF-OBS) for the summers of 2000–2013.

The WRF simulation accurately captures the spatial pattern of the TX90 threshold, with two hot regions aforementioned and one cold region in the North and mountainous area. Figure 2.2c shows the difference of TX90 between WRF and observation, revealing a warm bias pattern straddled along the western edge of the Great Plains. For many global and regional climate model (Ma et al. 2014; Whan and Zwiers 2016), the summer warm bias is a common issue in near-surface temperature simulation over central North America for both mean and maximum temperature. The highest warm bias is about 3–4 °C in the Midwest and North Great Plains, mostly in Iowa, Nebraska, Minnesota and South Dakota. A noticeable cold bias of about 2–3 °C appears in the mountainous and valley regions west of the Rocky Mountains.

HWF characterizes the average number of HW days in a month, which is well simulated in WRF (Figure 2.3b). However, WRF underestimates the spatial extent of the number of days contributing to HWF in the Midwest, Ohio Valley, Mississippi Basin, East Coast, and around the Great Basin.

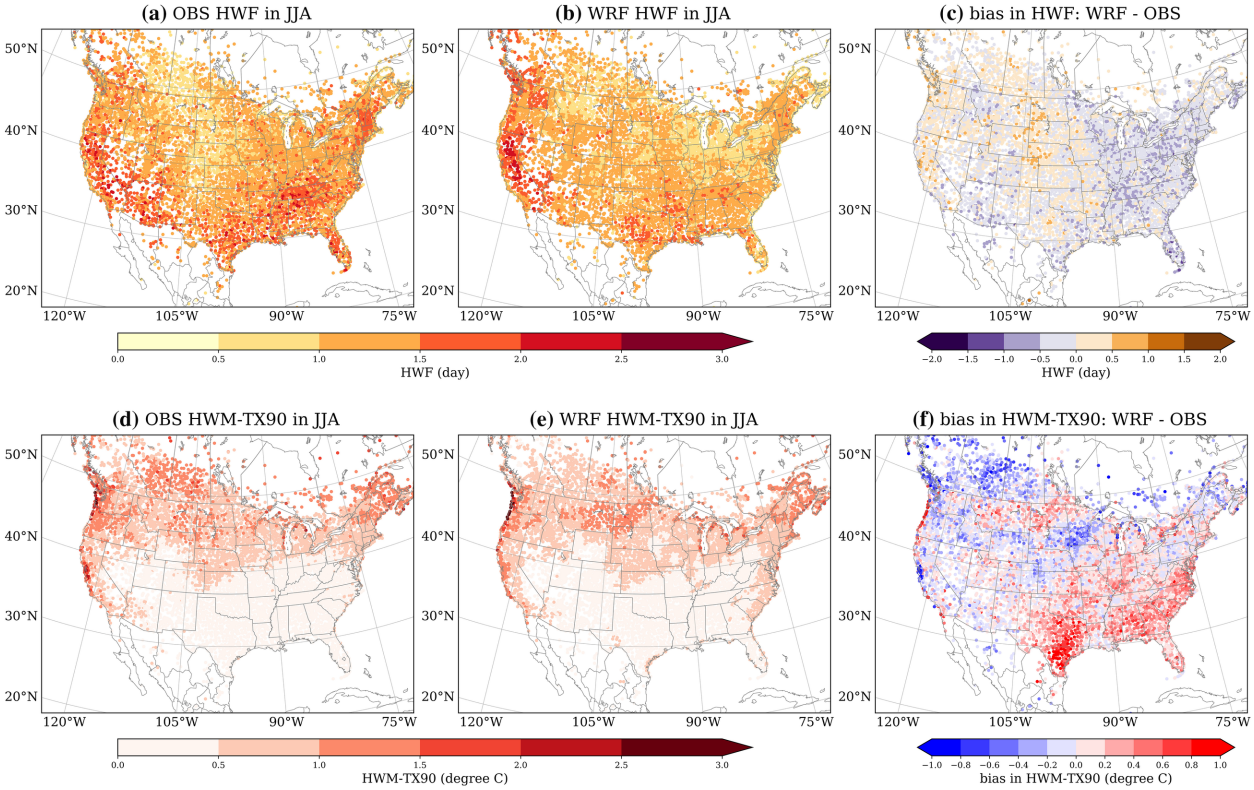

Figure 2.3. Same as Figure 2.2 but for HWF (a–c) and (HWM-TX90) (d–f).

The HWM is an index depicting the average magnitude of daily Tmax among HW days, which is identified based on the threshold temperature TX90. We show the HWM minus the TX90 threshold (HWM – TX90) in Figure 2.3d–f. (HWM – TX90) can also be considered as an indicator of the variability of daily Tmax beyond its 90th percentile threshold. Both observations and WRF (Figure 2.3d, e) show a larger magnitude ($\geq$ 2 °C) in the northern part of domain (north of 40 N), and near both east and west coast in daily Tmax. But in the southern part of the domain, the departure of HWM to TX90 are generally small. This may imply a heavier tail in the distribution of daily Tmax for the northern part than the southern part of the domain. The WRF model captured correctly this feature with small difference (less than ± 1 °C). Overall, the HW threshold and HW simulated by the WRF CONUS simulation are reasonable in representing the observations and can be trusted in further analysis.

Table 2.1 Pearson correlation coefficient between monthly timeseries of soil moisture anomaly and SPEI-3, from both observation and WRF model in two regions (MW and SGP)

Region	SMA_obs vs SMA_wrf	SMA_obs vs SPEI_obs	SPEI_obs vs SPEI_wrf	SMA_wrf vs SPEI_wrf
MW	0.706	0.546	0.905	0.762
SGP	0.692	0.716	0.965	0.826

For soil moisture evaluation, the simulated top 1-m soil moisture anomaly from WRF model is compared with the SCAN measurement. The timeseries of monthly soil moisture anomaly for two selected regions (MW and SGP) are shown in Figure 2.4. Since determining if the SPEI can represent soil moisture anomaly is of interest in these two regions, the SPEI-3 calculated for each month using meteorological data and WRF simulation are shown in dashed lines. The Pearson correlation coefficients between two soil moisture proxies, SMA and SPEI-3, from observation

(OBS) and WRF model are shown in Table 2.1, with bold numbers indicating statistical significance ($p < 0.01$). In general, WRF model well captured the temporal variability of soil moisture anomaly accurately in both regions, with high correlation and statistical significance. SPEI is a good indicator for soil moisture anomaly, with higher correlation in SGP than in MW. The SPEI-3 derived from WRF model in both regions are in good agreement with that from observation, thus it is reasonable to use SPEI-3 as a soil moisture indicator and WRF model has accurately simulated this index.

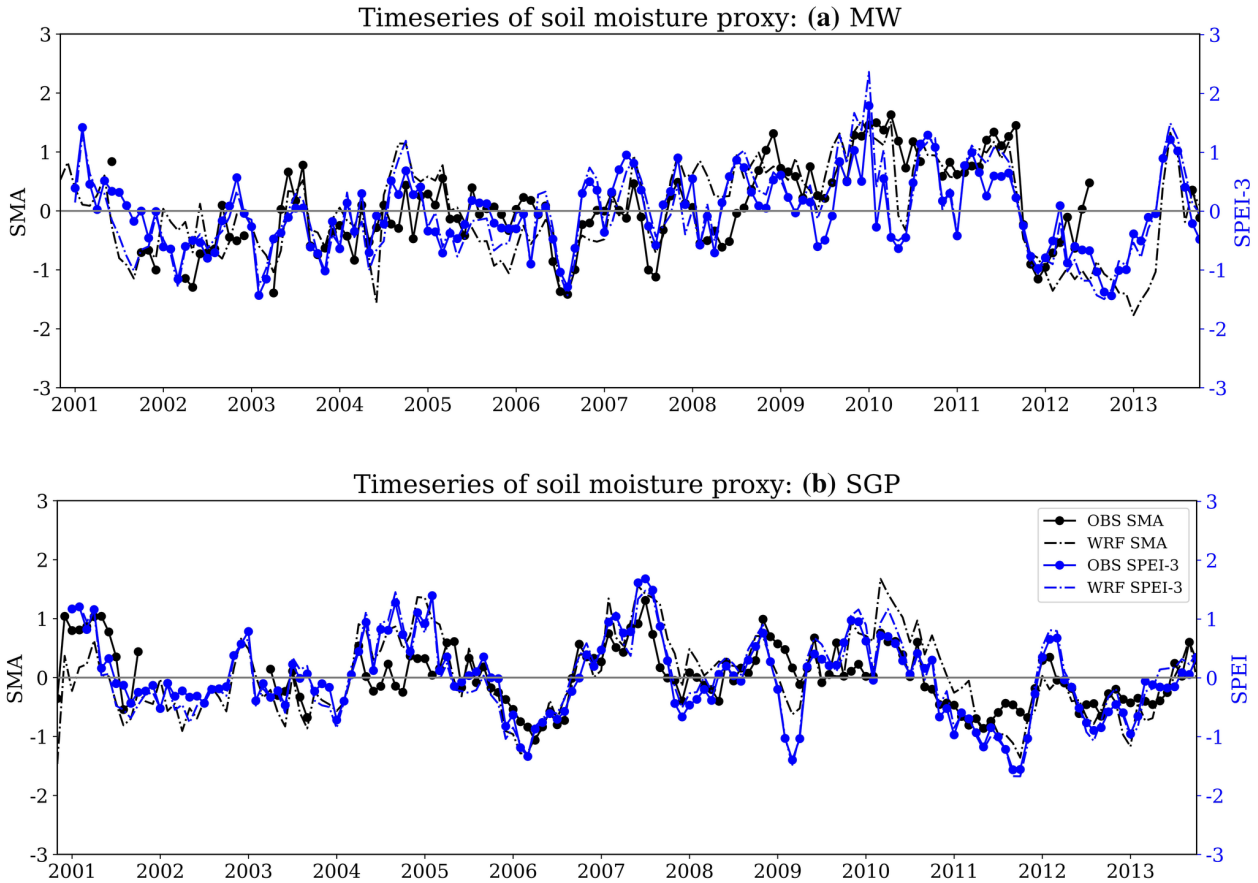

Figure 2.4. Monthly soil moisture anomaly and SPEI-3 in selected two regions **a** in MW, and **b** in SGP. Solid dotted lines are from observational results, and dashed lines are from WRF model; black lines are for soil moisture anomaly and blue lines are for SPEI-3 index

2.3.2 Correlation between heatwaves and antecedent soil moisture

To determine the statistical relationship between antecedent soil moisture represented by SPEI-3 and the HW indices used in this study, we calculated their Pearson correlation coefficients over the 13-year period (Figure 2.5). Significant anti-correlations with SPEI-3 exist for both HWF and HWM ($p < 0.01$) and appear in most regions in the continent, except for the Southwest region of the Pacific coast. The significant regions in HWM are generally further east compared to those in HWF, both in the observation and WRF. These anti-correlations suggest dry (wet) springs are associated with more (less) HW days and higher (lower) HW temperature in summer months.

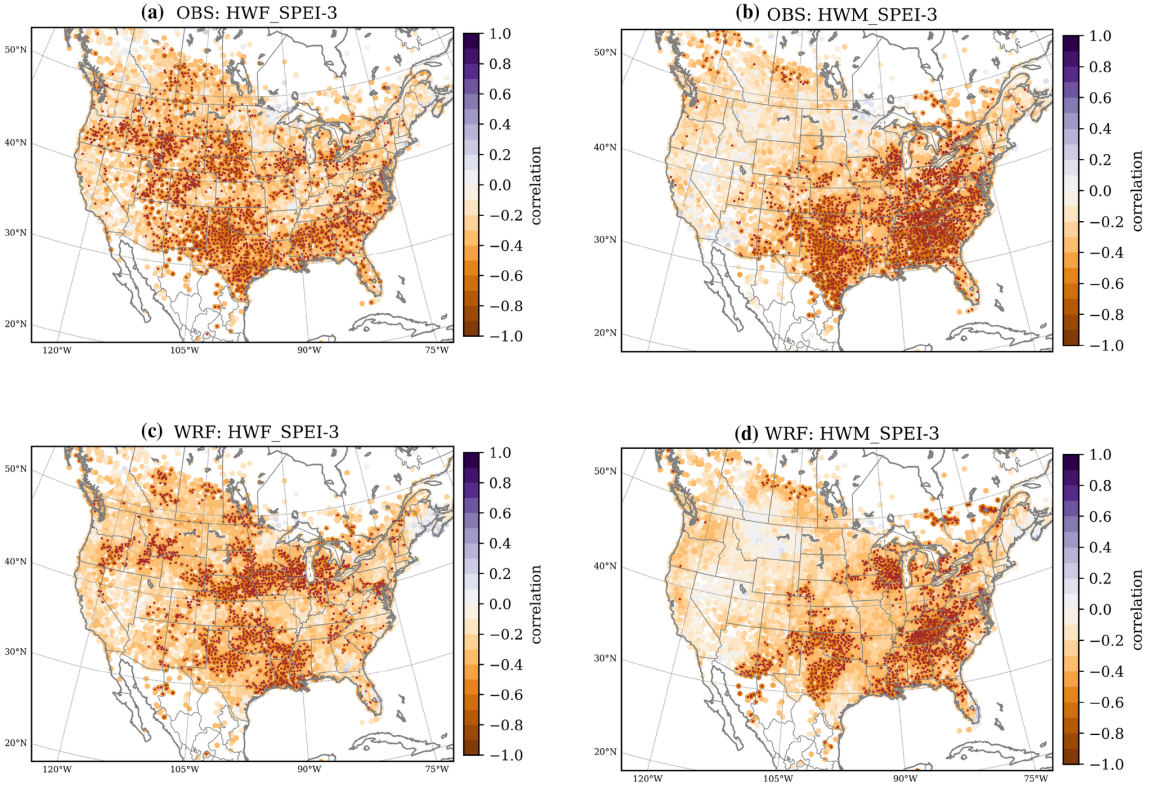

Figure 2.5. Pearson's correlation coefficient between SPEI-3 and HWF (a, c) and HWM (b, d), from observation (a, b) and WRF model (c, d). Highlighted stations/grid points indicate significant correlations at the 99% confidence level

The WRF model accurately captures these significant anti-correlations between antecedent soil moisture and summer heatwaves in most regions, including the South Great Plains (North Texas, Oklahoma, Kansas, Nebraska), Midwest (Wisconsin, Illinois, Iowa, Minnesota) and Gulf Coast (Louisiana, Arkansas, Mississippi). The WRF simulation shows less areas with statistical significance in the Canadian Prairies and Central US and more significant in Michigan ($p < 0.01$). These regions with significant anti-correlations resemble the land–atmosphere coupling "hot spots" in previous studies (Koster et al. 2004, 2006; Guo et al. 2006). In these regions the antecedent soil moisture has strong influence on both frequency and magnitude of HWs and, thus, may possess some predictability for HWs, especially in the Midwest, South Great Plains, and Gulf Coast.

2.3.3 Quantile regression analysis

The purpose of introducing quantile regression is to show how antecedent soil moisture impacts on the two HW indices varies across different quantiles. The regression slope of antecedent soil moisture (expressed as SPEI-3) and HW indices represents the differences in the effects of soil moisture at various quantiles. Figure 2.6 and 2.7 show the spatial distribution of regression slopes for three quantiles (0.1, 0.5 and 0.9 for low, median and high quantile) of HWF and HWM against antecedent soil moisture (SPEI-3) for both observation (a–c) and WRF (d–f). The impacts of soil moisture deficits on HWF become stronger from the lower to the upper end of HWF distribution (Figure 2.6a–c) and are prominently negative for 0.9 quantile (Figure 2.6c, f). For the lower quantile (Figure 2.6a, d) the regression slopes are close to zero across the domain. For the higher quantile (Figure 2.6c, f), the strongest impacts of antecedent soil moisture on HWF are in the Midwest, South Great Plains and along the Gulf Coast, where significant anti-correlations are shown in Figure 2.5a, c too. These results show that antecedent soil moisture has strong impacts on HWF, especially on the higher quantile, and can be used as a predictive index in these regions.

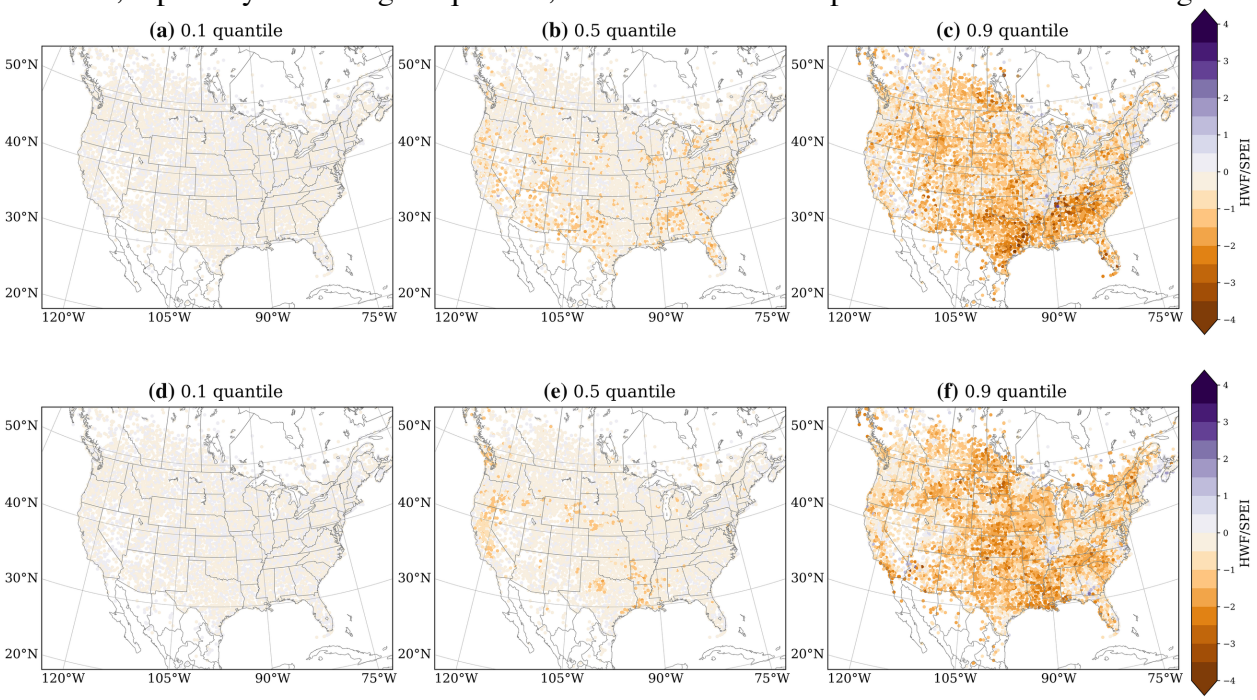

Figure 2.6. Quantile regression slope between SPEI-3 and HWF at three quantiles, 0.1, 0.5 and 0.9, for low, median and high quantiles in OBS (a–c) and WRF (d–f)

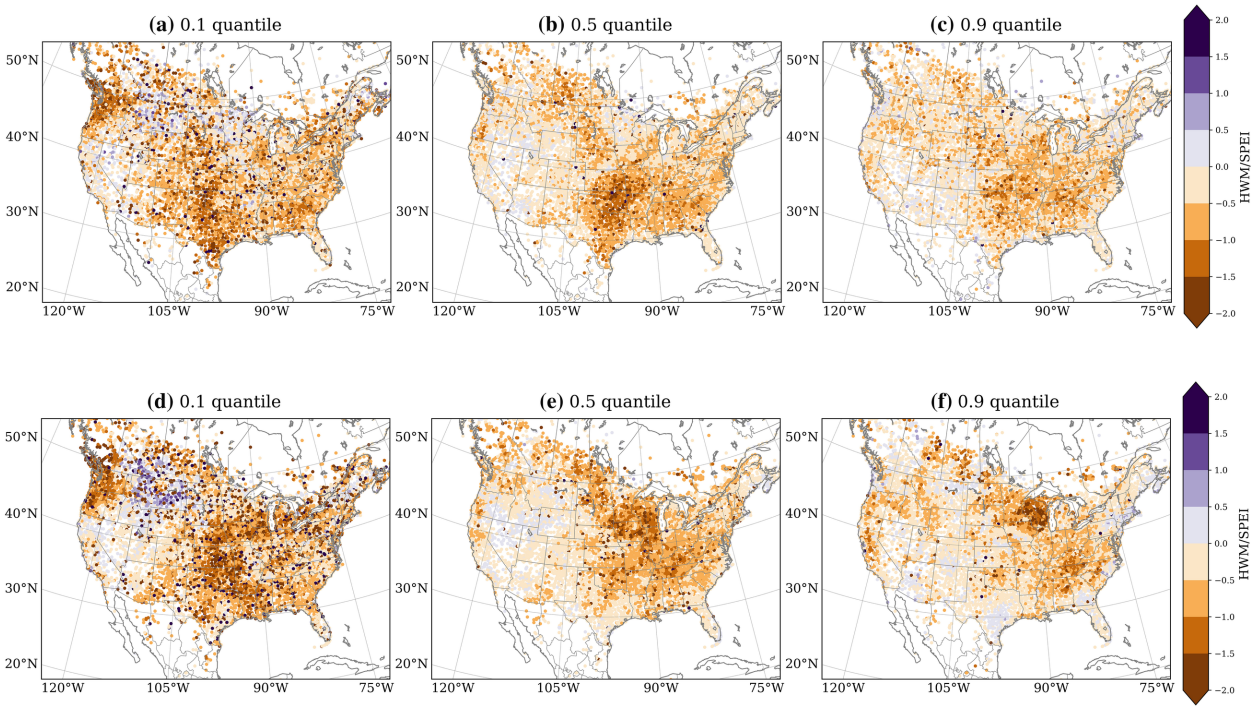

Figure 2.7. Same as Figure 2.6, but for quantile regression slope between SPEI-3 and HWM in OBS (a–c) and WRF (d–f).

Unlike HWF, HWM exhibits strong relationships with antecedent soil moisture in the low quantile, which is most obvious in the South Great Plains and Pacific Northwest. It implies that antecedent soil moisture has a stronger impact on the low quantile HWM than the high quantile in these regions. The strong impacts of antecedent soil moisture on low HWM are accurately simulated in SGP region in WRF compared to that of the observations. However, antecedent soil moisture impacts on the higher quantiles (0.5 and 0.9 quantile) are underestimated. Quantile regression slopes in this region become smaller in WRF simulation than in the observations. There are also some regions, where strong relationship between SPEI-3 and HWM in all quantiles is seen, for example in the MW region. The correlation becomes even stronger towards the high quantiles. Conversely, the WRF model simulate stronger impacts of antecedent soil moisture for the high quantiles than the observations in the MW region.

The heatwave indices in two regions, Midwest (MW) and South Great Plains (SGP), are analyzed further. For these two regions, the scatter plots of both HWF and HWM against SPEI-3 derived from observation and WRF simulation are shown in Figure 2.8. The regression lines for five different quantiles (0.1, 0.3, 0.5, 0.7, 0.9) are overlaid with different colors. For HWF (Figure 2.8a, c), for both regions, observations show a decreasing trend of regression slopes towards higher quantile with the slope values becoming more negative, which suggests a stronger impact of antecedent soil moisture on high HWF occurrence.

But for HWM, the scatter plots and quantile regression for these two regions show different features. In MW (Figure 2.8c, d), although the trends of five regression lines are not as clear as that of HWF, it does show stronger impacts (with steeper slope) of antecedent soil moisture on high quantile (Figure 2.8c) in both the WRF simulation and observation. On the contrary, in SGP, the regression

slopes are flat for the 0.9 quantile and steep for the 0.1 quantile, indicating stronger impacts of soil moisture on lower quantiles (less negative) as shown in Figure 2.8d.

The difference in HWM responses at various quantiles in two regions can be attributed to their different evaporation or soil moisture regimes (Schwingshackl et al. 2017). MW belongs to transitional-to-wet or transitional-to-energy limited evaporation regime. Summer precipitation amount is close to its potential evapotranspiration, so the region relies on moisture storage from last spring and winter as well as moisture input from current summer (Quiring and Kluver 2009). Thus, the occurrence and intensity of summer heatwaves rely on its antecedent soil moisture and summer weather condition. The dependence becomes even stronger for the high quantile of HWF and HWM. But SGP belongs to dry-to-transitional or soil moisture limited-to-transitional evaporation regime. Summer potential evapotranspiration is much stronger than precipitation. Summer convective weather in this region is more related to the moisture input, which is usually associated with the low-level jet as part of North Atlantic Subtropical High (NASH) that brings moisture from Gulf of Mexico but is less related to antecedent moisture storage in the soil. Thus, the high intensity heatwave events are more a response to summer weather condition than to antecedent soil moisture condition. Nonetheless, all three drivers including the summer weather conditions, antecedent low soil moisture and anomalous SSTs induced by climate variability will contribute to the occurrence of intensive HW events in SGP (Hoerling et al. 2013).

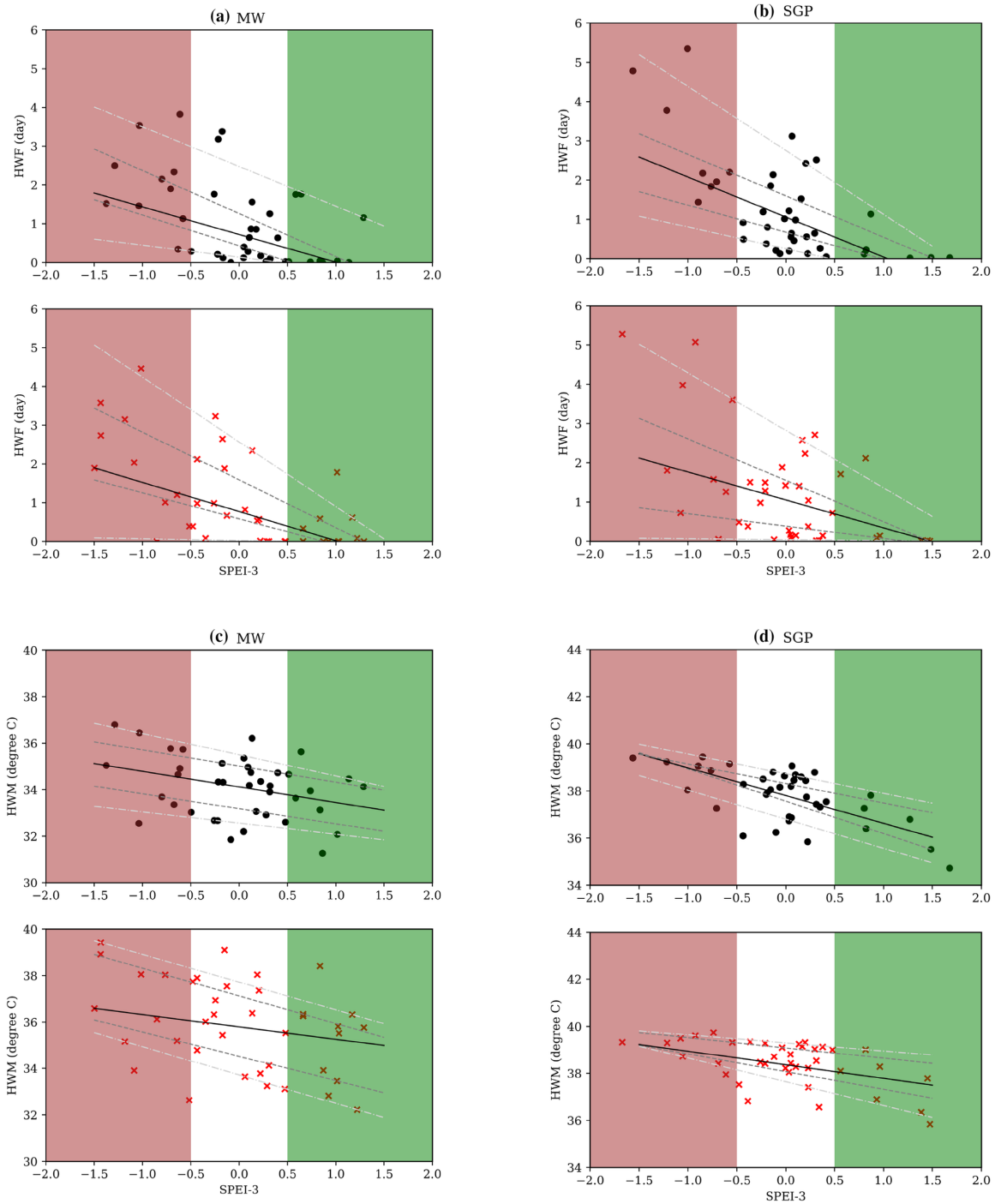

Figure 2.8. Scatter plots of monthly HWF (a, b) and HWM (c, d) against SPEI-3 from high-density observation (top) and from WRF simulation (bottom), based on stations/grid points averaged values for Midwest (MW) (a, c) and South Great Plains (SGP) (b, d). Regression lines for five different quantiles (0.1, 0.3, 0.5, 0.7 and 0.9) are shown with different colors. SPEI value larger (less) than 0.5 (− 0.5) are shaded in green (brown) to distinguish abnormal wet (dry) condition.

To evaluate WRF model performance, the quantile regression slope between antecedent soil moisture and HWF/HWM were calculated from both observations and WRF simulation. Figure 2.9 shows the regression slopes of 9 quantiles for both HWF and HWM in MW and SGP, with the shaded area representing the 95% confidence interval. The decreasing trends (slopes getting more

negative for higher quantile) of HWF and SPEI-3 in both regions are accurately simulated by WRF, except for high (low) quantiles in MW (SGP), where the WRF model overestimated (underestimated) the effect of antecedent soil moisture. For HWM, the decreasing trend in MW is not as obvious as that in SGP, given a large spread in the confidence interval; and an overestimation (underestimation) of the effects of antecedent soil moisture in MW (SGP) is shown for almost all quantiles. These two features are consistent with the spatial distribution of slopes shown in Figure 2.7c–f.

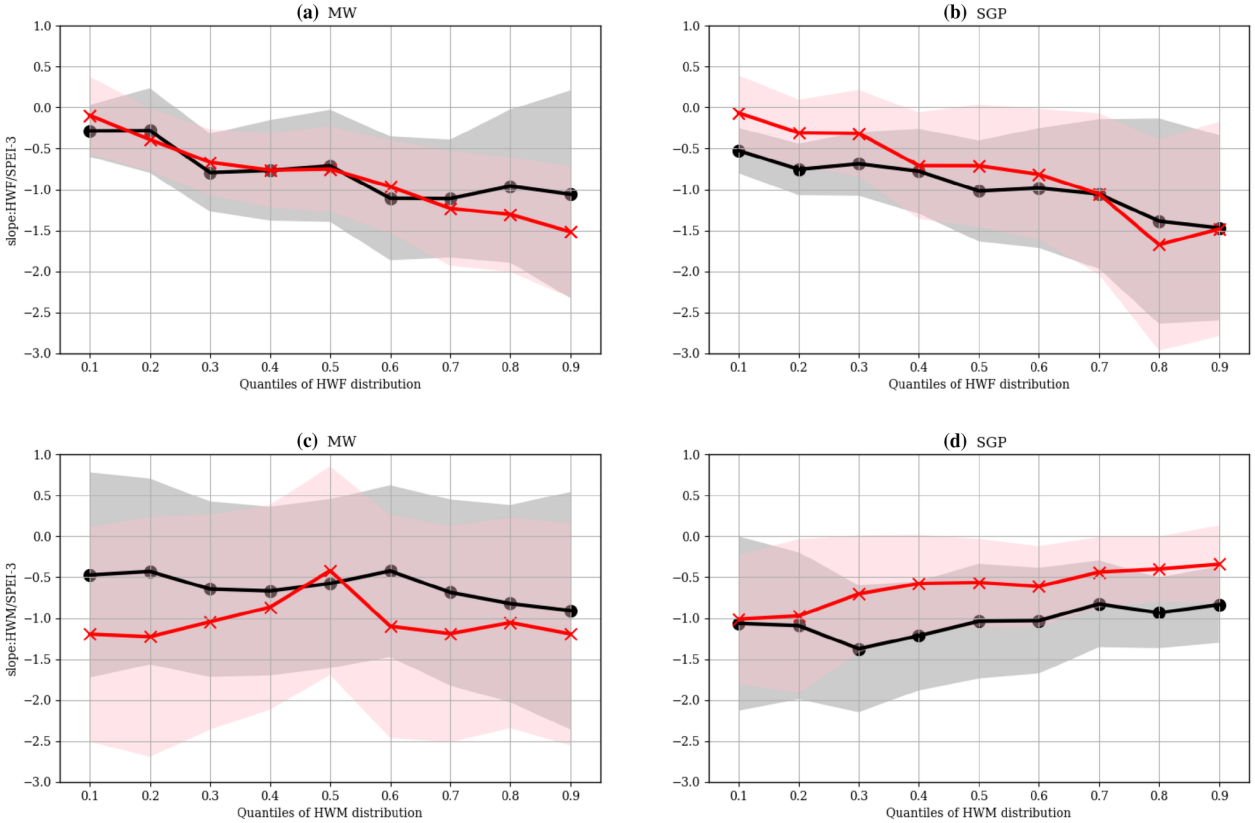

Figure 2.9. Quantile regression slopes of the 0.1–0.9 quantiles for HWF (a, b) and HWM (c, d) in relation to SPEI-3 for the two regions (a, c: MW, b, d: SGW), for both OBS (black dot) and WRF (red cross). The shaded areas are the 95% confidence interval for quantile regression slopes for each given quantile.

2.4 Discussion

Multiple physical drivers exist behind heatwaves and the contribution of each driver may vary across events and regions. In a recent review paper on heatwaves by Perkins (2015), the physical drivers of HWs are summarized in three main categories: synoptic condition, soil moisture and land surface interaction, and climate variability. Our study focuses on the impacts of antecedent soil moisture on HWs through soil moisture-temperature feedback. The results show that the feedback is stronger in a transitional regime, while its manifestation requires interacting with other drivers.

For example, soil moisture variation shows little impacts on low quantile HWF in two focus regions, suggesting synoptic conditions may be more important for regions with insufficient surface energy, which would prohibit evapotranspiration regardless soil moisture condition (Li et al. 2018) (Figure. 2.6a, d, 2.8a, b). But for high quantile HWF, which are likely associated with anticyclonic static synoptic condition, antecedent soil moisture becomes a critical driver, amplifying the soil moisture feedback after dry spring but suppressing it when spring wet. This result about HWF is consistent with other studies using observational data from Europe and the globe (Hirschi et al. 2011; Herold et al. 2016; Mueller and Seneviratne 2012).

On the other hand, the quantile regression between SPEI-3 and HWM show different results. In SGP, where antecedent soil moisture has stronger impacts on low quantile HWM (Figure 2.8d), the result is similar to a quantile regression study conducted for North and East part of Australia (Herold et al. 2016), which is also in dry regime in summer. However, in MW the antecedent soil moisture shows strong impacts on HWM in all quantiles (Figure 2.8c), suggesting antecedent soil moisture is very important for HWM in this region.

Furthermore, the asymmetric response of HWF/HWM to antecedent soil moisture for different quantiles suggests potential predictive skill based on antecedent soil moisture condition, especially for high quantile of HWF in both focus regions and low quantile of HWM in SGP. This is described as “asymmetric predictability” by Quesada et al. (2012), who found that the occurrence of summer extreme heat events is more sensitive to certain weather regime after dry winter/spring compared to a wet season. Our results extend the conclusion to the magnitude of summer heatwaves, which depends more on synoptic weather systems in SGP under wet soil condition, while the predictive skill of high HWM with dry soil is always high.

The different responses of HWM on different quantiles to antecedent soil moisture in these two regions (MW and SGP) could be explained by their different evaporation regimes and weather regimes in summer (Figure 2.8c, d). In the summer in SGP, evaporation is moisture-limited and the synoptic conditions are largely dependent on the activities of the static anticyclonic high pressure systems North Atlantic Subtropical High, which brings moisture from Gulf of Mexico. Thus, antecedent soil moisture has stronger influence on low quantile of HWM, while synoptic conditions are a more dominant factor for the high quantile of HWM. On the contrary, summer precipitation in the MW depends largely on antecedent rainfall/snowfall in previous spring/winter. In this region, the moisture recycling through soil moisture-precipitation feedback (Li et al. 2017) confirms that it is in energy-limited-to-transitional regime. That explains why antecedent soil moisture is important for all quantiles of HWM (Figure 2.8c), and a strengthening trend is observed towards higher quantiles (Figure 2.9c).

In the relationship between antecedent soil moisture and summer HW indices, the biggest differences between WRF simulation and observation found in Figures 2.6, 2.7, 2.8 and 2.9 could be explained by warm temperature bias and dry precipitation bias in both regions (Liu et al. 2017). In the MW, where summer precipitation relies on local moisture recycling, less precipitation and higher summer temperature introduce dry bias in soil moisture, higher evaporation demand further desiccating soil under the dry condition. This over-coupling between land and atmosphere contributes to a systematic overestimation of the impact of antecedent soil moisture on HWM in the MW (Figures 2.7e, f, 2.9c). On the other hand, the warm bias and dry bias in SGP is more related to the activities of NASH, which is the dominant factors for the summer weather in SGP. Thus, the contribution of antecedent soil moisture to HWM is underestimated with less negative slope value in Figures 2.7e, f and 2.9d.

Despite the warm and dry bias in the central US in summer have limited the model performance on HW magnitude, the WRF model accurately simulated the relationship between HW frequency and SPEI-3 in both regions. Other studies, comparing regional climate simulations with observations, found overestimation of the impacts of antecedent soil moisture deficits in wet regime (Hirschi et al. 2011). Our results showed reasonable estimation of soil moisture impacts on HW occurrence. This could be due to the improved representation of land surface properties in high-resolution model as well as the explicit simulation of convection in the model.

Although warm bias (3–4 °C) in daily maximum temperature exhibited in central US is a challenging issue in CPM simulation, our results showed considerable improvement in simulated precipitation compared to coarser-resolution non-convection-permitting regional climate model in North America (Whan and Zwiers 2016). In addition, efforts in the Hydrometeorology Applications Program group in NCAR/RAL are being undertaken to reduce the warm and dry biases in this region. This study showed a statistical approach of evaluating the relationship between antecedent soil moisture and temperature, which contributes to the knowledge of antecedent soil moisture's impacts on HW aspects, the asymmetric predictive skill towards HWF/HWM and the diagnosis of land–atmosphere coupling in regional climate models.

2.5 Conclusion

Antecedent soil moisture has significant impacts on summer heatwaves, as it can amplify the frequency and intensity of heatwaves. Thus, it is essential to understand the physical mechanism behind soil moisture and heatwaves and evaluate how this relationship is represented in current regional climate models. This study investigates the impacts of spring soil moisture on summer heatwaves from station observations and the WRF regional climate model in convection-permitting configuration (WRF CONUS). We started with evaluating the 90th percentile of the daily maximum temperature in June–July–August (JJA) and used it as the threshold for defining heatwave events (TX90). The SPEI-3 is used as a proxy for 3-month antecedent soil moisture as the supplement to meteorological station soil moisture measurement. The WRF model simulated the spatial patterns of a statistical threshold temperature (TX90) of heatwaves reasonably well, except for a 3–4 °C of warm bias in Midwest and 2–3 °C of cold bias in western mountainous regions. Despite the high temperature bias in central US in WRF CONUS, the frequency and magnitude of HWs are reasonably simulated by WRF CONUS compared to the observation, when using a statistical threshold to define HW events (TX90). A soil moisture proxy, SPEI-3, is then evaluated against in-situ soil moisture measurement and the results showed that SPEI-3 is a good indicator for monthly soil moisture anomaly.

The soil moisture-temperature feedback is represented by anti-correlations between antecedent soil moisture, the SPEI-3, and two HW indices, HWF and HWM across the domain. These strong anti-correlations are significant over many areas in the North America, including the Midwest, North and South Great Plains, South Coast as well as the Canadian Prairie. The spatial distribution of these strong coupling regions has been captured reasonably by the WRF model.

Quantile regression analysis shows that the impacts of antecedent soil moisture are asymmetric for the occurrence and magnitude of HWs. The quantile regression slopes represent the strength of the impact of soil moisture on HWF and HWM for different quantiles. For HWF, soil moisture has stronger impacts on the higher quantiles of the HWF, suggesting other have a larger effect in certain regions with sufficient surface energy, such as where anticyclonic synoptic conditions may play a dominant role. On the other hand, the asymmetric effect of soil moisture on HWM varies spatially. For two regions in interest, the Midwest (MW) and South Great Plains (SGP), the impacts of antecedent soil moisture are stronger for the lower quantile of HWM in SGP, while strong for all the quantiles in MW. This difference could be related to their different summer weather regimes - summer weather in SGP is highly impacted by large synoptic scale processes, while in MW it is largely depended on local feedback through moisture recycling of the antecedent rain/snowfall.

The asymmetric response of heatwave occurrence and magnitude to antecedent soil moisture (stronger for higher quantiles of HWF in both regions but for lower quantiles of HWM in SGP) provide important information for the improvement of their predictive skill, as it is confident that less heatwave events and lower heatwave temperatures will appear after a wet spring than a dry spring in two regions. In SGP, antecedent low soil moisture embedded higher predictability for high HWM while less predictability for high HWF.

The WRF model also represents well the regression slopes for HWF in most of the quantiles in both regions but overestimates the slopes for HWM in MW and underestimates the slopes in SGP. The warmer temperature and less precipitation bias in these two regions in summer led to increased

evaporative demands and further desiccated soil moisture, hence, strengthened local feedback in the MW. On the other hand, other processes might be responsible for underestimated land–atmosphere coupling in SGP, such as the activities of NASH. Overall, the WRF CONUS simulation is capable of capturing the soil moisture-temperature feedbacks in these two regions, which has strong connection in summer heatwaves.

The role of soil moisture in land–atmosphere interaction, particularly in heatwaves are complicated and need further analysis. Our study has important implications for land–atmosphere coupling research as well as heatwave monitoring and forecasting. Here we list a few non-exhaustive implications as well as our future research plan:

1. Predictive skill for agriculture activities: agriculture is very important but highly diverse in both regions, with the eastern part of MW and SGP mainly rain-fed crop but western part irrigated. Rain-fed crop production, in particular, is critically dependent on weather conditions in the warm season. Extreme temperature-induced heat stress can seriously affect crop production. These two regions are also major places for livestock production, including dairy and beef cattle, hogs and others, which are also sensitive to heatwaves.

2. Diagnosis on land–atmosphere coupling: the overestimation of soil moisture impacts on summer heatwaves in the MW regions, both seen in the high quantile of HWF and HWM, could be attributed to too strong land–atmosphere coupling. There have been many theories regarding the over-coupling issue, including too strong surface coupling due to out-of-date assumption on short vegetation in this region, which are mainly crop and grassland, which transport higher heat flux from the surface to the atmosphere, hence, intensifying the soil moisture-temperature feedback. (Chen et al. 1997; Chen and Zhang 2009). Another theory is related to lack of irrigation over this region in the land surface model, where irrigation water could be a significant input that increases soil moisture and evapotranspiration and cools the air (Huber et al. 2014). These are strong motivations and potentials for future land–atmosphere coupling studies.

3. High resolution convection permitting model: the initial motivation of performing high resolution regional climate modeling is its advantages in simulating convective precipitation. However, a recent study on the summer convection storms using the same model data showed less convection population simulated in the current climate than observation (Rasmussen et al. 2017). This result is connected to our findings here that a warm and dry bias in the Great Plain region amplify soil moisture-temperature feedback while suppress soil moisture-precipitation feedback. The diagnosis and improvement of land–atmosphere coupling in regional climate model can potentially benefit the performance of convection-permitting regional climate model.

4. Climate change impacts on land–atmosphere coupling: In the second part of the WRF CONUS simulation, a Pseudo Global Warming (PGW) method is applied to add a climate perturbation from RCP8.5 scenario to current climate, implying global warming. How global warming impacts on land–atmosphere coupling, particularly how soil moisture could impact heatwaves in future climate, could be an interesting research topic.

Heatwaves are extreme temperature events that has disastrous effects on human health and societies. Thus, it is important to understand the physical mechanism of soil moisture, and its interaction with

synoptic condition and climate variability and how they relate to HWs. This can provide useful information for heatwave forecast and mitigation approaches.

Key points for the next chapter

- Antecedent soil moisture plays an important role in influencing the regional climate through soil moisture-temperature feedback.
- Strong and significant anti-correlations between soil moisture anomalies and heatwave characteristics indicate that the North American Central Great Plains is a coupling of "hot spots" in land-atmosphere interactions.
- A consistent warm temperature bias and low soil moisture exist during summer in the central U.S., as exhibited in the CONUS WRF simulations.
- CONUS WRF simulations show a reliable capability for representing the relationship between the soil moisture anomaly and summer heatwave events.

Acknowledgments
The authors Zhe Zhang, Yanping Li, Zhenhua Li gratefully acknowledge the support from the Changing Cold Regions Network (CCRN) funded by the Natural Science and Engineering Research Council of Canada (NSERC), as well as the Global Water Future project and Global Institute of Water Security at University of Saskatchewan. Yanping Li acknowledge the support from NSERC Discovery Grant. Fei Chen, Michael Barlage appreciate the support from the Water System Program at the National Center for Atmospheric Research (NCAR), USDA NIFA Grants 2015-67003-23508 and 2015-67003-23460, and NSF Grant #1739705. NCAR is sponsored by the National Science Foundation. Any opinions, findings, conclusions or recommendations expressed in this publication are those of the authors and do not necessarily reflect the views of the National Science Foundation.

Chapter 3 – Irrigation improves crop yield through relieving soil water stress

This manuscript has been modified for inclusion in this thesis. It was originally published as:

Zhang, Z. Barlage, M., Chen, F., Li, Y., Helgason, W., Xu, X., Liu, X., Li, Z. Joint modeling of crop and irrigation in the Central United States using the Noah-MP land surface model. J. Adv. Model. Earth Syst. (2020) doi:10.1029/2020MS002159.

Author contributions: Z. Zhang, F. Chen and M. Barlage designed the study and wrote the paper. Y. Li, W. Helgason and Z. Li contributed to the interpretation of the results and reviewed the manuscript. X. Liu and X. Xu provided supports on model consultation and manuscript reviewing.

Keywords
Land surface model, Earth system model, crop irrigation, parameters, model uncertainties

Abstract
The representation of climate-crop interactions is critical to Earth system modeling. Despite recent progress in modeling dynamic crop growth and irrigation in land surface models (LSMs), transitioning these models from field to regional scales is still challenging. This study applies the Noah-MP LSM with dynamic crop-growth and irrigation schemes to jointly simulate the crop yield and irrigation amounts for corn and soybeans in the central United States. The model performance of crop yield and irrigation amounts are evaluated at the county-level against the USDA reports and USGS water withdrawal data, respectively. The bulk simulation (with uniform planting/harvesting management and no irrigation) produces significant biases in crop yield estimates for all planting regions, with root-mean-square-errors (RMSEs) being 28.1% and 28.4% for corn and soybean, respectively. Without an irrigation scheme, the crop yields in the irrigated regions are reduced due to water stress with RMSEs of 48.7% and 20.5%. Applying a dynamic irrigation scheme effectively improves crop yields in irrigated regions and reduces RMSEs to 22.3% and 16.8%. In rainfed regions, the model overestimates crop yields. Applying spatially varied planting and harvesting dates at state-level reduces crop yields and irrigation amount for both crops, especially in northern states. A "nitrogen-stressed" simulation is conducted and found that the improvement of irrigation on crop yields is limited when the crops are under nitrogen stress. Several uncertainties in modeling crop growth are identified, including yield-gap, planting date, rubisco capacity, and discrepancies between available data sets, pointing to future efforts to incorporating spatially varying crop parameters to better constrain crop growing seasons.

Motivation

In the previous chapter, I analyzed the impacts of antecedent soil moisture on extreme heatwave events in summer—an aspect of soil moisture-temperature feedback. In this chapter, I explore the importance of soil moisture in both biogeophysical and biogeochemical processes in large, extensive croplands in the central U.S. In addition, this chapter will describe the challenges and uncertainties involved in modeling dynamic crop growth and cropland land-atmosphere interactions.

This study also extends the investigation of two previous studies: Research by Liu et al. (2016), who developed the dynamic crop growth scheme in Noah-MP LSM for corn and soybeans, and a study by Xu et al. (2019), who focused on the transition of dynamic irrigation modeling from field to regional scales. These two studies built the foundation of this chapter and facilitated this research by establishing essential modeling parameters and datasets. In bringing these two contributions together as a joint simulation of crop growth and irrigation, this study investigates interactions with the land and atmosphere in croplands.

3.1 Introduction

The purpose of this chapter is to assess the benefits and uncertainties in joint crop-growth and irrigation modeling in the context of capturing climate-crop-irrigation interactions in Earth System Models (ESMs). It has been recognized that climate change and variability play a major role in crop production (Drewniak et al., 2013; Ray et al., 2015; Leng et al., 2016) from regional to global scales (Leng et al., 2016). Climate change has already impacted global agricultural production (Ray et al., 2019), and negative trends on crop yield per degree warming have been projected for major cultivars across the globe (National Research Council, 2011). In addition to mean climatic conditions, extreme climate events, such as drought and flooding, have also been emphasized as an important contributor to crop yield reduction (Hlavinka et al., 2009; Lobell et al., 2014).

Agriculture management activities such as irrigation and fertilization also play an essential role in increasing crop yields, especially in semi-arid climates and regions with strong seasonal variability of precipitation during crop reproductive stages (Grassini et al., 2009). Globally, ~20% of croplands are equipped for irrigation systems and contribute to ~40% of the world's food production (Siebert and Doll, 2010). Over the 55.8 million acres of irrigated U.S. farmland in 2012, 115 billion gallons of water was withdrawn for irrigation per day, accounting for more than one third of water-use nationwide in 2015 (Maupin et al., 2014; Dieter et al., 2018). Furthermore, climate change impacts on freshwater availability and groundwater over-exploitation are challenging for efficient water use in agriculture (Vorosmarty et al., 2000). Therefore, understanding the capability for freshwater to supply the world's major food production, such as in the U.S. Great Plain and Canadian Prairies, under climate change background, has become an overarching science goal in the Global Energy and Water Exchanges project (GEWEX, Grand Challenge on Water for the Food Baskets of the World: https://www.gewex.org/about/science/wcrps-grand-challenges/water-for-the-food-baskets-of-the-world/).

In addition, agricultural management modifies surface water and energy balances, alters characteristics of land-atmosphere interactions, and hence impacts local and regional climate (Pielke et al., 2007). Furthermore, irrigation practices add additional water to eliminate water stress,

which in turn increases humidity and decreases air temperature (Chen et al., 2018; Xu et al., 2019). This irrigation-cooling effect has shown to not only modify the local environment and regional precipitation but also to reduce the chance of extreme heatwaves in the U.S. (Lu et al., 2015) and globally (Thiery et al., 2017).

To better understand the climate change, crop yield, and freshwater nexus, as well as critical cropland-atmosphere interactions, it is important and necessary to improve the representation of dynamic crop growth and irrigation in ESMs. Recent efforts have been dedicated to integrating crop growth dynamics and agricultural management into land surface models (LSM) within ESMs (Levis et al., 2012; Drewniak et al., 2013; Liu et al., 2016; Leng et al. 2016; McDermid et al., 2016). For instance, crop growth models were introduced into the Community Land Model version 4 with carbon-nitrogen cycle (CLM4CN) by Levis et al. (2012), which focused on the crop coverage in mid-latitude regions. The results showed improvement on simulating leaf area index (LAI), an index for crop growth, and summer precipitation, compared to the default setting of CLM4.5. This work also highlights the importance of accurate representation of the cropping calendar, as a "late-planting" sensitivity test improved the simulated annual cycle of net ecosystem exchange (NEE) in midwestern North America. More recently, a dynamic crop growth model was incorporated into the Noah with multiple-physics (Noah-MP, Niu et al. 2011) model and tested for two field sites in Illinois and Nebraska for corn and soybean (Liu et al., 2016). In Noah-MP-Crop, crop growth stages are solely dependent on growing degree days (GDD). The Noah-MP-Crop model improved the simulation of surface energy balance and LAI and provided reasonable estimates of biomass. While these works demonstrated widespread potential for agriculture-climate interactions in some key agroecology regions, it is still challenging to accurately represent crop-climate-hydrology interactions in general and specifically the spatial variations of crop-model parameters across various scales.

Similarly, irrigation parameterizations have been incorporated into various LSMs using the "soil moisture deficit" approach. For example, Ozdonga et al. (2010) used the soil field capacity as a threshold, below which irrigation is triggered, and calculated the irrigation demand from subtracting current root-zone soil moisture from field capacity. Lawston et al. (2015) applied this soil moisture deficit approach in the coupled Weather Research and Forecast (WRF) model and found the regional climate is highly sensitive to the irrigation method chosen (drip, flood, and sprinkler). Xu et al. (2019) used a similar approach to mimic sprinkler irrigation at the county level in the central U.S. Instead of using a uniform value of field capacity, a spatially varying soil moisture threshold parameter is determined through regional calibration against the USGS water withdrawal data, which enables transforming model parameters from field to regional scale.

The above-mentioned crop-only and irrigation-only modeling approaches are inadequate to comprehensively address climate-crop-water interactions. In crop-only models, a significant amount of irrigation water as important input to the surface-water-budget equation is neglected in semi-arid croplands and will result in a warm/dry surface environment through land-atmosphere interactions, as well as loss in crop yield due to water stress. On the other hand, irrigation-only models fail to capture the feedback between irrigation water demand and crop growth stages. Therefore, regional irrigation modeling will benefit from the dynamic representation of crop heterogeneity, such as constraining simulated irrigation amount by crop planting/harvest date. Thus, it is necessary to perform joint crop-irrigation modeling in LSMs.

Leng et al. (2016) provided the first joint modeling effort with crop and irrigation on large-scale in the U.S., and optimized irrigation and fertilization practice in CLM4.5CN. The results showed that without optimization, the corn yield is much underestimated, due to the quick denitrification in CLM4.5CN previously reported by Oleson et al. (2013). The irrigation optimization increases yield only in the irrigated region and the fertilization optimization showed significant improvement in all regions. However, the improvement of irrigation scheme on crop yield under sufficient nutrition condition is not discussed. Moreover, uncertainties associated with crop model parameters, sparse agricultural datasets at both spatial and temporal scales, and even discrepancies between available datasets still remain unsolved.

Given the wide use of Noah-MP LSM in the community WRF model and in the operational National Water Model (NWM), it is important to understand and improve its capability in simulating concurrently crop growth and irrigation, because both processes affect surface heat and water-vapor fluxes (as lower boundary conditions in WRF) and streamflow. Therefore, the primary objectives of this study are to: (1) assess the Noah-MP model's performance in joint crop and irrigation modeling; (2) investigate methods of transforming irrigation and crop modeling from field to regional scales; and (3) identify uncertainties and challenges in crop modeling in LSMs. We focus on two crops (corn and soybean) in this study, since they are the two crops currently represented in Noah-MP-Crop and are two major field crops in the central U.S. Section 2 introduces the data required for model input and evaluation, and the Noah-MP crop and irrigation schemes. The model results for crop yield and irrigation amount are presented in Section 3. The uncertainties in simulating crop yield are discussed in Section 4. We conclude our findings in Section 5.

3.2 Description of input data, evaluation data, and models

3.2.1 Data Preparation

In this work, several agriculture management data sets are used to help constrain crop and irrigation models and to define the crop growing season, cultivated land fraction, and irrigated fractions. The planted areas for corn and soybean are obtained from the 30-m CropScape data from the U.S. Department of Agriculture's (USDA) National Agricultural Statistics Service (NASS)/George Mason University (GMU) (**https://nassgeodata.gmu.edu/CropScape/**). This is a geo-referenced, crop-specific land cover data layer created for the contiguous United States using satellite imagery and has been supported by extensive agricultural ground truthing. The CropScape data set is originally derived from the planting frequency in 11 years (from 2008 to 2018) and used to calculate the fractional coverage of total cropland (relative to the grid cell's vegetated area; hereafter F_{crop}) and of each crop type (relative to the grid cell's total cropland area; F_{corn} and $F_{soybean}$). In this study, the planting areas are determined on two criteria: (1) the $F_{crop} > 0.5$; and (2) F_{corn} or $F_{soybean} > 0.3$, for corn and soybean, respectively. The planting area for these two crops and their planting fraction are shown in Figure 3.1.

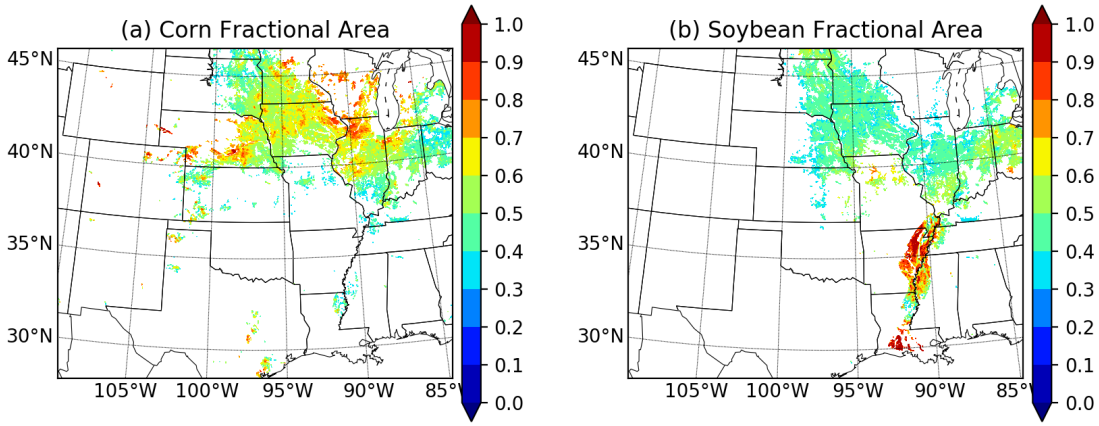

Figure 3.1. Planted-area fractions for (a) corn and (b) soybean in the Central U.S. domain derived from the USDA-NASS CropScape dataset.

The 2010 USDA report on usual planting and harvesting dates is used to define the length of growing season for corn and soybean. This survey reports the most active period of usual planting and harvesting dates for each state. In our study, the middle dates of planting and harvest windows are selected for the states within our study domain (see Figure 3.2). Although the middle dates for each crop in each state may not reflect the complex decision of actual planting and harvesting, it represents to some degree the spatial variation of planting and harvesting at state-level. The impacts of uncertainties in planting/harvesting dates on simulated crop yield and irrigation amount are discussed in section 3.3.2. For details of the planting and harvesting dates in each state, please see Appendix B.

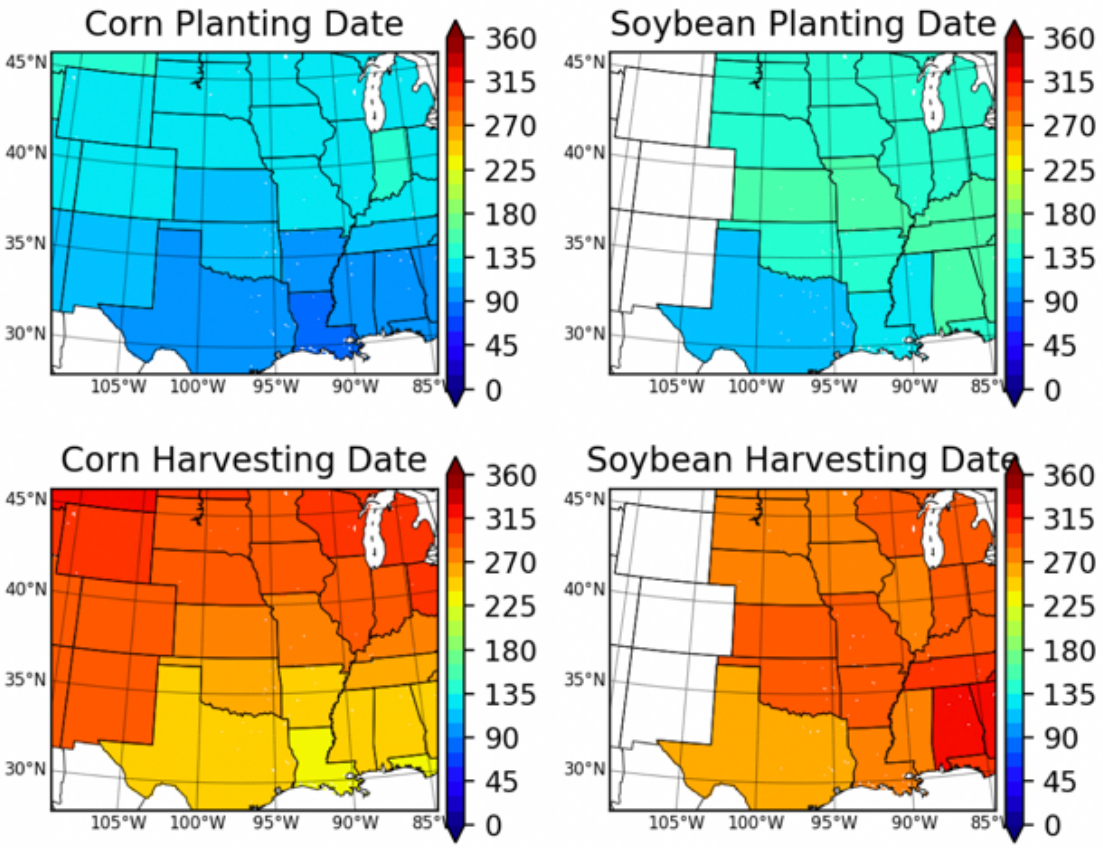

Figure 3.2. USDA-NASS state-level planting and harvest dates in Julian day for corn and soybean.

For each year, the USDA NASS reports the average yields for various crops at the county-level over the U.S (https://quickstats.nass.usda.gov/). These data are based on harvested yields, reported by a sample of farmers within each county, and verified with independent yield samples taken by USDA staff when the crop reaches maturity (FAO and DWFI, 2015). Therefore, the model simulated biomass (g/m^2) will need to be converted to standard yield (bushel/acre, bu/ac) to compare with the USDA county-level data, following the instruction:
(see http://www.ag.ndsu.edu/pubs/plantsci/crops/ae905w.htm)

$$\text{corn yield } [bu/ac] = \text{biomass}\left[\frac{g}{m^2}\right] * (1 - 0.155) * 4.046[km^2/ac] \,/25.4[kg/bu] \quad (3.1)$$

$$\text{soybean yield } [bu/ac] = \text{biomass}\left[\frac{g}{m^2}\right] * (1 - 0.13) * 4.046[km^2/ac] \,/27.4[kg/bu] \quad (3.2)$$

In the Eq. (3.1) and (3.2), 0.155 and 0.13 are the standard moisture content (15.5% and 13%) for corn and soybean, respectively. Harvested corn usually contain an initial moisture content greater than 15.5% (15.5~32%). For transportation and storage purpose, mechanical drying method is typically applied to reduce the initial moisture to the standard moisture. Two sources of weight loss are associated with this process: 1) the weight of the moisture loss (also known as "water shrink") and 2) the weight loss due to handling processes (Hicks and Cloud, 1992). The handling loss could range from 0.04% to 5.22%, depending on the initial moisture content and water shrink loss. But the water shrink loss varies among different growers. Therefore, the calculated dry mass losses

tend to be variable. This uncertainty is worth noting when comparing the model simulated dry mass with standard yield in the USDA survey.

The irrigation locations are defined by the 500-m MODIS-based irrigation fraction map (Ozdogan and Gutman, 2008) and the critical irrigation threshold parameter, IRR_CRI, from Xu et al. (2019) is applied in this study (see Figure 3). IRR_CRI is a threshold parameter for the soil water content, below which the irrigation scheme will be activated and was calibrated at county-level in Xu et al. (2019). To evaluate the model irrigation amount, the five-year report from the U.S. Geological Survey (USGS) on freshwater withdrawals for irrigation (http://water.usgs.gov/watuse/) is used to constrain and calibrate the irrigation parameters in the irrigation module (for details of irrigation modeling, see next section 2.3 and Xu et al., 2019).

Two Ameriflux sites with irrigated agriculture (Ne1 and Ne2 in Mead, NE; https://ameriflux.lbl.gov/sites/) are analyzed. Ne1 is an irrigated continuous maize site and Ne2 is an irrigated maize-soybean rotation site. Data collected at the Ameriflux sites, including LAI, leaf mass per area (LMA), and harvested biomass, are used to evaluate the model output at these two locations with and without the irrigation scheme. Also, the measured leaf biomass per area (LMA; g/m2) is equivalent to the Noah-MP-Crop parameter that converts biomass to LAI (BIO2LAI), which is assumed to be a constant.

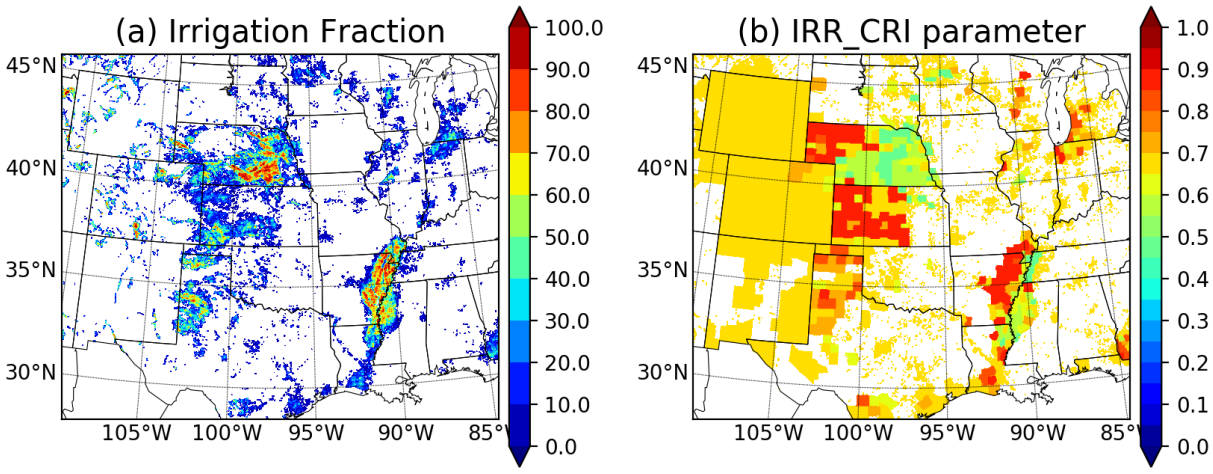

Figure 3.3. (a) The irrigation fraction used in this study. (b) The critical irrigation threshold parameter used in this study, calibrated in Xu et al. (2019).

3.2.2 Noah-MP-Crop model

Noah-MP is a land component of the Weather Research and Forecast (WRF) model (Skamarock et al., 2008; Niu et al., 2011; Yang et al., 2011), which has been widely applied in numerical weather prediction (NWP), regional climate and hydrology studies (Liu et al., 2017; Barlage et al., 2015; Zhang et al., 2020). It has been also used to simulate the land surface processes for streamflow forecasts in the National Water Model (www.water.noaa.gov/about/nwm).

The Noah-MP-Crop crop module consists of three components: a photosynthesis (PSN)-stomata scheme, a carbon allocation scheme, and a dynamic crop growth scheme. The leaf-level PSN rate and stomatal conductance are calculated based on the model of Farquhar et al. (1980) and Collatz et al. (1992) for C3 and C4 plants, respectively. However, there is only one set of PSN parameters for a generic C3 crop in the default Noah-MP. This simplified treatment doesn't represent corn (C4), a major productive species in Central U.S. Therefore, it is critical to adapt a set of C4 PSN parameters from a synthesis of literature and model sensitivity tests (see Appendix B).

Following a similar approach used in traditional crop models (Hybrid-Maize for corn, Yang et al., 2004; DSSAT for soybean, the Decision Support System for Agrotechnology Transfer, Jones et al., 2003), the dynamic crop growth model in Noah-MP-Crop uses the accumulated growing degree days (GDD) to determine eight plant growth stages (PGS, Liu et al., 2016): before seeding, emergence, initial vegetative, normal vegetative, initial reproductive, to maturity, after maturity, and after harvesting. The dynamic crop growth parameters, such as planting/harvest dates and GDD-based thresholds to determine plant growth stages are calibrated at two Ameriflux sites in Bondville (Bo1), IL, for corn and Mead (Ne3), NE, for soybean.

Finally, the Noah-MP-Crop model allocates the assimilated carbohydrate to different parts of plant, depending on the growth stages. For each stage, the total carbohydrate from the PSN scheme is partitioned to the leaf, stem, root and grain according to stage-function fraction parameters (from 0 to 1). For example, during the vegetative stage, more carbon is allocated to leaf relative to stem and root; while in the reproductive stage, most of the assimilated carbon is allocated to grain. Then, the simulated leaf biomass is converted to LAI based on a model parameter, BIO2LAI (or specific leaf area, SLA), in the following equation:

$$LAI = Leaf_{mass} * BIO2LAI \qquad (3.3)$$

The values of BIO2LAI are constants and are different for corn (0.015) and soybean (0.030), respectively (Liu et al., 2016).

3.2.3 Irrigation scheme

A dynamic irrigation scheme was integrated into Noah-MP and tested at field and regional scales without using the Noah-MP-Crop model (Xu et al. 2019). In this study, we adopt the same approach and couple it with dynamic crop growth, enabling two-way crop-irrigation interactions.

Plant photosynthesis and respiration processes are limited by water stress during droughts. Therefore, irrigation plays a critical role in both the water and carbon cycle through relieving water stress, especially for crops planted in arid and semi-arid regions. In Noah-MP, the water stress function is plant- and soil-dependent and is determined by the integrated soil moisture availability (SMA) in root zones. As in Xu et al. (2019), the root-zone SMA is also employed as a basic irrigation trigger. For the irrigated cropland, the root-zone SMA is defined as the ratio of the current root-zone available soil moisture (current SM–SM_{wlt}, wilting point) and non-stress soil moisture ($SM_{ref} - SM_{wlt}$):

$$SMA = (SM - SM_{wlt})/(SM_{ref} - SM_{wlt}) \qquad (3.4)$$

The irrigated cropland is defined as the fraction within a cultivated grid cell $F_{irr-crop}$ and takes the smaller value of F_{irr} and $F_{crop} \cdot F_{veg}$ (cropland fraction relative to the model grid cell's total area) in Figure 3(a):

$$F_{irr-crop} = \min(F_{irr}, F_{crop} \cdot F_{veg}) \qquad (3.5)$$

The irrigation triggering mechanism includes: (1) $F_{irr-crop} > IRR\_FRC$ (an irrigation fraction threshold); (2) within the growing season, defined by the planting/harvesting date map above; (3) $SMA < IRR\_CRI$ (soil moisture trigger, see Figure 3.3(b)); and (4) stop irrigation on rainy days. These criteria are checked daily, and if irrigation is triggered, the potential irrigation amount for the day (IWA) is computed to maintain *SMA* to a non-stress level (SM_{ref}): $IWA = \min(SM_{ref} - SM, IRR\_LIM)$, where *IRR_LIM* is the daily maximum irrigation amount, which is associated with irrigation systems and water availability.

The above irrigation scheme would be executed for the crop type in each irrigated grid cell to obtain the irrigation water amount for corn (IWA_{corn}) and soybean ($IWA_{soybean}$), respectively.

3.2.4 Model setup

The model domain is identical to the central U.S. domain in Xu et al. (2019). The model domain is 600 grids (north-south) × 700 grids (west-east) at 4-km resolution, covering major part of the corn-belt in the Central U.S. The simulation period ranges from 1999-10-01 to 2004-12-31, covering five growing seasons. The atmospheric forcing data are from the North American Land Data Assimilation System (NLDAS, Cosgrove et al., 2003) forcing dataset at 0.125-degree and hourly resolutions. The precipitation forcing are generated by combining observations from field stations, Stage IV radar retrievals from Next Generation Weather Radar System and satellite. A 10-year spin-up period was used to ensure the soil moisture and temperature reach an equilibrium state. An elevation adjustment was applied to the surface pressure, longwave radiation, near-surface temperature and humidity fields to account for topography differences between the model and NLDAS grids.

Six experiments were performed to assess Noah-MP's performance in joint crop-irrigation modeling (see Table 1). The first experiment (BULK) is a simulation with dynamic crop but without irrigation, in which a uniform planting and harvest date is applied in the whole domain. It adopts the default planting/harvest date (day of year) initially calibrated for corn in Bondville, IL, and soybean in Mead, NE (for corn: Julian day 111/300; for soybean: Julian day 130/280). The second experiment (BULK_IRR) is the same as BULK but with the calibrated dynamic irrigation scheme activated (Xu et al., 2019). The third (STATE) and the fourth simulation (STATE_IRR) are the same as the BULK and BULK_IRR but used the state-level planting and harvest date as shown in Figure 3.2. The BULK/BULK_IRR simulations were referred as the baseline simulations and the difference between BULK/BULK_IRR and STATE/STATE_IRR represents the impacts of spatially varying planting/harvest date on crop yield and irrigation amount. The fifth (0.5N) and the sixth (0.5N_IRR) simulation are the same as STATE and STATE_IRR but reduce the nitrogen concentration by half. The difference between STATE/STATE_IRR and 0.5N/0.5N_IRR can be attributed to the impacts of nitrogen concentration. Furthermore, comparing the results between STATE_IRR and STATE with 0.5N_IRR and 0.5N will see the impacts of irrigation under nitrogen sufficient and stressed condition.

Table 3.1. Description of the Numerical Experiments.

#	Experiment	Dynamic Crop	Dynamic Irrigation	PLT/HS	Nitrogen Concentration	Note
1	**BULK**	Yes	No	Uniform date	Sufficient	Baseline simulation
2	**BULK_IRR**	Yes	Yes (calibrated)	Uniform date	Sufficient	
3	**STATE**	Yes	No	State-level	Sufficient	To test the impacts planting/harvest date at state-level
4	**STATE_IRR**	Yes	Yes (calibrated)	State-level	Sufficient	
5	**0.5N**	Yes	No	State-level	Reduced by half	To assess the impacts of nitrogen-stress
6	**0.5N_IRR**	Yes	Yes (calibrated)	State-level	Reduced by half	

3.3 Results

3.3.1 Model Performance

Figure 3.4 shows the county-level corn yields reported by USDA and results from the six experiments. Yield results from the BULK and STATE compare well with the USDA report in the magnitude and spatial pattern in the rainfed region but are underestimated in heavily irrigated regions such as Southeast Nebraska. Using the dynamic irrigation scheme in BULK_IRR and STATE_IRR reduces the yield bias in irrigated regions. The differences between the BULK and STATE will be further discussed in section 3.2. The 0.5N experiment significantly reduces yield for more than 60% of the domain due to nitrogen stress, which is similar to the CROP_DFLT scenario in Leng et al. (2016) for the fast denitrification in the default version of CLM4.5. In this case, using irrigation scheme (0.5N_IRR) has little improvement under nitrogen stress.

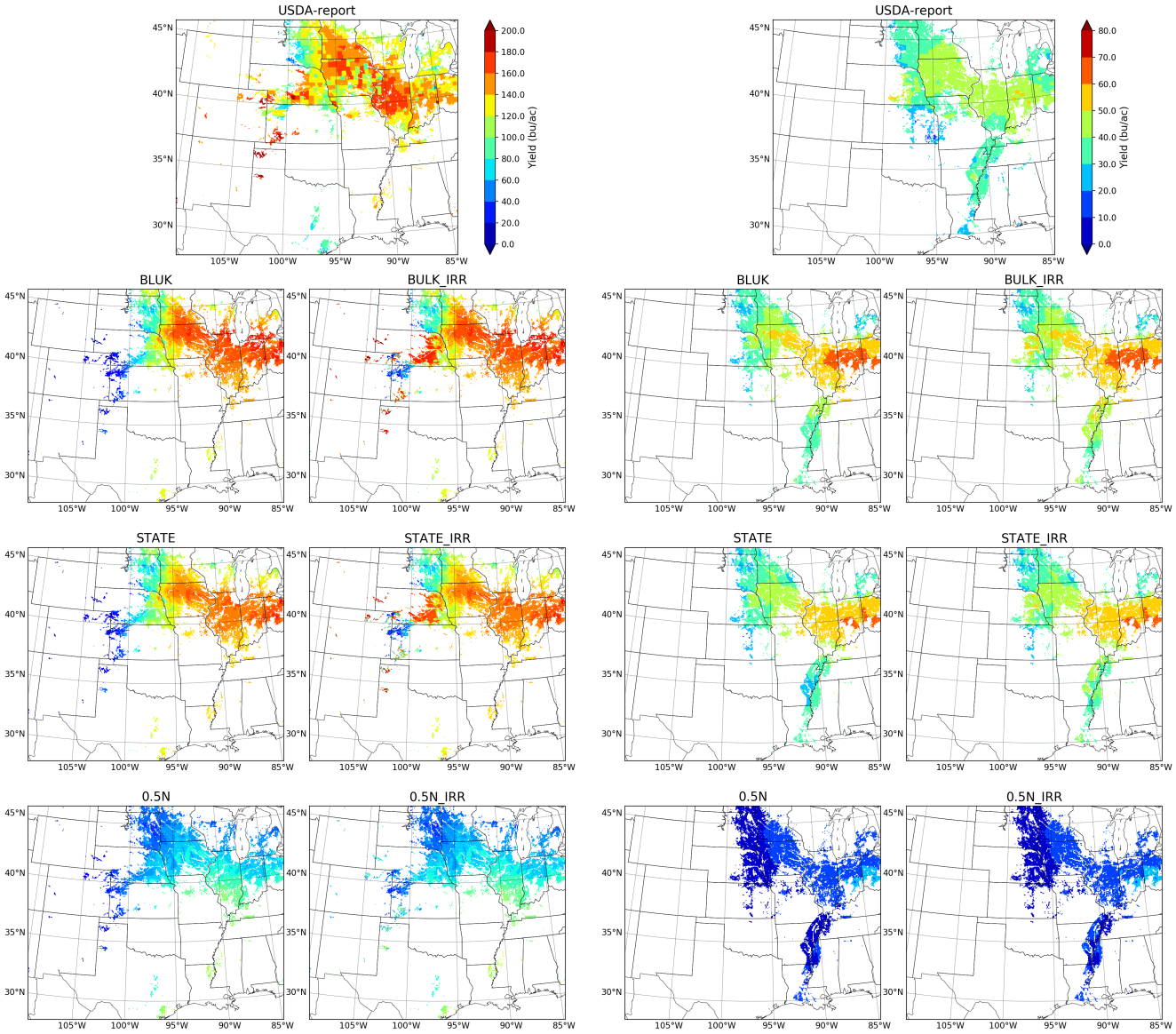

Figure 3.4. For Corn: Yield (bushel/acre) from USDA NASS county survey and six model simulations.
Figure 3.5. For Soybean: Yield (bushel/acre) from USDA NASS county survey and six model simulations.

As for soybean yields shown in Figure 3.5, BULK and STATE show good estimate of yield in the major soybean production areas in the U.S (MI, IL, IN, IO, WI, MN, SD), but underestimate significantly the yield in the irrigated regions such as NE, AR and MS. In the 0.5N nitrogen-stressed condition, soybean yields are much under predicted for the entire domain. The dynamic irrigation scheme can help improve yield in the BULK_IRR and STATE_IRR simulation, but it doesn't show much impact under nitrogen stress condition in 0.5N_IRR. These results from corn and soybean suggest that the impacts of irrigation on yields in the irrigated regions are significant but only occur with sufficient fertilization supply.

3.3.2 Transition from field to regional scale crop modeling

The second objective of this study is to transition crop modeling from field to regional scale by first exploring the use of spatially varying planting/harvesting dates for regional simulation. The impacts of spatially varying planting/harvest date on modeling crop yield and irrigation amount can be assessed by comparing the results from the BULK_IRR and STATE_IRR simulation as shown in Figure 3.6. The bars are ranked by the yield from low to high in each of these states and the black lines represent the delayed days in planting date compared to the uniform planting date in BULK_IRR (111 for corn and 130 for soybean in Julian day). The delayed planting for each state implies a shorter growing season, which results in lower yields in STATE_IRR than in BULK_IRR for both corn and soybean. These reduced yields help improve the high bias of BULK_IRR in all states, except for South Dakota and Minnesota, where STATE_IRR underestimates in both corn and soybean yield.

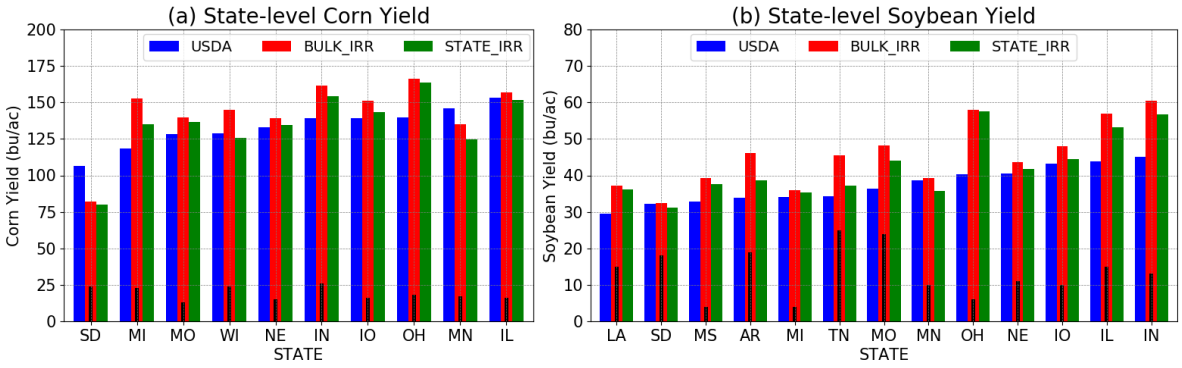

Figure 3.6. Bar plot of the USDA and modeled yield for each state from the BULK_IRR and STATE_IRR simulation for (a) corn and (b) soybean. The delayed days in planting date in STATE_IRR (compared to the uniform date in BULK_IRR) are shown in black lines.

Figure 3.7 shows the impacts of delayed planting date on reduced yield (bu/ac/day) for corn and soybean. This impact of planting date on yield may be more complex than a linear relationship, but strong spatial variation exists across states on the sensitivity of modeled yield to delay in planting date. For both corn and soybean, a clear north-to-south gradient can be witnessed, as the impacts of planting date are strong in Northern states, such as Minnesota, Iowa, Wisconsin and Michigan. While for soybean, the planting region in lower Mississippi river valley shows a clear dependence on planting day as well. Moreover, this north-to-south gradient of yield dependence on planting date also exhibits in each particular state as well. This is most obvious in Minnesota, Iowa, Illinois, and Indiana, for both corn and soybean, that the modeled yields in northern part of the states are more sensitive to delay in planting date than in the south.

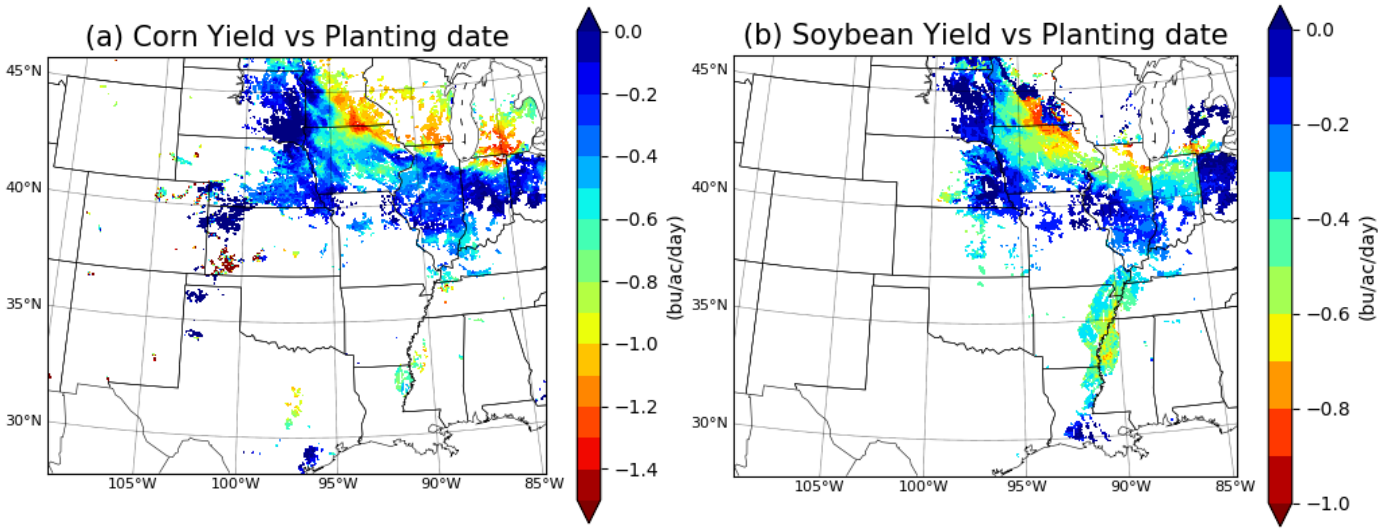

Figure 3.7. The impacts of delayed planting date on modeled yield (bu/ac/day) for (a) corn and (b) soybean.

On the other hand, in South Dakota the model shows very little sensitivity to the planting date, suggesting the modeled yield may be impacted by water stress (Figure S1 confirms this speculation that the underestimated yields in Eastern South Dakota and Western Minnesota are water-limited). However, the low irrigation fractions in these two regions (Figure 3.3a) suggested irrigation is not a significant water source for crop production. Therefore, we suspect that the perched shallow water table in the northern corn belt plays a role in supplying water for corn production. Note that the model applies a free drainage scheme for deep soil drainage and the complex two-way groundwater exchange processes are not considered in this study.

Transforming the planting date from uniform value at point scale to spatially varying at state-level could also influence the modeled irrigation amount, as the irrigation period is constrained by the crop growing season. Figure 3.8 shows the spatial distribution of USGS water withdrawal report at county-level in 2000 and the modeled irrigation amount from the BULK_IRR and STATE_IRR. The BULK_IRR, with uniform planting/harvesting date, overestimates irrigation amount compared to the USGS reported data, especially in the Lower Mississippi River Basin (LMRB). The largest overestimation in irrigation amount is over 100 mm and occurs in Poinsett, Arkansas, with USGS reported 459.2 mm and the BULK_IRR simulated 561.3 mm. The overestimated irrigation amount in the BULK_IRR has an intuitive explanation; the longer the growing season, the more water is needed to maintain soil moisture at the critical level. The scatter plot in Figure 9 for the irrigation amount from two simulations also confirms the overestimate of irrigation amount in the BULK_IRR, especially in the LMRB. After applying the spatially varying planting/harvesting date, the performance in STATE_IRR is improved compared to the BULK_IRR (RMSEs improve from 29.67 to 26.24 mm, and coefficient of determination, R^2, increases from 0.89 to 0.92) in LMRB. The STATE_IRR also reduces irrigation amount in Nebraska as well, but not as much as in LMRB. In fact, the USGS county-level report represents an upper bound of the total water withdrawal, but the water is not necessarily used all for irrigation. Therefore, the model simulated irrigation amount shouldn't exceed the USGS report. Hence, the STATE_IRR simulates less irrigation amount and provides better performance than the BULK_IRR.

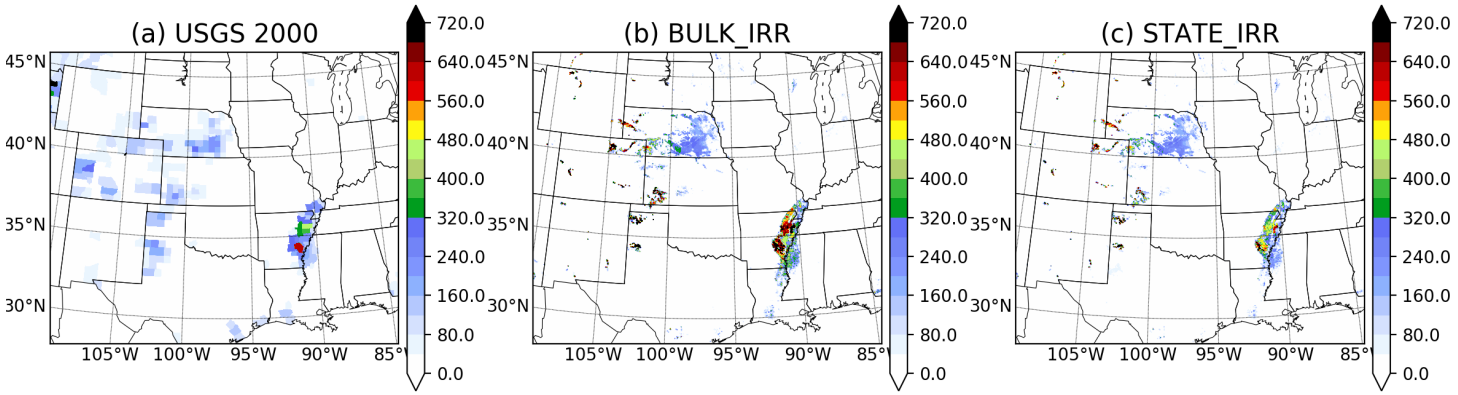

Figure 3.8. Irrigation amount from (a) USGS county-level water withdrawal report; (b) modeled irrigation amount from the BULK_IRR simulation; and (c) the STATE_IRR simulation.

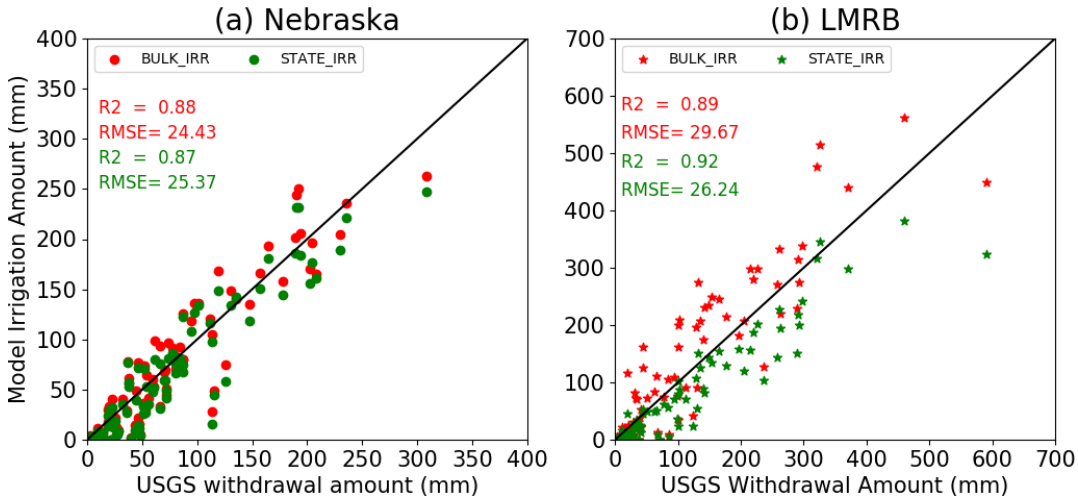

Figure 3.9. Scatter plot of the model irrigation amount against the USGS water withdrawal data in two heavily irrigated region, Nebraska and Lower Mississippi River Basin (LMRB).

3.3.3 Impacts of irrigation on crop yield

Figure 3.10 shows the LAI and grain mass at the two Ameriflux sites (Ne1 and Ne2). STATE and STATE_IRR simulated LAI have good agreement in Ne1 for corn throughout the growing season, but underestimate LAI in Ne2 in 2002 for soybean. When it comes to the crop reproductive stage (grain production), the differences in yield between these two simulations are evident. The STATE simulation significantly underestimates corn yield at both sites, ranging from 31% to 80%, but using the irrigation scheme greatly improves corn yield at both sites.

As for the soybean yield, irrigation doesn't improve soybean yield as much as it did for corn yield, even with similar total irrigation amount. This is also noticed in Chen et al. (2018), as the increase in crop yield due to irrigation has a strong dependence on crop species. This may be attributed to the different biogeochemical characteristics between these two plants (corn is C4 and soybean is C3) in their water-use efficiency, including photosynthesis and respiration.

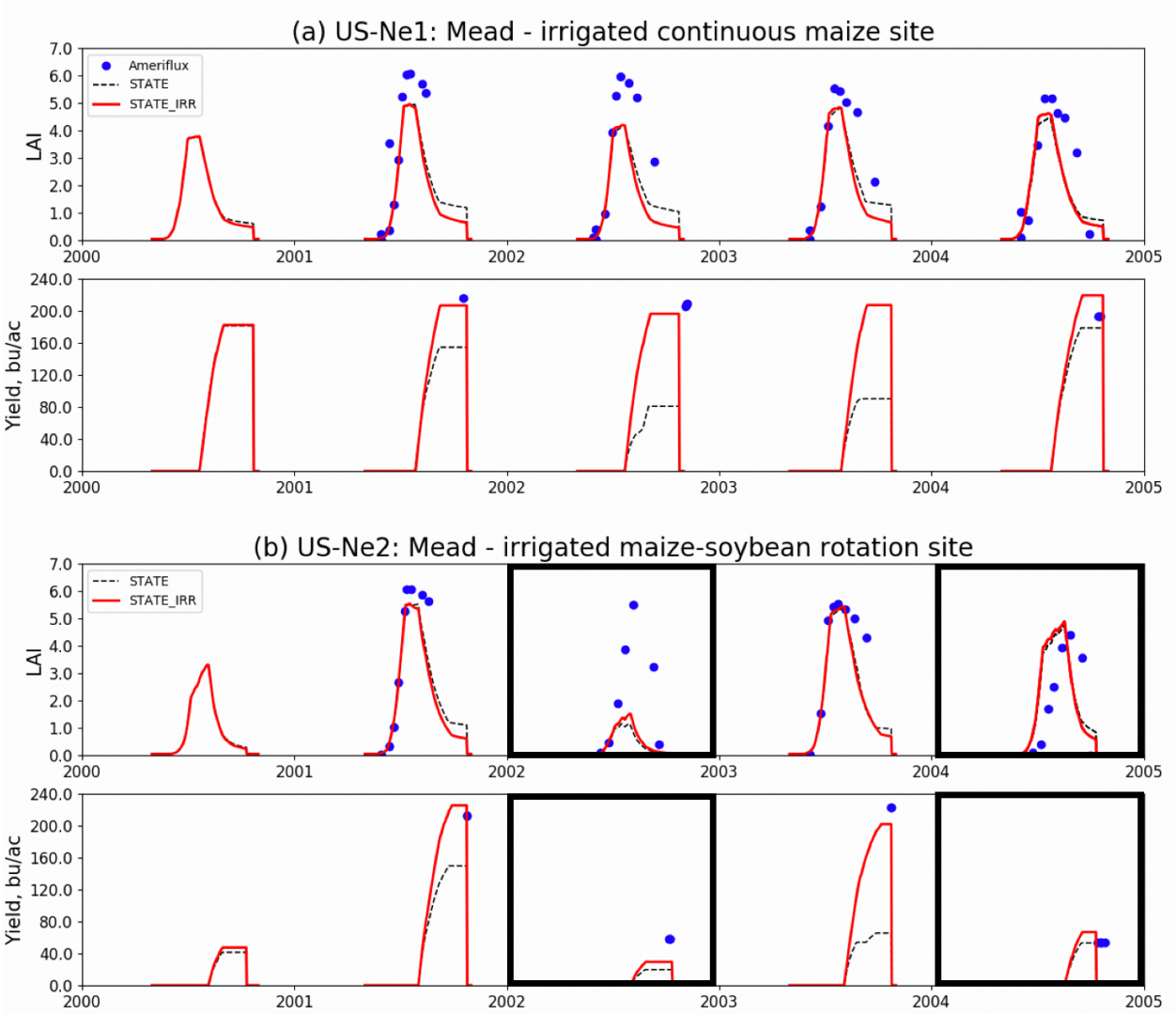

Figure 3.10. Timeseries of LAI and harvested grain in Ne1 and Ne2 sites from 2000 to 2005. Ne1 is irrigated continuous corn site and Ne2 is irrigated maize-soybean rotation; black boxes in Ne2 indicate soybean years.

Figure 3.11 shows the USDA yield data and the six simulations in this study, aggregated at state level. The comparison between BULK and BULK_IRR, and STATE and STATE_IRR in irrigated regions shows the improvement of yield with the irrigation scheme activated. The yield in BULK_IRR (156.5 bu/ac) is even double the amount than in BULK (74.61 bu/ac) for corn. The difference between BULK_IRR and STATE_IRR shows the impacts of prolonged growing season on overestimating modeled yield in BULK_IRR, due to the increase in modeled irrigation amount.

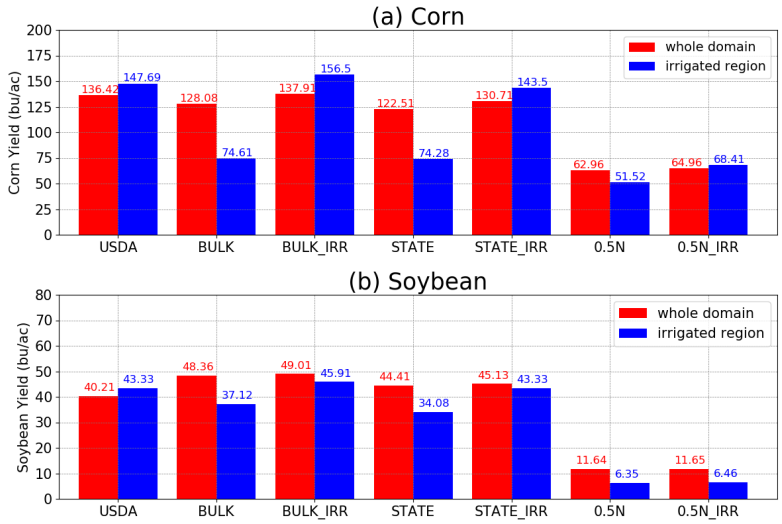

Figure 3.11. Bar plots of yield from (a) corn and (b) soybean from USDA survey and six simulations in this study. The red and blue bars represent the crop yields in the whole domain and in the irrigated region, respectively.

Moreover, the STATE_IRR and 0.5N_IRR represents the impacts of irrigation on crop yield under the conditions of sufficient and stressed nitrogen, respectively. The doubled irrigated yield in STATE_IRR (from 74.28 to 143.5 bu/ac) decreases under nitrogen stress condition (from 51.52 to 68.41 bu/ac) in 0.5N_IRR. This is similar to Leng et al. (2016) results, in which the irrigation scheme was applied to the default CLM4.5 run with fast denitrification rate. Thus, the irrigation impacts in such nitrogen-stressed conditions is limited. However, when the nitrogen concentration is unstressed, the impacts of irrigation manifest and improve crop yield.

Table 3.2 presents the statistics from all simulations, including RMSE (in both bu/ac and relative to USDA report) and the coefficient of determination (R^2). These statistics confirm that under sufficient nitrogen concentration and state-level planting/harvest management, the application of a dynamic irrigation scheme (STATE_IRR) improves the modeled yield performance for both corn and soybean, reducing RMSE from 47.8 to 22.3% for corn and from 18.9% to 16.8% for soybean.

Table 3.2. Summary of the model performance in simulating county-level corn and soybean yield from 2000-2004 (5 growing seasons) as compared to USDA report data for the whole domain and only irrigated regions (in parentheses).

Experiment	Cultivar	RMSE [bu/ac]	RMSE [% relative to USDA]	R^2
BULK	Corn	38.3 (72.0)	28.1% (48.7%)	0.70 (0.23)
	Soybean	11.4 (8.9)	28.4% (20.5%)	0.84 (0.83)
BULK_IRR	Corn	32.2 (34.1)	23.6% (23.1%)	0.79 (0.72)
	Soybean	11.3 (8.5)	28.1% (19.61)	0.86 (0.91)
STATE	Corn	35.9 (70.6)	26.3% (47.8%)	0.71 (0.24)
	Soybean	10.9 (8.2)	27.1% (18.9%)	0.80 (0.83)
STATE_IRR	Corn	29.4 (33.0)	21.5% (22.3%)	0.80 (0.71)
	Soybean	10.6 (7.3)	26.4% (16.8%)	0.82 (0.90)
0.5N	Corn	65.4 (78.6)	47.9% (53.2%)	0.71 (0.51)
	Soybean	23 (17)	57.4% (46.2%)	0.50 (0.38)
0.5N_IRR	Corn	64.1 (68.8)	47.0% (46.7%)	0.74 (0.72)
	Soybean	22 (17)	57.0% (44.8%)	0.50 (0.37)

3.4 Discussion

Several uncertainties can contribute to the differences between simulated crop yields and the USDA report, including those associated with discrepancies between available datasets, crop yield gaps, and crop/irrigation model parameters, which is the subject of discussion in this section.

3.4.1 Yield gaps between actual yield and modeled potential or water-limited yield

The yield potential (Y_p) is defined as the yield an adapted crop cultivar could achieve by alleviating all abiotic and biotic stresses through optimal crop and soil management (Lobwell et al., 2009). Thus, Y_p is achieved when management eliminates all limitations to crop growth and yield from nutrient deficiencies, water deficit or surplus, toxicities, salinity, weeds, insect pests, and pathogens. In our study, for irrigated corn and soybean, the model provides sufficient water and nitrogen, hence, the modeled yield should be close to Y_p. For rainfed crops, the modeled yield is not potential due to water limitation (Y_w, water-limited yield). The relative yield gap (Y_g) can be calculated in:

$$Y_g = \left(1 - Y_a/Y_p\right) * 100\%; \text{for irrigated crop} \quad (3.6)$$

$$Y_g = (1 - Y_a/Y_w) * 100\%; \text{for rainfed crop} \quad (3.7)$$

Quantifying the yield gaps for each crop cultivar in different growing regions is still a research topic in the food production community. The Global Yield Gap Atlas (GYGA, www.yieldgap.org) provides estimates of untapped crop production potential on existing farmland based on current climate and available soil and water resources. GYGA's estimated Y_g in US are 10~20% for irrigated corn and 20~30% for rainfed corn, respectively. In our study, Y_g are calculated between USDA county-level data and our model simulations and listed in Table 3, which are 13~25% for irrigated corn and 17~28% for rainfed corn. These numbers are comparable to the numbers given by GYGA. However, the yield gaps for soybean are 15~32% for irrigated and 14~39% for rainfed soybean, which are higher than other studies (e.g., 9~24% in Egli and Hatfield, 2014; 10~30% in Grassini et al., 2015), especially for the rainfed soybean, which agrees with the overestimation in IL, IN and OH.

3.4.2 Uncertainties in crop model parameters

The development of LSMs has expanded from its initial purpose to provide reliable lower boundary conditions for the coupled climate and weather models by including terrestrial biogeochemical processes, land use change, and dynamic vegetation growth (Bonan et al., 2011). Many LSMs adopt the Faquhar-Ball-Berry scheme to simulate the coupled leaf-level photosynthesis and stomatal conductance (Farquhar and von Caemmerer, 1982; Ball et al., 1987; Collatz et al., 1991; Collatz et al., 1992; Niu et al., 2011; Oleson et al., 2013). Those biophysiological models require a variety of plant-specific parameters, such as the minimum stomatal conductance, respiration rate, and rubisco capacity (V_{cmx25}), and they are usually measured under field experimental conditions. Bonan et al. (2011) reviewed the past literatures on PSN-stomata parameterization in LSMs and found that V_{cmx25} is the most critical parameter in modeling plant photosynthesis. This parameter characterizes the maximum carbon assimilation rate and is measured in laboratory conditions, given sufficient radiation upon leaf level and CO_2 concentration at 25 °C. Bonan et al. (2011) concluded that the leaf-level measured V_{cmx25}, when scaled up to LSM model grid cell, could lead to higher photosynthetic rates when nitrogen was non-limiting (such as for cropland systems). Furthermore, the V_{cmx25} is little constrained and remains model dependent over LSMs.

Table B1 in Appendix B provides a synthesis of the parameters used in several studies. The wide range of V_{cmx25} values (from 30 to 101 $\mu mol\, m^{-2}\, s^{-1}$) and different treatments of product-limiting pathway in PSN calculation (K_p) demonstrate a significant uncertainty in specifying the model-dependent PSN parameters. Hence, calibration of the PSN parameters becomes critical, but has been usually conducted at field scales using measurements of moisture and carbon fluxes. The Noah-MP-Crop model (Liu et al. 2016) uses the generic crop PSN parameters, which don't distinguish C3 and C4 crops. To incorporate corn-specific PSN parameters into Noah-MP-Crop parameter table, we performed a calibration for C4 corn using the LAI and biomass data in the Ameriflux Bo1 site in Bondville, IL. The calibrated values are listed at the bottom row of Table S1, noted as "Adjust", meaning they are calibrated and subject to adjustment. The main result of the calibration is to reduce overestimated rain-fed corn yield by reducing V_{cmx25} from the default value (80 $\mu mol\, m^{-2}\, s^{-1}$) to a lower value (60 $\mu mol\, m^{-2}\, s^{-1}$). The calibration results are presented in Figure S2. As for soybean, the default crop parameters for C3 were used in this study.

He et al. (2019) provides a global rubisco capacity map from satellite-observed solar-induced chlorophyll fluorescence (SIF) record. Through data assimilation methods, the 11-year record of SIF shows both spatial and temporal variation of V_{cmx25} in world's major crop production regions. Future efforts of incorporating the spatial map of V_{cmx25} into ESMs and LSMs would be highly useful to address the wide range of this model parameter.

3.4.3 Crop Model parameter uncertainties – planting/harvesting management

Representing dynamic crop phenology in LSMs is critical for predicting the energy, water, and carbon budgets in croplands and may even influence the atmospheric boundary layer, especially in areas with large cropland coverage (Betts, 2005; Ma et al., 2012). In some LSMs, the determination of planting and harvesting, as well as plant growth stages are calibrated against field data. Therefore, these calibration efforts are local and there are few studies quantifying the impacts of planting on simulating crop phenology over a large region. For example, in the CLM4-Crop, the planting is activated by three temperature thresholds, a 20-year averaged GDD threshold, a threshold of 10-day running mean of air temperature, and a threshold of daily minimum temperature (Levis et al., 2012). Chen et al. (2018) evaluated the CLM4-Crop over multiple Ameriflux sites over the U.S. corn belt and found there is an early season overestimate of LAI, due to a too-early start of planting. A modified simulation with delayed the planting showed improvement in simulating energy and water fluxes, as well as the NEE.

In Noah-MP-Crop, the planting and harvesting date are prescribed parameters to reflect the spatial and year-to-year variation of planting/harvesting date for Bo1 and Ne3 sites in Liu et al. (2016). In this study, the BULK_IRR simulation with an early and spatially invariant planting date overestimated the crop yield and irrigation amount for corn and soybean, consistent with the results of Chen et al. (2018). By contrast, the STATE_IRR simulation with spatially varying and delayed planting dates effectively mitigated those overestimations (Figure 3.6). Figure 3.7 shows that the northern states in the corn belt are relatively more affected by delayed planting date than the southern states, and this north-to-south gradient is evident within each state as well.

Although the state-level planting/harvesting date applied in STATE_IRR represented to some degree of their spatial variations, uncertainties still exist. The USDA usual planting/harvesting date report gives the most active window for planting and harvesting through the survey of last 20 years.

In the STATE and STATE_IRR simulation, the middle date of the window time is selected for each state. However, applying the single planting/harvesting date on state-level is still unrealistic. Figure 3.7 shows the spatial variations of the modeled crop yield sensitivities to delay in planting date and the range of these crop yield responses are calculated in Table 3.3.

To better constrain the crop growing seasons, it is necessary to incorporate the spatially detailed crop calendars. For example, the planting and harvesting windows can be dynamically modeled based on field workability, considering snow cover and rainfall, and crop biological requirement for heat and moisture (Iizumi et al., 2018). Dynamically modeling the crop calendar will likely reduce the uncertainties of specifying crop growing seasons in future crop model development, especially in regions where agricultural management data are sparse.

3.4.4 Crop Model Parameter Uncertainties – convert leaf mass to LAI

Figure 3.12 shows the reciprocal of measured leaf mass per unit area (LMA, g/m^2) from Ne1 and Ne2 from 2001 to 2007, which demonstrates significant in-season variations for both corn and soybean. For corn, this reciprocal decreases from 0.03 at the early growing stage to 0.01 m^2/g at the end of the growing season. This characterizes a general corn leaf growth feature: grow bigger (larger LAI) at the beginning of the growing season with small amount of mass, and later growing thicker (more mass) with slight increase in LAI. The inverse of LMA for soybean has less variability and the values are generally higher than for corn during the growing season (ranging from 0.018 to 0.029 m^2/g).

The ranges of LMA are listed in Table 3 as compared to the default constant value of BIO2LAI in Noah-MP-Crop that has the same physical meaning as the 1/LMA and is used to convert the prognosed leaf mass to diagnosed LAI. BIO2LAI is set as constants for corn (0.015) and soybean (0.030). Such a constant conversion coefficient is used in other LSMs too, e.g., the specific leaf area parameter (SLA) in CLM (Oleson et al., 2013). The substantial seasonal variations of 1/LMA in Figure 3.12 points to the challenges of using a constant BIO2LAI throughout the entire crop growing season, and a time-varying conversion coefficient is needed in future model development.

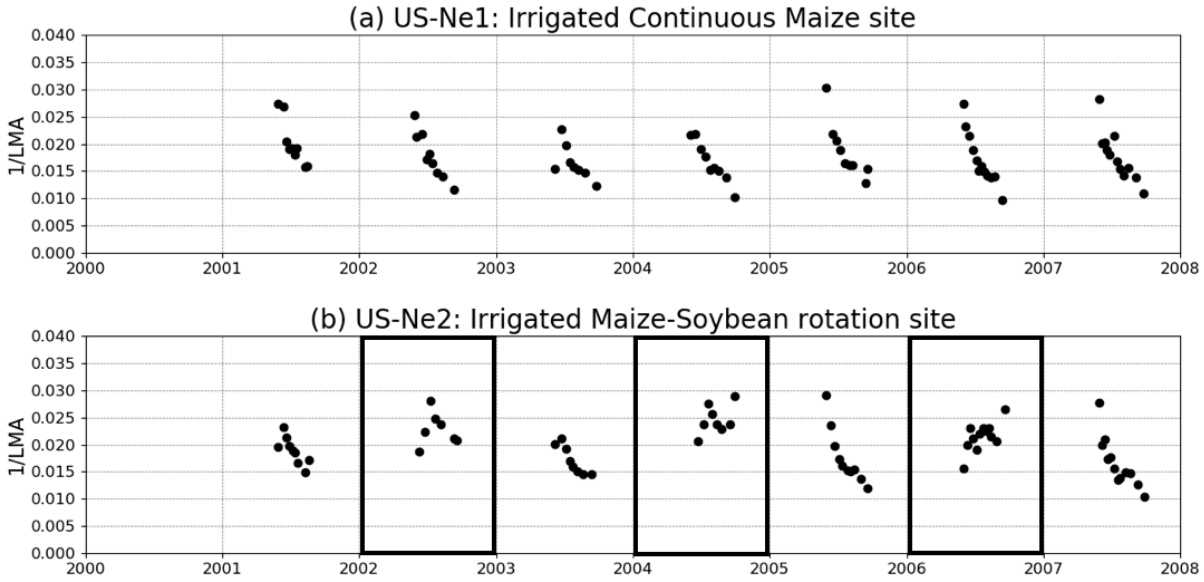

Figure 3.12. The reciprocal of the measured leaf mass per area (LMA) from two Ameriflux sites, US-Ne1 and US-Ne2. The inverse of LMA is the same as BIO2LAI parameter in the Noah-MP-Crop model. The black boxes in US-Ne2 indicates soybean years.

3.4.5 Summary of the uncertainties in validating crop modeling

Table 3.3 summarizes the aforementioned uncertainties and provides the default values in Noah-MP-Crop and the ranges of uncertainties of three parameters: yield gaps (between USDA-report actual yield and modeled yield), model parameters (V_{cmx25}, planting date, and BIO2LAI). The uncertainty associated with mechanical drying after harvest mentioned in Section 2 are also include in Table 3.3.

Table 3.3. Summary of the sources of uncertainties in conducting crop modeling and validating model outputs.

Uncertainty source	Default setting	Range	Unit
Yield gap	[-]	13~25% for irrigated corn 17~28% for rainfed corn 15~32% for irrigated soybean 14~39% for rainfed soybean	% relative to potential yield for irrigated corn and water-limited yield for rainfed corn.
Model parameter, V_{cmx25}	80 for generic crop parameter	30~101 for corn 80~101 for soybean	$\mu molm^{-2}s^{-1}$
Model parameter, planting date*	111 for corn 130 for soybean	-0.04~-1.22 -0.06~-0.72	*bu*/*ac*/*day* delayed after the default date
Model parameter, BIO2LAI	0.015 for corn 0.030 for soybean	0.010~0.030 0.018~0.029	m^2/g
Handling loss in mechanical drying	[-]	0.04 ~ 5.22 % for corn	% relative to final standard yield at 15.5% moisture content

3.5 Conclusion

This study evaluated the performance of Noah-MP-Crop's joint modeling of crop and irrigation at in the Central U.S. By incorporating spatial datasets of high-resolution crop and irrigation fraction, and state-level planting/harvesting date, the crop model can be applied to regional scale. The impacts of irrigation on crop yield are assessed from field to regional scale as well as under nitrogen sufficient and stressed conditions. Also, several uncertainties including model parameters, yield gaps, and discrepancies between available datasets are assessed.

The results showed that in the U.S corn-belt the bulk simulation (with uniform planting/harvesting date and no irrigation) captured the magnitude and spatial variation of corn yield against the USDA county-level report (RMSE = 28.1% for the whole domain). But in the heavily irrigated region, for example in Nebraska, the yield was much underestimated (RMSE = 48.7% in the irrigated region). Adding irrigation modeling capability effectively improved yield simulation over irrigated region (RMSE=23.1%). The RMSEs for soybean over the whole domain and irrigated region are 28.4% and 20.5%, respectively. The irrigation improvements on soybean yield are relatively small compared to that for corn. Noticeable overestimation of yield for corn and soybean still exist in Northeast of the domain in Indiana and Ohio, which may be attributed to early planting biases and the yield gap between actual yield and modeled yield.

To transition the crop modeling from field to regional scale, two simulations with state-level planting/harvesting date were conducted. These spatially varying planting/harvesting dates were in general later than the uniform planting dates. The delayed planting dates across states resulted in reduction in modeled yield and irrigation amount, which improved the overestimated yield bias associated with early planting bias. A spatial analysis also showed that the modeled yield in northern states was more sensitive to delayed planting than in southern states for rainfed corn and soybean. This north-to-south gradient was evident within each northern state as well (IL, IN, IO, MN, WI). This indicates that using one single value for planting/harvesting date for each state is still an over-simplified assumption, which is inadequate to address the complex decision of agricultural management. Comprehensive datasets of cropping calendar at high-resolution are needed for future crop model development.

Dynamic modeling of crop growth and irrigation application is challenging and there are many uncertainties. Several sources of uncertainties were identified, including yield gaps, model parameters associated with photosynthetic rubisco capacity and planting date, and discrepancies between different observation data. The rubisco capacity (V_{cmx25}), is a significant source of uncertainty and we calibrated it according to single-point simulation in Bondville for corn (C4 corn).

Fertilization has been identified as a source of uncertainties in previous studies (Leng et al., 2016). In this study, it was assumed that the crops are not nitrogen-stressed. To investigate the impacts of irrigation on crop yield under nitrogen-stress, two sets of additional simulations are conducted which halved the nitrogen concentration. When nitrogen concentration is reduced to half, nitrogen stress could cut crop yield by 48.6% and 73.8% for corn and soybean, respectively (comparing 0.5N with STATE). The irrigation improvements on crop yields under nitrogen stress are restricted (comparing 0.5N and 0.5N_IRR), with 32% and 1% increase for corn and soybean. These numbers are much less than under sufficient nitrogen condition (comparing STATE and STATE_IRR, 93%

for corn and 27% for soybean). This concludes that the manifestation of irrigation improvement on crop yield relies on sufficient nitrogen concentration.

The present study contributed to the knowledge of simulating crop yield and irrigation water amount in one of the world's most productive agriculture regions in the North America Great Plains and investigated the impacts of irrigation on crop yields. The irrigation effects on crop yield under no nutrition-stress condition is addressed in this study, which was often ignored in previous research. This is mediated through adding additional amount of water from irrigation to supply soil moisture fulfilling till a critical level. The wet soil moisture supports photosynthesis and transpiration through maintaining the openness of stomata, hence, sustaining normal physiological activities during dry periods. On the other hand, other sources of uncertainties arise from crop model photosynthesis and phenology parameters, yield gap and unit conversion. To mitigate these uncertainties, we demonstrated that calibrating the crop rubisco capacity parameters and constrain growing season with spatially varying planting/harvesting date can improve crop simulation results. Finally, future efforts should be dedicated to incorporating spatially detailed rubisco capacity parameters and crop calendar to better constrain the crop growth dynamics.

Key points for the next chapter

- The soil moisture impacts on crop photosynthesis and carbon allocation is accessed through simulations w/wo irrigation schemes. These simulations are particularly important for croplands in the semi-arid regions.
- Crop models and irrigation models in Noah-MP can provide reasonable estimates of crop yields and irrigation water amounts.
- Large uncertainties remain in model parameters, related to planting and irrigation areas, planting/harvesting dates, crop photosynthesis parameters and unit conversion during model evaluation.
- Reasonably representing the crop growth dynamics and irrigation process in LSMs could potentially improve the land surface heterogeneity in the study region. In particular, the application of irrigation may also influence the withdrawal and recharge from groundwater aquifers, which will be discussed in the next chapter.

Acknowledgments

The authors Zhe Zhang, Yanping Li, Warren Helgason, and Zhenhua Li gratefully acknowledge the support from the Global Water Future project and Global Institute of Water Security at University of Saskatchewan. Yanping Li acknowledge the support from NSERC Discovery Grant. Michael Barlage and Fei Chen appreciate the support from by NCAR Water System, USDA NIFA Grants 2015 - 67003 - 23460, NSF INFEWS Grant #1739705, and NOAA OAR Grant NA18OAR4590381. NCAR is sponsored by the National Science Foundation. Any opinions, findings, conclusions, or recommendations expressed in this publication are those of the authors and do not necessarily reflect the views of the National Science Foundation.

Chapter 4 – Shallow groundwater dynamics in the Prairie Pothole region

This manuscript has been modified for inclusion in this thesis. It was originally published as:

Zhang, Z. Li, Y., Barlage, M., Chen, F., Miguez-Macho, G., Ireson, A., Li, Z. Modeling groundwater responses to climate change in the Prairie Pothole Region. *Hydrol. Earth Syst. Sci.*, 24, 655-672, (2020), https://doi.org/10.5194/hess-24-655-2020.

Author contributions: Z. Zhang, F. Chen and M. Barlage designed the study and wrote the paper. Y. Li, A. Ireson and Z. Li contributed to the interpretation of the results and reviewed the manuscript. G. Miguez-Macho provided valuable supports on model consultation and manuscript reviewing.

Keywords

Groundwater, Recharge, Climate Change, Prairie Pothole Region, Hydrological cycle

Abstract

Shallow groundwater in the Prairie Pothole Region (PPR) is predominantly recharged by snowmelt in the spring and supplies water for evapotranspiration through the summer and fall. This two-way exchange is underrepresented in current land surface models. Furthermore, the impacts of climate change on the groundwater recharge rates are uncertain. In this paper, we use a coupled land–groundwater model to investigate the hydrological cycle of shallow groundwater in the PPR and study its response to climate change at the end of the 21st century. The results show that the model does a reasonably good job of simulating the timing of recharge. The mean water table depth (WTD) is well simulated, except for the fact that the model predicts a deep WTD in northwestern Alberta. The most significant change under future climate conditions occurs in the winter, when warmer temperatures change the rain/snow partitioning, delaying the time for snow accumulation/soil freezing while advancing early melting/thawing. Such changes lead to an earlier start to a longer recharge season but with lower recharge rates. Different signals are shown in the eastern and western PPR in the future summer, with reduced precipitation and drier soils in the east but little change in the west. The annual recharge increased by 25 % and 50 % in the eastern and western PPR, respectively. Additionally, we found that the mean and seasonal variation of the simulated WTD are sensitive to soil properties; thus, fine-scale soil information is needed to improve groundwater simulation on the regional scale.

Motivation

In the last two chapters, I explored the soil moisture interactions with the atmosphere and biosphere through soil moisture-temperature feedback and biogeochemical processes. In the study's region—the Canadian Prairies and Great Plains—shallow groundwater is a typical feature, as is an exchange of water with soil moisture. In wet seasons groundwater receives recharge from the upper soil layers, and in dry seasons the shallow groundwater can also supply soil moisture through capillary rise. This two-way exchange has been a challenge to represent in models and, hence, has been neglected in previous LSMs. In this chapter, I will explore the exchanges between shallow groundwater and soil moisture, as well as the water table dynamics under future climate change scenarios in the North American Prairie Pothole region.

4.1 Introduction

The Prairie Pothole Region (PPR) in North America is located in a semi-arid and cold region, where evapotranspiration (ET) exceeds precipitation (PR) in summer and near-surface soil is frozen in winter (Gray, 1970; Granger and Gray, 1989; Hayashi et al., 2003; Pomeroy et al., 2007; Ireson et al., 2013; Dumanski et al., 2015). These climatic conditions have introduced unique hydrological characters to the groundwater flow in the PPR (Ireson et al., 2013). During winters, frozen soils reduce permeability and snow accumulates on the surface, prohibiting infiltration (Niu and Yang 2006; Mohammed et al., 2018). At the same time, the water table slowly declines due to a combination of upward transport to the freezing front by the capillary effect and discharge to rivers (Ireson et al., 2013). In early spring, snowmelt becomes the dominant component of the hydrological cycle and the melt water runs over frozen soil, with little infiltration contributing to recharge. As the soil thaws, the increased infiltration capacity allows snowmelt recharge to the water table, the previously upward water movement by capillary effect to reverse and move downwards, and the water table to rise to its maximum level. In summer and fall, when high ET exceeds PR, capillary rise may draw water from the groundwater aquifers to supply ET demands, declining water table. These processes characterize the critical two-way water exchange between the unsaturated soils and saturated groundwater aquifers.

Previous studies have suggested that substantial changes to groundwater interactions with unsaturated soils are likely to occur under climate change (Tremblay et al., 2011; Green et al., 2011; Ireson et al., 2013, 2015). Existing modeling studies on the impacts of climate change on groundwater are either at global or basin/location-specific scales (Meixner et al., 2016). Global-level groundwater studies focus on potential future recharge trends (Doll and Fiedler, 2008; Doll, 2009; Green et al., 2011), yet coarse resolution analysis from global climate models (GCMs) provided insufficient specificity to inform decision making. Basin-scale groundwater studies connect the climate with groundwater-flow models to understand the climate impacts on specific systems (Maxwell and Kollet, 2008; Kurylyk and MacQuarrie, 2013; Dumanski et al., 2015). Regional groundwater modeling studies, such as in the Colorado River Basin (Christensen et al., 2004) and in the western U.S. (Niraula et al., 2017), have applied downscaled climate scenarios from GCMs to drive large scale hydrology models. These studies identified research gaps associated with poor representation of groundwater-soil interactions in models and uncertainties in future climate projections.

It is challenging to represent groundwater flows in LSMs because the important two-way water exchange between unsaturated soils and groundwater aquifers was neglected in previous LSMs.

Recently, this two-way exchange has been implemented in coupled land surface – groundwater models (LSM-GW). For example, Maxwell and Miller (2005) used a groundwater model (ParFlow) coupled with the Common Land Model (CLM) as a single column model. They found that the coupled and uncoupled models were very similar in simulated sensible heat flux (SH), ET, and shallow soil moisture (SM), but differed greatly in simulated runoff and deep SM. Later on, Kollet and Maxwell (2008) incorporated the ET effect on redistributing moisture upward from shallow water table depth (WTD) and found the surface energy partitioning is highly sensitive to the WTD when the WTD is less than 5 m below ground surface. Niu et al. (2011) implemented a simple groundwater model (SIMGM, Niu et al., 2007), into the community Noah LSM with multi-parameterization options (Noah-MP LSM), by adding an unconfined aquifer at the bottom of soil layers. More complex features such as three-dimensional subsurface flow and two-dimensional surface were included in ParFlow v3 and evaluated over much of continental North America for a very fine 1-km resolution (Maxwell et al., 2015). These recent development in coupled land and groundwater models have advanced our knowledge on the important interactions between soil and groundwater aquifer.

In cold regions, soil freeze-thaw processes further complicate this two-way exchange. Field studies have found that frozen soil not only influences the timing and amount of downward recharge to aquifers by reducing the soil permeability (Koren et al., 1999; Niu et al., 2006; Kelln et al., 2007), but may also induce upward water transport from aquifers to soil freezing fronts (Spaans and Baker, 1996; Remenda et al., 1996; Hansson et al., 2004). In the modeling community, a range of approaches have been applied to deal with frozen soil parameterizations. Earlier LSMs assumed no significant heat transfer and soil water redistribution for sub-freezing temperature, for example, in simplified SiB and BATS (Xue et al., 1991; Dickinson et al., 1993; Niu and Zeng, 2012). Koren et al. (1999) suggested that the frozen soil is permeable due to macropores that exist in soil structural aggregates, such as cracks, dead root passages, and worm holes. The NoahV3 model adopted this scheme as its default option. Niu and Yang (2006) suggested to separate a model grid into frozen and unfrozen patches, and these two patches have a linear effect on the soil hydraulic properties. This treatment was incorporated into CLM 3.0 and Noah-MP in 2007 and 2011, respectively.

The spatial heterogeneity of soil moisture and WTD requires high-resolution meteorological input that direct outputs from GCMs are too coarse to provide. In GCMs, differences in simulated precipitation stem from the choice of convection parameterization scheme (Sherwood et al., 2014; Prein et al., 2015). An important approach to improve precipitation simulation is to conduct dynamical downscaling using the convection-permitting model (CPM) (Ban et al., 2014; Prein et al., 2015; Liu et al., 2017). The CPM uses a high spatial resolution (usually under 5-km) to explicitly resolve convection without activating convection parameterization schemes. CPMs can also improve the representation of fine-scale topography and spatial variations of surface fields (Prein et al., 2013). These CPM added-values provide an excellent opportunity to investigate water table dynamics in the PPR.

The objectives of this paper are to 1) investigate the performance of a regional scale coupled land-groundwater model in simulating groundwater water levels, recharge and storage in a seasonally frozen environment in PPR; and 2) explore the possible impacts of climate change on these processes. In this paper, we use a physical process-based LSM (Noah-MP) coupled with a

groundwater dynamics model (MMF model). The coupled Noah-MP-MMF model is driven by two sets of meteorological forcing for 13 years under current and future climate scenarios. These two sets of meteorological datasets are from a CPM dynamical downscaling project using the Weather Research & Forecast (WRF) model with 4-km grid spacing covering the Contiguous U.S. and Southern Canada (WRF CONUS, Liu et al., 2017). The paper is structured as follows: Section 4.2 introduces the groundwater observations for WTD evaluation in the PPR, the coupled Noah-MP-MMF model, and the meteorological forcing from the WRF CONUS project. Section 4.3 evaluates the model simulated WTD timeseries and shows the groundwater budget and hydrological changes due to climate change. Section 4.4 and 4.5 offer a broad discussion and conclusion.

4.2 Data and Methods

4.2.1 Observation data

Groundwater observation data were obtained through several agencies: (1) the United States Geological Survey (USGS) National Water Information System in the U.S. (https://waterdata.usgs.gov/nwis/gw), (2) the Alberta Environment (http://aep.alberta.ca/water/programs-and-services/groundwater/groundwater-observation-well-network/default.aspx), (3) the Saskatchewan Water Security Agency (https://www.wsask.ca/Water-Info/Ground-Water/Observation-Wells/).

Initially, groundwater data from 160 wells were acquired, 72 in the U.S., 43 from Alberta, and 45 from Saskatchewan. We used the following criteria to select qualified stations for our study and evaluate our model performance against these observations:

1) the locations of the wells are within the PPR region.
2) a sufficiently long data record exists during the simulation period. We define the observation availability as the available observation period within the 13-year simulation period and select wells with observation availability greater than 80%.
3) we only take data from unconfined aquifers with shallow groundwater levels (mean WTD > 5 m).
4) we only take data with minimal anthropogenic effects (such as from pumping or irrigation).

These criteria reduced the observation data to 33 well records, with six in Alberta, 13 in Saskatchewan and 14 from the U.S. Table 4.1 summarizes the information for each selected well, and Figure 4.1(a) shows the location of the wells in our study area. It is noteworthy that most of the groundwater sites have more permeable deposits (sand and gravel) as provincial and state agencies don't monitor low permeability formations. More information about the selecting criteria is provided in the Appendix C.

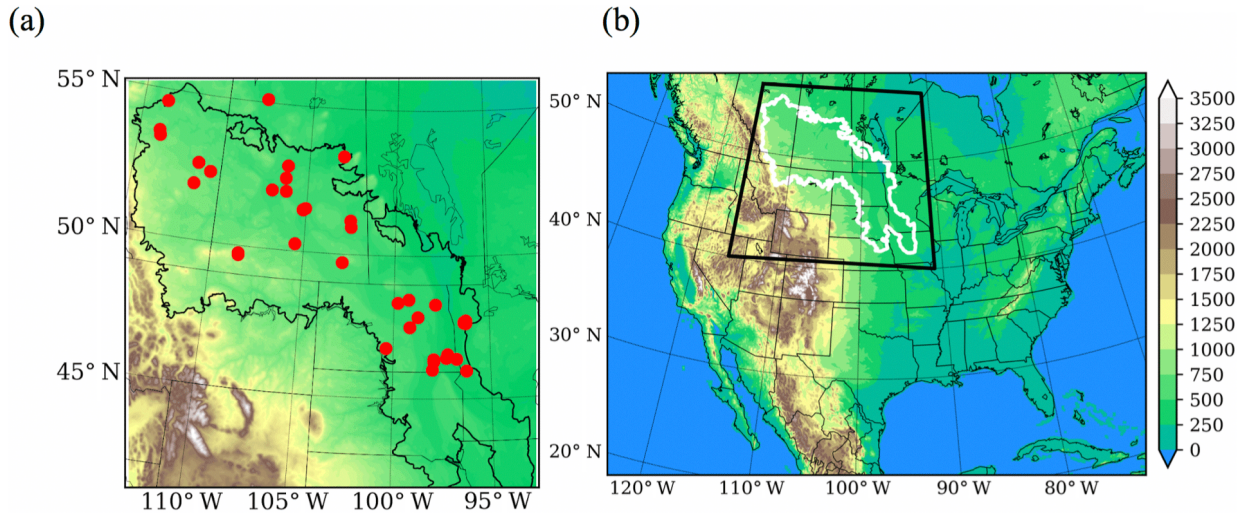

Figure 4.1. (a) Topography of the Prairie Pothole Region (PPR) and station location of rain gauges (black dots) and groundwater wells (red diamonds); (b) Topography of the WRF CONUS domain, with the black box indicating the PPR domain.

Table 4.1. Summary of the locations and aquifer type and soil type of the 33 selected wells.

Site Name/ Site No.	Lat	Lon	Elev (m)	Aquifer type	Aquifer Lithology	Model Elevation (m)	Model Soil type
Devon 0162	53.41	-113.76	700.0	Unconfined	Sand	697.366	Sandy loam
Hardisty 0143	52.67	-111.31	622.0	Unconfined	Gravel	633.079	Loam
Kirkpatrick Lake 0229	51.95	-111.44	744.5	Semi-confined	Sandstone	778.311	Sandy loam
Metiskow 0267	52.42	-110.60	677.5	Unconfined	Sand	679.516	Loamy sand
Wagner 0172	53.56	-113.82	670.0	Surficial	Sand	670.845	Silt loam
Narrow Lake 252	54.60	-113.63	640.0	Unconfined	Sand	701.000	Clay loam
Baildon 060	50.25	-105.50	590.184	Surficial	-	580.890	Sandy loam
Beauval	55.11	-107.74	434.300	Intertill	Sand	446.500	Sandy loam
Blucher	52.03	-106.20	521.061	Intertill	Sand/Gravel	523.217	Loam
Crater Lake	50.95	-102.46	524.158	Intertill	Sand/Gravel/Clay	522.767	Loam
Duck Lake	52.92	-106.23	502.920	Surficial	Sand	501.729	Loamy sand
Forget	49.70	-102.85	606.552	Surficial	Sand	605.915	Sandy loam
Garden Head	49.74	-108.52	899.160	Bedrock	Sand/Till	894.357	Clay loam
Nokomis	51.51	-105.06	516.267	Bedrock	Sand	511.767	Clay loam
Shaunavon	49.69	-108.50	896.040	Bedrock	Sand/Till	900.433	Clay loam
Simpson 13	51.45	-105.18	496.620	Surficial	Sand	493.313	Sandy loam
Simpson 14	51.457	-105.19	496.600	Surficial	Sand	493.313	Sandy loam
Yorkton 517	51.17	-102.50	513.643	Surficial	Sand/Gravel	511.181	Loam
Agrium 43	52.03	-107.01	500.229	Intertill	Sand	510.771	Loam
460120097591803	46.02	-97.98	401.177	Alluvial	Sand/Gravel	400.381	Sandy loam
461838097553402	46.31	-97.92	401.168	-	Sand/Gravel	404.719	Clay loam
462400097552502	46.39	-97.92	409.73	-	Sand/Gravel	407.405	Sandy loam
462633097163402	46.44	-97.27	325.52	Alluvial	Sand/Gravel	323.728	Sandy loam
463422097115602	46.57	-97.19	320.40	Alluvial	Sand/Gravel	314.167	Sandy loam
464540100222101	46.76	-100.37	524.91	-	Sand/Gravel	522.600	Clay loam
473841096153101	47.64	-96.25	351.77	Surficial	Sand/Gravel	344.180	Loamy sand
473945096202402	47.66	-96.34	327.78	Surficial	Sand/Gravel	328.129	Sandy loam
474135096203001	47.69	-96.34	325.97	Surficial	Sand/Gravel	327.764	Sandy loam
474436096140801	47.74	-96.23	341.90	Surficial	Sand/Gravel	336.210	Sandy loam
475224098443202	47.87	-98.74	451.33	-	Sand/Gravel	450.463	Sandy loam
481841097490301	48.31	-97.81	355.61	-	Sand/Gravel	359.568	Clay loam
482212099475801	48.37	-99.79	488.65	-	Sand/Gravel	488.022	Sandy loam
CRN Well WLN03	45.98	-95.20	410.70	Surficial	Sand/Gravel	411.400	Sandy loam

4.2.2 Groundwater and Frozen soil scheme in Noah-MP LSM

In the present study, we used the community Noah-MP LSM (Niu et al., 2011; Yang et al., 2011) coupled with a GW model – the MMF model (Fan et al., 2007; Miguez-Macho et al., 2007). This coupled model has been applied in many regional hydrology studies in offline mode (Miguez-Macho and Fan, 2012; Martinez et al., 2016) and has also been coupled with regional climate models (Anyah et al., 2008; Barlage et al., 2015). Here, we present a brief introduction to the MMF groundwater scheme and the frozen soil scheme in Noah-MP; further details can be found in previous studies (Fan et al., 2007; Miguez-Macho et al., 2007; Niu and Yang, 2006).

Figure 4.2 is a diagram of the structure of four soil layers (0.1, 0.3, 0.6, and 1.0 m) and the underlying unconfined aquifer in Noah-MP-MMF. The MMF scheme explicitly defines an unconfined aquifer below the 2 m soil level and an auxiliary soil layer stretching to the WTD, which varies in space and time (m). The thickness of this auxiliary layer, z_{aux} (m), is also variable, depending on the WTD:

$$z_{aux} = \begin{cases} 1, & WTD \geq -3 \\ -2 - WTD, & WTD < -3 \end{cases} \qquad (4.1)$$

The vertical fluxes include gravity drainage and capillary flux, solved from the Richards' equation,

$$q = K_\theta \left(\frac{\partial \psi}{\partial z} - 1\right), \quad K_\theta = K_{sat} * \left(\frac{\theta}{\theta_{sat}}\right)^{2b+3}, \quad \psi = \psi_{sat} * \left(\frac{\theta_{sat}}{\theta}\right)^{b} \qquad (4.2)$$

where q is water flux between two adjacent layers [m/s], K_θ is the hydraulic conductivity [m/s] at certain soil moisture content θ [m3/m3], ψ is the soil matric potential [m] and b is soil pore size index. The subscript sat denotes saturation. The recharge flux from/to the layer above WTD, R, can be obtained according to WTD:

$$R = \begin{cases} K_k * \left(\frac{\psi_i - \psi_k}{z_{soil(i)} - z_{soil(k)}} - 1\right), & WTD \geq -2 \\ K_{aux} * \left(\frac{\psi_4 - \psi_{aux}}{(-2) - (-3)} - 1\right), & -2 > WTD \geq -3 \\ K_{sat} * \left(\frac{\psi_{aux} - \psi_{sat}}{(-2) - (WTD)} - 1\right), & WTD < -3 \end{cases} \qquad (4.3)$$

In the first case, WTD is in the resolved soil layers and z_{soil} is the depth of soil layer with the subscript k indicating the layer containing WTD while i is the layer above. The calculated water table recharge is then passed to the MMF groundwater routine.

The change of groundwater storage in the unconfined aquifer considers three components: recharge flux (R), river discharge (Q_r), and lateral flows (Q_{lat}):

$$\Delta S_g = (R - Q_r + \sum Q_{lat}) \qquad (4.4)$$

where S_g [mm] is groundwater storage, Q_r [mm] is the water flux of groundwater-river exchange, and $\sum Q_{lat}$ [mm] are groundwater lateral flows to/from all surrounding grid cells. The groundwater lateral flow ($\sum Q_{lat}$) is the total horizontal flows between each grid cell and its neighbouring grid cells, calculated from Darcy's law with the Dupuit–Forchheimer approximation (Fan and Miguez-Macho 2010), as:

$$Q_{lat} = wT \left(\frac{h - h_n}{l}\right) \qquad (4.5)$$

where w is the width of cell interface [m], T is the transmissivity of groundwater flow [m^2/s], h and h_n are the water table head [m] of local and neighboring cell, and l is the length [m] between cells. T depends on hydraulic conductivity K and WTD:

$$T = \begin{cases} \int_{-\infty}^{h} K\,dz & WTD \geq -2 \\ \int_{-\infty}^{(z_{surf}-2)} K\,dz + \sum K_i * dz_i & WTD < -2 \end{cases} \quad (4.6)$$

For $WTD < -2$, K is assumed to decay exponentially with depth, $K = K_4 \exp(-z/f)$, K_4 is the hydraulic conductivity in the 4-th soil layer and f is the e-folding length and depends on terrain slope. For WTD ≥ -2, i represents the number of layers between the water table and the 2-m bottom and z_{surf} is the surface elevation.

The river flux (Q_r) is also represented by a Darcy's law–type equation, where the flux depends on the gradient between the groundwater and the river depth and the riverbed conductance:

$$Q_r = RC \cdot (h - z_{river}) \quad (4.7)$$

with z_{river} is the depth of river [m] and RC is dimensionless river conductance, which depends on the slope of the terrain and equilibrium water table. Eq. (8) is a simplification which uses z_{river} rather than the water level in the river and, for this study, we only consider one-way discharge from groundwater to rivers. Finally, the change of WTD is calculated as the total fluxes fill or drain the pore space between saturation and the equilibrium soil moisture state (θ_{eq} [m3/m3]) in the layer containing WTD:

$$\Delta\text{WTD} = \frac{\Delta S_g}{(\theta_{sat} - \theta_{eq})} \quad (4.8)$$

If ΔS_g is greater than the pore space in the current layer, the soil moisture content of current layer is saturated and the WTD rises to the layer above, updating the soil moisture content in the layer above as well. Vice versa for negative ΔS_g as water table declines and soil moisture decreases.

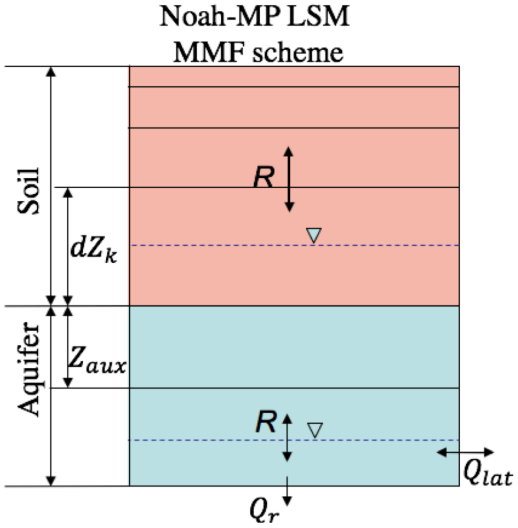

Figure 4.2. Structure of the Noah-MP LSM coupled with MMF groundwater scheme, the top 2-m soil of 4 layers whose thicknesses are 0.1, 0.3, 0.6 and 1.0 m. An unconfined aquifer is added below the 2-m boundary, including an auxiliary layer and the saturated aquifer. Positive flux of R denotes downward transport. Two water table are shown, one within the 2-m soil and one below, indicating the model is capable to deal with both shallow and deep water tables.

There are two options in Noah-MP LSM for frozen soil permeability; option 1, the default option in Noah-MP, is from Niu and Yang (2006) and option 2 is inherited the Koren et al. (1999) scheme from NoahV3. Option 1 assumes that a model grid cell consists of permeable and impermeable patches and the area weighted sum of these patches gives the grid cell soil hydraulic properties. Thus, the total soil moisture (θ) in the grid cell is used to compute hydraulic properties as:

$$\theta = \theta_{ice} + \theta_{liq} \qquad (9)$$

$$K = \left(1 - F_{frz}\right)K_u = \left(1 - F_{frz}\right)K_{sat}\left(\frac{\theta}{\theta_{sat}}\right)^{2b+3} \qquad (4.10)$$

the subscript frz and u denote the frozen and unfrozen patches in the grid point. The impermeable frozen soil fraction is parameterized as:

$$F_{frz} = e^{-\alpha(1-\theta_{ice}/\theta_{sat})} - e^{-\alpha} \qquad (4.11)$$

α = 3.0 is an adjustable parameter. The amount of the liquid water in soil layer is either θ_{liq} or $\theta_{liq,max}$, the maximum amount of liquid water, which is calculated by a more general form of the freezing-point depression equation:

$$\theta_{liq,max} = \theta_{sat}\left\{\frac{10^3 L_f\left(T_{soil} - T_{frz}\right)}{gT_{soil}\psi_{sat}}\right\}^{-\frac{1}{b}} \qquad (4.12)$$

where T_{soil} and T_{frz} are soil temperature and freezing point [K]; L_f is the latent heat of fusion [J kg^{-1}]; g is gravitational acceleration [m s^{-2}].

On the other hand, the option 2 uses only the liquid water volume to calculate hydraulic properties and assumes a non-linear effect of frozen soil on permeability. Also, the option 2 uses a variant of freezing-point depression equation with an extra term, $(1 + 8\theta_{ice})^2$, to account for the increased interface between soil particles and liquid water due to the increase of ice crystals. Generally, option 1 assumes that soil ice has a smaller effect on infiltration and simulates more permeable frozen soil than option 2 (Niu et al., 2011). For this reason, the option 1 allows the soil water to move and redistribute more easily within the frozen soil and we decide to use option 1 in our study.

4.2.3 Forcing Data

The output from the WRF CONUS dataset (Liu et al. 2017) are used as meteorological forcing to drive the Noah-MP-MMF model. The WRF CONUS project consists of two simulations. The first simulation is referred as the current climate scenario, or control run (CTRL), from Oct 2000 to Sep 2013, and forced with the 6-hourly 0.7° ERA-Interim reanalysis data. The second simulation is a perturbation to reflect the future climate scenario, closely following the pseudo global warming (PGW) approach in previous works (Rasmussen et al., 2014). The PGW simulation is forced with 6-hourly ERA-Interim reanalysis data plus a delta climate change signal derived from an ensemble of CMIP5 models under the RCP8.5 emission scenario and reflects the climate change signal between the end of the 21st and 20th century.

Figure 4.3 shows the annual precipitation in the PPR from 4-km WRF CONUS from the current climate and 32-km North America Regional Reanalysis (NARR, another reanalysis dataset commonly used for land surface model forcing). Both datasets show similar annual precipitation pattern and bias patterns compared to observations: underestimating of precipitation in the east and overestimating in the west. However, the WRF CONUS shows significant improvement of percentage bias in precipitation ((Model-Observation)/Observation) over the western PPR. For the consistency of the same source of data for current and future climate, the WRF-CONUS is the best available dataset for the coupled land-groundwater study in the PPR.

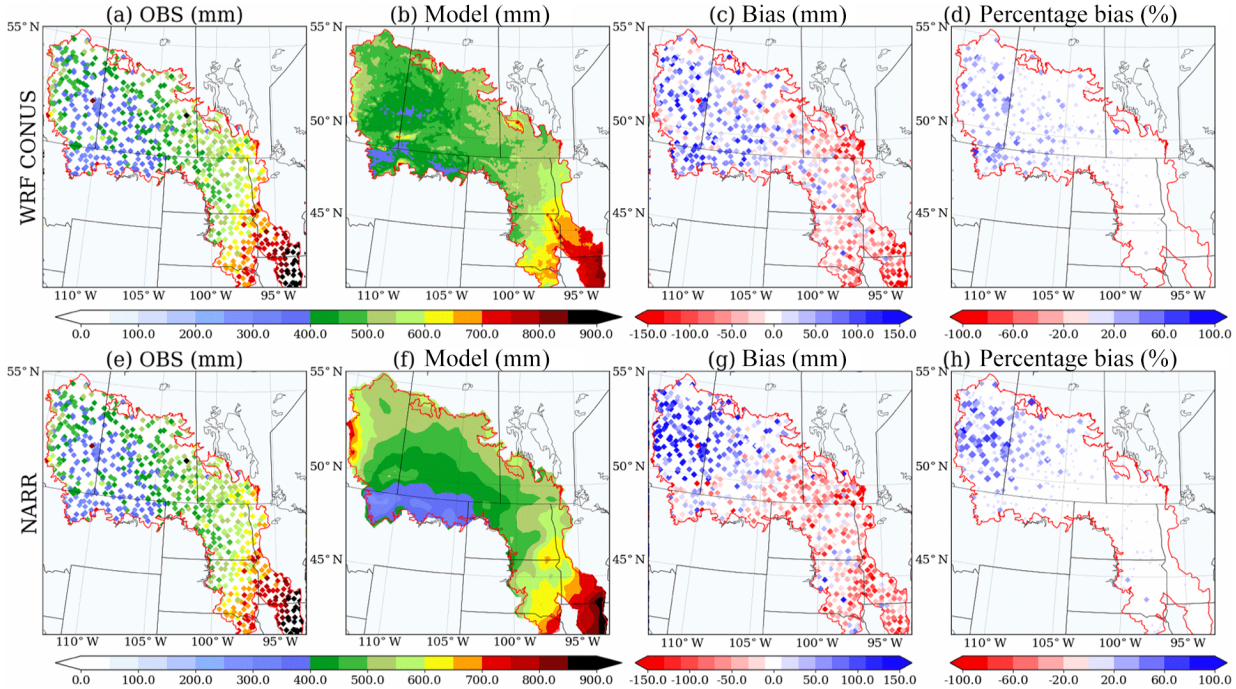

Figure 4.3. Evaluation of the annual precipitation from WRF CONUS (top) and NARR (bottom) against rain gauge observation.

For the future climate study, the precipitation and temperature of the PGW climate forcing are shown in Figure 4.4 and 4.5. WRF CONUS projects more precipitation in the PPR, except in the southeast of the domain in summer, where it shows a precipitation reduction of about 50–100 mm. In contrast, WRF CONUS projects that the strongest warming will occur in the northeastern PPR in winter (about 6–8 ◦C

as shown in Figure 4.5). Another significant warming signal occurs in summer in the southeast of the domain, corresponding to the reduction of future precipitation, as seen in Figure 4.4.

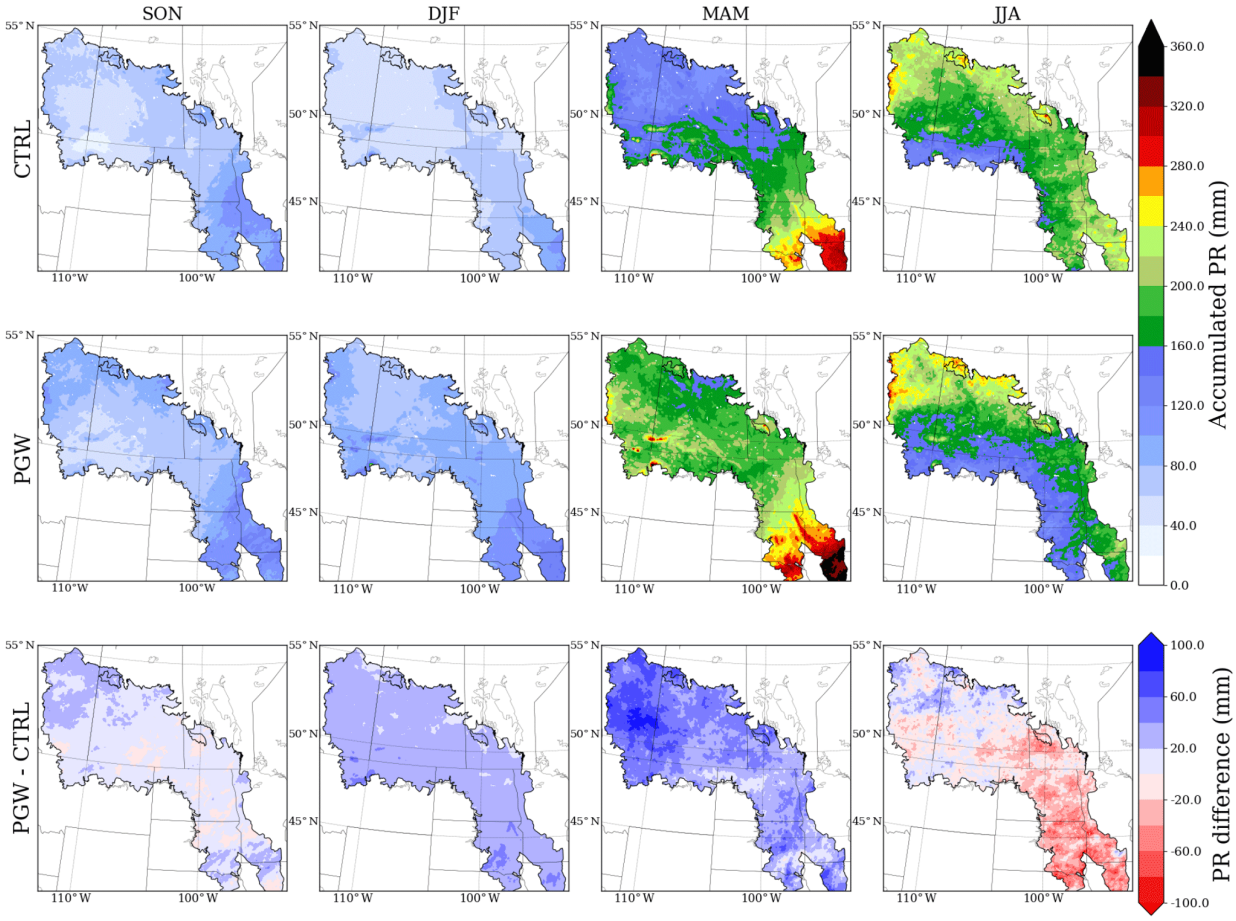

Figure 4.4. Seasonal accumulated precipitation from current climate scenario (CTRL), future climate scenario (PGW) and projected change (PGW-CTRL) in the forcing data.

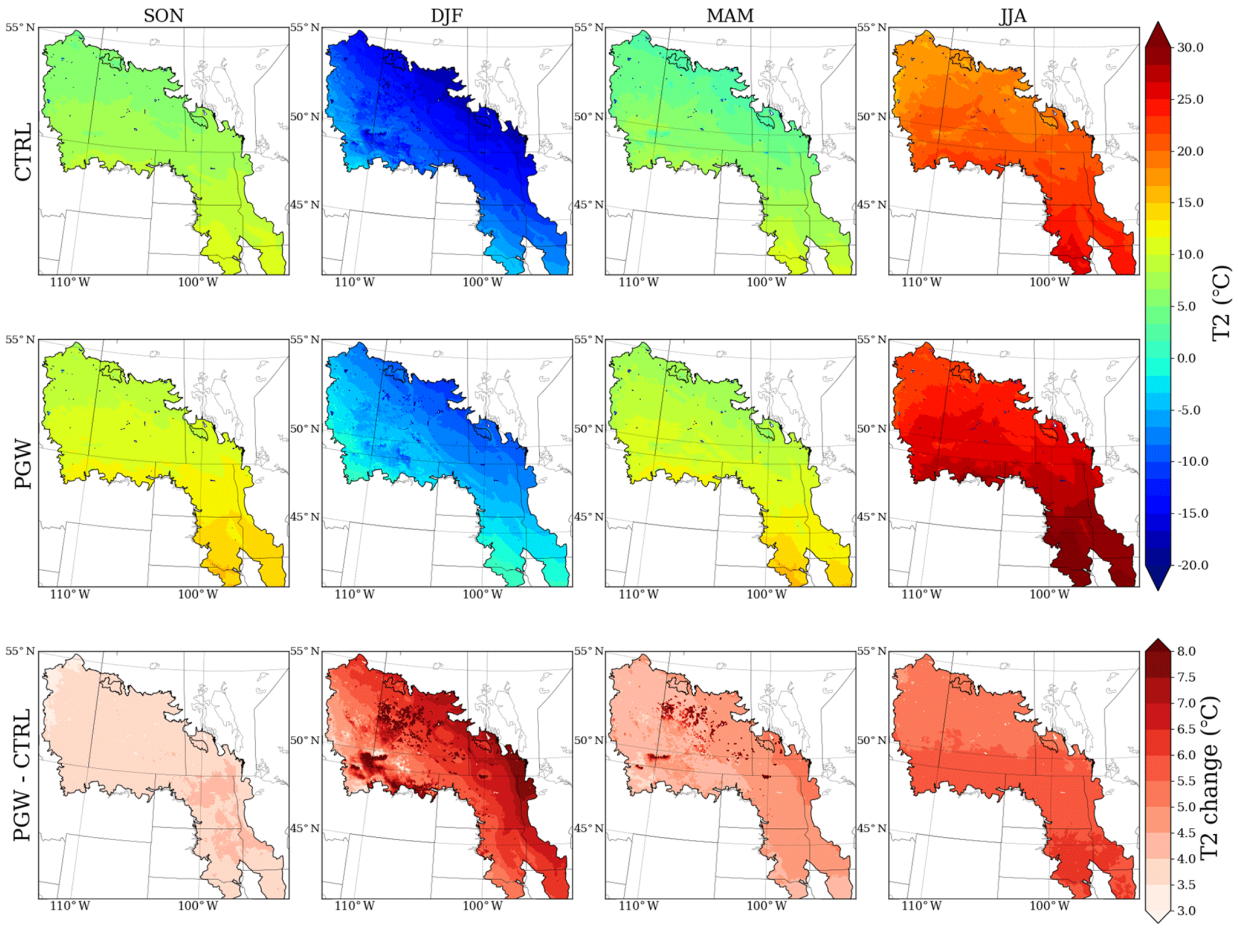

Figure 4.5. Seasonal averaged temperature from CTRL, PGW, and the projected change (PGW-CTRL).

2.4 Model Setup

The two Noah-MP-MMF simulations representing the current climate and future climate are denoted as CTRL and PGW, respectively. The initial groundwater levels are from a global 1-km equilibrium groundwater map (Fan et al., 2013) and the equilibrium soil moisture for each soil layer is calculated at the first model timestep with climatology recharge, spinning up for 500 years. Since the model domain is at a different resolution than the input data, the appropriate initial WTD at 4-km may be different than the average at 1-km. To properly initialize the simulation, we spin up the model using the forcing of current climate (CTRL) for the years from 2000 to 2001 repeatedly (in total 10 loops).

Due to different data sources, the default soil types along the boundary between the U.S. and Canada are discontinuous. Thus, we use the global 1-km fine soil data (Shangguan et al., 2014, http://globalchange.bnu.edu.cn/research/soilw) in our study region. The soil properties for the aquifer use the same properties as the lowest soil layer from the Noah-MP 2-m soil layers.

4.3 Results

4.3.1 Comparison with groundwater observations

According to the locations of 33 groundwater wells in Table 1, the simulated WTD from the closest model grid points are extracted. Figure 4.6 shows the modeled WTD bias from the CTRL run. We also select the monthly WTD timeseries from 8 sites, the observations are in black dots and CTRL in blue lines. See Appendix C for the timeseries of 33 sites. The model produces reasonable values of mean WTD, the mean biases are smaller than 1 m in most of sites, except in Alberta, where the model predicts deep bias about 5 m in the northwestern part of PPR. The model also successfully captures the annual cycle of WTD, which rises in spring and early summer, because of snowmelt and rainfall recharge, and declines in summer and fall, because of high ET, and in winter because of frozen near-surface soil. In all observations, the timing of the water table rising, and dropping is well simulated, as the timing and amount of infiltration and recharge in spring is controlled by the freeze-thaw processes in seasonally frozen soil.

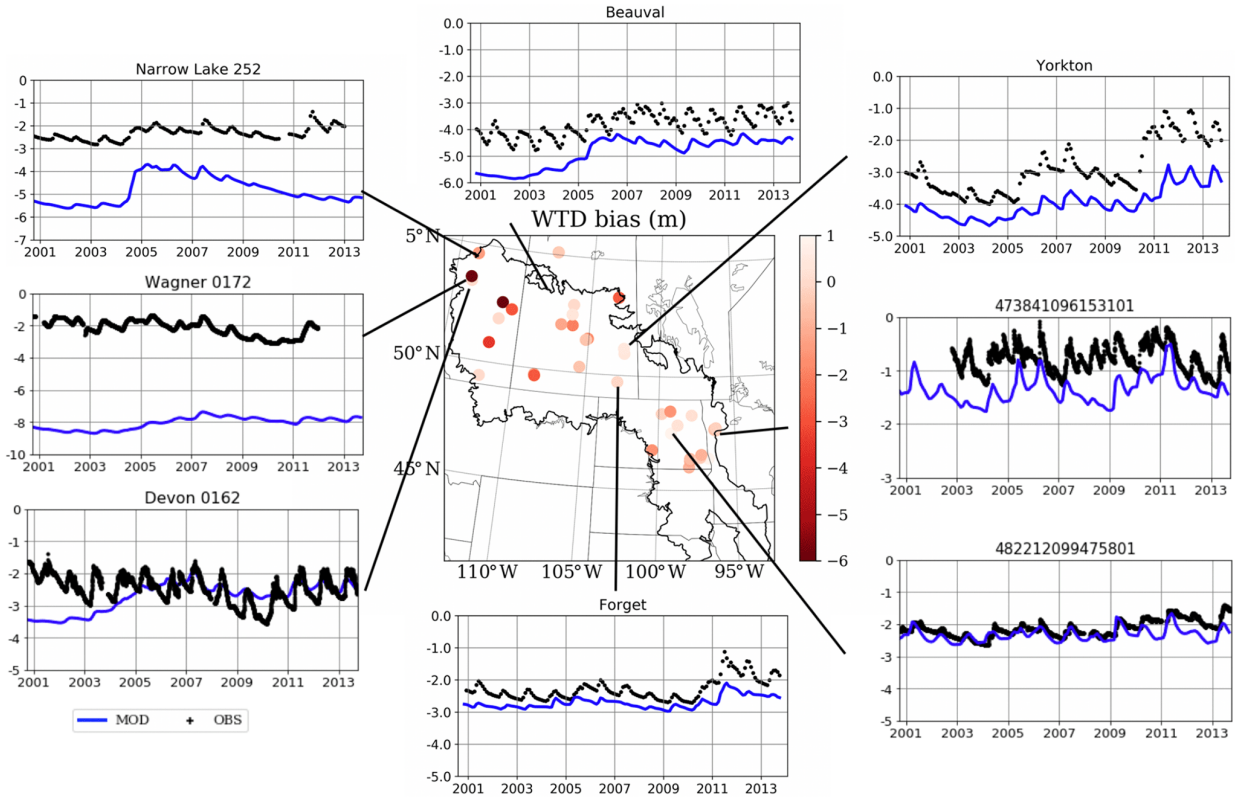

Figure 4.6. WTD (m) bias from CTRL simulation and timeseries from 8 groundwater wells in PPR (black for observation and blue for CTRL model simulation). See Table 4.2 CTRL column for the model statistics and Appendix C for complete timeseries from 33 wells.

On the other hand, the model simulated WTD seasonal variation is smaller than observations. The small seasonal variation could be due to the misrepresentation between the lithology from the observational surveys and the soil types in the model grids. As mentioned in Section 4.2.2, the groundwater aquifer uses the same soil types as the bottom layer of the resolved 2-m soil layers. While sand and gravel are the dominant lithology in most of the sites, they are mostly clay and loam in the model (Table 4.1). For sandy soil reported in most of the sites, small capacity and fast responses to infiltration lead to large water table fluctuations, whereas, in the model, clay and loam soil allows low permeability and large capacity and smoothens responses to recharge and capillary

effects. Furthermore, the 4-layer soils are vertically homogeneous in soil type and the groundwater model uses the lowest level soil type as the aquifer lithology. For many parts of the PPR, where groundwater levels are perched at the top 5-m due to a layer called glacial till. These geohydrological characteristics cannot be reflected in this model and contribute to the deep WTD bias simulated in Alberta. This shortcoming of the model was also reported in a study taken place in the Amazon rainforest (Miguez-Macho et al., 2012).

4.3.2 Climate change signal in Groundwater fluxes

The MMF groundwater model simulates three components in the groundwater water budget, the recharge flux (R), lateral flow (Q_{lat}), and discharge flux to rivers (Q_r). Because the topography is usually flat in the PPR, the magnitude of groundwater lateral transport is very small (Q_{lat} less than 5 mm per year). On the other hand, the shallow water table in the PPR region is higher than the local riverbed, thus, the Q_r term is always discharging from groundwater aquifers to rivers. As a result, the recharge term is the major contributor to the groundwater storage in the PPR, and its variation (usually between -100 to 100 mm) dominates the timing and amplitude of the water table dynamics. The seasonal accumulated total groundwater fluxes in the PPR (R+$Q_{lat} - Q_r$) are shown in Figure 4.7. The positive (negative) flux in blue (red) means the groundwater aquifer is gaining (losing) water, causing the water table to rise (decline).

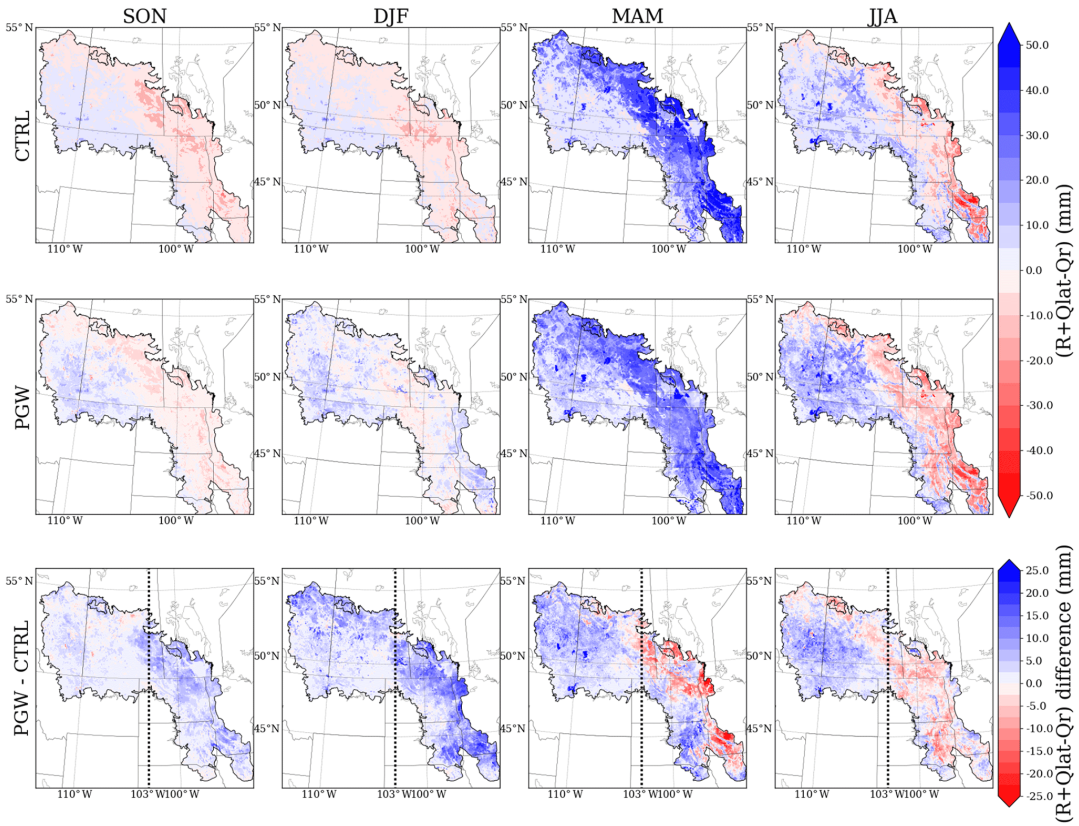

Figure 4.7. Seasonal accumulated total groundwater fluxes ($R + Q_{lat} + Q_r$) for current climate (CTRL, top), future climate (PGW, middle) and projected change (PGW-CTRL, bottom) in forcing data. Black dashed lines in PGW-CTRL separate the PPR into eastern and western halves.

Under current climate conditions, the total groundwater fluxes show strong seasonal fluctuations, consistent with the WTD timeseries shown in Figure 4.6. On average, in fall (SON) and winter (DJF), there is a 20-mm negative recharge, driven by the capillary effects and drawing water from aquifer to dry soil above. Spring (MAM) is usually the season with a strong positive recharge because snowmelt provides a significant amount of water, and soils thawing allow infiltration. The large amount of snowmelt water contributes to more than 100 mm of positive recharge in the eastern domain. It is until summer (JJA), when strong ET depletes soil moisture and results in about 50 mm of negative recharge.

Under future climate conditions, the increased PR in fall and winter leads to wetter upper soil layers, resulting in a net positive recharge flux (PGW – CTRL in SON and DJF). However, the PGW summer is impacted by increased ET under a warmer and drier climate, due to higher temperature and less PR. As a result, the groundwater uptake by the capillary effect is more critical in the future summer. Furthermore, there is a strong east-to-west difference in the total groundwater flux change from PGW to CTRL. In the eastern PPR, the change in total groundwater flux exhibits obvious seasonality while the model projects persistent positive groundwater fluxes in the western PPR.

4.3.3 Water budget analysis

Figure 4.8 and 4.9 show the water budget analysis for the eastern and western PPR (divided by the dotted line in 103° W in Figure 4.7), respectively. Four components are presented in the figures, i.e. (1) PR and ET; (2) surface and underground runoff (*SFCRUN* and *UDGRUN*); and surface snowpack; (3) the change of soil moisture storage and (4) groundwater fluxes and the change of storage. In the current and future climate, these budget terms are plotted in annual accumulation ((a) and (b) for CTRL and PGW), whereas their difference are plotted in each month individually ((c) for PGW-CTRL).

Under current climate conditions, during snowmelt infiltration and rainfall events, water infiltrates into the top soil layer, travels through the soil column and exits the bottom of the 2-m boundary, hence, the water table rises. During the summer dry season, ET is higher than PR and the soil layers lose water through ET, therefore, the capillary effect takes water from the underlying aquifer and the water table declines. In winter, the near-surface soil in the PPR is seasonally frozen, thus, a redistribution of subsurface water to the freezing front results in negative recharge, and the water table declines.

In the eastern PPR, the effective precipitation (PR-ET) is found to increase from fall to spring but decrease in summer in PGW (Figure 4.8(1c)). Warmer falls and winters in PGW, together with increased PR, not only delay snow accumulation and bring forward snowmelt, but also change the precipitation partition – more as rain and less as snow. This warming causes up to 20 mm of snowpack loss (Figure 4.8(2c)). The underground runoff starts much earlier in PGW (December) (Figure 4.8(2b)) than in CTRL (February) (Figure 4.8(2a)). On the other hand, the warming in PGW also changes the partitioning of soil ice and soil water in unsaturated soil layers (Figure 4.8(3c)). For late spring in PGW, the springtime recharge in the future is significantly reduced due to early melting and less snowpack remaining (Figure 4.8(4c)). In the PGW summer, reduced PR (50 mm less) and higher temperatures (8 °C warmer) lead to reduction in total soil moisture, and a stronger negative recharge from the aquifer. Therefore, the increase of recharge from fall to early

spring compensates the recharge reduction due to stronger ET in summer in the eastern PPR, and changes little in the annual mean groundwater storage (1.763 mm per year).

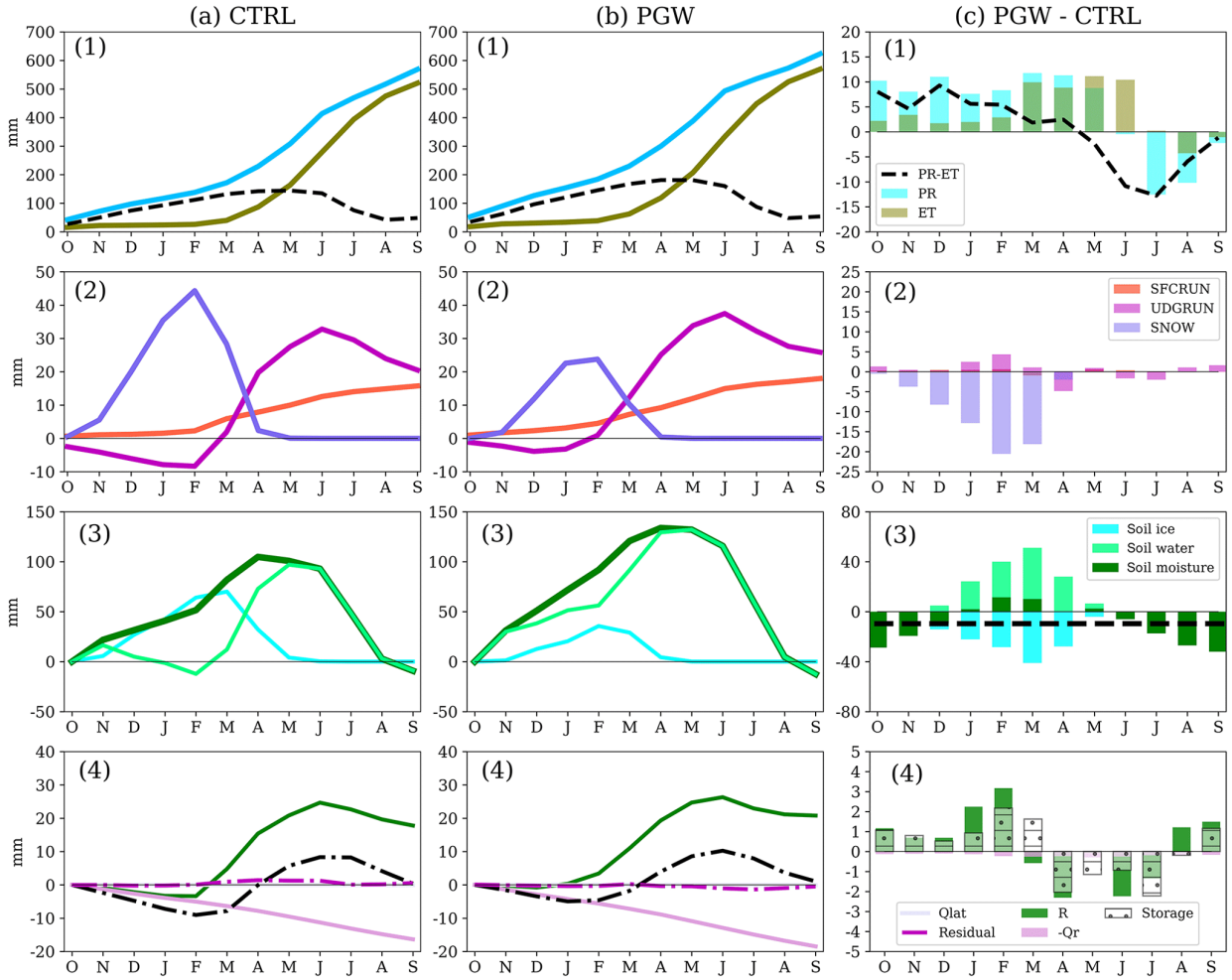

Figure 4.8. Water budget analysis in the eastern PPR in (a) CTRL, (b) PGW and (c) PGW – CTRL. Water budget terms include: (1) *PR & ET*, (2) surface snow, surface runoff and underground runoff (*SNOW*, *SFCRUN*, and *UDGRUN*), (3) change of soil moisture storage (soil water, soil ice and total soil moisture, ΔSMC) and (4) groundwater fluxes and the change of groundwater storage (R, Q_{lat}, Q_r, ΔS_g). The annual mean soil moisture change (PGW-CTRL) is shown with black dashed line in (3). The Residual term is defined as $Res = (R+Q_{lat}-Q_r)-\Delta S_g$ in (4). Note that in (a) and (b) the accumulated fluxes and change in storage are shown in lines, whereas in (c) the difference in (PGW-CTRL) is shown for each individual month in bars.

These changes in water budget components in the western PPR (Figure 4.9) are similar to those in the eastern PPR (Figure 4.8), except in summer. The reduction in summer PR in the western PPR (less than 5 mm reduction) is not as obvious as that in the eastern PPR (50 mm reduction) (Figure 4.4). Thus, annual mean total soil moisture in future is about the same as in current climate (Figure 4.9(3c)) and results in little negative recharge in PGW summer (Figure 4.9(4c)). Therefore, the increase in annual recharge is more significant (10 mm per year), an increase of about 50% of the annual recharge in the current climate (20 mm per year) (Figure 4.9(4c)).

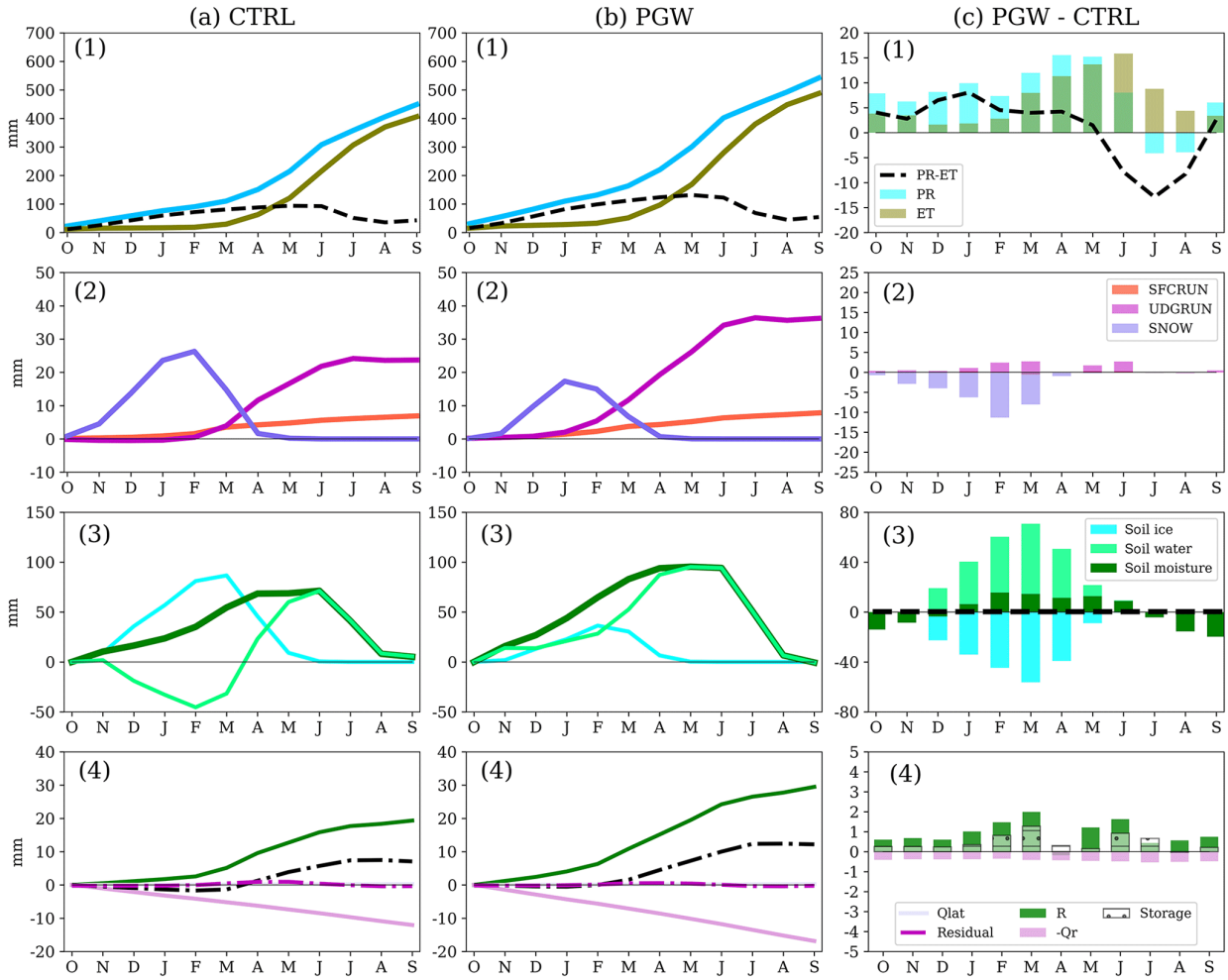

Figure 4.9. Same as Figure 4.8. Water budget analysis in the **western PPR**: in (a) CTRL, (b) PGW and (c) PGW – CTRL. Water budget terms include: (1) *PR & ET*, (2) surface snow, surface runoff and underground runoff (*SNOW*, *SFCRUN*, and *UDGRUN*), (3) change of soil moisture storage (soil water, soil ice and total soil moisture, ΔSMC) and (4) groundwater fluxes and the change of groundwater storage ($R, Q_{lat}, Q_r, \Delta S_g$). The annual mean soil moisture change (PGW-CTRL) is shown with black dashed line in (3). The Residual term is defined as $Res = (R+Q_{lat}-Q_r)-\Delta S_g$ in (4). Note that in (a) and (b) the accumulated fluxes and change in storage are shown in lines, whereas in (c) the difference in (PGW-CTRL) is shown for each individual month in bars.

In both the eastern and western PPR, the water budget components for the groundwater aquifer are plotted in Figure 4.8(4) and Figure 4.9(4), with the changes of each flux (PGW-CTRL) printed at the bottom. The groundwater lateral flow is a small term in areal average and has little impact on the groundwater storage. Nearly half of the increased recharge in both the eastern and western PPR is discharged to river flux (Q_r = 2.26 mm out of R = 4.15 mm in the eastern PPR and Q_r = 5.20 mm out of R = 10.72 mm in western PPR). Therefore, the groundwater storage change in the eastern PPR (1.76 mm per year) is not as great as that in the western PPR (5.39 mm per year).

These two regions of the PPR show differences in hydrological response to future climate because of the spatial variation of the summer PR. As shown in both Figure 4.4 (PGW-CTRL), Figure 4.8(1) and Figure 4.9(1), the reduction of future PR in summer in the eastern PPR is significant (50 mm).

The spatial difference of precipitation changes in the PPR further results in the recharge increase doubling in the western PPR compared to the eastern PPR.

4.4. Discussion

4.4.1 Improving WTD Simulation

In Section 4.3.1, we show that the model is capable of simulating the mean WTD in most sites yet predicts deep groundwater in Alberta and underestimates its seasonal variation. These results may be due to misrepresentations between model default soil type and the soil properties in the observational wells. To test this theory, an additional simulation, REP, is conducted by replacing the default soil types in the locations of these 33 groundwater wells with sand-type soil, which is the dominant soil types reported from observational surveys. The timeseries of the REP and default CTRL are shown in Figure 4.10 (also see Appendix C for the complete 33 sites) and a summary of the mean and standard deviation of the two simulations are provided in Table 4.2.

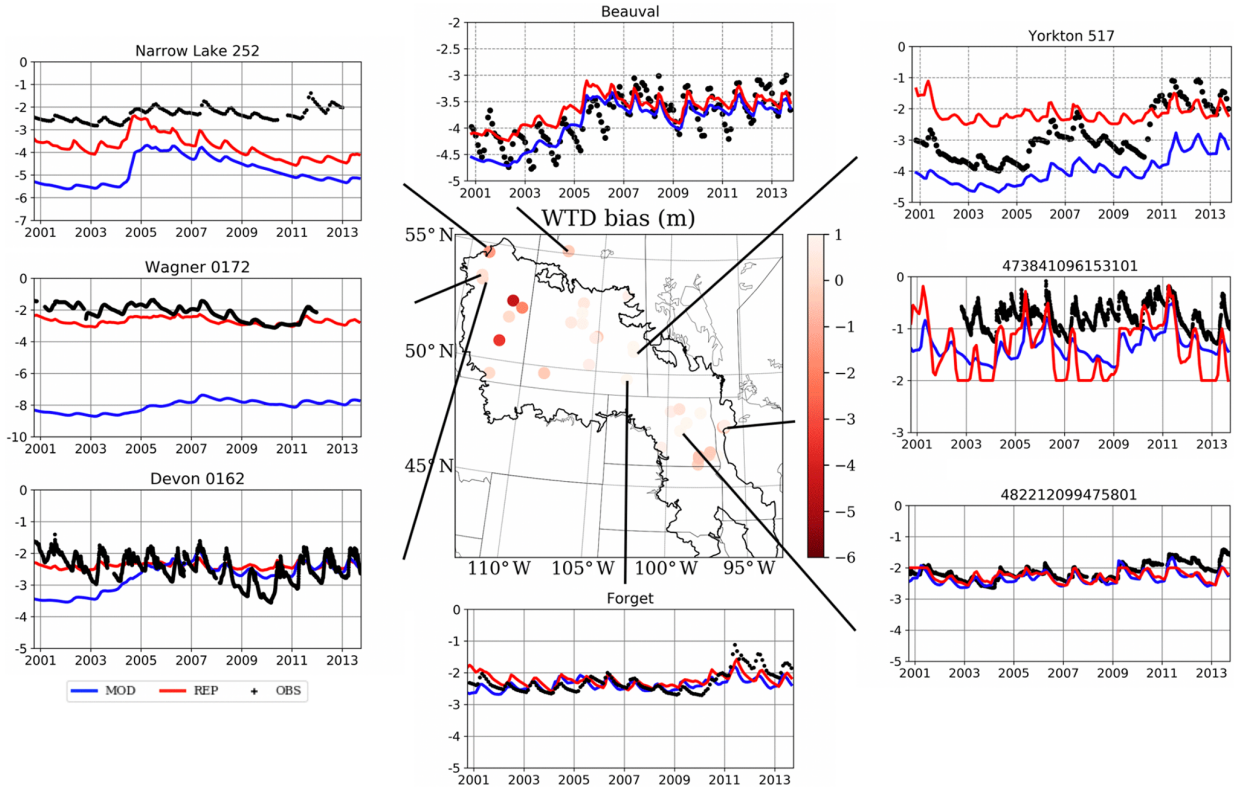

Figure 4.10. Same as Figure 4.6, WTD (m) bias from CTRL simulation and timeseries from 8 groundwater wells in PPR (black for observation and blue for CTRL model simulation, and red for the replacing soil type simulation). REP is the additional simulation by replacing the default soil type in the model with sandy soil type.

Table 4.2. Summary of mean and standard deviation (std) of WTD from 33 groundwater wells, from observation records (OBS), default model (CTRL) and replacing with sand soil simulation (REP). Bold texts indicate improvement in the REP than the CTRL run.

Site Name/Number	OBS_mean	CTRL_mean	REP_mean	OBS_std	CTRL_std	REP std
Devon 0162	-2.46	-2.69	**-2.38**	0.43	0.45	0.09
Hardisty 0143	-2.44	-8.91	**-6.88**	0.41	0.64	**0.36**
Kirkpatrick Lake 0229	-4.22	-4.03	-3.45	0.43	0.98	**0.22**
Metiskow 0267	-2.54	-5.39	**-4.43**	0.34	0.78	**0.55**
Narrow Lake 252	-2.31	-4.81	**-3.75**	0.28	0.60	0.51
Wagner 0172	-2.14	-8.06	**-2.70**	0.48	0.37	0.21
Baildon 060	-2.80	-3.29	**-3.20**	0.47	0.58	0.30
Beauval	-3.78	-4.85	**-4.20**	0.44	0.56	0.32
Blucher	-2.20	-4.24	**-2.16**	0.30	0.92	**0.26**
Crater Lake	-4.33	-3.97	-3.64	1.10	0.4	0.28
Duck Lake	-3.65	-3.69	-3.17	0.54	0.41	**0.62**
Forget	-2.28	-2.37	**-2.23**	0.33	0.17	0.19
Garden Head	-3.67	-4.85	**-3.77**	0.88	0.70	0.30
Nokomis	-1.04	-2.70	**-2.17**	0.23	0.55	**0.17**
Shaunavon	-1.62	-4.41	**-2.58**	0.42	0.69	0.20
Simpson 13	-4.82	-4.83	-3.02	0.31	0.91	**0.17**
Simpson 14	-2.03	-2.61	**-1.82**	0.34	0.18	**0.27**
Yorkton 517	-2.87	-3.97	**-1.98**	0.80	0.46	0.32
Agrium 43	-2.66	-3.75	**-3.38**	0.32	1.05	**0.36**
460120097591803	-1.44	-2.33	**-1.63**	0.56	0.24	**0.50**
461838097553402	-1.17	-2.32	**-1.68**	0.27	0.24	0.43
462400097552502	-4.9	-5.61	**-5.37**	0.29	0.09	**0.17**
462633097163402	-1.18	-1.49	**-1.02**	0.46	0.29	**0.54**
463422097115602	-1.36	-2.28	**-1.66**	0.34	0.23	0.49
464540100222101	-2.02	-3.64	**-2.78**	0.52	0.43	0.32
473841096153101	-0.77	-1.48	**-1.37**	0.24	0.18	0.51
473945096202402	-1.59	-1.58	-1.56	0.32	0.24	0.51
474135096203001	-0.72	-1.48	**-1.30**	0.33	0.25	0.54
474436096140801	-2.44	-2.29	-1.96	0.39	0.21	**0.40**
475224098443202	-4.52	-4.28	-5.31	0.75	0.52	0.34
481841097490301	-4.39	-4.24	-4.58	0.79	0.28	0.17
482212099475801	-2.13	-2.32	**-2.26**	0.24	0.20	0.17
CRN WLN 03	-2.04	-2.18	-1.88	0.24	0.18	0.43

The REP simulation with sandy soil shows two sensitive signals: (1) REP WTD are shallower than the default simulation; (2) and exhibit stronger seasonal variation. These two signals can be explained by the WTD equation in the MMF scheme:

$$\Delta WTD = \frac{\Delta(R + Q_{lat} - Q_r)}{(\theta_{sat} - \theta_{eq})} \quad (4.13)$$

Eq. (4.13) represents that the change of WTD in a period of time is calculated by the total groundwater fluxes, $\Delta(R + Q_{lat} - Q_r)$, divided by the available soil moisture capacity of current layer ($\theta_{sat} - \theta_{eq}$). In REP simulation, the parameters θ_{sat} for the dominant soil type in observational sites (sand/gravel) is smaller than those in default model grids (clay loam, sandy loam, loam, loamy sand, etc.). Therefore, changing the θ_{sat} is essentially reducing the storage in the aquifer and soil in this model grid. Given the same amount of groundwater flux, in the REP simulation, the mean WTD is higher and the seasonal variation is stronger than the default CTRL run.

In the REP simulation, we replaced soil type only at a limited number of sites because the geological survey data in high resolution and large area extent is not yet available for the whole PPR. At point scale, the WTD responses to climate change over these limited number of sites show diverse results and uncertainties (see Appendix C). For the rest of the domain, the default soil type from global 1-km soil map is used. The REP modifications of soil types at point-scale have small contribution to the water balance analysis (Figure 4.8 & 4.9) at regional-scale. Our results and conclusions for groundwater response to PGW doesn't change. We are currently undertaking a soil property survey project in the PPR region to obtain soil properties at high spatial resolution, both horizontal and vertical. This may provide better opportunity to improve WTD simulation as well as assess climate-groundwater interaction in future studies.

4.4.2 Climate Change Impacts on Groundwater Hydrological Regime

The warming and increased precipitation in cold seasons in future climate will lead to later snow accumulation, higher recharge in winter and earlier melting in spring compared to current climate. Such changes in snowpack loss have been hypothesized in mountainous as well as high-latitude regions (Taylor et al 2013; Ireson et al., 2015; Meixner et al., 2016; Musselman et al., 2017). In addition to the amount of recharge, the shift of recharge season is also noteworthy. Under current climate conditions in spring, soil thawing (in March) is generally later than snowmelt (in February) by a month in the PPR. Thus, the snowmelt water in pre-thaw spring would either re-freeze after infiltrating into partially frozen soil or become surface runoff. Under the PGW climate, the warmer winter and spring allows snowmelt and soil thaw to occur earlier in the middle of winter (in January and February, respectively). As a result, the recharge season starts earlier in December, and last longer until June, results in longer recharge season but with lower recharge rate.

Future projected increasing evapotranspiration demand in summer desiccates soil moisture, resulting in more water uptake from aquifers to subsidize dry soil in the future summer. This groundwater transport to soil moisture is similar to the "buffer effect" documented in an offline study in the Amazon rainforest (Pokhrel et al., 2014). In the PPR, shallow water tables exist in the critical zone, where WTD ranges from 1 to 5 meters below surface and could exert strong influence on land energy and moisture fluxes feedback to the atmosphere (Kollet and Maxwell, 2008; Fan et al., 2015). Previous coupled atmosphere-land-groundwater studies at 30-km resolution showed that groundwater could support soil moisture during summer dry period but has little impacts on

precipitation in Central U.S. (Barlage et al., 2015). It would be an interesting topic to study the integrated impacts of shallow groundwater to regional climate in the convection permitting resolution (resolution < 5-km).

4.3 Fine-scale interaction between groundwater and prairie wetlands

Furthermore, groundwater exchange with prairie pothole wetlands are complicated and critical in the PPR. Numerous wetlands known as potholes or sloughs provide important ecosystem services, such as providing wildlife habitats and groundwater recharge (Johnson et al., 2010). Shallow groundwater aquifers may receive water from or lose water to prairie wetlands depending on the hydrological setting. Depression-focused recharge generated by runoff from upland to depression contributes to sufficient amount of water input to shallow groundwater (5-40 mm/year) (Hayashi et al., 2016).

On the other hand, groundwater lateral flow exchange center of a wetland pond to its moist margin is also an important component in the wetland water balance (van der Kamp and Hayashi, 2009; Brannen, et al., 2015; Hayashi et al., 2016). However, this groundwater-wetland exchange typically occurs on local scale (from 10 to 100 m) and thus, is challenging to represent in current land surface models or climate models (resolution from 1 km to 100 km). In this paper, we focus on the groundwater dynamics on regional scale, which is still unable to capture these small wetland features in this study. We admit this limitation and are currently developing a sub-grid scheme to represent small scale open water wetlands as a fraction within a grid cell and calculate its feedback to regional environments. Future studies on this topic will provide valuable insights on these key ecosystems and their interaction under climate change.

4.5 Conclusion

In this study, a coupled land-groundwater model is applied to simulate the interaction between the groundwater aquifer and soil moisture in the PPR. The climate forcing is from a dynamical downscaling project (WRF CONUS), which uses the convection-permitting model (CPM) configuration in high resolution. The goal of this study is to investigate the groundwater responses to climate change, and to identify the major processes that contribute to these responses in the PPR. To our knowledge, this is the first study applying CPM forcing in a hydrology study in this region. We have three main findings:

(1) the coupled land-groundwater model shows reliable simulation of mean WTD, however underestimates the seasonal variation of the water table against well observations. This could be attributed to several reasons, including misrepresentation of topography and soil types, as well as vertical homogenous soil layers used in the model. We further conducted an additional simulation (REP) by replacing the model default soil types with sand-type soil and the simulated WTDs were improved in both mean and seasonal variation. However, inadequacy of soil properties in deeper layer and higher spatial resolution is still a limitation.

(2) Recharge markedly increases due to projected increased PR, particularly from fall to spring under future climate conditions. Strong east-west spatial variation exists in the annual recharge increases, 25% in the eastern and 50% in the western PPR. This is due to the significant projected PR reduction in PGW summer in the eastern PPR but little change in the western PPR. This PR reduction leads to stronger ET demand, which draws more groundwater uptake due to the capillary effect, results in negative recharge in the summer. Therefore, the increased recharge from fall to spring is consumed by ET in summer, and results in little change in groundwater in the eastern PPR, while gaining water in the western PPR.

(3) The timing of infiltration and recharge are critically impacted by the changes in freeze-thaw processes. Increased precipitation, combined with higher winter temperatures, results in later snow accumulation/soil freezing, partitioned more as rain than snow, and earlier snowmelt/soil thaw. This leads to substantial loss of snowpack, shorter frozen soil season, and higher permeability in soil allowing infiltration. Late accumulation/freezing and early melting/thawing leads to an early start of a longer recharge season from December to June, but with a lower recharge rate.

Our study has some limitations where future studies are encouraged:
(1) Despite the large number of groundwater wells in PPR, only a few are suitable for long-term evaluation, due to data quality, anthropogenic pumping, and length of data record. As remote sensing techniques advance, observing terrestrial water storage anomalies derived from the GRACE satellite may provide substantial information on WTD, although the GRACE information needs to be downscaled to a finer scale before comparisons can be made with regional hydrology models at km-scale (Pokhrel et al., 2013).

(2) This study is an offline study of climate change impacts on groundwater. It is important to investigate how shallow groundwater in the earth's critical zone could interact with surface water and energy exchange to the atmosphere and affect regional climate. This investigation would be important to the central North America region (one of the land atmosphere coupling "hot spots", Koster et al., 2004).

Key points for the next chapter

- The shallow groundwater in the PPR is key to the region's hydrological cycle, buffering the land surface and unsaturated soil moisture. The groundwater aquifer receives recharge during wet periods and supports soil moisture through capillary rise in dry periods.
- The shallow groundwater in the PPR exhibits strong spatial heterogeneity, which is closely related to topography and climatic conditions. This strong heterogeneity requires a high-resolution model grid cell and meteorological forcing to resolve its small-scale features.
- Future projections of groundwater dynamics strongly reflect the heterogeneity of meteorological forcing, which has shown a large east-west contrast.
- Including the shallow groundwater processes in LSMs is required to make reasonable estimates of soil moisture, which are important to sustaining the prairie pothole wetlands. This topic will be addressed in the next chapter.

Acknowledgments

The authors, Zhe Zhang, Yanping Li, and Zhenhua Li, gratefully acknowledge support from the Changing Cold Regions Network (CCRN), funded by the Natural Science and Engineering Research Council of Canada (NSERC), as well as the Global Water Future project and the Global Institute for Water Security at the University of Saskatchewan. Yanping Li acknowledges support from a NSERC Discovery Grant. Zhe Zhang acknowledges support from a MITACS Accelerate Fellowship. Fei Chen and Michael Barlage appreciate support from the Water System Program at the National Center for Atmospheric Research (NCAR), USDA NIFA (grant nos. 2015-67003-23508 and 2015-67003-23460), NSF INFEW/T2 (grant no. 1739705), and NOAA CFDA (grant no. NA18OAR4590381). NCAR is sponsored by the National Science Foundation. Any opinions, findings, conclusions, or recommendations expressed in this publication are those of the authors and do not necessarily reflect the views of the National Science Foundation. The authors acknowledge the helpful comments from Lauren Bortolotti from Ducks Unlimited Canada.

Chapter 5 – Heterogenous changes to wetlands in the Canadian Prairies suggests diversified conservation strategies

This manuscript has been modified for inclusion in this thesis. It was originally accepted as:

Zhang, Z., Bortolotti, E. L., Li, Z., Armstrong, L. M., Bell, T. W., Li, Y. Heterogeneous changes to North America Prairie Pothole wetlands under future climate. (2020). Water Resources Research.

Author contributions: Z. Zhang and L. E. Bortolotti designed the study, construct the statistical model and wrote the paper. Y. Li, T. W. Bell and Z. Li contributed to the interpretation of the results and reviewed the manuscript. L. M. Armstrong provided valuable technical supports on GIS and static datasets.

Keywords

Wetland, Hydrology, Climate change, Prairie Pothole Region, Waterfowl, Conservation

Abstract

Numerous wetlands in the prairies of Canada provide important ecosystem services yet are threatened by climate and land-use changes. Understanding the impacts of climate change on prairie wetlands is critical to effective conservation planning. In this study, we construct a wetland model with surface water balance and ecoregions to project future distribution of wetlands. The climatic conditions downscaled from the Weather Research and Forecasting model were used to drive the Noah-MP land surface model to obtain surface water balance. The climate change perturbation is derived from an ensemble of general circulation models using the pseudo global warming method, under the RCP8.5 emission scenario by the end of 21st century. The results show that climate change impacts on wetland extent are spatiotemporally heterogenous. Future wetter climate in the western Prairies will favor increased wetland abundance in both spring and summer. In the eastern Prairies, particularly in the mixed grassland and mid-boreal upland, wetland areas will increase in spring but experience enhanced declines in summer due to strong evapotranspiration. When these effects of climate change are considered in light of historical drainage, they suggest a need for diverse conservation and restoration strategies. For the mixed grassland in the western Canadian Prairies, wetland restoration will be favorable, while the highly drained eastern Prairies will be challenged by the intensified hydrological cycle. The outcomes of this study will be useful to conservation agencies to ensure that current investments will continue to provide good conservation returns in the future.

Motivation

In the previous chapter, I explored the shallow groundwater dynamics in the PPR and tested the capacity of the Noah-MP LSM model in reasonably simulating shallow groundwater and its exchange with soil moisture. In this chapter, I explore the hydrological changes associated with the future climate, as well as the future climate's impacts on the spatial wetland extents in this region.

5.1 Introduction

The Prairie Pothole Region (PPR) contains millions of small wetlands within topographic depressions (also known as prairie potholes) across five states in the U.S. (Iowa, Minnesota, North Dakota, South Dakota, Montana) and three provinces in Canada (Alberta, Saskatchewan, Manitoba). These wetlands provide important ecosystem services, including improving water quality, water regulation, and supporting biodiversity (Gleason et al., 2008; Johnson et al., 2010; Niemuth et al., 2014; Hayashi et al., 2016). The PPR is known as one of the most important landscapes for breeding waterfowl in North America (Batt et al. 1989), but it also provides crucial habitat for nesting and migration for other wetland- and grassland-associated birds (Beyersbergen et al. 2004, Rich et al. 2004, Niemuth et al. 2008). As a result, the PPR is the focus of conservation programs in both Canada and the U.S. The major conservation partnerships of this region (i.e., the Prairie Habitat Joint Venture (PHJV) and Prairie Pothole Joint Venture (PPJV)) recognize that wetlands in the PPR face threats from land-use conversion to cropland and possible threats from climate change-related drying (PHJV, 2014; PPJV, 2017). Niemuth et al. (2014) hypothesized that land use change may be more influential on wetlands and wildlife than the direct effects of climate change, and work incorporating land use into projecting the effect of climate on wetlands suggests that regions most climatically suitable for wetlands in the future may not coincide with areas that show lower land use pressures (Sofaer et al. 2016).

In the PPR, prairie wetlands exist because of key interactions among topographic, geological, and climatic conditions (van der Kamp and Hayashi, 2009; Hayashi et al., 2016). These local depressions were formed by clay-rich glacial till deposition from the continental ice sheet during Pleistocene glaciation. The local topographic variation (hollow and hummock) favors the convergence of surface and shallow groundwater runoff in local depressions. In addition, cold winters allow snow accumulation on the ground and spring snowmelt is an important source of surface runoff filling these closed depressional wetlands (Ireson et al., 2013). The PPR also has a semi-arid climate, with wetland water most abundant in May after snowmelt but continuously evaporating through the summer. The duration of inundation/permanence of prairie wetlands varies widely, depending on the water balance (Hayashi et al., 2016), which is influenced by factors such as seasonal precipitation, snowmelt runoff, and recharge from shallow groundwater. Moreover, water in neary depressions can be connected by ephemeral streams during wet condition, through a "fill-and-spill" mechanism, suggesting dynamic connectivity of surface runoff interacting with water availability and depressional topography (Ehsanzadeh et al., 2012; Shaw et al., 2012, Mekonnen et al., 2014). These surface wetland expansions under wet conditions and contractions under drought conditions response to climate inputs and are varied spatially (Vanderhoof et al., 2016, 2018).

Observational studies have documented recent changes in climatic conditions, e.g., temperature and precipitation, and hydrological regime shifts, with implications for waterfowl populations in various parts of the PPR (e.g., Niemuth et al., 2010; Dumanski et al., 2015). Since the early 1990s,

an extended period of high precipitation has caused a hydrological regime shift to a novel "wet continuum", with corresponding increases in pond numbers, lake levels, streamflow amount, soil moisture, as well as waterfowl populations in the southern PPR (South and North Dakota) (Niemuth et al., 2010, 2014; McKenna et al., 2017). On the other hand, the western PPR (mostly in the western Canadian Prairies, Alberta) has shown a decreasing trend in precipitation, glaciers, streamflows (St. Jacques et al., 2013) and number of inundated ponds in July (Niemuth et al., 2014). These contrasting trends in the recent observation record have been demonstrated by Liu and Schwartz (2012), in a reconstruction of the surface water body numbers based on moisture residual in the last five years in 27 locations across the PPR.

Modeling studies have attempted to project future wetlands and hydrological conditions across the PPR from a range of possible climate change scenarios (Johnson et al., 2005; Forbes et al., 2011; MacDonald et al., 2012; Kienzle et al., 2012). These studies have simulated a baseline condition under current climate and added a delta climate change on temperature or precipitation for future climate. For example, in Johnson et al. (2005), the climate change scenarios were designed with a temperature warming of 3°C and a precipitation increase or decrease of 20%, applied uniformly across the PPR. In Forbes et al. (2011), MacDonald et al. (2012) and Kienzle et al. (2012), delta climate changes in temperature and precipitation were derived from monthly means of general circulation models (GCMs) ensembles and were imposed upon current station observations in three watersheds in the western PPR. Despite the range of climate change projections considered, this type of delta climate change method, is may be unsuitable for wetland water balance studies asit lacks constraints on energy and moisture conservation in the coupled atmosphere and land system and is unable to capture possible combined extreme hydroclimatic conditions as in processes-based models.

Other modelling studies have established statistical relationships between long-term climatic conditions and wetland surveys to generate predictions of wetland distributions in the PPR. For example, Niemuth et al. (2014) and Herfindal et al. (2012) developed linear regression models describing to predict wetland counts as function of climate (precipitation and temperature) and other (e.g., plant phenology, land use) variables. Garris et al. (2015) used 35 climate variables from GCM ouputs from CMIP4 in a linear model paired with an artificial neural network technique to predict a potential increase of wetland areas in Southwest Minnesota. Sofaer et al. (2016) used yet another approach, choosing climate outputs downscaled from 10 GCMs in CMIP5 and forcing them through a land surface hydrology model (VIC). They built a statistical relationship between 15 hydrological variables from VIC gridded output and wetland density in the US portion of the PPR, with the overall surface water balance (i.e., precipitation minus potential evapotranspiration) as the most sensitive predictor of wetland density.

The coarse resolution of GCM outputs (~50-100 km) is not suitable for modelling prairie wetlands, where a finer scale (~10-1000 m) is more appropriate, and discrepancies among GCM projections restrict the reliability of future wetland projections. Additionally, GCM-projected future precipitation forecasts are highly uncertain depending on the choice of convection parameterizations, a mathematical description of the convection processes within each model grid cell (Prein et al., 2015; Kendon et al., 2017). This is problematic as precipitation is the key water input for prairie wetlands.

Using GCM outputs to study the impact of climate change on wetlands requires downscaling. Recent progress in dynamical downscaling using high-resolution regional climate models (RCMs) with the pseudo global warming (PGW) method provides us with a surrogate climate change scenario for studying hydrological responses to climate change (Schär et al., 1996). The PGW method usually consists of two dynamical downscaling simulations. The first simulation is from a retrospective dataset of current climate (control simulation, CTRL). The other applies a climate change perturbation derived from an ensemble of GCMs to the current climate to generate a future climate simulation using RCM (pseudo global warming, PGW). The PGW method has multiple advantages. The CTRL simulation is reasonably reliable compared to direct downscaling from GCMs and allows detailed climate and hydrological process studies (Schär et al., 1996). Additionally, dynamical downscaling with a high-resolution convection-permitting regional climate model (CPRCM) improves precipitation forecast as well as provides detailed representation of surface properties. Multiple studies have shown great potential of the PGW method downscaled with a CPRCM in studying atmosphere processes, hydrological responses, and model inter-comparison in the climate science community (Prein et al., 2016; Liu et al., 2017; Musselman et al., 2017; Li et al., 2019; Zhang et al., 2020; Fang and Pomeroy, 2020). It offers a novel and powerful for studying climate change and its impacts on the hydrological conditions for prairie wetlands.

The purpose of this study is to investigate the impacts of climate change on the future abundance and distribution of wetland ponds in the Canadian portion of the PPR (hereafter, the Canadian prairies), using the PGW method. More specifically, our objectives were to: (1) model the impacts of climate change on spatial distribution of wetland ponds as well as seasonal variation under the PGW climate scenario, focusing on the water availability (van der Kamp et al., 2016); (2) explain these changes by water balance analysis; (3) explore potential joint effects of climate change and historical drainage patterns on future wetland ecosystem services and conservation policies. This is achieved by applying the hydroclimatic outputs from previous CPRCM simulations in the Noah-MP land-surface hydrology model and statistically fitting a fractional wetland index for each grid point in the Canadian prairies in high-resolution (4-km). Results of this study have important implication for wetland conservation, especially for decision-making on prioritizing conservation investments across the Canadian prairies. For example, the PHJV uses spatial targeting to maximize the return on conservation investments (PHJV, 2014). Understanding how the patterns (including wetland density) that drive current conservation delivery prioritization may change in the future is key to ensuring that investments made now deliver benefits in perpetuity or give conservation organizations the information needed to adapt their programs to changing conditions.

5.2 Data and Models

5.2.1 Wetland Datasets

The Canadian Wetland Inventory (CWI) classifies wetlands according to the Canadian Wetland Classification System (National Wetlands Working Group, 1997) and, in the prairies, delineates wetland basins from stereo pairs, with a minimum mapping unit of 0.02 ha. In the protocol used, the wetland extent spans the wet meadow vegetation zone to the deepest point of the basin and represents the depressional area capable of holding water. Shapefiles from the CWI were compiled into a high-resolution single geodatabase for the Canadian prairies to represent wetland fractional area in 4-km grid cells (F_{wet}, Figure 1a). Given the challenges in mapping small wetland features, the CWI represents the best available map of prairie wetlands, though it has incomplete coverage of the Canadian prairies.

For a product with prairie-wide coverage, we used a modelled spatial layer, the Adjusted CanVec layer (hereafter, "Adj_CanVec"; Figure 5.1b). CanVec is a vector dataset developed by Natural Resources Canada (Natural Resources Canada, 2008). It has good spatial coverage but does not capture all small wetlands and has variable scale (~1:10000-1:50000) and accuracy. Ducks Unlimited Canada (DUC) used CanVec hydrography and water saturated soils features, Soil Landscape of Canada data (Soil Landscapes of Canada Working Group, 2007), and CWI to generate predictive equations to scale CanVec 3.0 data to the high-resolution CWI data in the prairies. Because it is difficult to separate out wetlands and lakes in the CanVec data, the Adj_CanVec includes some non-wetland waterbodies such as shallow prairie lakes. A layer of MODIS-derived water mask was applied to remove large water bodies at 4-km grid scale (n = 174 grid cells).

Figure 5.1a&b shows the distribution of F_{wet} from CWI and Adj_CanVec in the Canadian prairies. The Adj_CanVec shows a high F_{wet} close to the northern boundary of the PPR in the aspen parkland ecoregion. Figure 5.1c is a scatter plot of F_{wet} from these two datasets with their histogram on the top. The majority of the data points are below 0.3, while Adj_CanVec has a longer tail of high F_{wet}. Figure 1d takes a closer look at the two datasets of F_{wet} from 0 to 0.4. It is evident that most data points are smaller than 0.3 and Adj_CanVec has a tendency for higher F_{wet} than the CWI.

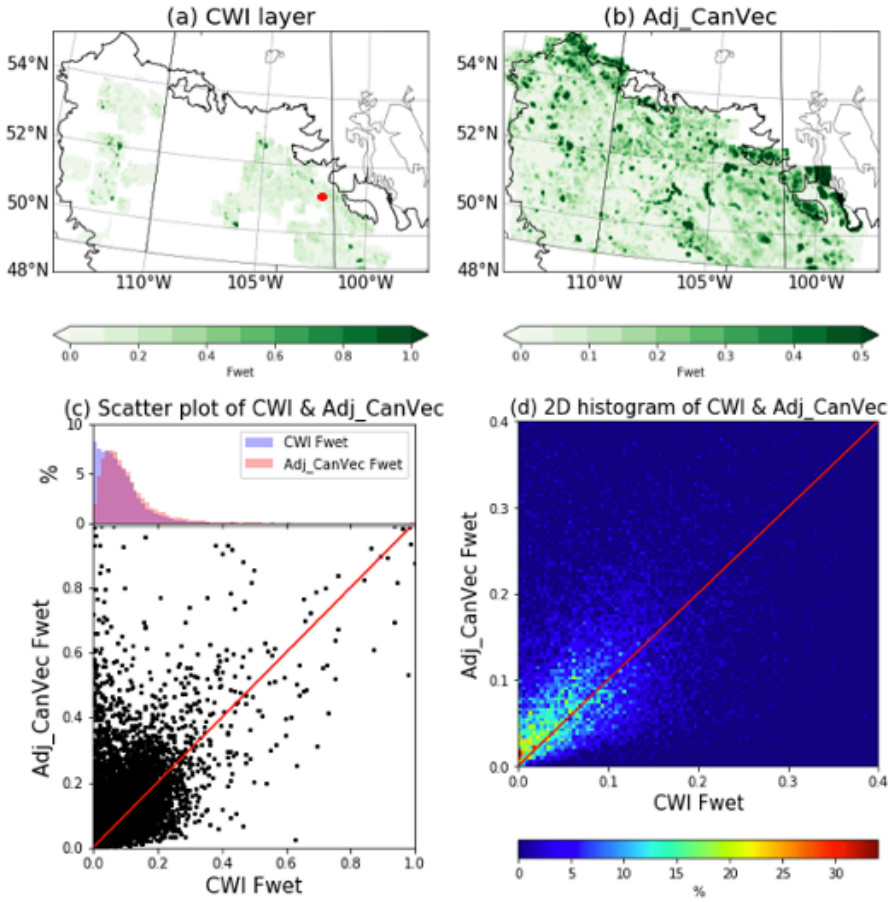

Figure 5.1. (a) F_{wet} (0-1) spatial distribution from the Canadian Wetland Inventory (CWI); (b) F_{wet} (0-1) spatial distribution from Adj_CanVec, a modelled wetland dataset; (c) scatter plot (bottom) and histogram (top) of F_{wet} of the CWI (blue) and Adj_CanVec (red) and (d) a 2D histogram of F_{wet} from 0 to 0.4. Red dot in Figure 1a represents the location of the Smith Creek watershed in Saskatchewan.

Due to the strong wet-dry cycles in the prairies, wetland extent varies both through space and time (Liu and Schwartz, 2012). However, the CWI and Adj_CanVec are both static products meant to represent long-term conditions and are thus not suitable for evaluating the temporal performance of the statistical model. Therefore, we investigated temporal changes in ponding depth at the St. Denis National Wildlife Area (SDNWA, 52°12'N 106°5'W) in Saskatchewan, Canada (red dot in Figure 1a). Although the site is relatively small in area (4 km^2), it contains hundreds of wetland ponds of various sizes and permanences and long-term monitoring records since 1968 (Bam et al., 2019). To study the temporal wetland dynamics in the SDNWA, the ponding depth records from 140 ponds are used to calculate the change in depth (exact value – all-time mean) at this site. Ponding depth and F_{wet} both reflect moisture conditions at this site and, hence, can provide some reference for evaluating the model performance in this study (see section 5.3.1).

Moreover, a supplemental analysis is conducted to show the interannual variation between model simulated F_{wet} and open water fraction in the Smith Creek Watershed (50°50'N 101°34'W) in Southeast Saskatchewan (Figure D5 in Appendix D). The Smith Creek Watershed is a long-term established research site for wetland hydrology in the Canadian prairies, though it has experienced high wetland loss due to anthropogenic drainage (Dumanski et al., 2015; Pattison-Williams et al., 2018). The open water fraction in the Smith Creek Watershed is estimated by Multiple Endmember

Spectral Mixture Analysis (MESMA, Roberts et al., 1998), a remote sensing technique to detect open water features in an area (see Appendix D for detailed methods).

Wetland drainage plays a significant role in the human modification of prairie landscapes. The Prairie Habitat Monitoring Program has collected data on the density of drainage ditches in the Canadian prairies. Figure 5.2 shows a qualitative wetland drainage score, based on the density of agricultural surface ditches as detected through aerial photography and high-resolution satellite imagery (for detailed methods and score descriptions see Appendix 11 in PHJV, 2014). Low drain score areas show minimal evidence of anthropogenic drainage whereas high drain scores exhibit extensive ditching and related drainage. Three examples of drain score photos are included in Figure 5.3: (b) a low drain score, most wetlands remain intact; (c) a medium drain score, many small wetlands have been drained; (d) a high drain score, most wetlands have been drained and converted to cropland.

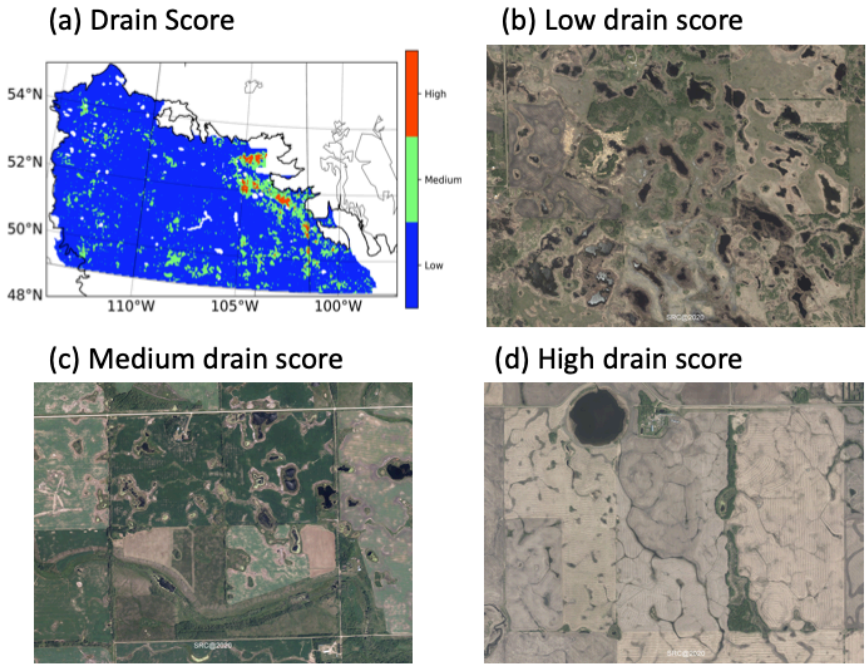

Figure 5.2. (a) A qualitative drain score map based on density of drainage ditches with (b-d) examples of the three drain scores (photos are from the Saskatchewan Geospatial Imagery Collaborative).

To answer the third objective of this paper, a joint analysis of both historical drainage condition and future wetland projection will be conducted. The two data layers, change in wetland distribution in future climate and the three-category drain score, will be combined where areas will become drier or wetter in future climate (ΔF_{wet}), as well as with low/medium/high drain score. A threshold condition of $|\Delta F_{wet}|$ ($|\Delta F_{wet}|$>0.1) is applied. Therefore, the current drained areas within three drain score categories will gain or lose surface wetland, impacted by climatic conditions, will be the interests of our study and conservation policies.

5.2.2 Study domain and ecoregions in the Canadian Prairies

Wetland density varies across the PPR, influenced by both geographic and climatic factors. Figure 5.3 shows eight major ecological regions in central Canada, as defined by the Ecological Land Classification (Statistics Canada, 2017). Ecoregions categorize broad landscapes based on distinctive regional ecological factors including climate, physiography, vegetation, and soil, and thus have the potential to explain spatial variation in wetland area not covered by hydrological or climatological variables. The ecoregions represented in Figure 3 only include those where there was overlapping coverage with the CWI. Ecoregions not represented in the CWI were either excluded from analysis (Lake Manitoba plain) or recoded to an adjacent ecoregion (cypress upland reclassified as mixed grassland, wabasca lowlands and interlake plain recoded as mid-boreal uplands). Reclassified grid cells represent less than 1% of all grid cells. These eight ecoregions are used in modeling of F_{wet} (section 5.2.4).

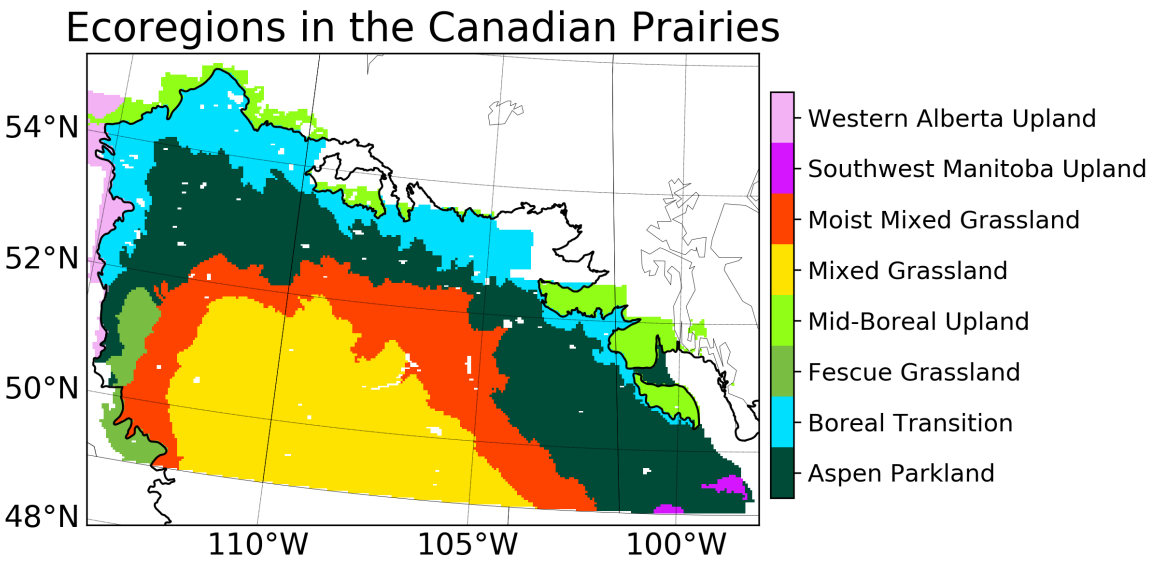

Figure 5.3. Ecoregions in the Canadian Prairies. Black contour outlines the Prairie Pothole Region, and the filled colors represent the 8 ecoregions as used in the wetland model. The areas where Adj_CanVec data are unavailable are blank.

5.2.3 Climate scenarios and surface water balance

The climate scenarios in this study were obtained from high-resolution (4-km) regional climate simulations in the Contiguous U.S. and Southern Canada, using the Weather Research and Forecasting (WRF, Skamarock et al., 2008) model (referred to as CONUS WRF, Liu et al., 2017). The future climate change scenario was generated using the PGW (Schär et al. 1996). For the CTRL simulation, the initial and boundary conditions were from a 6-hr ERA-Interim re-analysis dataset (equation 5.1). For the PGW simulation, the initial and boundary conditions were created by adding a climate change perturbation, derived from an ensemble of GCMs by the end of the 21st century in RCP8.5 emission scenario, upon the ERA-Interim reanalysis (equation 5.2) (see Liu et al. (2017) for the full list of GCMs ensemble).

The climate change perturbation includes wind, geopotential height, temperature, specific humidity, sea surface temperature, soil temperature, sea level pressure, and sea ice (equation 5.3) (Liu et al., 2017). The perturbation in these fields impacts large-scale planetary waves and associated thermal dynamics, while synoptic scale weather events remain structurally constrained by the boundary

conditions in terms of frequency and intensity (Schär et al., 1996; Rasmussen et al., 2011). Both CTRL and PGW simulations were dynamically downscaled from above initial and boundary conditions, using the WRF model, and the simulations span from 2000-10-01 to 2013-10-01 (Liu et al., 2017) at convection-permitting resolution (4-km). The PGW method has gained popularity in the climate science and hydrology communities, as it concomitantly allows certain processes to be examined in isolation, such as snowfall and snowpack (Rasmussen et al., 2011; Musselmen et al., 2018), meso-scale convection systems (Prein et al., 2017), land-atmosphere interactions (Zhang et al., 2018) and groundwater responses to climate change (Zhang et al., 2020).

$$\text{CTRL: } \mathrm{WRF_{input}} = \text{ERA–Interim} \quad (5.1)$$

$$\text{PGW: } \mathrm{WRF_{input}} = \text{ERA–Interim} + \Delta\mathrm{CMIP5_{RCP8.5}} \quad (5.2)$$

$$\Delta\mathrm{CMIP5_{RCP8.5}} = \mathrm{CMIP5_{2071-2100}} - \mathrm{CMIP5_{1976-2005}} \quad (5.3)$$

The hourly output data from CONUS WRF, including temperature, precipitation, humidity, wind, pressure, short and long-wave radiation, were used to drive a land-surface model (LSM), Noah-MP (Niu et al., 2011; Yang et al., 2011) with groundwater component (Fan et al., 2007; Miguez-Macho et al., 2007), to simulate the hydrological cycle in the study domain. The Noah-MP LSM is a physical process-based model which explicitly simulates major storage, such as snow water equivalent (SWE) and soil moisture (SM), and hydrological processes, including snow accumulation, sublimation, evaporation, runoff, and groundwater recharge. Snow is a key water source for prairie wetlands at the beginning of snowmelt seasons. The Noah-MP snow model simulates the snowpack for up to three layers according to the snow depth and snow cover fraction as determined by snow density, depth, and ground roughness length. The snow surface energy balance is calculated separately over two semitiles of the grid cell, vegetated and bare ground. The snow albedo scheme is adopted from the CLASS model (Verseghy, 1991), which accounts for snow age, grain size, and accumulated debris on the snow surface. We also included an evaluation of model simulated snow processes in the Canadian Prairies in the Supporting Information. Furthermore, the Noah-MP LSM is coupled with a dynamic groundwater model, enabling two-way interactions between soil moisture and an underlying unconfined aquifer, as well as lateral flow from surrounding grid cells. The groundwater dynamics were reasonably simulated and evaluated in Zhang et al. (2020) against multiple well observations in the PPR.

In this study, we used the Noah-MP LSM output SM to represent surface water balance and compute a fractional index (soil moisture content, SMC) as a key input to forecast spatial wetland distribution in the Canadian prairies. The surface water balance can be represented as:

$$\Delta SM + \Delta SNOW = PR - ET - SR - G \quad (5.4)$$

$$SMC = \frac{\theta}{\theta_{SAT}} \quad (5.5)$$

The change in soil moisture storage (ΔSM) is calculated by volumetric soil moisture times soil depth ($\Delta SM = \Delta\theta \cdot z$, where z is a 2-m soil layer). Collectively, ΔSM and snow ($\Delta SNOW$) are a product of precipitation (*PR*), evapotranspiration (*ET*), surface runoff (*SR*) and groundwater recharge (*G*). The fractional *SMC* is calculated from the volumetric soil moisture (θ) divided by saturated soil moisture content (θ_{SAT}). θ varies from 0 to θ_{SAT}, so that *SMC* varies from 0 to 1. θ_{SAT} is a parameter determined by soil types and can be found in a parameter look-up table in the Noah-MP LSM: (https://github.com/NCAR/hrldas/blob/master/hrldas/run/SOILPARM.TBL).

5.2.4 Model of wetland fraction

In this study, we used a generalized additive model (GAM) to analyze the relationship between F_{wet} and hydrological and ecological covariates. GAMs accommodate a variety of response distributions/link functions and allow for flexible, additive effects of predictor variables (Hastie and Tibshirani, 1986). We fit the following statistical model in R (R Core Team, 2020) using the mgcv package (Wood, 2011):

$$g\big(E(F_{wet})\big) = s(SMC) + ER \qquad (5.6)$$

We used a binomial distribution and logistic link of wetland fraction (i.e., $g(p)$ = ln(p/(1-p)), a smooth function of soil moisture content ($s(SMC)$), and included ecoregion (ER) as a factor predictor variable in the model to allow for different baseline wetland fractions (or intercepts) among the eight ecoregions. More model details are provided in the Appendix D. The fitted model was used to predict current wetland fraction (F_{wet}_CTRL), which was evaluated against Adj_CanVec data in the Canadian prairies. The *SMC* input for equation (5.6) is averaged from March to August, representing a mean moisture condition of the warm season, hence, the modeled F_{wet} is a seasonal averaged wetland distribution. Finally, to study the impacts of future climate change, we substituted SMC from the future climate model scenario (PGW) to predict future wetland fraction (F_{wet}_PGW). The difference between F_{wet}_PGW and F_{wet}_CTRL can be attributed to the impacts of climate change. SMC is the only hydrological variable in this model, and it can be computed over different timescale, monthly or seasonal, etc. As for simulating F_{wet}_CTRL, we obtained the mean SMC from March to August over 13-year to represent the wetness condition over the warm season. It is assumed that, over the long term, SMC is the net result of hydrological processes from equation (5.4) including precipitation, snowmelt, evapotranspiration, runoff, and groundwater recharge.

5.3 Results

5.3.1 Validation and sensitivity of the GAM model

Figure 4 shows the evaluation results from F_{wet}_CTRL, predicted by the GAM, and the Adj_CanVec, at the grid (Figure 4a) and ecoregion scale (Figure 4b). The average ecoregion F_{wet}_CTRL tends to be lower than average F_{wet} from Adj_CanVec, but they covary positively, with both indices similarly ranking the ecoregions with respect to wetland fraction. The root-mean-square-error of the model prediction in current climate is 0.102 and for 98% of the grids, abs (F_{wet}_CTRL - Adj_CanVec) < 0.1.

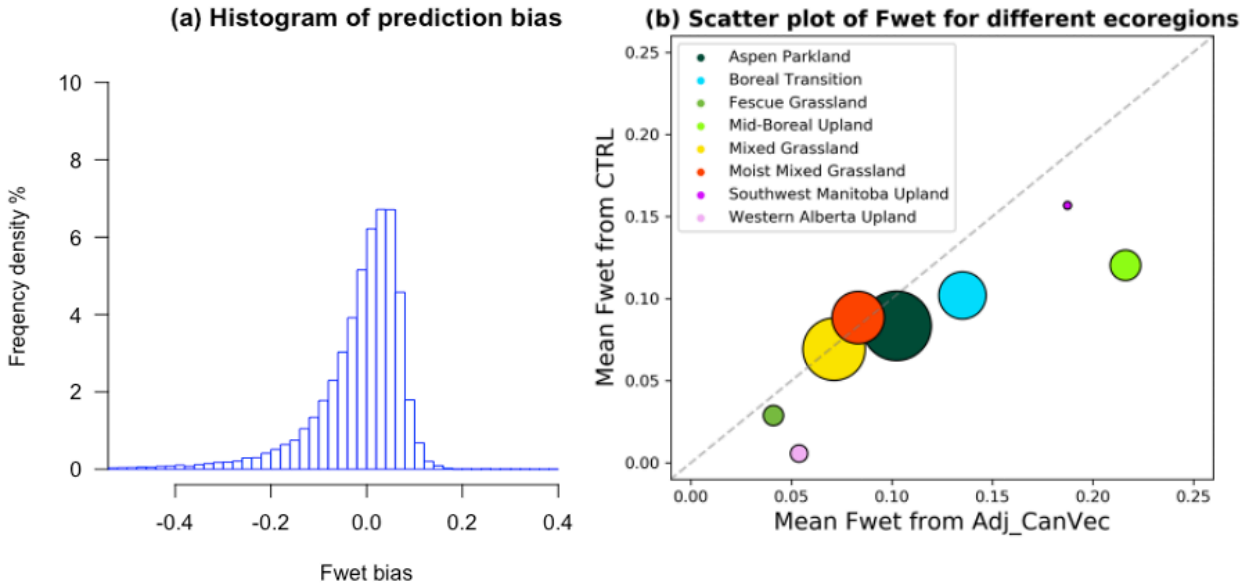

Figure 5.4. (a) Histogram of the model bias (F_{wet}_CTRL-F_{wet}_Adj_CanVec) showing the relative frequency density of grid cells in the Canadian prairies; (b) scatter plot of mean F_{wet}_CTRL compared with mean F_{wet} from Adj_CanVec by ecoregion. Point sizes are proportional to the square root of sample sizes.

As SMC and ecoregions are the two predictors in the GAM, wetlands in different ecoregions may respond differently to climate change impacts. In order to test the sensitivity of modeled F_{wet} by ecoregion, we artificially added a 1% change to the input SMC, with the changes in resulting F_{wet} solely attributable to the ecoregions' intercept-adjustments. Figure 5 shows the aggregated change in F_{wet} in eight ecoregions in the Canadian prairies with perturbed 1% SMC. Given that the statistical model fitted is additive in the effects of ecoregion and $s(SMC)$, the perturbed change may translate into non-linear responses in F_{wet}. For the whole domain, the model-predicted F_{wet} increased at twice the rate of the perturbed change in SMC in the Canadian prairies. There is a clear gradient in the response of wetland fraction to SMC, with a weaker response in the moist southwest Manitoba uplands and aspen parkland compared with strong responses in drier regions including the western Alberta uplands, mid-boreal uplands, and fescue grassland.

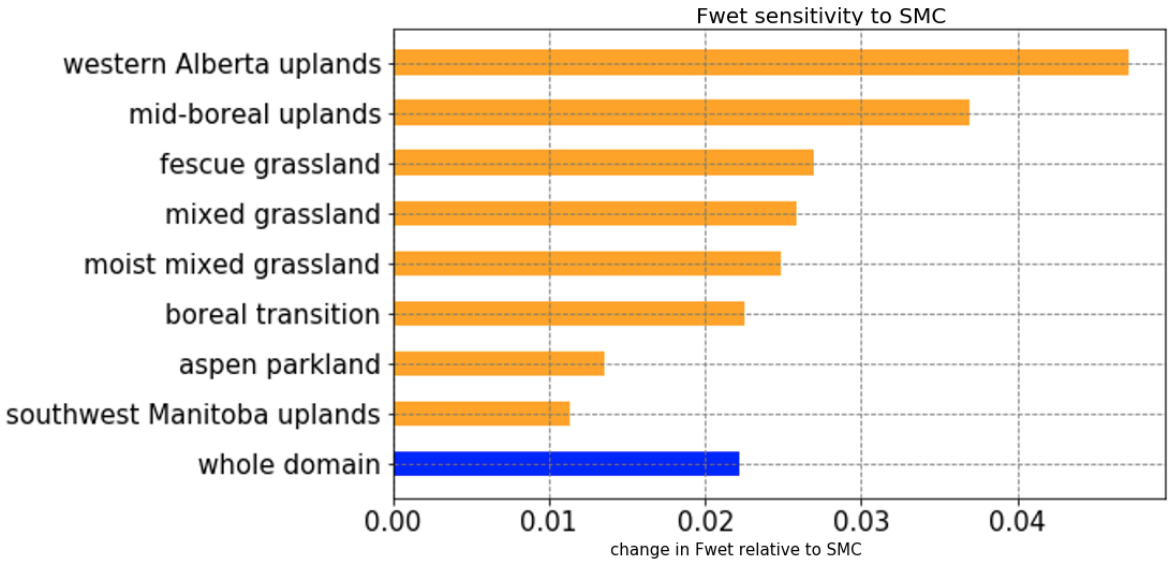

Figure 5.5. Bar plot of change in F_{wet} relative to a 1% increase in soil moisture content (SMC) for the entire domain and eight ecoregions.

In addition to the ecoregion-wise validation, we also compared the interannual F_{wet} change with the wetland ponding depth records at the St. Denis National Wildlife Area (SDNWA). Figure 6 shows the long-term ponding depth record from 140 ponds in the SDNWA (Δ ponding depth on the left axis) with annual F_{wet} values from CTRL and PGW in the corresponding 4-km grid cell (on right axis). Most of the SDNWA records are from Apr to Sep, so those same monthly F_{wet} values from the GAM are selected. Both ponding depth and F_{wet}reflect the moisture conditions in this area. From 2001 to 2013, an increasing trend of ponding depth and F_{wet} are evident. Additionally, although the SDNWA ponding depth is also affected by hydrological and ecological processes other than soil moisture content, the general trend of SDNWA ponding depth largely agrees with that of CTRL F_{wet}. In 2001 and 2002, both datasets show values below the multi-year mean. An increasing trend of ponding depth and F_{wet} is obvious in the following years from 2003 to 2006, though the model predicts a stronger increase in F_{wet} in CTRL than the SDNWA ponding depth. For the rest of the timeseries from 2007 to 2013, both F_{wet} and ponding depth remain high with some interannual fluctuation. For the corresponding period in the PGW climate at the end of the century, the red line indicates a stronger increase in moisture conditions and larger interannual variations. This analysis adds credibility to our statistical model, demonstrating reasonable representation of interannual wetland variability in the Canadian prairies.

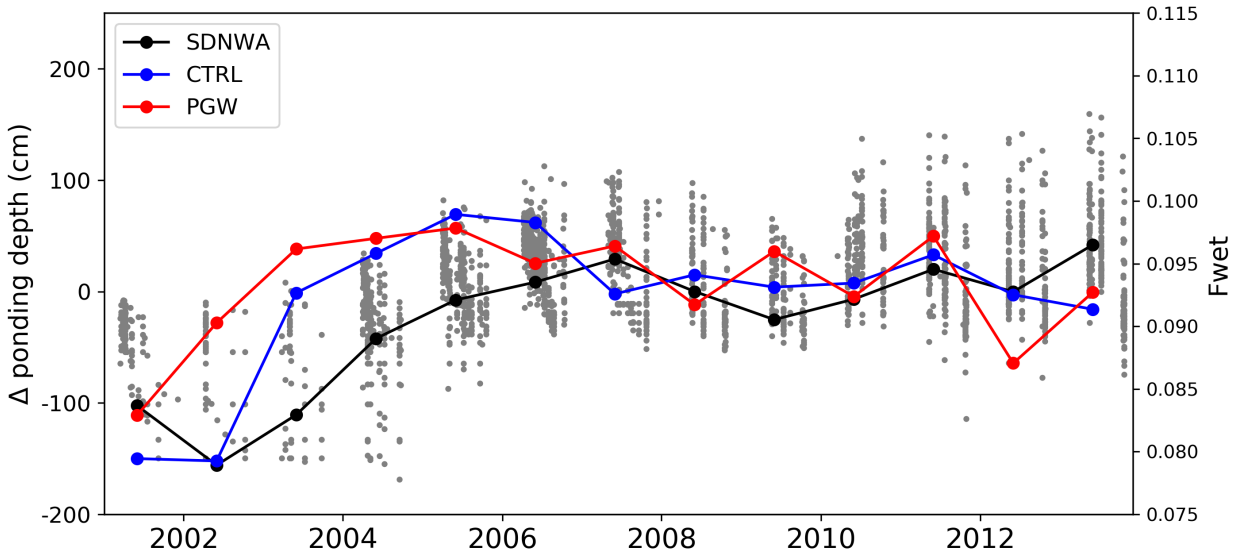

Figure 5.6. Scatter plot of Δ ponding depth (cm) (exact ponding depth – all-time mean depth) from 140 ponds in SDNWA with annual F_{wet} value from the GAM model (gray dots). Records from Apr to Sep are shown. The black line is the mean Δ ponding depth averaged over 140 ponds for each year. The blue line is the mean F_{wet} value for each year from 2001 to 2013 and red line is for the corresponding period under the PGW climate at the end of the 21st century.

5.3.2 Future climate conditions between PGW and CTRL

Figure 5.7 shows the impacts of climate change (PGW-CTRL) in temperature ($\Delta T2, ℃$) and monthly precipitation (ΔPR in mm and %) and their regional average by ecoregion in four seasons in the Canadian prairies. All ecoregions exhibit a warming signal from 4 to 7 ℃, with the strongest warming in winter (DJF). The changes in precipitation vary across seasons and ecoregions, though mostly increase except in summer (JJA). In all seasons, the climate change scenario shows a negative correspondence between temperature warming and precipitation change. Ecoregion-wide, southwest Manitoba uplands experience the most warming in all seasons and usually the least precipitation increases, implying possible drying conditions in the eastern Canadian prairies. On the other hand, western Alberta uplands and fescue grassland receive the most precipitation increase and least temperature warming, indicating potentially wetter conditions in the western Canadian Prairies. These spatially heterogeneous changes in climatic conditions in future climate, in both temperature and precipitation, will manifest in hydrological change, i.e. soil moisture, and reflect in the change of F_{wet} from the GAM model.

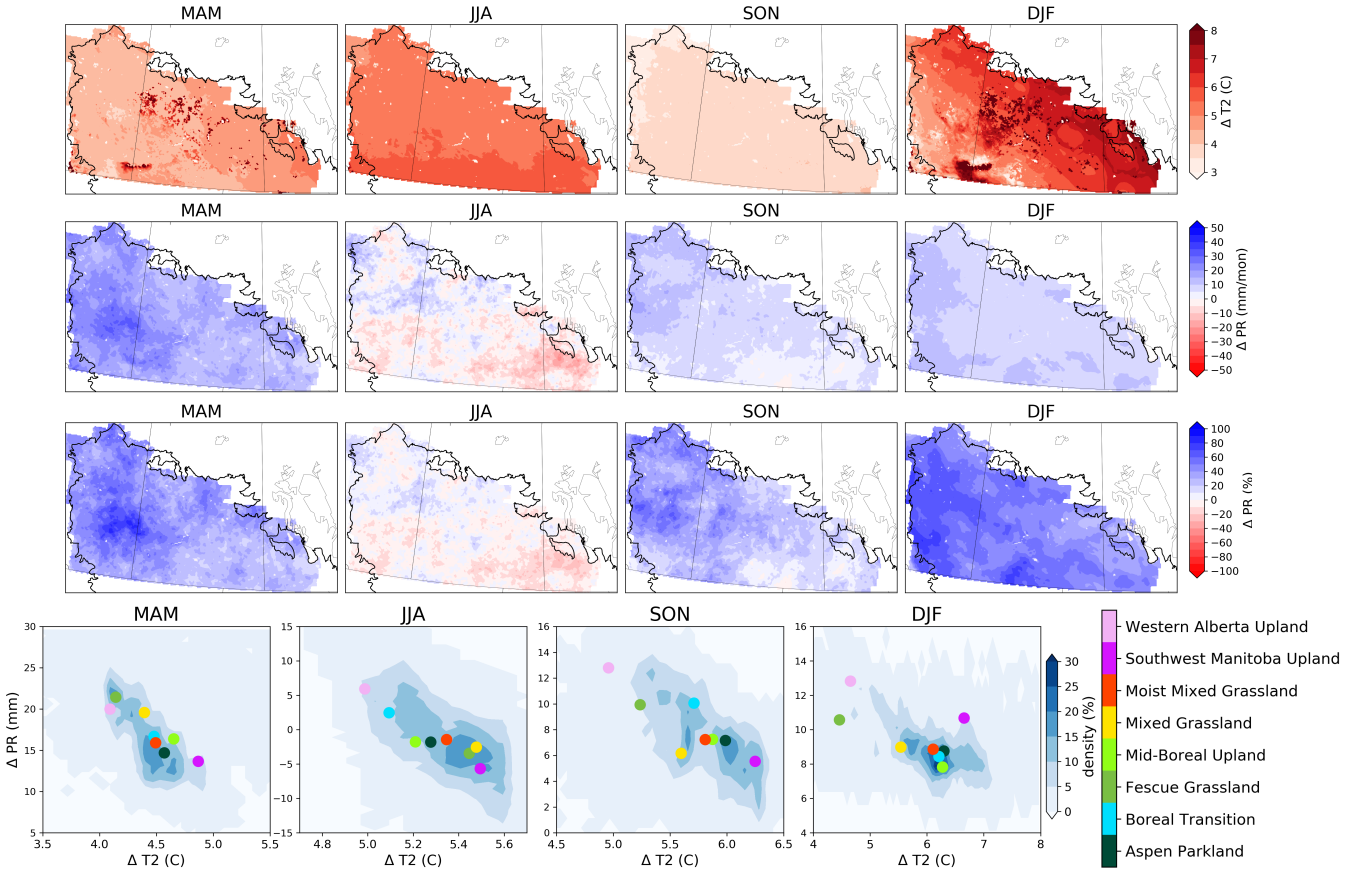

Figure 5.7. The first three rows show the PGW- CTRL Δ change in 2-m temperature (ΔT2, ℃), monthly precipitation (ΔPR, mm/mon), and precipitation in %, in four seasons. The fourth row shows the temperature change (ΔT2, ℃) and precipitation change ((ΔPR, mm) in the Canadian prairies by season and ecoregion. The blue shading represents the probability density for all the grid points in the study domain.

5.3.3 Spatially and temporally heterogenous water balance and wetland changes

Climate change impacts on wetlands showed strong spatial heterogeneity. In Figure 5.8, we present the differences in F_{wet} (from March to August) between current and future climate (PGW-CTRL) as the relative change, calculated as ((F_{wet}_PGW- F_{wet}_CTRL)/ F_{wet}_CTRL). For the area in the southwest mixed grassland ecoregion in Alberta and Saskatchewan, projected F_{wet} increases by about 30% (Figure 5.8a). In contrast, for the moist mixed grassland and mid-boreal uplands regions in southwest Manitoba and eastern Saskatchewan, which is a region with high F_{wet} under current climate (Figure 5.2), a decline in F_{wet} of about 20% is evident.

Changes in F_{wet} also demonstrate strong seasonal variation. Figure 5.8b & c show the changes in F_{wet} in spring (MAM) and summer (JJA). In spring, there are extensive increases in F_{wet} in the southwest Canadian prairies. In contrast, many areas in summer may see declining F_{wet}. This is due to both temperature warming and precipitation decline in the Canadian prairies in summer (Figure 5.6). As such, the southwest Canadian prairies are getting warmer and wetter with higher F_{wet} in future springs, while the mid-boreal uplands and moist mixed grassland in the eastern Canadian prairies will experience warmer and drier summers and reduced wetland extents. On the other hand, two regions show consistent change in F_{wet} in spring and summer (highlighted by blue and red circles in Figure 5.8a), corresponding to the mixed grassland and mid-boreal uplands ecoregions.

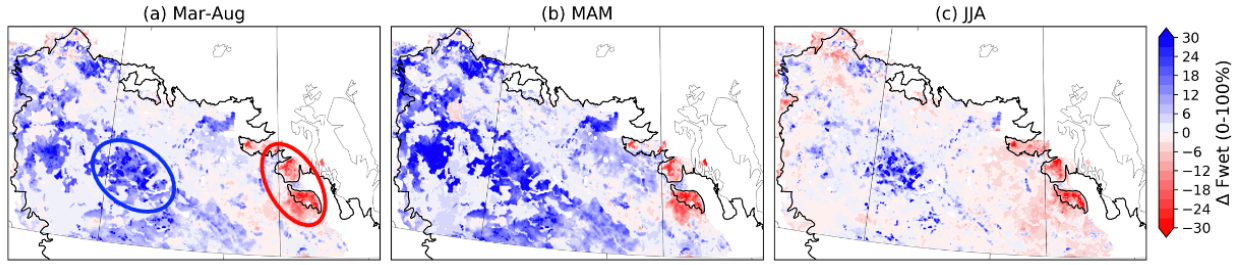

Figure 5.8. (a) Mean relative change in (F_{wet} _PGW-F_{wet}_CTRL)/F_{wet}_CTRL from March to August; (b) in spring (March to May) and (c) in summer (June to August). The blue and red circles in (a) highlight the areas of wetland gain in mixed grassland and loss in mid-boreal uplands ecoregions, respectively.

Figure 5.9 depicts the hydrological cycle of precipitation, SWE and SMC in the mixed grassland and mid-boreal uplands, the two ecoregions highlighted with increasing and decreasing F_{wet} in Figure 5.8a. In the mixed grassland, precipitation increases in almost all seasons, especially in the spring. However, the increased precipitation during cold seasons does not result in a greater snowpack due to warming winter temperatures. The combined effect of increased winter precipitation and temperature result in early melting of snow and higher soil moisture content at the beginning of spring in PGW than CTRL. These wetter conditions in PGW can persist through spring and summer such that F_{wet} shows consistent increases in both spring and summer.

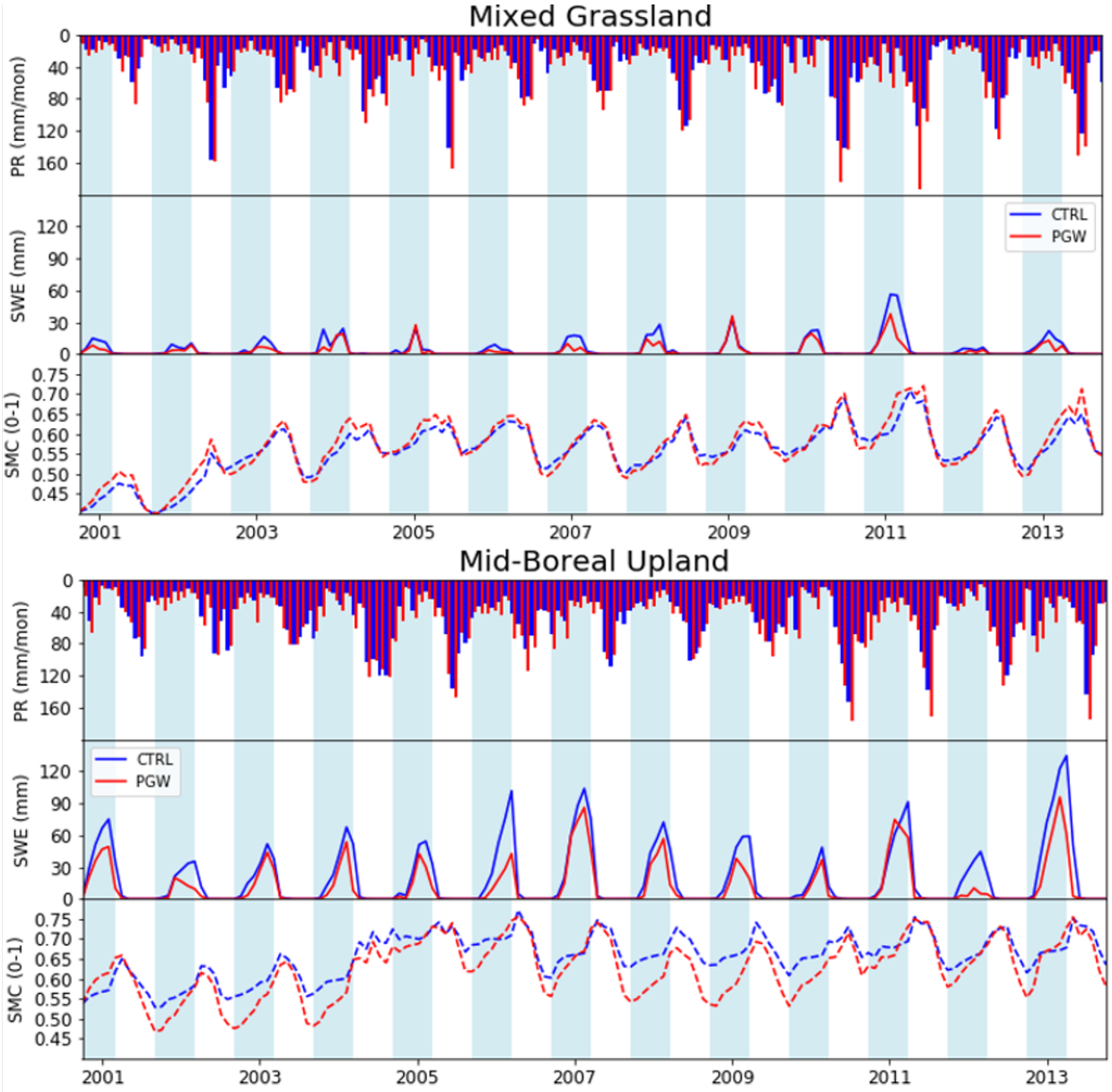

Figure 5.9. Hydrological cycle of precipitation (PR), snow water equivalent (SWE) and fractional soil moisture content (SMC) for two ecoregions highlighted in **Figure 5.8**, the mixed grassland and the mid-boreal upland. Blue and red lines represent the CTRL and PGW climate scenarios, respectively. The light blue shaded blocks correspond to the period from September to February, and the white blocks from March to August.

In the mid-boreal uplands, precipitation shows a strong decline in summer while still increasing in other seasons in Figure 5.9. Both late and slow accumulation, as well as early and rapid snowmelt, is revealed by the significant snowpack loss in this region. These conditions lead to higher infiltration, shown by the steeper increase of SMC in PGW compared to CTRL in spring. On the other hand, hotter summers combined with reduced precipitation result in stronger ET demand, shown by the steeper SMC decline in the summer of PGW than in CTRL, characterizing a strengthened hydrological cycle in this region. Overall, the increase in precipitation in other seasons cannot compensate for the stronger ET demand in summer, thus, F_{wet} is smaller in PGW in both spring and summer.

Furthermore, for these two regions, it is recognized that SMC are shown to increase through winters. This could be due to intermittent warming during winter that causes snowmelt and infiltration into soil layers. So that soil moisture increase is even stronger in the PGW winters. A detailed water balance analysis is presented in the Appendix D (Figure D6). As SMC is the key input for the GAM model, it is important to recognize this increase over winter. However, large scale soil moisture observations are required to validate this feature in the future.

5.3.4 Joint impacts of climate and land use change

The third objective of this study is to explore the joint effects of climate change and historical drainage on prairie wetlands and their ecosystem services. For this purpose, we merge the changes in F_{wet} induced by climate change and the drain score data in the Canadian prairies (Figure 5.2). This is done by: (1) calculating the ΔF_{wet} (PGW-CTRL) under extreme dry or wet conditions; (2) overlaying the ΔF_{wet} with the three categories in drain score map. Figure 10 shows the concordance of future climate change impacts and the drainage score under extreme dry and wet conditions. The change in extreme dry and wet conditions (PGW-CTRL) is characterized by the 5^{th} and 95^{th} percentile of F_{wet} (i.e., F_{wet}_PGW_95^{th}- F_{wet}_CTRL_95^{th} and F_{wet}_PGW_5^{th}- F_{wet}_CTRL_5^{th}). Extreme dry conditions usually occur in summer months and the extreme wet conditions in spring months. We visualize only those grids where $|\Delta F_{wet}|$ is at least 0.1 and overlap it with the three categories of qualitative drain score, creating six cateories as shown in Figure 10. Although some areas are anticipated to be wetter even under the driest (5^{th} percentile) conditions, parts of Saskatchewan with high drainage intensity may experience both amplified dryness and wetness.

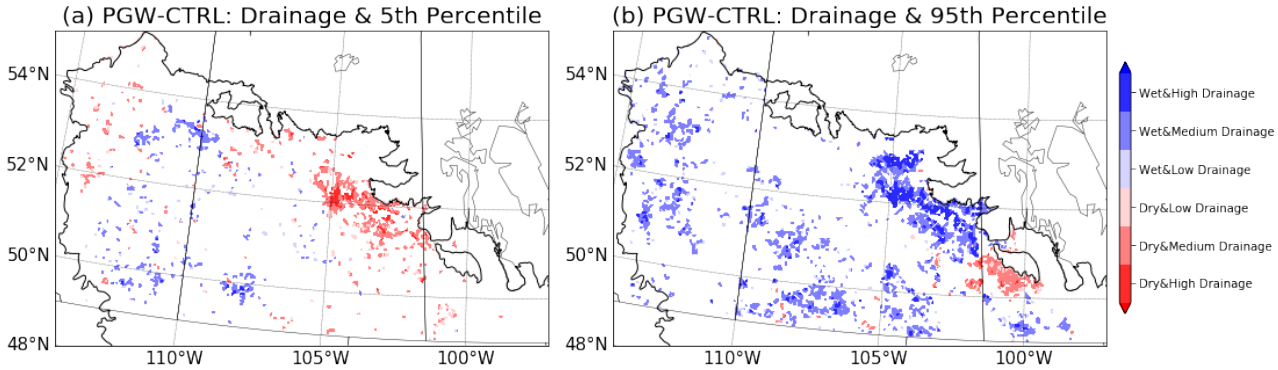

Figure 5.10. Combined effect of climate change and drainage in extreme (a) dry and (b) wet conditions. The dry and wet conditions are selected from the 5^{th} and 95^{th} percentile of the monthly wetland fraction results from CTRL and PGW climate.

5.4 Discussion

5.4.1 Climate change studies in the PPR

Several studies have projected climate change impacts on wetland densities in the PPR, ranging from local-scale (Johnson et al., 2005; Liu and Schwartz, 2012) to regional-scale (Niemuth et al., 2014; Garris et al., 2015; Sofaer et al., 2016) investigations. Variable study scales and data sources have made linking wetland spatial distribution and climatic conditions a challenge. The most common approach has been to statistically relate different climatic variables, landscape management types, and human footprints with wetland abundance (Herfindal et al., 2015, Niemuth et al. 2014, Sofaer et al., 2015, Garris et al., 2015). Typically, the key variable in these studies has been water balance (P-PET, Herfindal et al., 2015). Less often, physical process-based hydrology or LSMs have been applied in wetland studies (Johnson et al., 2005; Capehart et al., 2011; Fan et al., 2012). These studies attempted to simulate hydroperiod, soil wetness, and shallow water table, to represent the dynamics of wetlands in the PPR. Importantly, these variables are analogous to the surface water balance, as represented by the fractional SMC in this study.

Wetland distribution under climate change reflects the change in climate forcing and thus is subject to differences in study periods and regions, data sources, the choice of GCMs, whether and how the GCMs are downscaled, and hydrological models used. Climate observation records show a wetting trend in precipitation, streamflow, soil moisture and wetland pond counts, etc., in the southern PPR (Niemuth et al., 2010; McKenna et al., 2017) and eastern Canadian prairies (St. Jacques et al., 2014). In the Smith Creek watershed, Dumanski et al. (2015) recorded an increasing trend and abnormally high values of streamflow volume, indicating that the watershed is already experiencing changes in the runoff mechanism, relying more on rainfall and less on snowmelt (Shook and Pomeroy, 2012). In our study, an increasing trend of F_{wet} index during the CTRL simulation period agrees with the above findings. However, in the PGW scenario, both warmer temperature and decreased summer precipitation contribute to reduced F_{wet} in the eastern Canadian prairies, especially in the mid-boreal uplands, boreal transition, and eastern aspen parklands ecoregions. This projection differs from recent observations mainly due to reduced summer precipitation from the PGW scenario (Figure 4). This finding highlights the importance of precipitation projections in assessing hydrological and ecological impacts from regional climate change.

The choice of climate change scenario and downscaling method will make fundamental differences to the projection results for hydrological responses and ecosystem impacts. Johnson et al. (2005) applied three climate change scenarios uniformly across the entire PPR and concluded that the region with greatest productivity in the central PPR will shift east- and southwards. However, these climate change scenarios are not realistic as GCM model projections are much more heterogeneous than a uniform increase of temperature or perturbations in precipitation for the entire PPR. Furthermore, St. Jacques et al. (2013) modeled the central Rocky Mountain river discharge (the western Canadian prairies in our study) using large-scale climate indices such as the Pacific Decadal Oscillation, El Nino Southern Oscillation and Arctic Oscillation/North Atlantic Oscillation, forced with CMIP3 until 2096. They found a general declining trend in the surface water availability. Climate model downscaling studies using the delta method in the Canadian Rockies (Cline River watershed, Kienzle et al., 2012; Beaver Creek watershed, Forbes et al., 2011; North Saskatchewan River watershed, MacDonald et al., 2012) also project a change in seasonality of the hydrological regime in this region: earlier onset of snowmelt and higher peak streamflow in

spring but lower streamflow in summer. This strong seasonal contrast of wetter spring and drier summer is consistent with our predictions. However, we predict greater summer precipitation compared to the above studies, highlighting the differences in projection scenarios, especially with respect to precipitation. Finally, another recent modeling study, using the same PGW method in the Marmot Creek Basin in the western Canadian prairies, also demonstrated declining and earlier melting of snowpack, inducing huge increases in streamflow (236%) in spring and reductions in summer (12%), and an overall increase of 18% annually (Fang and Pomeroy, 2020).

The main limitation of the PGW method is the trade-off between selection of climate scenarios, simulation time and high model resolution. With high-resolution convection-permitting configuration, these simulations require great computational resources, which limits the selection of climate change scenarios. For example, only one emission scenario (RCP8.5) from an ensemble of 19 GCM members and shorter simulation time is used in this study, compared to the delta method which can afford to explore climate change impacts on longer time scales or for more emissions scenarios. Nonetheless, the PGW method with high-resolution is currently considered the best option to assess future climate changes and their impacts on hydrology and ecology for large regions (Liu et al., 2017; Prein et al., 2017; Li et al., 2019) for a specific scenario.

We also recognized the limitations regarding the equation (4.6) used in the GAM model. In equation (4.6), the variation in SMC is assumed to represent the hydrological responses to climate change and the ecoregion factors are treated as constants. In this approach, critical hydrological processes at local and watershed scales, such as blowing snow redistribution and fill-and-spill, are underrepresented in our model. These processes, which occur at sub-grid resolution (Shaw et al., 2012) much smaller than the 4-km resolution, are not sufficiently monitored in observation over large regional scale in the Canadian Prairies, nor are represented in the typical scale LSMs. Although Noah-MP doesn't directly simulate the blowing snow process, its capability of reasonably simulating snow accumulation and snowmelt is demonstrated against gridded distributed snow observation (see Supporting Information). One recent study applied the Cold Region Hydrological Model (CRHM) in the Mauvais Coulee Basin (MCB) and demonstrated the spatiotemporal variation in snow redistribution and sublimation can be significant for surface water balance, though requires fined field observations to verify (Van Hoy et al., 2020). We are also actively developing a dynamic surface water storage scheme in Noah-MP LSM, incorporating inflow, outflow, and ET feedback from wetland ponds to the atmosphere.

On the other hand, ecoregion factors are treated as constants for two reasons: first is because it allows us to attribute the changes of F_{wet} solely to soil moisture content, driven by two sets of climate forcings from the current and future climate; second is that the ecoregion map is utilized by conservation agencies as boundaries and design strategies for each ecoregion. The eight ecoregions used in this study represent clearly their geographical locations while incorporating their ecofunctions to the modeling framework is outside the scope of this study and would require and entirely separate study.

5.4.2 Implications for wetland conservation

The spatial heterogeneity of climate change impacts on wetland fraction in the Canadian prairies is a challenge to conservation decision-makers, especially under extreme climate conditions and uncertainties associated with anthropogenic drainage. Considering extreme climate conditions (droughts and floods) can constrain the magnitude of possible wetland area change, complementing an assessment of effects of climate change on average wetland conditions (Figure 7). Including anthropogenic drainage can help spatially prioritize conservation efforts by revealing both areas that may remain robust to climate change and areas where wetland ecosystem services may be imperilled by climate change and drainage.

Projected changes in F_{wet} suggest the need for a diversified approach to wetland conservation, one that considers both the future hydrological suitability of wetland retention and restoration efforts, as well as how historical drainage patterns will interact with changes in wetland extent to affect the availability of wetland ecosystem services. For example, the consistent wetland increases in the western PPR, under both wet and dry extremes, suggests wetland retention and restoration will be hydrologically favourable under climate change, with water available to fill wetlands and maintain wildlife habitats even in relatively dry summers. Relatively wet areas may act as refuges for mobile wetland-associated species like waterfowl, as long as upland conditions (i.e., sufficient perennial cover for nesting) are favourable. In contrast, highly drained areas in eastern Saskatchewan will be challenged under fluctuating hydrological conditions. The combination of high wetland loss and intensified drought conditions under climate change will mean a shortage of wildlife habitat in dry years. In contrast, extreme wet conditions may lead to flooding in spring snowmelt season, exacerbated by wetland loss. Therefore, conserving and restoring wetlands in the aspen parkland and boreal transition regions in eastern Saskatchewan may act as a buffer against flooding during intensified future wet periods. Other areas of the Canadian prairies, like western Manitoba, could become challenged by moisture deficits (even in the wettest years) that will not favour the inundation and persistence of wetlands. Conservation planning will benefit from the incorporation of future wetland distributions for multiple applications such as refining spatial targeting (e.g., by the PHJV for waterfowl habitat), targeting wetland restorations to maximize ecosystem services, and more.

In addition to impacting wetlands via change in the surface water balance, climate change may have indirect effects on wetlands via land use change. Wetland conservation strategies should take into account these direct and indirect climate effects. For example, Beaman (2016) found that climate change may alter agricultural economics such that annual-seeded crops increase at the expense of natural and semi-natural landcovers. Given that drainage for agriculture has been the historical driver of wetland loss on the prairies (Watmough and Schmoll, 2007; Doherty et al., 2018), with ongoing losses of ~ 3% of wetland area per decade, land use change could augment or offset direct climate effects on wetlands (PHJV 2014). Previous research combining modelling the direct effects of climate change with changes in land use in the US portion of the PPR suggested that projected changes in land use are not expected to greatly modify the direct effects of climate change (Sofaer et al. 2016). However, the Canadian PPR may exhibit different patterns, which should be investigated.

5.5 Conclusion

Conservation of prairie wetlands is crucial to protect the vital services they provide including regulating floods, improving water quality, and supporting biodiversity. It is necessary to consider the impacts of climate change in conservation planning, for they pose a threat to wetland habitats through alteration of the hydrological cycle. The approach used in this study, a dynamical downscale from a high-resolution convection-permitting regional climate simulation as our climate projection, has better representation of land surface properties and less uncertainty in the precipitation forecast than many previous efforts to model the effects of climate change in the PPR. It is also more realistic and informative than using GCM-scale of uniform climate forcings to simulate hydrological responses in this region.

Overall, the climatic change is projected to be wetter in all seasons, except in summer, with strong spatial heterogeneity and seasonal variation and corresponding effects on wetlands. For the western Canadian prairies, in particular in the mixed grassland ecoregion in Saskatchewan, wetland fraction is expected to to increase in future climate in both the spring and summer seasons. Increased precipitation with warmer temperatures over winter results in higher late accumulation and early melting of snow. This is manifested in a substantial increase in soil moisture in future springs when compared with the current climate. However, in the eastern Canadian prairies, wetlands are expected to increase in spring but decrease in summer, due to reduced summer precipitation and intensified ET demand in this region. Moreover, this precipitation reduction and stronger ET demand lead to declining wetland fraction in both spring and summer for the mid-boreal uplands along the northeast boundary of the Canadian prairies.

The heterogeneous change in projected climatic and hydrological conditions may alter the current wetland distribution of the Canadian prairies, where wetlands are more abundant in the east. This has implications for wetland conservation and ecosystem services, especially when considered in light of historical wetland losses due to drainage. Areas expected to experience extended summer drying coinciding with areas with high density of drainage ditches (and thus already high wetland loss) may be challenged through loss of wetland ecosystem services. The western PPR, with moisture conditions conducive to wetland persistence through the spring and summer, will remain a safe choice for wetland conservation efforts. Assessments of the effects of climate change on wetland conservation must fully consider ecological, economic, and social realities along with the potential for climate-induced changes to determine the most effective spatial targeting of wetland conservation and restoration.

Key points for the next chapter

- The GAM model used in this study with input from soil moisture and ecoregion factors could effectively estimate the surface wetland fraction in the PPR region.
- Future projections of wetland extents are strongly controlled by the input of meteorological forcing, which are supplied from CONUS WRF convection-permitting simulations. High-resolution precipitation input is critical to estimating small-scale soil moisture and wetland extents.
- This study uses a statistical approach to estimate wetland extents under current and future climate states. To deepen the understanding and improve the representation of the wetland hydrological cycle and land-atmosphere interaction, a dynamic approach is needed to incorporate LSM and coupled RCM, which will be the topic of the next chapter.

Acknowledgments
The authors thank L. Boychuk and S. Witherly for GIS support and M. Watmough for providing access to drainage score data. Z. Zhang was funded by a Mitacs Accelerate Fellowship funded by Ducks Unlimited Canada's Institute for Wetland and Waterfowl Research. Z. Zhang, Z. Li and Y. Li acknowledge the financial support from the Natural Sciences and Engineering Research Council of Canada (NSERC) Discovery Grant, and Global Water Futures Program, Canada First Research Excellence Fund. This project was supported by grants from Wildlife Habitat Canada, Bass Pro Shops Cabela's Outdoor Fund, and the Alberta NAWMP Partnership.

Chapter 6 – Evident wetland cooling effects to temperature relieves heat stress and mitigates climate change

This manuscript has been modified for inclusion in this thesis. It was originally submitted as:

Zhang, Z., Chen, F., Barlage, M., Bortolotti, E. L., Famiglietti, J., Ma, X., Li, Z., Li, Y. Evident cooling effects of surface wetlands to mitigate climate change – a study of North America Prairie Pothole Region. (2021). Water Resources Research.

An **addendum** is added by the end of this thesis for revision made to this manuscript.

Author contributions: Z. Zhang and M. Barlage designed the study and wrote the paper. F. Chen and J. Famiglietti provided valuable experience on the TOPMODEL and insight on the topic. Y. Li, L. E. Bortolotti and Z. Li contributed to the interpretation of the results and reviewed the manuscript. X. Ma provided great supports on observation data collection.

Keywords

Wetland, Hydrology, Land surface model, Land-atmosphere interaction, Convection-permitting model, Climate change mitigation

Abstract

Wetlands are an important land type on Earth's surface, significantly alter surface energy and water balance, and provide vital ecosystem functions such as regulating floods, storing carbon, supporting wildlife habitats. The ability to reasonably simulate their spatial extent and hydrological processes are important to valuing wetlands' function and mitigating climate change impacts. The purpose of this study is to dynamically simulate wetlands' energy and water balance, as well as its feedback to regional climate in the North America Prairie Pothole Region (PPR), where a large number of surface wetlands exist. In this study, we incorporate a dynamic wetland scheme into the Noah-MP LSM, which includes two major modifications, (1) modifying the sub-grid fraction of F_{sat} to represent spatial wetland extent; (2) incorporating a dynamic surface water storage to simulate wetland hydrological processes. These two modifications are tested in the Fen site in central Saskatchewan, Canada and applied regionally in the PPR with high-resolution convection permitting climate forcing for 13 years. The difference between wetland and no-wetland simulations are significant in increasing latent heat and evapotranspiration while decreasing in sensible heat and runoff. Finally, the dynamic wetland scheme is tested using the WRF model over three summers. The wetland simulations show an evident cooling effect of 1~3℃ in summer where wetlands are abundant, which is linearly related to the wetland extent when water is not limited. In particular, the wetland simulation shows reduction in the frequency of extreme hot days over the summer of 2006, when a long-lasting and widespread heatwave occurred in the U.S. Midwest and Southern Canada. This research has great implications for land surface/regional climate modeling, as well as wetland conservation, for valuing wetlands in providing a moisture source and mitigating extreme heatwaves, especially under climate change.

Motivation

In the previous chapter, a statistical method was developed to estimate spatial wetland extents under the future climate using hydrological outputs and factors involving ecoregions. The next step forward is to represent wetland hydrological processes in the Prairie Pothole region. For this purpose, two major modifications are applied to address the wetlands spatial extents and to dynamic hydrological processes in this chapter. The modifications in this chapter also show significant feedback to the atmosphere when the dynamic wetland scheme is coupled with a regional climate model (WRF) for summertime simulation. The finding of this paper will benefit both the climate science community and the waterfowl and wetland conservation community.

6.1 Introduction

Wetlands are important and unique ecosystems around the world that play vital roles in Earth's ecosystem balance and biodiversity. Although wetlands occupy a small portion of the Earth's global land surface (~6%), they store about one third of terrestrial carbon (Lehner and Doll, 2004; Mitra et al., 2005; Mitsch and Gosselink, 2007). Moreover, due to their unique abundance in nutrient and aquatic ecosystems, wetlands also support a wide variety of plants, birds, and amphibians; areas of high biodiversity, they are especially important for migratory waterfowl (The Ramsar Convention, 2007). They can effectively regulate regional surface energy balance and hydrological cycle, potentially influencing regional climate through complex land-atmosphere interactions. Wetlands are natural reservoirs to prevent flooding, especially in high latitudes and mountainous regions (Hayashi et al., 2016; Pattison-Williams et al., 2018). After springtime snowmelt or heavy rainfall, surface runoff can be stored in wetlands, effectively bending the curve and delaying the peak time of flooding. The presence of surface water and the moisture conditions of wetland soils can effectively store surface energy and favor energy partitioning to latent heat flux over sensible heat. Specifically, the more partitioning to latent heat flux over sensible heat flux that occurs in wetland water bodies, the more summer temperatures (Bonan, 1995) and daily air temperature variability will decrease (Hostetler et al. 1993). This land-atmosphere interaction is analogous to soil moisture-temperature feedback (Seneviratnes et al., 2010), inducing a cooling effect on surrounding environments.

With unique geology, hydrology, and climate conditions, the North American Prairie Pothole regions (PPR) contains millions of small wetlands known as "potholes". The retreat of continental ice sheets over 11, 000 years ago left glacial deposition upon the landscape, forming millions of depressional terrains. Poorly hydraulic connected, these depressions are isolated from large river networks. The cold winters allow snow to accumulate over cold seasons, and springtime runoff and seasonal rainfall provide major water input to these wetlands. Over the warm season, evaporation exceeds precipitation, drying the surface water and exposing the underlying soils. The persistence and storage of wetland ponds depend on receiving seasonal rainfall and connection with shallow groundwater. Under extremely wet conditions, strong rainfall or sudden snowmelt increases the water level of wetlands, exceeding the maximum capacity. In a "fill-and-spill" process, water from several filled wetlands will spill over to other surrounding wetlands, depicting a "fill-and-spill" process, and form a largely connected wetland complex (van der Kamp and Hayashi, 2009; Mekonnen et al., 2014; Vanderhoof et al., 2018). These complex interactions between climate, wetland, and groundwater are challenging to simulate in traditional hydrological models and land surface models (LSMs).

Given the importance of wetlands to the global and regional environment, representing wetland hydrological processes in earth system models and land surface models has emerged as an area of interest in recent decades. In the CLM (Oleson et al., 2008) and Noah-MP LSM (Niu et al., 2011; Yang et al., 2011), a relationship has been established between the grid-cell's saturated fraction and the depth of groundwater, based on the TOPMODEL a hydrological model (Beven and Kirkby, 1979) and its application in LSMs (Famiglietti and Wood, 1991, 1994a)– TOPMODEL (Beven and Kirkby, 1979). This method assumes that the sub-grid representation of grid-cell saturation is based on a redistribution of the water table depth, given the variation of slope and contributing areas to the grid cell. A sub-grid saturated fraction F_{sat} is defined for the local water table at the surface and can be used for runoff generation as in saturated excess runoff. While this may be sufficient estimation over a large grid resolution in many GCM models (~50-100 km), it is not sufficiently detailed reasonable and too crude for high resolution regional simulation (~5-10 km). Despite its limitations and insufficiency, TOPMODEL- based F_{sat} is widely used in many LSMs and ESMs, particularly in representing global wetland extents. The discrepancies in projecting wetland extents have major implications for modeled CH4 emissions, as summarized in a wetland CH4 inter-comparison modeling project (WETCHIMP, Wania et al., 2013, Melton et al., 2013).

On the other hand, to represent the dynamics in lakes and wetlands and investigate their impacts on energy and water cycle, many models have incorporated surface water storage schemes. For example, Pitman (1991) incorporated a sub-grid scheme for the water surface and its contribution to latent and sensible heat is taken as the weighted average over the fraction of water, vegetated and bare ground surface in a coarse resolution (~2°) GCMs. The Variable Infiltration Capacity model (VIC, Liang et al., 1994) has developed a dynamic lake and wetland scheme to study the impacts of surface water heterogeneity on energy and water balance (Bowling and Lettenmaier, 2010). Results show that incorporating wetlands increases the annual ET by 5% and decreases runoff by ~ 12% in the U.S. Midwest region. As latent heat fluxes increase, sensible heat fluxes decrease. Despite robust results in surface energy and water balance, this research is not coupled with regional climate models, therefore omitting the feedback from wetlands to temperature and precipitation.

The purpose of this study is to study the **impacts of dynamic wetlands on the surface energy and water balances, as well as their feedback to the regional climate** in high-resolution convection-permitting regional climate model with spatial resolution < 5-km, (CPRCM, Prein et al., 2015). For this purpose, we have established three steps: (1) Develop a physical process-based parameterization of sub-grid wetland extent and dynamic wetland storage scheme; (2) Explore the impacts of including this wetland parameterization on the surface energy and water balance in offline regional land-surface hydrology simulations using Noah-MP; (3) Investigate the interactions between the wetland hydrological cycle and its feedback to the regional climate using the coupled Weather Research & Forecasting model (Skamarock, et al., 2008) system with Noah-MP LSM. In particular, it is worth highlighting the potential cooling effect of surface wetlands in mitigating summertime heat stress, especially during the widespread high-intensity heatwave, which occurred in 2006 in Southern Canada and the U.S.

6.2 Data and Model

6.2.1 Global Inundation Extent from Multiple Satellites (GIEMS-2)

The 1993-2007 Global Inundation Extent from Multiple Satellites (GIEMS-2) is a unique dataset that provides estimates on surface water extents and dynamics, based on a collection of satellite observations (https://lerma.obspm.fr/spip.php?article91&lang=en). The satellite data are used to calculate monthly-mean inundated fractions of equal-area grid cells (0.25°x0.25° at the equator), taking into account the contribution of vegetation (Prigent et al., 2001, 2007, 2012; Papa et al., 2010). Such estimates use both passive and active microwave measurements, along with visible and near-infrared reflectance to capitalize on their complementary strengths, to extract maximum information about inundation characteristics, and to minimize problems related to one instrument only. The technique is globally applicable without any tuning for particular environments. The GIEMS data have been widely used to evaluate surface wetland extents in multiple GCMs intercomparison studies for simulating wetland extents (Wania et al., 2012; Melton et al., 2012).

6.2.2 Convection-permitting regional climate simulation

The convection-permitting model (CPM) refers to the atmospheric models whose grid spacing is fine enough (usually < 4-km) to permit convection and resolve mesoscale orography (Rasmussen et al., 2011; Prein et al., 2015; Liu et al., 2017). Long-term high-resolution climate downscaling using CPM provides important added-values to improve precipitation forecasting, which is critical in surface wetland hydrology, as well as in resolving fine scale land surface heterogeneity (Kenden et al., 2017).

The WRF convection-permitting regional climate simulation over the CONtiguous U.S. (CONUS WRF, Liut et al., 2017) provides a good opportunity for long-term (13-year), high-resolution (4-km) land surface modeling (Zhang et al., 2020). The CONUS WRF consists of simulations for the current climate and for the future climate using the Pseudo Global Warming method (PGW) (Schär et al., 1996, Rasmussen et al. 2011). The current climate simulation is a retrospective run from 2000-10-01 to 2013-10-01, forced by ERA-Interim as boundary and initial condition. For the future simulation, a delta climate perturbation, derived from the 19-model ensemble in the CMIP5 project under RCP8.5 scenario at the end of 21st century, is added upon the ERA-Interim forcing (Simons et al., 2007). The future simulation represents an equivalent 13-year period at the end of the 21st century. The CONUS WRF forcing has been used in multiple climates, hydrology, and land surface studies (Zhang et al., 2020; Fang et al., 2021). In this study, we also use CONUS WRF forcing in the PPR region for offline land-surface model regional simulations to study the impacts of incorporating a surface wetland scheme on regional energy and water balance in the PPR.

6.2.3 Application of TOPMODEL in LSMs

TOPMODEL (TOPography based hydrological MODEL) is a rainfall-runoff model that uses topography data to reflect its dynamic processes responses in downslope hydrology, especially in the runoff generation in a variable contributing area, which was developed about 45 years ago (Kirkby 1975; Beven and Kirkby, 1979; Beven et al., 2020). TOPMODEL's basic assumption is that the runoff generation responses to a steady state rainfall is proportional to the spatial variation of moisture contents in a drainage basin and can be characterized by its topography variation by digital topography analysis, which is the name of the model. In the model, a topographic index was defined, $\Lambda = ln\,(\frac{a}{tan\beta})$, where a is the area draining through a point from upslope and $tan\beta$ is the

local slope angle. High index values are likely to saturate first, hence, indicate potential subsurface or surface contributing areas (Beven, 1997).

The simplicity of the model comes from the assumption that all the points of the same value of the index respond similarly in the catchment. As a result, it is not necessary to calculate all the points in a catchment, but the integration of each interval of index values must be calculated through the distribution function. In a steady state, a critical threshold value for local topographic index (Λ_{cri}) can be obtained when the local water table depth is at the surface, compared to the grid cell mean water table depth. A sub-grid fraction F_{sat} can be defined by integrating the topographic index interval from this critical value to the maximum, following its probability distribution function:

$$F_{sat} = \int_{\Lambda_{cri}}^{\infty} pdf(\Lambda)d\Lambda \quad (6.1)$$

This probability distribution function was assumed to be a three-parameter gamma distribution by Sivapalan et al. (1987).

This F_{sat} fraction is an important parameter in partitioning surface water using the saturation runoff mechanism, i.e., the F_{sat} portion of the surface water from rainfall and snowmelt becomes surface runoff and the remaining (1-F_{sat}) becomes infiltration. The sub-grid F_{sat} is also critical in controlling the surface energy balance and land-atmosphere interaction (Famiglietti and Wood, 1994a&b). In Famiglietti and Wood (1994a&b), a Soil-Vegetation-Atmosphere Transfer Scheme (SVATS) is applied in local, catchment and macroscale to demonstrate the sub-grid soil moisture heterogeneity in controlling both evapotranspiration and runoff. The total evapotranspiration over the sub-grid topographic index in a grid cell is the integration of the potential evaporation from the saturated portion to drier land surface outside the transitional region, where evapotranspiration is restricted by active vegetation and soil moisture (Famiglietti and Wood 1994a). This framework for incorporating TOPMODEL into LSMs (TOPLATS) was utilized in the NASA GISS land surface model (Stieglitz et al., 1997) and the NASA Catchment Land Surface Model (CLSM, Koster 2000; Bechtold et al., 2018) among others.

Due to its computational simplicity, the F_{sat} fraction is also very popular in representing surface wetland extents in large scale global models (Gedney and Cox, 2003; Ringeval er al., 2011). The temporal and spatial variation of the F_{sat} is based on the groundwater dynamics interacting with soil moisture, hence the expansion and shrinking of the surface wetland. Although the meaning of saturation is not necessarily the same as inundation or wetland soil, this fractional area to some degree reflects the wetness condition in a given grid cell, as well as its function partitioning surface water in the "saturation excess" runoff generation. Thus, the F_{sat} fraction has been widely applied in various LSMs and multiple modeling studies simulating wetland extents (WETCHIMP, wetland CH4 multi-model intercomparison, Wania et al., 2013; Melton et al., 2013).

In Noah-MP LSM, the energy balance is calculated separately for two sub-grid semitiles: a fractional vegetated area (F_{veg}) and a fractional bare ground area (1-F_{veg}). In this semitile scheme, shortwave radiation transfer is computed over the entire grid, while longwave radiation, sensible, latent heat flux, and ground heat flux are computed separately over these two tiles. As a result, these two tiles in the Noah MP grid neglects the large extending and seasonally variable open water wetlands. The total latent (LH) and sensible heat (SH) of these two semitiles are aggregated in a weighted function:

$$LH = F_{veg}\left(LE_{gv} + LE_v\right) + (1 - F_{veg})LE_{gb} \quad (6.2)$$
$$SH = F_{veg}\left(SH_{gv} + SH_v\right) + (1 - F_{veg})SH_{gb} \quad (6.3)$$

where subscript *v* representing vegetation canopy, *gv* is ground under canopy, and *gb* is bare ground fluxes.

Additionally, the TOPMODEL based runoff generation model is utilized for surface water partitioning. In Niu and Yang (2005), the pdf of F_{sat} is replaced by an exponential function of the water table depth and utilized in both CLM3.0 (Oleson et al., 2008) and Noah-MP LSM (2011).

$$R_{srf} = Q_{insurf} * F_{sat} \quad (6.4)$$
$$Q_{infil} = Q_{insurf} * (1 - F_{sat}) \quad (6.5)$$
$$F_{sat} = F_{satmx} * exp\,(-0.5 * f * (Z_\nabla - 2)) \quad (6.6)$$

However, the above water balance setting does not reflect the dynamical water movement in prairie wetlands. These wetland depressions actively receive surface water from snowmelt and rainfall, but there is no surface water storage process in Noah-MP, so that the simulated surface runoff component will leave the model grid point. Additionally, this setting further neglects evaporation from the wetland surface to the atmosphere and discharge to surrounding wetlands in the fill-and-spill process. Therefore, a dynamical surface wetland storage scheme, incorporating both sub-grid energy and water balance, is needed to represent the complex hydrological processes in the prairie wetland landscape and their potential feedback to the atmosphere.

6.2.4 Modifying F_{sat} fraction to represent wetland extents

The original TOPMODEL-based F_{sat}, based on an exponential function of the water table depth, does not reasonably reflect the magnitude and seasonal variation of wetland extents in the Prairies. Figures 6.1 and 6.2 shows the spatial distribution and temporal evolution of the inundation fraction from GIEMS and Noah-MP simulated F_{sat} fraction in the PPR region from 2000 to 2014. It is clear that the modeled F_{sat} has underestimated the maximum extent while overestimated the minimum extent. This occurs for two reasons: first, the parameter F_{satmx} is a fixed value (0.38) for the global mean; second, the seasonally frozen soil and glacial till with low hydraulic conductivity prevent direct a groundwater connection with the surface water; hence, the water table dynamic is not a good indicator for the surface water extents in the PPR. Detailed speculations on this discrepancy are provided in the discussion section.

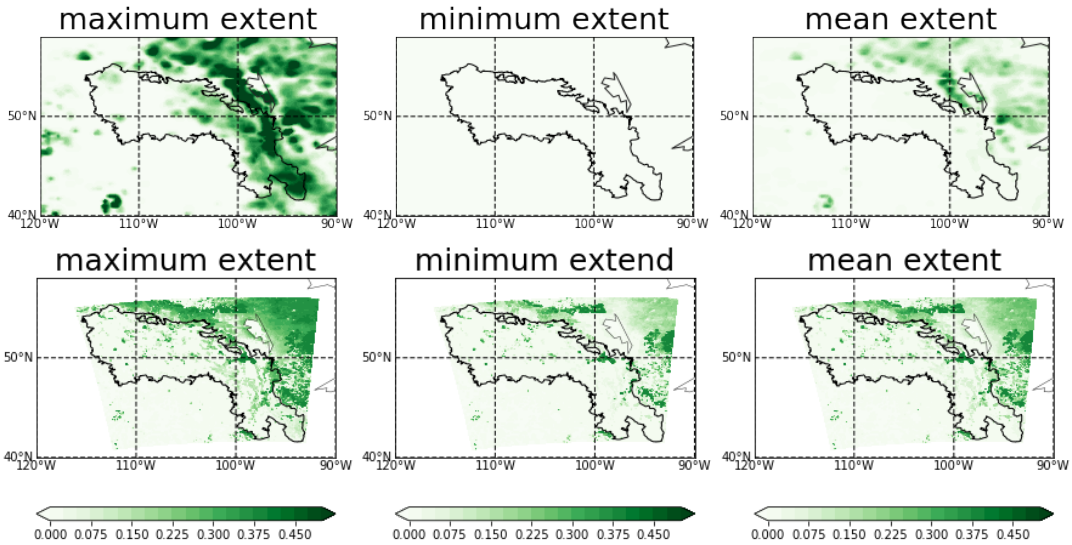

Figure 6.1. Spatial distribution of surface water extent from GIEMS (top) and Noah-MP modeled F_{sat}(bottom), on the maximum, minimum and mean extent.

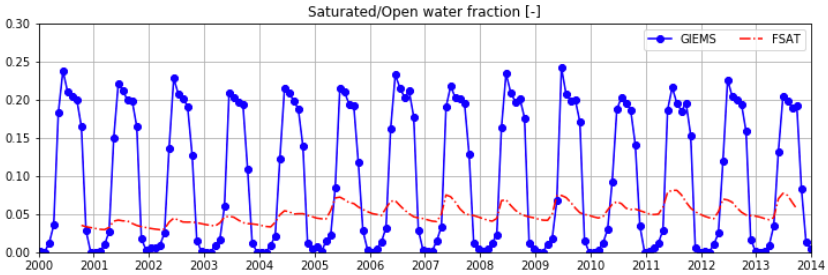

Figure 6.2. Temporal evolution of the inundation fraction from GIEMS and modelled F_{sat} in the PPR region.

Therefore, we propose a new formula for the saturated fraction F_{sat}, based on the first layer of soil moisture, instead of the water table depth:

$$F_{sat} = F_{satmx} * \left(\frac{SH_2O - SM_{wlt}}{SM_{max} - SM_{wlt}}\right) \quad (6.7)$$

The first layer of soil moisture will respond more rapidly to surface hydrological processes, such as snowmelt infiltration and evapotranspiration. F_{sat} is determined by the maximum saturated fraction (F_{satmx}) and a relative soil moisture saturation condition. This modification is basically assuming the mean soil moisture saturation at the first layer soil can empirically represent the spatial heterogeneity of soil saturation at the sub-grid scale.

6.2.5 Implementing surface wetland storage scheme

In this study, we incorporate a sub-grid bucket-style surface water storage scheme to represent the surface water dynamics in Prairie Pothole wetlands in North America by capturing three important processes in its water balance: (1) wetland storage receives water from snowmelt runoff and rainfall; (2) water in wetland storage would evaporate at the potential rate; (3) when the water exceeds the wetland maximum storage capacity (W_{cap}), it will spill out and become the outflow term. This wetland storage scheme operates at a sub-grid scale and uses F_{sat} to determine the inflow of water input from precipitation and snowmelt and contributes to the latent heat flux as a weighted average over all three sub-grid types, similar to the treatment in Pitman (1991). The sensible heat flux is calculated as the residual term from the energy balance equation.

$$Q_{insur} = Q_{snowmelt} + Q_{rain} \quad (6.8)$$

$$Q_{inflow} = Q_{insur} * F_{sat} \quad (6.9)$$

$$Q_{evap} = \frac{mR_n + \rho c_p (\Delta e) g_a}{\lambda_v (m+\gamma)} \quad (6.10)$$

$$LH_{all} = (1 - F_{sat})(F_{veg}(LE_{g,v} + LE_v) + (1 - F_{veg})LE_{g,b}) + F_{sat} * Q_{evap}\lambda_v \quad (6.11)$$

$$Q_{outflow} = max(Q_{inflow} - W_{cap}, 0) \quad (6.12)$$

$$\Delta W_{surf} = Q_{inflow} - Q_{evap} * F_{sat} - Q_{outflow} \quad (6.13)$$

In many traditional LSMs treatments, surface runoff is treated as a drainage term that leaves the grid cell and is a lost term in the water balance. In our new scheme, the surface runoff from snowmelt and rainfall becomes the inflow to surface water storage (Q_{inflow}). The water in surface wetlands evaporates to the atmosphere at the potential rate, which is calculated by the Penman equation. The outflow is a result of total water exceeding the maximum water storage (W_{cap}), characterizing the "fill-and-spill" process. Notably, this surface wetland storage scheme is not connected to another wetland storage or river network, so that the outflow term will leave the grid point and is a lost term in the water balance, as was the surface runoff term in the default Noah-MP. The change of surface water storage (ΔW_{surf}) is calculated by the net result of inflow, evaporation, and outflow.

Figure 6.3 below is a diagram illustrating the difference between the default Noah-MP and the modified surface runoff scheme in this study. The left-hand side shows the default Noah-MP surface runoff scheme based on the TOPMODEL saturation-excess concept. The inflow from rain and snowmelt (Q_{insur}) is be partitioned to infiltration by the 1-F_{sat} portion, which enters soil moisture, and to surface runoff by the F_{sat} portion, which eventually leaves the grid cell. The right-hand side shows the two modifications in our study: (1) modified F_{sat} parameterization based on first layer soil saturation; (2) the creation of a surface water storage W_{cap} representing surface wetland dynamics. The F_{sat} portion of the inflow will now be collected within the W_{cap} storage and evaporate into the atmosphere with a weighted function. The water amount exceeding the maximum capacity will become the outflow from the wetland (which also refers to the new runoff term, R_{srf}).

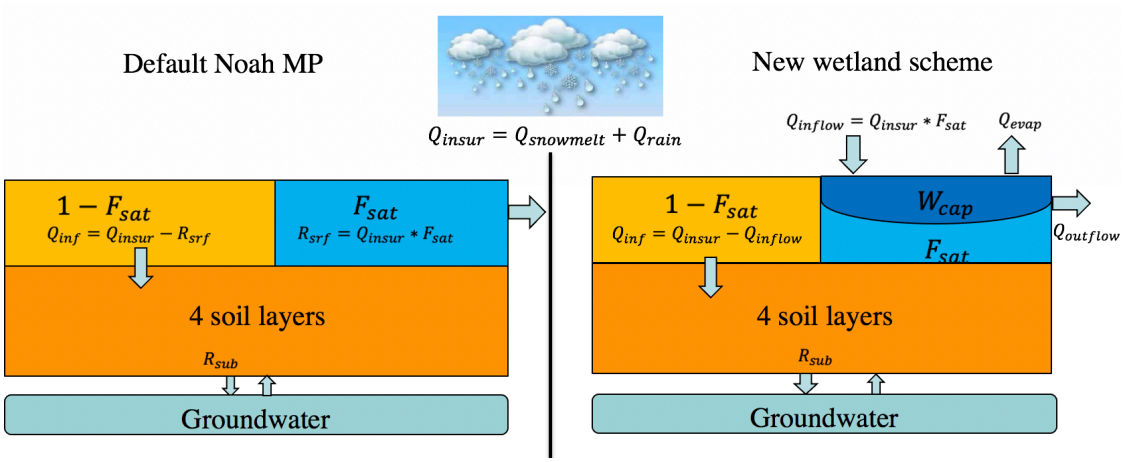

Figure 6.3. Simple diagram demonstrating the modifications in this study, which includes the modification of surface saturated fraction and the incorporation of a surface wetland storage scheme in Noah-MP LSM.

6.2.6 Simulations design

Three sets of numerical simulations are conducted to study the impacts of wetland representation on the simulated energy and water balance in the Noah-MP LSM, as well as feedback to the regional climate in the coupled WRF system. A summary of these three simulations is presented in Table 6.1.

The first set of simulations is a single-point test, driven by the observation forcing, in a half-water/half-vegetation Fen site in central Saskatchewan. These simulations aim to study the impacts of modifying F_{sat} parameterization and the sensitivity of dynamic storage and its impacts on energy/water balance.

The second set of simulations is on the regional scale in the PPR, driven by a 4-km WRF regional climate simulation (CONUS-I, Liu et al., 2017). In this simulation, we constrain the maximum F_{satmx} by satellite observation data (GIEMS) and combine the surface water storage with fine-scale 90-m DEM (MERIT data: http://hydro.iis.u-tokyo.ac.jp/~yamadai/MERIT_DEM/). The purpose of this offline simulation is to investigate the implementation on a regional scale, with respect to spatial heterogeneity of F_{satmx} and W_{cap}.

The third set is the coupled WRF regional climate simulation for three summers in 2005 (wet), 2006 (dry), and 2007 (normal) with strong inter-annual variability. The purpose of this set of simulations is to study the impacts of surface wetland dynamics and their feedback to the regional climate, particularly under a high-resolution convection-permitting configuration. It is noteworthy that, in the summer of 2006, an intense and prolonged heatwave occurred in the Central U.S. and Southern Canada from mid-July to early August. One interesting highlight of this simulation is to examine the cooling effect induced by wetlands and its interactions with the atmosphere, which can help relieve the heat stress imposed by large-scale atmospheric circulation.

Table 6.1. Summary of the three simulations conducted in this study.

Simulation design	Location	Period	Purpose
Single-point Noah-MP	Fen site, SK	20030101-20101231	Exam the sensitivity of the F_{sat} formula and different levels of storage
Offline regional Noah-MP	PPR region	20001001-20131001	Incorporate spatially varied F_{satmx} and W_{cap} parameters in the PPR
Coupled regional WRF	PPR region	2005-2007, three summers from Apr to Aug	Conduct coupled WRF-NoahMP-Wetland simulations and study the feedback to temperature

6.3 Results

6.3.1 Implementation and sensitivity tests on single-point LSM

We first perform a single-point LSM simulation in the Fen site in North Saskatchewan. Two modifications are tested: first, the modified F_{sat} formula and, second, a sensitivity test for surface water dynamics with various storage capacities. Figure 4 shows the F_{sat} parameter, energy and water balance in the Fen site simulated by Noah-MP. In Figure 6.4a, the default F_{sat} formula by the exponential function of the water table depth fails to represent the large magnitude and strong seasonal variation, as shown by the GIEMS results. The modified formula using the first layer of soil moisture improves both the magnitude and seasonal cycle of the F_{sat} parameter. This larger F_{sat} will effectively change the surface water partitioning, by increasing the surface runoff, which leaves the grid point water balance, and reducing the infiltration to soil moisture, which further reduces ET and underground runoff (Figure 6.4b). Furthermore, the increased F_{sat} will reduce latent heat fluxes and enhanced sensible heat fluxes from March to September, with the strongest decrease in July (Figure 6.4c).

The surface wetland scheme (Section 6.2.4) basically collects the increased surface runoff in wetland storage and allows evaporation to the atmosphere. The scheme's contribution to surface water and energy balance depends on its storage capacity. Figure 6.4d shows the sensitivity of water storage in this wetland with four different capacities (0, 5, 50 and 500 mm). For the "WS=5", the wetland water will be depleted during the dry seasons in summer, while with larger capacity (WS=50 or 500), the water storage from the previous year can be sustained through dry seasons. The greater capacity of holding water allows greater contribution to evaporation and reduces surface runoff (Figure 4e). The changing storage capacity has little impact on underground runoff. Moreover, greater storage capacity also allows greater latent heat fluxes and fewer sensible heat fluxes. This threshold mediated effect is clear between WS=5 and WS=50, as water may be dried in smaller capacities, while the contribution is similar between WS=50 and WS=500.

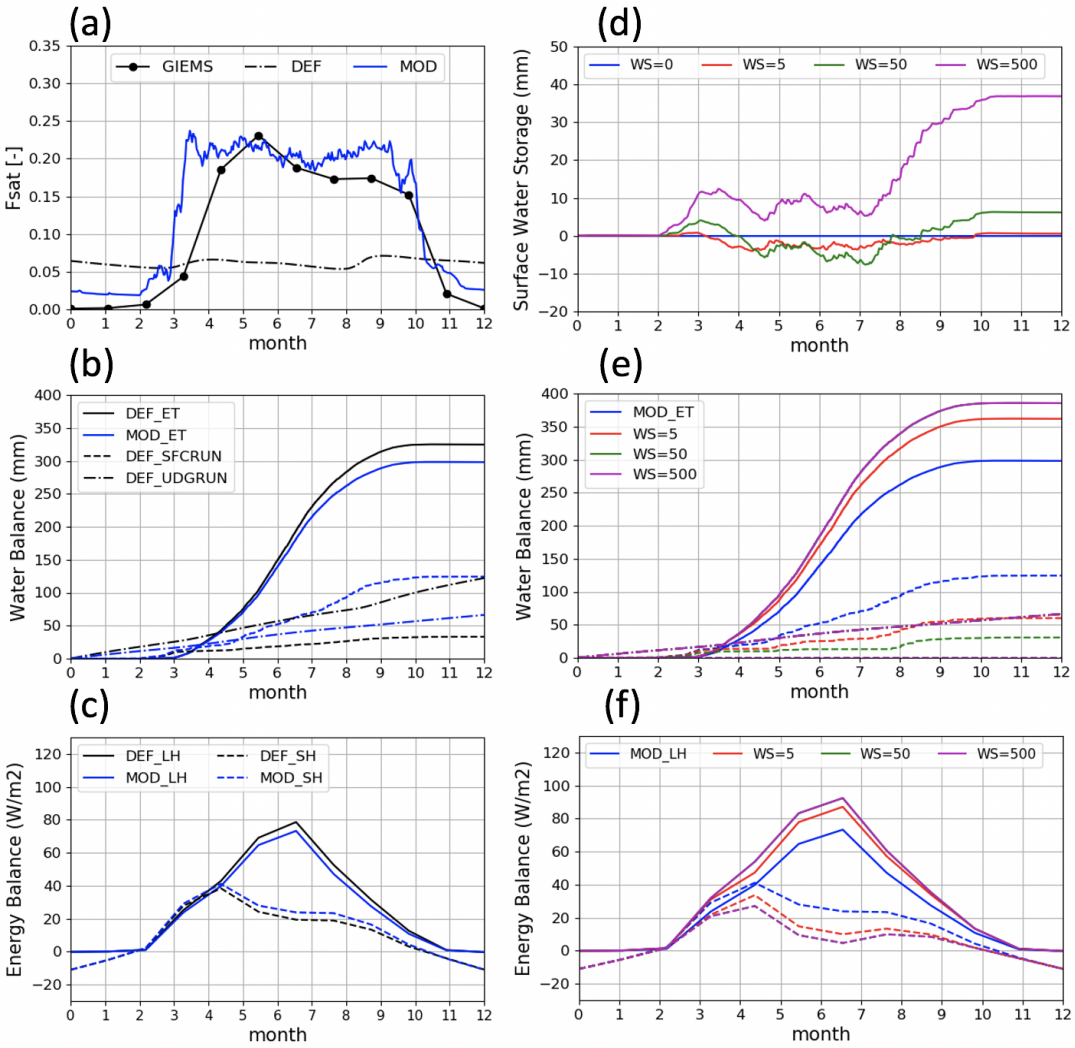

Figure 6.4. Single-point simulation of F_{sat} modification (a-c) and incorporation of dynamic wetland storage (d-f) in Fen site in central Saskatchewan: (a) surface saturated fraction from default and modified formula and GIEMS inundation extent, (b) surface water balance in ET, surface and underground runoff, (c) surface energy balance in sensible and latent heat fluxes; (d) water level change in wetland storage, (e) surface water balance in ET, surface and underground runoff, (f) surface energy balance in sensible and latent heat fluxes.

6.3.2 Regional scale land model simulation constrained by spatially varied parameters

To simulate the wetland dynamics at regional scales, it is essential to constrain two spatially varied parameters, F_{satmx} and the storage capacity, W_{cap}, as they are critical to wetland energy and water balance shown in the last section. Figure 5 shows the spatial map of F_{satmx} and W_{cap} in the PPR region. Here, Fsatmx is derived from the GIEMS inundation fraction to represent the sub-grid maximum saturation, and W_{cap} is derived from MERIT 90-m DEM and aggregated to a 4-km resolution grid (the same resolution as in CONUSI WRF 4-km meteorological forcing).

$$W_{cap} = \sum_{i=1}^{n} min\left((H_i - \bar{H}), 0\right) \quad (6.14)$$

H_i represents the 90-m elevation and $\underline{H}$ is the mean elevation averaged at 4-km grid, so that W_{cap} represents the collective topographical variation in the depressional area from 90-m DEM and aggregated into the 4-km grid.

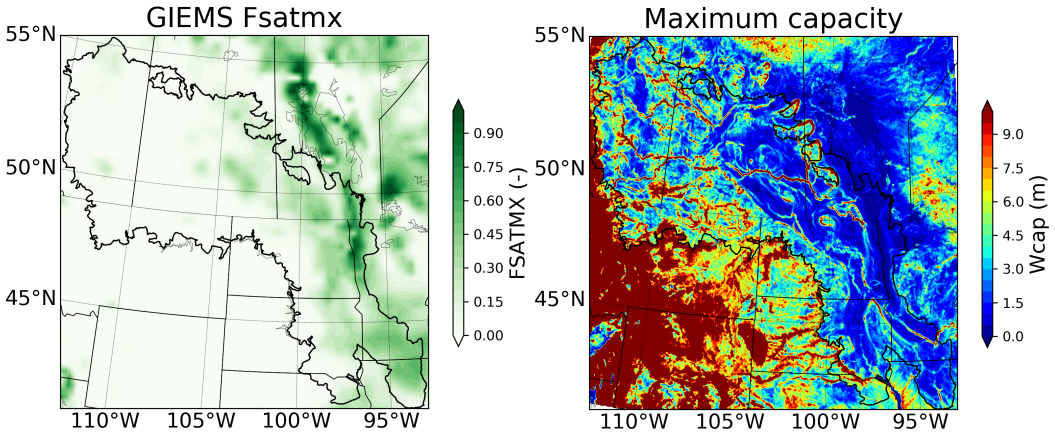

Figure 6.5. Spatial map of F_{satmx} and W_{cap} in the PPR region, derived from GIEMS product and MERIT DEM, respectively.

It is clear that the high F_{satmx} regions are located in the Northeast part of the domain, near Lake Winnipeg in Manitoba and the Red River Valley. These regions are also in correspondence with the low W_{cap} regions in the W_{cap} map.

Two 13-year offline Noah-MP simulations are conducted: one with the default setting and one with the new surface wetland scheme. The 13-year average surface water balance (surface runoff and ET) and energy balance (sensible heat and latent heat) are shown in Figure 6.6. Figure 6.6a shows substantial wetland water storage availability – more than 200 mm average over the summer months, in the north domain and in the southeastern PPR in the Red River valley. In the central and western PPR, wetland storage is generally less than 100 mm, with some deeper storage in large water bodies surrounding lakes and rivers.

The surface water and energy balance in the PPR are greatly altered by the presence of surface wetlands and the differences between WS and DEF simulation follow their spatial distribution. The presence of surface wetlands generally holds inflow water from rain and snowmelt, reducing surface runoff while increasing evaporation by about 100~200 mm in summer months. The water in the saturated fraction of the grid cell creates an open water surface, reducing (increasing) the sensible (latent) heat fluxes by about 0~50 W/m2 in summer months. These impacts on surface energy and water compensate for each other, and the presence of open water storage may induce

potential feedback to the atmosphere through land-atmosphere interactions, which we will discuss in next section.

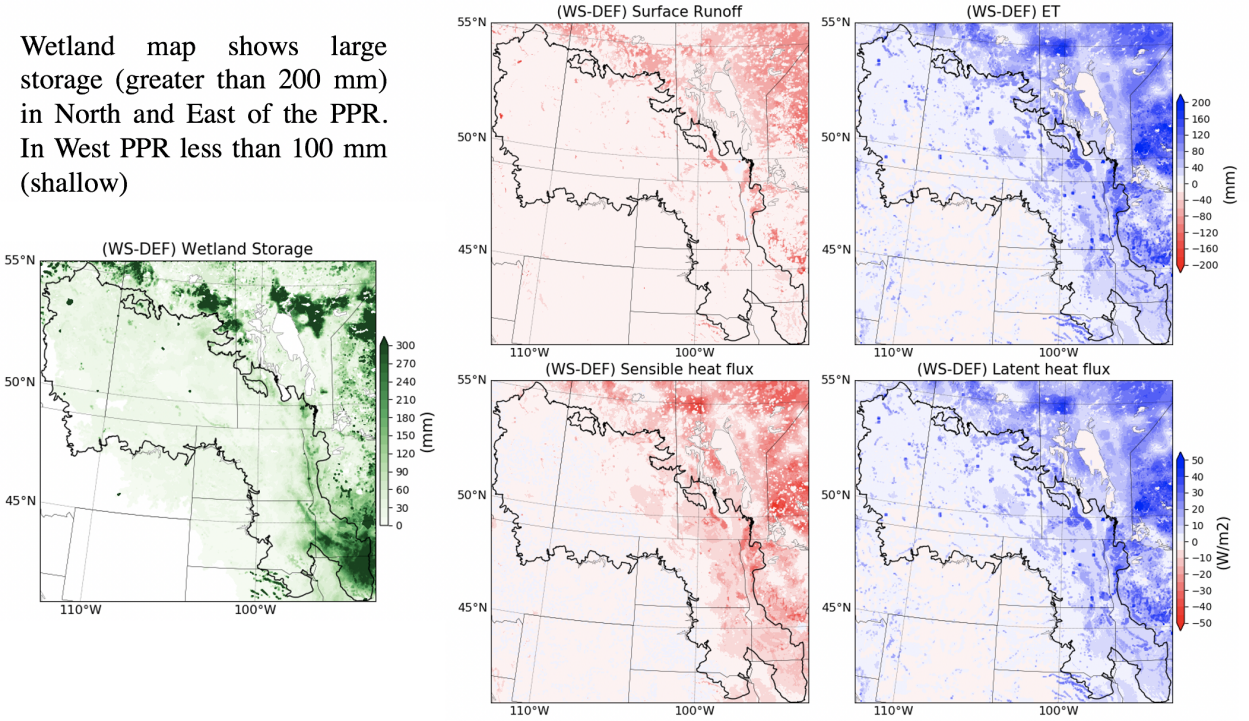

Figure 6.6. 13-year summertime (MJJA) mean wetland storage level (a); and the difference between WS and DEF simulations in surface runoff (b), evapotranspiration (ET, c), sensible heat flux (d), and latent heat flux (e).

6.3.3 Regional climate simulation with coupled wetland dynamics

To study the feedback from surface wetland dynamics to the regional climate, we perform two coupled WRF-wetland simulations for the summer of 2005, 2006, and 2007 years. The first simulation already includes the shallow groundwater scheme from Miguez-Macho et al. (2007), which is referred to as the DEF simulation. The second simulation incorporates the wetland scheme upon the shallow groundwater scheme, which is referred to as the WS simulation. These simulations start from April and run through August, with the first month as the spin-up period. Our analysis focuses on the temperature and precipitation from May to August for these three years, especially in 2006 when an intense summer heatwave occurred from mid-July to early August in the Central U.S. and Southern Canada.

Figure 6.7 shows the monthly temperatures from station observation, model biases from two simulations, and the cooling effect induced by the WS scheme in 2006. It is evident that a warm bias exists in the southern part of the domain, ranging from 2°C in the Central U.S. to 1°C in the Western Canadian Prairies. This warm bias grows stronger in July and August. The WS simulation shows a significant cooling effect in the Northeast portion of the domain, where the saturated fraction is high. The cooling in temperature ranges from less than 1°C in May to about 1~2°C in July. This cooling signal is evident in high-F_{sat} regions in the domain in all three-year simulations.

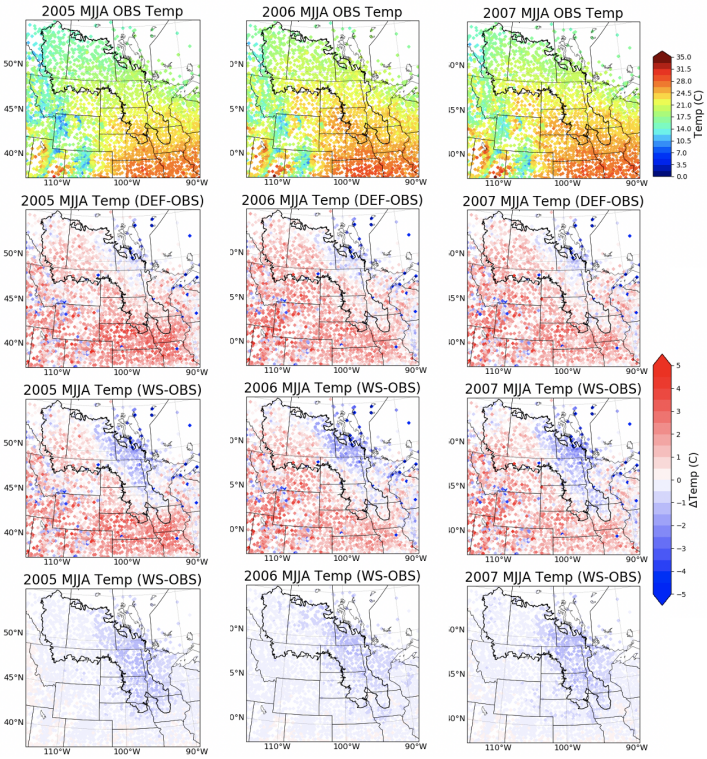

Figure 6.7. Monthly temperatures from station observation, temperature biases from two simulations, and the cooling effect induced by WS in the summer for three-year simulations.

In the summer of 2006, a record-breaking heatwave hit the major part of the U.S. and Southern Canada. The extreme heat conditions can be represented by the number of "hot days" during the summer, with the daily maximum temperature exceeding the 90th percentile of climatological records. We accumulated the number of hot days from May to August in 2006 from two simulations and the results are shown in Figure 8. Through these four months, the hottest region is in the southeast of the domain in Nebraska, Iowa, Kansas and Missouri – for more than 40 days of hot days – while in the Northern Great Plains and Canadian Prairies, the hot days are about 10~20 days. The WS simulation shows the dynamic wetland could effectively reduce the number of hot days by about 10 days in the entire domain. Two regions receive greater impacts from the wetlands, including southern Manitoba and the area between Nebraska and Iowa. This result manifests the important role of wetlands in mitigating climate change, especially in extreme heat events.

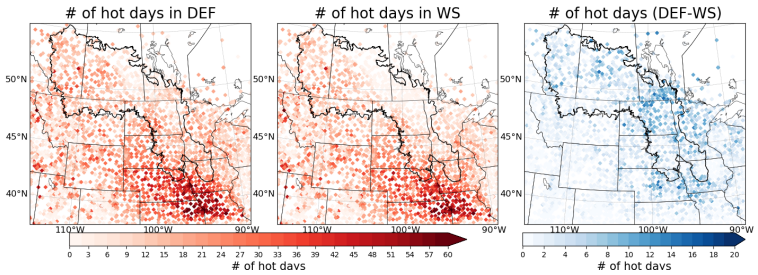

Figure 6.8. Number of hot days in two simulations and the reduction in hot days from WS to DEF.

Figure 6.9 shows the effect of wetland cooling on temperature against its maximum saturated fraction for the domain. The F_{satmx} parameter generally depicts the spatial pattern of a highly

saturated region with high water availability. The cooling effect from wetlands is evident for almost every month in the simulation period and is stronger in June and July than in May and August. The strongest effect is shown in 2005 July, which is almost 1.5 ℃ cooler. There exists a linear relationship between F_{satmx} and ΔTEMP – the larger of the F_{satmx}, the stronger the cooling effect is, especially in 2005 and 2007, but not as clear in 2006. This relationship indicates that the wetland cooling effect relies on the available water input from precipitation: under normal and wet conditions, the greater the F_{satmx}, the more water can be stored in wetland storage and the more surface energy partitioned into latent heat, hence the stronger the cooling effect. However, in the 2006 dry conditions, there was not sufficient precipitation to fill these wetlands, limiting the wetlands' cooling effects and evaporation, regardless of F_{satmx} values. This wetland cooling effect is analogous to the classic soil moisture-temperature feedback in land-atmosphere interactions.

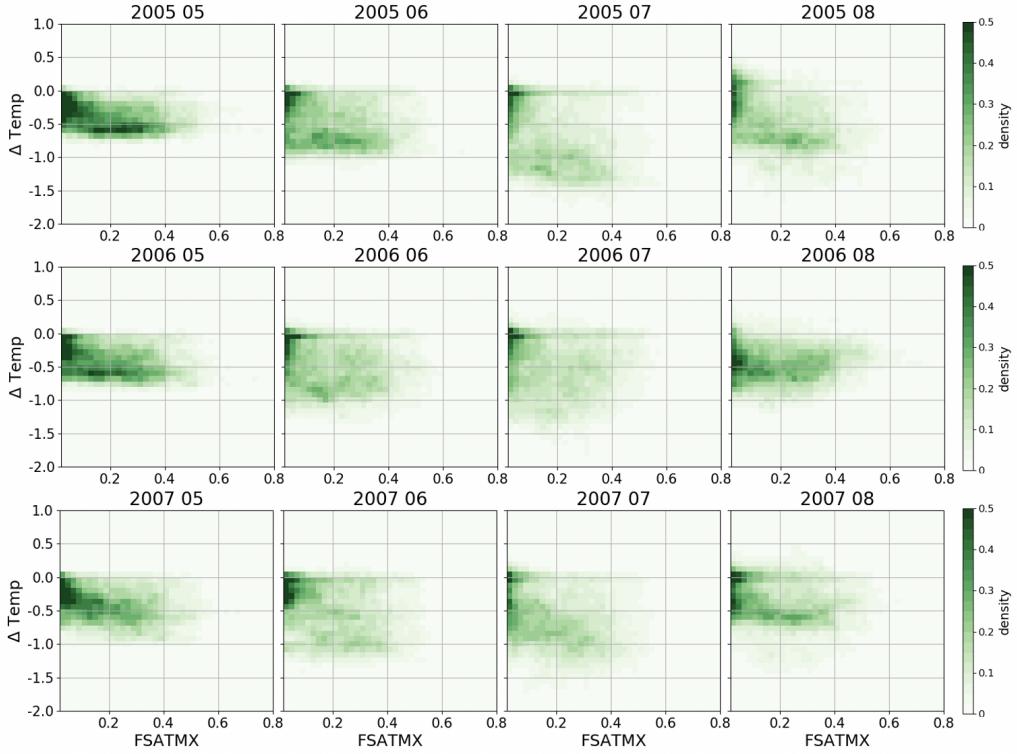

Figure 6.9. Scatter plot of ΔTEMP (DEF-WS, ℃) against the F_{satmx}, maximum saturated fraction in grid cell, from three-year summer monthly data.

Compared to the uniform cooling effect on temperature, the feedback of surface wetlands to regional precipitation is more ambiguous than the uniform cooling effect in temperature. Figure 6.10 shows the monthly precipitation from observation, model biases from two simulations and their difference in three-year summers. The precipitation bias corresponds well with the temperature bias in Figure 6.7, with a significant dry bias in the southeast part of the domain while the precipitation is not as obvious in the Canadian Prairies. The WS simulations show little difference in precipitation from the DEF simulation and the signals of changes are almost random in the last row. This almost random and patchy precipitation signal is shown in all three-year simulations and for the accumulated period of four months.

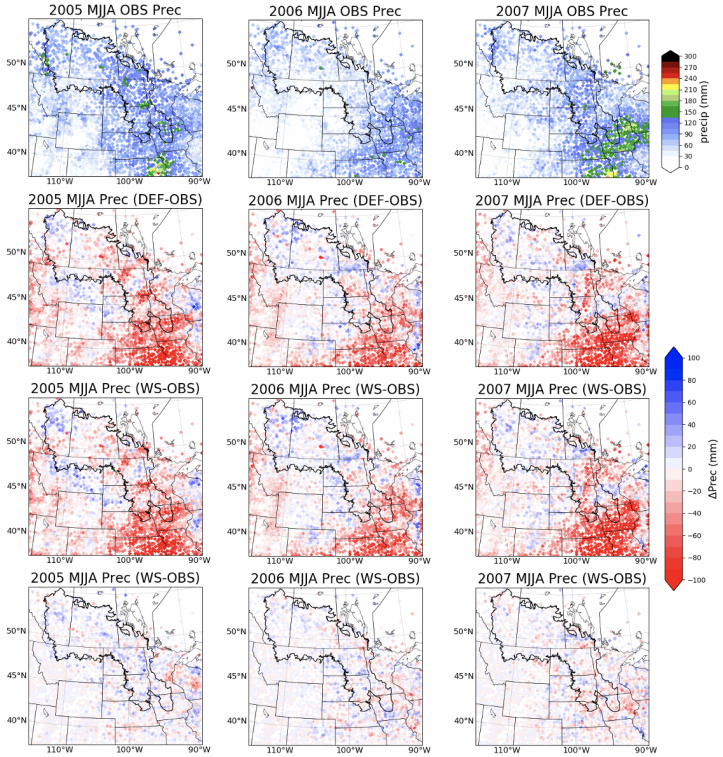

Figure 6.10. Monthly precipitation from station observation, precipitation biases from two simulations, and the difference in precipitation induced by WS in three years' summer.

6.4 Discussion

In LSMs and coupled ESMs, reasonable representations of wetland spatial extents and dynamic water storage are challenging in light of data scarcity, coarse model resolution, and insufficient understanding of the physical processes (Prigent et al., 2007). However, because wetland extents play a key role in land-atmosphere interactions and carbon feedback to the climate system, researchers have long been of great interest to estimate wetland extents in hydrology-climate simulation from global to regional scales. For example, the WETCHIMP project gathered 10 participating GCMs for simulating the global wetland extents as well as CH4 contributions (Wania et al., 2013; Melton et al., 2013). Many of these GCMs used prescribed wetland maps from global surveys or remote sensing products, such as the Global Lake and Wetland Database (Lehner and Doll, 2004) and GIEMS (Prigent et al., 2007), or used the TOPMODEL-based F_{sat} to simulate a subgrid "saturated" fraction to represent wetlands extents.

Although the TOPMODEL method provides some spatial heterogeneity and temporal dynamics to the wetland extent estimate, it generally underestimates both the maximum value and the seasonal variability. As we showed in Section 6.2.1 that the TOPMODEL based method in Noah-MP simulates a much lower F_{sat} value than the highly dynamic GIEMS product. Here we provide two possible reasons for the discrepancy between TOPMODEL F_{sat} and surface water dynamics from satellites. (1) The first underlying assumption of the TOPMODEL method requires a "steady state" precipitation and soil moisture heterogeneity, which is more likely in wet, relatively shallow soils on moderate slopes (Beven and Kirkby, 1979; Kirkby et al., 2021). However, this is not the case in the Prairie Pothole region, where the climate is usually semi-arid and the large-scale topography is flat with small scale variation. (2) Another possible reason for this discrepancy is that the TOPMODEL method calculates a critical topographic index value when the local water table is at the surface; this value is used to determine the F_{sat} fraction through the integration of its probability distribution function. However, in the PPR region, the freezing soils in wintertime prevent interaction between the soil moisture and groundwater (Ireson et al., 2013). Therefore, in the TOPMODEL method, the exponential function will simulate less seasonal variation in the surface water dynamics. As well, a large portion of the global wetlands and peatlands are located in high latitude regions where winter soil freezing is very common.

In our modification of the F_{sat} formulation, we used the first layer of soil saturation to indicate the sub-grid spatial extent of the saturated portion – the extent of wetlands. This method empirically assumes the grid cell mean soil moisture saturation can be translated into a spatial fraction for surface saturation and shows a highly variable F_{sat} value compared to the default TOPMODEL method, in terms of the maximum and minimum extent, and seasonality (in section 6.3.1). Moreover, we also incorporate a spatially varied maximum F_{satmx} map from the GIEMS product to replace the default global mean value (0.38) in Noah-MP and WRF. Both these modifications improve the spatial heterogeneity and the temporal dynamics of wetland extents in the PPR region.

Additionally, we incorporated a dynamic surface water storage scheme to simulate the hydrological processes in wetlands. Although this scheme is simple, we aim to capture three important processes – the filling of wetlands by snowmelt and rainfall, the evaporation of wetland water into the atmosphere, and the excess water spilling to surface runoff. These three processes are the key components in the wetlands water and energy cycle during the warm season open water period. Our results showed increase of ET with a decrease of surface runoff and an increase of latent heat

with decreases of sensible heat. This finding aligns with our expectations, as well as with previous VIC model wetland and lake simulations in the U.S. Midwest region (Mishra and Cherkauer et al., 2010).

Moreover, our scheme provides greater potential to explore wetlands' feedback to the atmosphere in coupled WRF-NoahMP-Wetland simulation. In the default simulation, which already includes the MMF groundwater scheme (Barlage et al., 2015, 2021), warm biases still exist at about 1~3 degrees in the U.S. Great Plains. Without the groundwater scheme, the summertime warm biases could be as high as 4~6 degrees. By adding the wetland scheme on top of the MMF groundwater scheme, the warm biases in the U.S. can be further reduced by 0.5~1.5 degrees, but it also introduces 1-degree cool biases in Southern Manitoba, where wetland extents are large. While the temperature cooling effect is evident, wetland feedback to precipitation is less obvious and is more ambiguous. A previous study using WRF with prescribed soil moisture threshold to indicate wetlands in the great plain in a coarser resolution (12-km) also showed a temperature cooling effect, but the precipitation effect was negligible (Capehart et al., 2012).

One of the highlights of this study is the wetland cooling effect to the atmospheric temperature. Previous studies have documented this effect in detail, but they have been specific to different wetland characteristics and dominant vegetation types. In our study, we used general open water storage to characterize wetland interactions with the atmosphere, omitting these variations in specific wetland types but gaining more generic conclusions in a much larger region. The wetland cooling effect to temperature, especially during extreme heatwave events, echoes a previous study in the Central U.S. where we found land surface characteristics could effectively reduce the frequency, intensity, and duration of extreme heatwaves (Zhang et al., 2018)

We also want to note that the land use and hydrological cycle in the PPR region is of great complexity. In recent years, the competition between agriculture and wetland conservation has been a serious topic of discussion among the public, universities, and government agencies. It has been shown that the agricultural land expansion at the cost of wetland drainage increases the risk of emerging flooding in springtime (Dumanski et al., 2015). The excessive amount of the organic carbon released from wetland deposition contributes greatly to the atmospheric carbon emission. The loss of wetlands for croplands also reduces the resilience to drought and high temperature, which may cause crop failures due to water and heat stress. As a tradeoff, the gains in agricultural yields are marginal and cannot compensate for the ecological value loss from wetland drainage.

However, the loss of wetlands to agricultural, industrial and residential land are not specific to only in the PPR region but are common problems worldwide and require humans' attention (Rasmar convention 2007; Nature Geoscience, 2021). These land use modifications not only threaten the local environment but also contribute to the global carbon balance and eventually cause problems for human beings. Understanding the effects of development is challenging. It is hoped that these threats to the future can inspire future studies on wetlands for their hydrological, climatic, ecological, environmental functions and that solutions can be found for humans to interact with nature peacefully and sustainably.

6.5 Conclusion

Wetlands play an irreplaceable role in Earth systems for their climatic, hydrological, and ecosystem surface. However, reasonably representing the spatial extents and water dynamics of these small-scale wetlands has been challenging to LSMs and coupled ESMs. This is particularly important and urgent in the Prairie Pothole Region (PPR) for the wetlands are critical to the region's ecology and the hydrological conditions are complex. In this research, we mainly developed a surface wetland scheme with two modifications to represent wetland dynamics in the Noah-MP LSM. One is modifying the sub-grid saturation fraction to indicate the spatial wetland extent based on grid cell soil moisture. Another is incorporating a dynamic surface water storage scheme to represent the hydrological processes in wetlands. This new wetland scheme is incorporated in single-point, offline regional simulation, and coupled WRF simulation in the PPR region.

The single-point simulation showed that the modified the sub-grid F_{sat} using the first layer soil saturation reasonably mimics the magnitude and seasonality of surface saturation condition in the PPR, compared to the default TOPMODEL-based formula. On the other hand, the modified increased F_{sat} formula partitions more water to surface runoff than infiltration to soil moisture. The enhanced surface inflow is then collected by the surface storage, mimicking the capacity of wetland depressions, with water exceeding the capacity will spill out to outflow. The single-point simulation also shows that the wetland modifying surface energy and water balance also depends on its maximum capacity. For shallow storage wetlands, both spring inflow and summer evaporation demand would exceed their maximum capacity, limiting their function in energy and water exchange with the atmosphere.

In the offline regional simulation in the PPR, two spatially varied parameters are incorporated, the maximum F_{satmx} fraction and maximum storage capacity W_{cap}. The results show that the model simulated wetlands are located in the Northeast portion of the PPR domain, where F_{satmx} is high but maximum capacity is shallow. By incorporating the wetland scheme, the summertime evaporation and latent heat fluxes are evidently increased, with decreasing surface runoff and sensible heat fluxes. These changes occur in where F_{satmx} is high and are compensating each other in different directions, which is up to our expectation.

Finally, we examine the wetlands' feedback to regional temperature and precipitation in the coupled WRF-NoahMP-Wetland model. Evident cooling effect induced by the presence of surface wetlands are shown in all three years' summer for about 0.5~1℃ in dry year (2006) and 0.7~1.5℃ in the wet year (2005), occurring in where the wetland fraction is high. This cooling is the result of wetland altering energy balance partitioning, increasing latent heat fluxes while reducing sensible heat fluxes. The cooling effect is strongest in July while weakest in May, representing the previous theory of evaporation regime in energy limited regions starting from early summer while transition to water limited regime in mid-summer. In the summer of 2006, when an extreme heatwave hit the Central U.S. and Southern Canada, the presence of wetland could profoundly reduce the number of extreme hot days by more than 10 days during the summer period, effectively relieving the heat stress to human comfort. On the other hand, wetland scheme impacts on regional precipitation doesn't manifest an obvious pattern, which is showing both positive and negative precipitation and seems randomly located.

In the PPR region, wetlands have always amid the competition with agricultural, industrial, and residential land use. Loss of wetlands through land use conversion has occurred since the last a few decades and the trend is still going up. Our results show that the presence of wetlands could be beneficial to many sectors, such as regulating surface runoff during flooding and cooling atmospheric temperature during heatwaves. These highlights are inspiring future studies to understand wetlands' value in regional environments and the Earth system, especially those that have been neglected at the cost of human expansion.

Acknowledgments
Z. Zhang and L. Botorlotti were funded by a Mitacs Accelerate Fellowship funded by Ducks Unlimited Canada's Institute for Wetland and Waterfowl Research. Z. Zhang, Z. Li and Y. Li acknowledge the financial support from the Natural Sciences and Engineering Research Council of Canada (NSERC) Discovery Grant, and Global Water Futures Program, Canada First Research Excellence Fund. This project was supported by grants from Wildlife Habitat Canada, Bass Pro Shops Cabela's Outdoor Fund, and the Alberta NAWMP Partnership.

Chapter 7 – Conclusion

- Concluding remarks—provide a summary of the thesis and discussion to address existing major challenges
- Potential future works on wetland-crop joint simulation in LSMs and coupled RCMs

7.1 Concluding Remarks

7.1.1 Concluding remarks – a summary of previous chapters

Key to this research was the representation of different land surface characteristics in offline LSMs and in convection-permitting models (CPM). The focus of this thesis is two land types: croplands and wetlands. First, the thesis evaluated the relationship between the soil moisture anomaly and the frequency and magnitude of heatwaves in a long-term CPM simulation, CONUS WRF, showing a significant negative correlation and the model reasonably simulate this feature. Second, it validated the jointly simulated dynamic crop growth and irrigation water for corn and soybeans, which exhibit strong uncertainties in model parameters. Third, it both characterized the shallow groundwater dynamics in the Prairie Pothole Region using a groundwater scheme coupled to the Noah-MP LSM and investigated the water table dynamics under the current and future climate, which is closely connected to wetland hydrology in this region. Fourth, it predicted the future wetland extents using a generalized additive model with soil moisture and ecoregions as inputs. The prediction for future wetlands overlapping with historical drainage information provides strong implications for wetland conservation. Fifth, a dynamic wetland storage scheme was incorporated into the Noah-MP LSM by modifying the TOPMODEL-based runoff scheme, showing the significant cooling effect of wetland physics during extreme heatwave events. All the objectives in this thesis have been addressed, as shown in the summary presented below.

7.1.2 Concluding discussion to address existing major challenges

Land surface is an important component in the earth system and LSMs have evolved from simplified representation to various complexity to address biogeophysical and biogeochemical processes, surface heterogeneity, as well as uncertainties in model parameters. These three aspects are also emphasized as the three major challenges in LSM developments proposed by Fisher and Koven (2020). Clark et al. (2015) also recognized similar major challenges in representing hydrological processes in ESMs. In their synthesis paper, these three challenges are summarized as:

(1) Managing and increasing model processes complexity
(2) Representing land surface heterogeneity
(3) Constraining and predicting model parameters

From my perspective in conducting my Ph.D. research and writing this thesis, I will provide a brief discussion of these three challenges using my studies as examples.

To reasonably represent the physical realism of processes on land surface, detailed descriptions of the processes themselves are required. For example, in this thesis, four detailed hydrological, biophysical, and biogeochemical processes are developed and applied, including dynamic crop and irrigation processes (Chapter 3), shallow groundwater dynamics (Chapter 4), and the surface wetland process (Chapter 6). Before these processes were applied, these features in croplands and wetlands were represented by simple parameters (cropland and wetland parameters) or even neglected (shallow groundwater). Adding specific descriptions of these dynamical processes will enrich researchers' understanding and enlarge their vision for investigating these processes. On the other hand, correctly representing these processes will inevitably uncover two other challenges: spatial heterogeneity and parameter uncertainties. Additional information on both these dimensions are needed to constrain the model performance on these newly added processes. Figure 7.1 provides a diagram of these three challenges, showing them overlapping with each other and revealing how the studies in this thesis fit into the three-challenge framework.

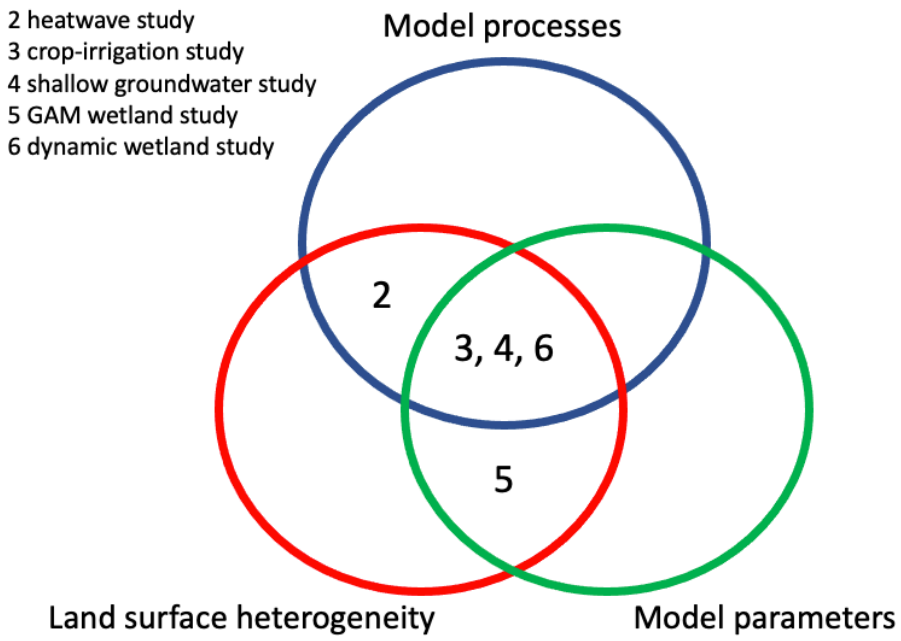

Figure 7.1. A diagram of three major challenges overlapping with each other and the five studies in this thesis framing this overlapping structure.

Figure 7.1 illustrates that some studies in this thesis touch on all three challenges. Although the initial intentions of these studies were not to explore all three challenges, to solve one challenge likely requires addressing some aspects of the others. I will use three examples to illustrate how my studies have tackled these challenges: the cropland study, the shallow groundwater study, and the dynamic wetland study.

Crop-irrigation study. The purpose of this study is to investigate the joint effect of dynamic crops and irrigation on crop growth. This purpose requires the application of two biogeophysical and biogeochemical processes: photosynthesis and carbon allocation. The land surface heterogeneity of cropland and irrigated land are characterized by sub-grid fractions, F_{irri}, F_{crop}, F_{corn} and $F_{soybean}$, respectively. To correctly represent the spatial extents of these land use types, high-resolution land information data from GMU and MODIS satellite are applied. Moreover, the parameters related to crop growth and irrigation embed great uncertainties. The sources of parameter uncertainties are summarized as plant physiology, phenology, and human management (planting/harvesting dates and the irrigation threshold). Some of these parameters can be calibrated. For example, the irrigation threshold, IRR_{cri}, is calibrated using USGS county-level water-use data in Xu et al. (2019). The planting/harvesting dates can be selected at the state-level, using the most frequent date within the planting and harvesting window of time in a long-term record. However, many other parameters, such as V_{cmx25} (maximum photosynthesis capacity at 25℃) and *BIO2LAI* (conversion ratio from leaf mass to LAI), are difficult to constrain in this study.

Recent studies have attempted to reasonably model human management given climate conditions and previous decisions (Izumi et al., 2019). This process is facilitated by dynamically modeling based on field workability, considering snow cover and rainfall and crop biological requirements for heat and moisture. Crop model parameters can also be constrained using data assimilation techniques. For example, Xu et al. (2021, under review) used the ensemble Kalman filter method

to assimilate solar-induced chlorophyll fluorescence (SIF) to constrain the maximum photosynthesis capacity, which was demonstrated with large uncertainties from laboratory results and the modeling literature. Both these attempts tackle constraining and estimating model parameters, processes which will in turn improve modeling performance.

Shallow groundwater study. The purpose of this study is to explore the two-way exchange between upper soil moisture and underlying unconfined shallow groundwater in the PPR in the current and future climate. Therefore, the shallow groundwater process is essential in this study. Adding an unconfined aquifer beneath the default 2-m soil column and allowing two-way water exchange between soil moisture and groundwater is the first step in this study. In addition to the process description in the model, land surface heterogeneity and model parameters are also critical to correctly represent this process. In this case, the spatial heterogeneity of the meteorological forcing from a convection-permitting simulation study is important, as it provides reliable precipitation forcing in current as well as future climate scenarios. Moreover, the vertical heterogeneity of soil texture should be accounted for, i.e., the hydraulic conductance and maximum soil water capacity decaying with depth, without too deep water table depths will be produced with small seasonal variations. On the other hand, spatial heterogeneity, as collected from well observations, leans towards sandy soil texture, because they are more often monitored by groundwater resource agencies than other soil textures. This feature is misrepresented as clay type soil in the model spatial soil type map. Replacing the soil texture at these sites in the model will result in improved simulation of groundwater depth and seasonal fluctuations. However, this study has limitations because little is known about spatial and vertical soil texture. Increasing this knowledge will require future development of observations and monitoring techniques.

Moreover, a recent finding on the scale-dependency of shallow groundwater coupled with the land surface and regional climate demonstrates that the processes and heterogeneity are closely linked (Barlage et al., 2021). Despite activating the shallow groundwater scheme, coarse resolution (27-km and 9-km) simulation results show that the soil moisture-groundwater exchange and feedback through land-atmosphere interaction are much weaker than in finer resolution (3-km and 1-km) simulation. These simulation results occur because the regions of shallow groundwater in the Central U.S. (Iowa) are shown on a high-resolution map (1-km), but they are blurred when represented on a coarser resolution map (27-km). This study strongly supports the argument that improving the representation of surface heterogeneity will contribute to understanding modeling processes and simulation.

Dynamic wetland study. The purpose of this study is to dynamically simulate spatial wetland extents and wetland hydrological processes as well as their climate feedback in the PPR. This study faces all three of the above-mentioned challenges in how to represent wetlands in LSMs. Previously, the spatial wetland extents were constrained mainly by global maps of land use types from land surveys or remote sensing or by dynamical modeling using the sub-grid saturated fraction in the TOPMODEL surface runoff scheme. In this study, a sub-grid bucket-style surface wetland storage model is combined with modified wetland fraction parameterization to represent the wetland's spatial extents and hydrological processes. The spatial heterogeneity is represented as a sub-grid fraction using the first layer of soil moisture saturation and constrained by remote sensing products for the seasonal cycle. This sub-grid fraction is critical because it determines the portion of available surface water flowing into the wetland storage, hence, the wetland water balance. The

newly added bucket-style surface wetland scheme, although simple, attempts to characterize basic hydrological processes occurring in wetland basins, inflow, evaporation, and outflow when water capacity is exceeded. In terms of model parameters, two key spatially varied parameters are used to constrain the spatial extent and water balance in wetland basins: the maximum saturated fraction F_{satmx} and maximum wetland capacity W_{cap}. The results show that the coupling surface wetlands processes strongly influence the surface energy and water balance, as well as the feedback to the regional climate. In particular, the cooling effect induced by the open water surface and increased latent heat fluxes can substantially reduce summertime temperature biases and relieve heat stress during extreme heatwaves.

Overall, these three examples from this thesis illustrate that to tackle any of the three major challenges will likely require tackling the others as well. This would typically involve having more detailed information on spatial extents and refining model parameters to increase understanding of processes and improving performance. It is also noteworthy that the purpose of these three studies is to investigate coupling these new processes with land surface characteristics and the regional climate. Therefore, the two pillars supporting the purpose are improving spatial heterogeneity and constraining model parameters. Nonetheless, these examples shed some light on future LSM development, not only incorporating process complexity but also accounting for land surface heterogeneity and model parameter uncertainties.

7.2 Potential future studies

The methods used and results shown in this thesis will potentially lead to multiple future land surface, hydrological, and agricultural studies in North America and globally. The advanced modeling processes in this thesis will be beneficial for researchers applying them in other regions of the world. Also, of interest to researchers will be interactions and feedback from the coupling of these advanced processes.

7.2.1 Wetland water availability under a future climate

In Chapter 6, the sub-grid surface wetland storage scheme is developed with the wetland water balance. This scheme allows future investigation of wetland water availability under different climate projections. The goal of this study is to understand future wetland distributions and water availability and to design conservation strategies for wildlife agencies, water management sectors, and government policymakers. This study can be conducted at both the global and regional levels i.e., the Prairie Pothole region. In detail, three specific goals can be setup:

- Evaluating the wetland distribution, duration, and water level, using current climate forcing
- Exploring future wetland characteristics under the future climate forcing using the Pseudo Global Warming method
- Understanding the hydrological component changes associated with these changes in wetland characteristics.

7.2.2 Wetland-cropland interaction as benefits to farms

In Chapter 3, the dynamic crop growth model is applied to two crop types, corn and soybeans. However, these two crops are not typical in the Canadian Prairies, where wheat and canola are more common. Thus, the first step of this study is to develop a set of Canadian crop species parameters (starting from wheat): phenology, photosynthetic characteristics, and carbon allocation. Turning to the other part of this study, Prairie pothole wetlands are facing land use conversion through drainage as the cropland expands. Especially in Chapter 6, the dynamic wetland simulation shows a significant cooling and moistening effect on the surface environment. It is critical to understand the potential impacts of converting wetlands to croplands on land surface energy, water, and crop yield. This study can be conducted using both the offline LSM mode and the coupled RCM mode with the WRF model. Three specific goals can be established:

- Conduct a wetland-conversion simulation to represent cropland expansion over the PPR.
- Explore the potential impacts on surface energy, water, and carbon balance from cropland expansion in offline mode.
- Investigate the benefits of wetlands for farms as a potential reason to maintain wetlands within cropland expansion.
- Study the feedback of joint cropland-wetland impacts on the regional climate, focusing on both temperature and precipitation changes induced by land use changes in the convection-permitting regional climate model.

The rapid development of representations of land surface processes and the progress of high-resolution convection-permitting simulations show promise in improving the integration of land surface processes into more advanced regional climate simulations. Along with an increased interest in more precise answers to the impact of uncertain climate changes, these strategies will lead to more robust understanding of the land surface processes and land-atmosphere interactions.

Reference

Ando, A. W., & Mallory, M. L. (2012). Optimal portfolio design to reduce climate-related conservation uncertainty in the Prairie Pothole Region. Proceedings of the National Academy of Sciences, 109(17), 6484–6489. https://doi.org/10.1073/pnas.1114653109

Anyah, R. O., Weaver, C. P., Miguez-macho, G., Fan, Y. and Robock, A.: Incorporating water table dynamics in climate modeling: 3 . Simulated groundwater influence on coupled land-atmosphere variability, 113, 1–15, doi:10.1029/2007JD009087, 2008.

Ball, J. T., I. E. Woodrow, and J. A. Berry (1987), A model predicting sto- matal conductance and its contribution to the control of photosynthesis under different environmental conditions, in Progress in Photosynthesis Research, vol. 4, edited by J. Biggins, pp. 221–224, Martinus Nijhoff, Dordrecht, Netherlands.

Ballard, T., Seager, R., Smerdon, J. E., Cook, B. I., Ray, A. J., Rajagopalan, B., et al. (2014). Hydroclimate Variability and Change in the Prairie Pothole Region, the "Duck Factory" of North America. Earth Interactions, 18(14), 1–28. https://doi.org/10.1175/EI-D-14-0004.1

Bam, E. K. P., Brannen, R., Budhathoki, S., Ireson, A. M., Spence, C., & van der Kamp, G. (2019). Meteorological, soil moisture, surface water, and groundwater data from the St. Denis National Wildlife Area, Saskatchewan, Canada. Earth System Science Data, 11(2), 553–563. https://doi.org/10.5194/essd-11-553-2019

Ban, N., Schmidli, J. and Schär, C.: Evaluation of the new convective-resolving regional climate modeling approach in decade-long simulations, J. Geophys. Res. Atmos., 119, 7889–7907, doi:10.1002/2014JD021478.Received, 2014.

Barlage M, Tewari M, Chen F, Miguez-Macho G, Yang ZL, Niu GY (2015) The efect of groundwater interaction in North American regional climate simulations with WRF/Noah-MP. Clim Change 129(3–4):485–498. https://doi.org/10.1007/s10584-014-1308-8

Barlage, M., Chen, F., Rasmussen, R., Zhang, Z. & Miguez-Macho, G. The importance of scale-dependent groundwater processes in land-atmosphere interactions over the central United States. Geophys. Res. Lett. (2021) doi:10.1029/2020GL092171.

Batt, B.J.D., Anderson, M.G., Anderson, C.D., & Caswell, F.D. (1989). The use of prairie potholes by North American ducks, In Northern Prairie Wetlands. ed A. van der Valk, pp. 204-227. Iowa State University Press, Ames, Iowa.

Beaman, Benjamin, C., Implications of Climate Change for Land Use and Waterfowl Productivity in Prairie Canada, M.S., Department of Agricultural and Applied Economics, August, 2016.

Betts, A. R. (2005). Integrated approaches to climate–crop modelling: needs and challenges. Philosophical Transactions of the Royal Society B: Biological Sciences, 360(1463), 2049–2065. https://doi.org/10.1098/rstb.2005.1739

Beven, K. J., & Kirkby, M. J. (1979). A physically based, variable contributing area model of basin hydrology / Un modèle à base physique de zone d'appel variable de l'hydrologie du bassin versant. Hydrological Sciences Bulletin, 24(1), 43–69. https://doi.org/10.1080/02626667909491834

Beven, K. (1997). TOPMODEL: A critique. *Hydrological Processes*, *11*(9), 1069–1085. https://doi.org/10.1002/(SICI)1099-1085(199707)11:9<1069::AID-HYP545>3.0.CO;2-O

Beven, K. J., Kirkby, M. J., Freer, J. E., & Lamb, R. (2021). A history of TOPMODEL. Hydrology and Earth System Sciences, 25(2), 527–549. https://doi.org/10.5194/hess-25-527-2021

Beyersbergen, G.W., Niemuth, N.D., & Norton, M.R. (2004). Northern Prairie & Parkland Waterbird Conservation Plan. A plan associated with the Waterbird Conservation for the Americas initiative. Prairie Pothole Joint Venture, Denver, Colorado. 183pp.

Bonan, G. B. (1995). Sensitivity of a GCM Simulation to Inclusion of Inland Water Surfaces. Journal of Climate, 8(11), 2691–2704. https://doi.org/10.1175/1520-0442(1995)008<2691:SOAGST>2.0.CO;2

Bonan, G. B., Lawrence, P. J., Oleson, K. W., Levis, S., Jung, M., Reichstein, M., et al. (2011). Improving canopy processes in the Community Land Model version 4 (CLM4) using global flux fields empirically inferred from FLUXNET data. Journal of Geophysical Research, 116(G2), 1–22. https://doi.org/10.1029/2010jg001593

Bowling, L. C., & Lettenmaier, D. P. (2010). Modeling the effects of lakes and wetlands on the water balance of arctic environments. Journal of Hydrometeorology, 11(2), 276–295. https://doi.org/10.1175/2009JHM1084.1

Brannen, R., Spence, C. and Ireson, A.: Influence of shallow groundwater-surface water interactions on the hydrological connectivity and water budget of a wetland complex, Hydrol. Process., 29(18), 3862–3877, doi:10.1002/hyp.10563, 2015.

Brooke Anderson G, Bell ML (2011) Heat waves in the United States: mortality risk during heat waves and efect modifcation by heatwave characteristics in 43 US communities. Environ Health Perspect 119(2):210–218. https://doi.org/10.1289/ehp.1002313

Budyko, M.I., (1974). Climate and Life. Academic Press. 508 pp.

Cai X, Yang ZL, David CH, Niu GY, Rodell M (2014a) Hydrological evaluation of the noah-MP land surface model for the Mississippi River Basin. J Geophys Res 119(1):23–38. https://doi.org/10.1002/2013JD020792

Cai X, Yang ZL, Xia YL, Huang M, Wei H, Leung LR (2014b) Assessment of simulated water balance from Noah, Noah-MP, CLM, and VIC over CONUS using the NLDAS test bed. J Geophys Res Atmos 119:1–20. https://doi.org/10.1002/2014JD022113

Capehart, W. J., Stamm, J., & Norton, P. (2011). Representing Great Plains Prairie Wetland Feedbacks in WRF. May.

Chen F, Janjic ZI, Mitchell K (1997) Impact of atmospheric surfacelayer parameterizations in the new land-surface scheme of the NCEP mesoscale eta model. Bound Layer Meteorol 85:391–421. https://doi.org/10.1023/A:1000531001463

Chen F, Dudhia J (2001) Coupling an advanced land surface—hydrology model with the Penn State—NCAR MM5 modeling system. Part I: model implementation and sensitivity. Mon Weather Rev. https://doi.org/10.1175/1520-0493(2001)129

Chen F, Zhang Y (2009) On the coupling strength between the land surface and the atmosphere. Geophys Res Lett 36:L10404. https://doi.org/10.1029/2009GL037980

Chen, F., Xu, X., Barlage, M., Rasmussen, R., Shen, S., Miao, S., & Zhou, G. (2018). Memory of irrigation effects on hydroclimate and its modeling challenge. Environmental Research Letters, 13(6). https://doi.org/10.1088/1748-9326/aab9df

Chen, F., Liu, C., Dudhia, J. and Chen, M.: A sensitivity study of high-resolution regional climate simulations to three land surface models over the western United States, J. Geophys. Res., 7271–7291, doi:10.1002/2014JD021827.Received, 2014.

Chen, L., Li, Y., Chen, F., Barr, A., Barlage, M. and Wan, B.: The incorporation of an organic soil layer in the Noah-MP land surface model and its evaluation over a boreal aspen forest, Atmos. Chem. Phys., 16(13), 8375–8387, doi:10.5194/acp-16-8375-2016, 2016.

Chen, L., Li, Y., Chen, F., Barlage, M., Zhang, Z. and Li, Z.: Using 4-km WRF CONUS simulations to assess impacts of the surface coupling strength on regional climate simulation, Clim. Dyn., doi:10.1007/s00382-019-04932-9, 2019.

Chen, M., Griffis, T. J., Baker, J. M., Wood, J. D., Meyers, T., & Suyker, A. (2018). Comparing crop growth and carbon budgets simulated across AmeriFlux agricultural sites using the Community Land Model (CLM). Agricultural and Forest Meteorology, 256–257(March), 315–333. https://doi.org/10.1016/j.agrformet.2018.03.012

Christensen NS, Wood AW, Voisin N, et al (2004) The Effects of Climate Change on the Hydrology and Water Resources of the Colorado River Basin. Clim Change 62:337–363. doi: 10.1023/B:CLIM.0000013684.13621.1f

Clark, M. P., Fan, Y., Lawrence, D. M., Adam, J. C., Bolster, D., Gochis, D. J., Hooper, R. P., Kumar, M., Leung, L. R., Mackay, D. S., Maxwell, R. M., Shen, C., Swenson, S. C., & Zeng, X. (2015). Improving the representation of hydrologic processes in Earth System Models. Water Resources Research, 51(8), 5929–5956. https://doi.org/10.1002/2015WR017096

Collatz, G. J., J. T. Ball, C. Grivet, and J. A. Berry (1991), Physiological and environmental regulation of stomatal conductance, photosynthesis and transpiration: A model that includes a laminar boundary layer, Agric. For. Meteorol., 54, 107–136, doi:10.1016/0168-1923(91)90002-8.

Collatz, G. J., M. Ribas-Carbo, and J. A. Berry (1992), Coupled photosynthesis-stomatal conductance model for leaves of C4 plants, Aust. J. Plant Physiol., 19, 519–538.

Cosgrove, B. A., et al. (2003), Land surface model spin-up behavior in the North American Land Data Assimilation System (NLDAS), J. Geo- phys. Res., 108(D22), 8845, doi:10.1029/2002JD00331603.

Dai, Y., Zeng, X., Dickinson, R. E., Baker, I., Bonan, G. B., Bosilovich, M. G., Denning, A. S., Dirmeyer, P. A., Houser, P. R., Niu, G., Oleson, K. W., Schlosser, C. A., & Yang, Z.-L. (2003). The Common Land Model. *Bulletin of the American Meteorological Society*, *84*(8), 1013–1024. https://doi.org/10.1175/BAMS-84-8-1013

Dai, A.: Precipitation Characteristics in Eighteen Coupled Climate Models, J. Clim., 19(18), 4605–4630, doi:10.1175/JCLI3884.1, 2006.

Dai A (2011) Drought under global warming: a review. Wiley Interdiscip Rev Clim Change 2(1):45–65. https://doi.org/10.1002/wcc.81

Deardorff, J. W. (1978). Efficient prediction of ground surface temperature and moisture, with inclusion of a layer of vegetation. *Journal of Geophysical Research*, *83*(C4), 1889. https://doi.org/10.1029/JC083iC04p01889

Dickinson, R. E. (1983). Land Surface Processes and Climate—Surface Albedos and Energy Balance (pp. 305–353). https://doi.org/10.1016/S0065-2687(08)60176-4

Dickinson RE, Henderson-Sellers A, Kennedy PJ (1993) Biosphere-Atmosphere Transfer Scheme (BATS) Version le as Coupled to the NCAR Community Climate Model. NCAR Technical Note, NCAR/TN-387+STR.

Dickinson, R. E., Berry, J. A., Bonan, G. B., Collatz, G. J., Field, C. B., Fung, I. Y., Goulden, M., Hoffmann, W. A., Jackson, R. B., Myneni, R., Sellers, P. J., & Shaikh, M. (2002). Nitrogen Controls on Climate Model Evapotranspiration. *Journal of Climate*, *15*(3), 278–295. https://doi.org/10.1175/1520-0442(2002)015<0278:NCOCME>2.0.CO;2

Dieter, C., Maupin, M., Caldwell, R., Harris, M., Ivahnenko, T., Lovelace, J., et al. (2015). Estimated use of water in the United States in 2015. Circular. https://doi.org/10.3133/cir1441

Difenbaugh NS, Ashfaq M (2010) Intensifcation of hot extremes in the United States. Geophys Res Lett 37(15):1–5. https://doi.org/10.1029/2010GL043888

Doherty, K.E., Howerter, D.W., Devries, J.H., & Walker, J. (2018). Prairie Pothole Region of North America. In The Wetland Book (Finlayson C., Milton G., Prentice R., Davidson N., eds.). Springer, Dordrecht.

Döll, P. and Fiedler, K.: Global-scale modeling of groundwater recharge, Hydrol. Earth Syst. Sci., 12(3), 863–885, doi:10.5194/hess-12-863-2008, 2008.

Döll, P.: Vulnerability to the impact of climate change on renewable groundwater resources: A global-scale assessment, Environ. Res. Lett., 4(3), doi:10.1088/1748-9326/4/3/035006, 2009.

Drewniak, B., Song, J., Prell, J., Kotamarthi, V. R., & Jacob, R. (2013). Modeling agriculture in the Community Land Model. Geoscientific Model Development, 6(2), 495–515. https://doi.org/10.5194/gmd-6-495-2013

Duda JD, Wang X, Xue M (2017) Sensitivity of convection-allowing forecasts to land surface model perturbations and implications for ensemble design. Mon Weather Rev 145(5):2001–2025. https://doi.org/10.1175/MWR-D-16-0349.1

Dumanski, S., Pomeroy, J. W., & Westbrook, C. J. (2015). Hydrological regime changes in a Canadian Prairie basin. Hydrological Processes, 29(18), 3893–3904. https://doi.org/10.1002/hyp.10567

Durre I, Wallace JM, Lettenmaier DP (2000) Dependence of extreme daily maximum temperatures on antecedent soil moisture in the contiguous United States during summer. J Clim 13(14):2641–2651

Egli, D. B., & Hatfield, J. L. (2014). Yield Gaps and Yield Relationships in Central U.S. Soybean Production Systems. Agronomy Journal, 106(2), 560–566. https://doi.org/10.2134/agronj2013.0364

Ehsanzadeh, E., Spence, C., van der Kamp, G., & McConkey, B. (2012). On the behaviour of dynamic contributing areas and flood frequency curves in North American Prairie watersheds. Journal of Hydrology, 414–415, 364–373. https://doi.org/10.1016/j.jhydrol.2011.11.007

Environment Canada: Municipal Water Use, 2009 Statistics, 2011 Munic. Water Use Rep., 24, doi:En11-2/2009E-PDF Information, 2011.

Famiglietti, J. S. & Wood, E. F. Multiscale modeling of spatially variable water and energy balance processes. Water Resour. Res. 30, 3061–3078 (1994a).

Famiglietti, J. S. & Wood, E. F. Application of multiscale water and energy balance models on a tallgrass prairie. Water Resour. Res. 30, 3079–3093 (1994b).

Fan, Y., Miguez-Macho, G., Weaver, C. P., Walko, R., & Robock, A. (2007). Incorporating water table dynamics in climate modeling: 1. Water table observations and equilibrium water table simulations. Journal of Geophysical Research Atmospheres, 112(10), 1–17. https://doi.org/10.1029/2006JD008111

Fan, Y. and Miguez-Macho, G.: A simple hydrologic framework for simulating wetlands in climate and earth system models, Clim. Dyn., 37(1), 253–278, doi:10.1007/s00382-010-0829-8, 2011.

Fan, Y., Li, H. and Miguez-Macho, G.: Global patterns of groundwater table depth, Science (80-.)., 339(6122), 940–943, doi:10.1126/science.1229881, 2013.

Fan, Y.: Groundwater in the Earth's critical zones: Relevance to large-scale patterns and processes, Water Resour. Res., 3052–3069, doi:10.1002/2015WR017037. 2015.

Fang, X., & Pomeroy, J. (2020). Diagnosis of future changes in hydrology for a Canadian Rocky Mountain headwater basin. Hydrology and Earth System Sciences Discussions, 1–40. https://doi.org/10.5194/hess-2019-640

FAO and DWFI. 2015. Yield gap analysis of field crops – Methods and case studies, by Sadras, V.O., Cassman, K.G.G., Grassini, P., Hall, A.J., Bastiaanssen, W.G.M., Laborte, A.G., Milne, A.E., Sileshi, G.,Steduto, P. FAO Water Reports No. 41, Rome, Italy.

Farquhar, G. D., S. von Caemmerer, and J. A. Berry (1980), A biochemical model of photosynthetic CO2 assimilation in leaves of C3 species, Planta, 149, 78–90.

Fischer EM, Seneviratne SI, Vidale PL, Lüthi D, Schär C (2007) Soil moisture–atmosphere interactions during the 2003 European summer heat wave. J Clim 20(20):5081–5099. https://doi.org/10.1175/JCLI4288.1

Fisher, R. A., & Koven, C. D. (2020). Perspectives on the Future of Land Surface Models and the Challenges of Representing Complex Terrestrial Systems. *Journal of Advances in Modeling Earth Systems*, *12*(4). https://doi.org/10.1029/2018MS001453

Forbes, K. A., Kienzle, S. W., Coburn, C. A., Byrne, J. M., & Rasmussen, J. (2011). Simulating the hydrological response to predicted climate change on a watershed in southern Alberta, Canada. Climatic Change, 105(3–4), 555–576. https://doi.org/10.1007/s10584-010-9890-x

Garris, H. W., Mitchell, R. J., Fraser, L. H., & Barrett, L. R. (2015). Forecasting climate change impacts on the distribution of wetland habitat in the Midwestern United states. Global Change Biology, 21(2), 766–776. https://doi.org/10.1111/gcb.12748

Gedney, N., & Cox, P. M. (2003). The Sensitivity of Global Climate Model Simulations to the Representation of Soil Moisture Heterogeneity. Journal of Hydrometeorology, 4(6), 1265–1275. https://doi.org/10.1175/1525-7541(2003)004<1265:TSOGCM>2.0.CO;2

Gleason, Robert A. Ecosystem services derived from wetland conservation practices in the United States Prairie Pothole Region with an emphasis on the U.S. Department of Agriculture Conservation Reserve and Wetlands Reserve Programs / edited by Robert A. Gleason, Murray K. Laubhan, and Ned H. Euliss, Jr. p. cm. –(U.S. Geological Survey professional paper ; 1745) Includes bibliographic references. ISBN 978-1-4113-2017-8

Granger RJ, Gray DM: Evaporation from natural non-saturated surface. J. Hydrol., 111, 21–29, 1989.

Grassini, P., Yang, H., & Cassman, K. G. (2009). Limits to maize productivity in Western Corn-Belt: A simulation analysis for fully irrigated and rainfed conditions. Agricultural and Forest Meteorology, 149(8), 1254–1265. https://doi.org/10.1016/j.agrformet.2009.02.012

Grassini, P., Yang, H., Irmak, S., Thorburn, J., Burr, C. and Cassman, K. G.: High-yield irrigated maize in the Western U.S. Corn Belt: II. Irrigation management and crop water productivity, F. Crop. Res., 120(1), 133–141, doi:10.1016/j.fcr.2010.09.013, 2011.

Gray DM: Handbook on the Principles of Hydrology: With Special Emphasis Directed to Canadian Conditions in the Discussion, Applications, and Presentation of Data. Water Information Center: Huntingdon, New York, 1970. ISBN:0-912394-07-2

Green, T. R., Taniguchi, M., Kooi, H., Gurdak, J. J., Allen, D. M., Hiscock, K. M., Treidel, H. and Aureli, A.: Beneath the surface of global change: Impacts of climate change on groundwater, J. Hydrol., 405(3–4), 532–560, doi:10.1016/j.jhydrol.2011.05.002, 2011.

Guo, Z., Dirmeyer, P. a., Koster, R. D., Bonan, G. B., Chan, E., Cox, P. M., Gordon, C. T., Kanae, S., Kowalczyk, E., Lawrence, D. M., Liu, P., Lu, C. H., Malyshev, S., MacAvaney, B., McGregor, J. L., Mitchell, K., Mocko, D., Oki, T., Oleson, K. W., Pitman, a., Sud, Y. C., Taylor, C. M., Verseghy, D., Vasic, R., Xue, Y. and Yamada, T.: GLACE: The Global Land

– Atmosphere Coupling Experiment. Part II: Analysis, J. Hydrometeorol., 7(4), 611–625, doi:http://dx.doi.org/10.1175/JHM511.1, 2006.
Hastie, T., & Tibshirani, R. (1986). Generalized Additive Models. Statistical Science, 1(3), 297–318.
Hauser M, Orth R, Seneviratne SI (2015) Role of soil moisture vs. recent climate change for hea waves in western Russia. Geophys Res Lett 43(10):2819–2826. https://doi.org/10.1002/2016GL068036
Hayashi, M., Van Der Kamp, G. and Schmidt, R.: Focused infiltration of snowmelt water in partially frozen soil under small depressions, J. Hydrol., 270(3–4), 214–229, doi:10.1016/S0022-1694(02)00287-1, 2003.
Hayashi, M., van der Kamp, G., & Rosenberry, D. O. (2016). Hydrology of Prairie Wetlands: Understanding the Integrated Surface-Water and Groundwater Processes. Wetlands, 36, 237–254. https://doi.org/10.1007/s13157-016-0797-9
He, L., Chen, J. M., Liu, J., Zheng, T., Wang, R., Joiner, J., et al. (2019). Diverse photosynthetic capacity of global ecosystems mapped by satellite chlorophyll fluorescence measurements. Remote Sensing of Environment, 232, 111344. https://doi.org/10.1016/j.rse.2019.111344
Herfindal, I., Drever, M. C., Høgda, K.-A., Podruzny, K. M., Nudds, T. D., Grøtan, V., & Sæther, B.-E. (2012). Landscape heterogeneity and the effect of environmental conditions on prairie wetlands. Landscape Ecology, 27(10), 1435–1450. https://doi.org/10.1007/s10980-012-9798-0
Herold N, Kala J, Alexander LV (2016) The influence of soil moisture defcits on Australian heatwaves. Environ Res Lett 11(6):64003. https://doi.org/10.1088/1748-9326/11/6/064003
Hicks, D. R., and Cloud, H. A. (1992). Calculating grain weight shrinkage in corn due to mechanical drying. National Corn Handbook-61, Purdue Extension, Purdue University.
Hirschi M et al (2011) Observational evidence for soil-moisture impact on hot extremes in southeastern Europe. Nat Geosci 4(1):17–21. https://doi.org/10.1038/ngeo1032
Hlavinka, P., Trnka, M., Semerádová, D., Dubrovský, M., Žalud, Z. and Možný, M.: Effect of drought on yield variability of key crops in Czech Republic, Agric. For. Meteorol., 149(3–4), 431–442, doi:10.1016/j.agrformet.2008.09.004, 2009.
Hoerling M et al (2013) Anatomy of an extreme event. J Clim 26(9):2811–2832. https://doi.org/10.1175/JCLI-D-12-00270.1
Hong S-Y, Noh Y, Dudhia J (2006) A new vertical difusion package with an explicit treatment of entrainment processes. Mon Weather Rev 134:2318–2341
Hostetler, S. W., Bates, G. T., & Giorgi, F. (1993). Interactive coupling of a lake thermal model with a regional climate model. Journal of Geophysical Research: Atmospheres, 98(D3), 5045–5057. https://doi.org/10.1029/92JD02843
Huber D, Mechem D, Brunsell N (2014) The effects of Great Plains irrigation on the surface energy balance, regional circulation, and precipitation. Climate 2(2):103–128. https://doi.org/10.3390/cli2020103
Iacono MJ, Delamere JS, Mlawer EJ, Shephard MW, Clough SA, Collins WD (2008) Radiative forcing by long-lived greenhouse gases: calculations with the AER radiative transfer models. J Geophys Res 113:D13103. https://doi.org/10.1029/2008JD009944
Iizumi, T., Kim, W., & Nishimori, M. (2019). Modeling the Global Sowing and Harvesting Windows of Major Crops Around the Year 2000. Journal of Advances in Modeling Earth Systems, 11(1), 99–112. https://doi.org/10.1029/2018MS001477

IPCC (2012) Managing the risks of extreme events and disasters to advance climate change adaptation. In: Field CB, Barros V, Stocker TF, Qin D, Dokken DJ, Ebi KL, Mastrandrea MD, Mach KJ, Plattner G-K, Allen SK, Tignor M, Midgley PM (eds) A special report of working groups I and II of the intergovernmental panel on climate change. Cambridge University Press, Cambridge, p 582

Ireson, A. M., Barr, A. G., Johnstone, J. F., Mamet, S. D., van der Kamp, G., Whitfield, C. J., Michel, N. L., North, R. L., Westbrook, C. J., DeBeer, C., Chun, K. P., Nazemi, A. and Sagin, J.: The changing water cycle: the Boreal Plains ecozone of Western Canada, Wiley Interdiscip. Rev. Water, 2(5), 505–521, doi:10.1002/wat2.1098, 2015.

Ireson, A. M., van der Kamp, G., Ferguson, G., Nachshon, U., & Wheater, H. S. (2013). Hydrogeological processes in seasonally frozen northern latitudes: understanding, gaps and challenges. Hydrogeology Journal, 21(1), 53–66. https://doi.org/10.1007/s10040-012-0916-5

Jaeger EB, Seneviratne SI (2011) Impact of soil moisture–atmosphere coupling on European climate extremes and trends in a regional climate model. Clim Dyn 36(9–10):1919–1939. https://doi.org/10.1007/s00382-010-0780-8

Johnson, W. C., Millett, B. V, Gilmanov, T., Voldseth, R. a, Guntenspergen, G. R., & Naugle, D. E. (2005). Vulnerability of Northern Prairie Wetlands to Climate Change. Bioscience, 55(10), 863–872. https://doi.org/10.1641/0006-3568(2005)055[0863:VONPWT]2.0.CO;2

Johnson, W. C., Werner, B., Guntenspergen, G. R., Voldseth, R. A., Millett, B., Naugle, D. E., et al. (2010). Prairie Wetland Complexes as Landscape Functional Units in a Changing Climate. BioScience, 60(2), 128–140. https://doi.org/10.1525/bio.2010.60.2.7

Jones, J. W., G. Hoogenboom, C. H. Porter, K. J. Boote, W. D. Batchelor, L. A. Hunt, P. W. Wilkens, U. Singh, A. J. Gijsman, and J. T. Ritchie (2003), The DSSAT cropping system model, Eur. J. Agron., 18, 235– 265.

Kelln C, Barbour L, Qualizza C (2007) Preferential Flow in a Reclamation Cover : Hydrological and Geochemical Response. 1277–1289

Kendon, E. J., Ban, N., Roberts, N. M., Fowler, H. J., Roberts, M. J., Chan, S. C., et al. (2017). Do Convection-Permitting Regional Climate Models Improve Projections of Future Precipitation Change? Bulletin of the American Meteorological Society, 98(1), 79–93. https://doi.org/10.1175/BAMS-D-15-0004.1

Kienzle, S. W., Nemeth, M. W., Byrne, J. M., & MacDonald, R. J. (2012). Simulating the hydrological impacts of climate change in the upper North Saskatchewan River basin, Alberta, Canada. Journal of Hydrology, 412–413, 76–89. https://doi.org/10.1016/j.jhydrol.2011.01.058

Kollet SJ, Maxwell RM (2008) Capturing the influence of groundwater dynamics on land surface processes using an integrated, distributed watershed model. Water Resour Res 44:1–18. doi: 10.1029/2007WR006004

Koren, V., Schaake, J., Mitchell, K., Duan, Q.-Y., Chen, F., & Baker, J. M. (1999). A parameterization of snowpack and frozen ground intended for NCEP weather and climate models. Journal of Geophysical Research: Atmospheres, 104(D16), 19569–19585. https://doi.org/10.1029/1999JD900232

Koster, R. D., & Milly, P. C. D. (1997). The Interplay between Transpiration and Runoff Formulations in Land Surface Schemes Used with Atmospheric Models. *Journal of Climate*, *10*(7), 1578–1591. https://doi.org/10.1175/1520-0442(1997)010<1578:TIBTAR>2.0.CO;2

Koster, R. D., Suarez, M. J., Ducharne, A., Stieglitz, M., & Kumar, P. (2000). A catchment-based approach to modeling land surface processes in a general circulation model: 1. Model structure. Journal of Geophysical Research: Atmospheres, 105(D20), 24809–24822. https://doi.org/10.1029/2000JD900327

Koster, R. D., Guo, Z., Bonan, G., Chan, E., Cox, P. (2004). Regions of strong coupling between. Science 1138(2004):10–13. https://doi.org/10.1126/science.1100217

Koster, R. D., Sud, Y. C., Guo, Z., Dirmeyer, P. A., Bonan, G., Oleson, K. W., Chan, E., Verseghy, D., Cox, P., Davies, H., Kowalczyk, E., Gordon, C. T., Kanae, S., Lawrence, D., Liu, P., Mocko, D., Lu, C.-H., Mitchell, K., Malyshev, S., … Xue, Y. (2006). GLACE: The Global Land–Atmosphere Coupling Experiment. Part I: Overview. *Journal of Hydrometeorology*, *7*(4), 590–610. https://doi.org/10.1175/JHM510.1

Koster, R. D., Schubert, S. D., Suarez, M. J. (2009). Analyzing the concurrence of meteorological droughts and warm periods, with implications for the determination of evaporative regime. J Clim 22(12):3331–3341. https://doi.org/10.1175/2008JCLI2718.1

Kucharik, C. J.: Evaluation of a Process-Based Agro-Ecosystem Model (Agro-IBIS) across the U.S. Corn Belt: Simulations of the Interannual Variability in Maize Yield, Earth Interact., 7(14), 1–33, doi:10.1175/1087-3562(2003)007<0001:eoapam>2.0.co;2, 2003.

KUMAR, S., PETERSLIDARD, C., TIAN, Y., HOUSER, P., GEIGER, J., OLDEN, S., LIGHTY, L., EASTMAN, J., DOTY, B., & DIRMEYER, P. (2006). Land information system: An interoperable framework for high resolution land surface modeling. *Environmental Modelling & Software*, *21*(10), 1402–1415. https://doi.org/10.1016/j.envsoft.2005.07.004

Kurylyk, B. L. and MacQuarrie, K. T. B.: The uncertainty associated with estimating future groundwater recharge: A summary of recent research and an example from a small unconfined aquifer in a northern humid-continental climate, J. Hydrol., 492, 244–253, doi:10.1016/j.jhydrol.2013.03.043, 2013.

Lawston, P. M., Santanello Jr., J. A., Franz, T. E. and Rodell, M.: Assessment of irrigation physics in a land surface modeling framework using non-traditional and human-practice datasets, Hydrol. Earth Syst. Sci., 21(6), 2953–2966, doi:10.5194/hess-21-2953-2017, 2017.

Lehner, B., & Döll, P. (2004). Development and validation of a global database of lakes, reservoirs and wetlands. Journal of Hydrology, 296(1–4), 1–22. https://doi.org/10.1016/j.jhydrol.2004.03.028

Leng, G., Huang, M., Tang, Q., Sacks, W. J., Lei, H., & Leung, L. R. (2013). Modeling the effects of irrigation on land surface fluxes and states over the conterminous United States: Sensitivity to input data and model parameters. Journal of Geophysical Research Atmospheres, 118(17), 9789–9803. https://doi.org/10.1002/jgrd.50792

Leng, G., Zhang, X., Huang, M., Asrar, G. R., & Leung, L. R. (2016). The Role of Climate Covariability on Crop Yields in the Conterminous United States. Scientific Reports, 6(September), 1–11. https://doi.org/10.1038/srep33160

Levis, S., B. B. Gordon, Erik Kluzek, P. E. Thornton, A. Jones, W. J. Sacks, and C. J. Kucharik (2012), Interactive crop management in the com- munity earth system model (CESM1): Seasonal influences on land-atmosphere fluxes, J. Clim., 25(14), 4839–4859, doi:10.1175/JCLI-D-11- 00446.1.

Li, Y., Szeto, K., Stewart, R. E., Thériault, J. M., Chen, L., Kochtubajda, B., et al. (2017). A Numerical Study of the June 2013 Flood-Producing Extreme Rainstorm over Southern

Alberta. Journal of Hydrometeorology, 18(8), 2057–2078. https://doi.org/10.1175/JHM-D-15-0176.1

Li, Y., Li, Z., Zhang, Z., Chen, L., Kurkute, S., Scaff, L., & Pan, X. (2019). High-resolution regional climate modeling and projection over western Canada using a weather research forecasting model with a pseudo-global warming approach. Hydrology and Earth System Sciences, 23(11), 4635–4659. https://doi.org/10.5194/hess-23-4635-2019

Li, Z., Li, Y., Bonsal, B., Manson, A. H., & Scaff, L. (2018). Combined Impacts of ENSO and MJO on the 2015 Growing Season Drought over the Canadian Prairies, (February).

Liu, C., Ikeda, K., Rasmussen, R., Barlage, M., Newman, A. J., Prein, A. F., et al. (2017). Continental-scale convection-permitting modeling of the current and future climate of North America. Climate Dynamics, 49(1–2), 71–95. https://doi.org/10.1007/s00382-016-3327-9

Liu, G., & Schwartz, F. W. (2012). Climate-driven variability in lake and wetland distribution across the Prairie Pothole Region: From modern observations to long-term reconstructions with space-for-time substitution. Water Resources Research, 48(8), 1–11. https://doi.org/10.1029/2011WR011539

Liu, X., Chen, F., Barlage, M., Zhou, G., & Niyogi, D. (2016). Noah-MP-Crop: Introducing dynamic crop growth in the Noah-MP land surface model. Journal of Geophysical Research: Atmospheres, 121(23), 13,953-13,972. https://doi.org/10.1002/2016JD025597

Lobell, D. B., Cassman, K. G., & Field, C. B. (2009). Crop Yield Gaps: Their Importance, Magnitudes, and Causes. Annual Review of Environment and Resources, 34(1), 179–204. https://doi.org/10.1146/annurev.environ.041008.093740

Lobell, D. B., M. J. Roberts, W. Schlenker, N. Braun, B. B. Little, R. M. Rejesus, and G. L. Hammer (2014), Greater sensitivity to drought accom- panies maize yield increase in the US Midwest, Science, 344, 516–519.

Lu, Y., & Kueppers, L. (2015). Increased heat waves with loss of irrigation in the United States. Environmental Research Letters, 10(6), 064010+. https://doi.org/10.1088/1748-9326/10/6/064010

Ma HY et al (2014) On the correspondence between mean forecast errors and climate errors in CMIP5 models. J Clim 27(4):1781–1798. https://doi.org/10.1175/JCLI-D-13-00474.1

Ma, S., Churkina, G., & Trusilova, K. (2012). Investigating the impact of climate change on crop phenological events in Europe with a phenology model. International Journal of Biometeorology, 56(4), 749–763. https://doi.org/10.1007/s00484-011-0478-6

MacDonald, R. J., Byrne, J. M., Boon, S., & Kienzle, S. W. (2012). Modelling the Potential Impacts of Climate Change on Snowpack in the North Saskatchewan River Watershed, Alberta. Water Resources Management, 26(11), 3053–3076. https://doi.org/10.1007/s11269-012-0016-2

Manabe, S. (1969) Climate and the ocean circulation 1, *Monthly Weather Review*., 97(11), 739-774. https://doi.org/10.1175/1520-0493(1969)097<0739:CATOC>2.3.CO;2

Martinez, J. A., Dominguez, F. and Miguez-Macho, G.: Effects of a Groundwater Scheme on the Simulation of Soil Moisture and Evapotranspiration over Southern South America, J. Hydrometeorol., 17(11), 2941–2957, doi:10.1175/JHM-D-16-0051.1, 2016.

Maupin, M. A., Kenny, J. F., Hutson, S. S., Lovelace, J. K., Barber, N. L., & Linsey, K. S. (2014). Estimated use of water in the United States in 2010: U.S. Geological Survey Circular 1405, 56 p., https://dx.doi.org/10.3133/cir1405. Circular. https://doi.org/10.3133/cir1405

Maxwell RM, Miller NL (2005) Development of a Coupled Land Surface and Groundwater Model. 233–247

Maxwell, R. M. and Kollet, S. J.: Interdependence of groundwater dynamics and land-energy feedbacks under climate change, Nat. Geosci., 1(10), 665–669, doi:10.1038/ngeo315, 2008.
Maxwell, R. M., Condon, L. E. and Kollet, S. J.: A high-resolution simulation of groundwater and surface water over most of the continental US with the integrated hydrologic model ParFlow v3, Geosci. Model Dev., 8(3), 923–937, doi:10.5194/gmd-8-923-2015, 2015.
McDermid, S. S., Mearns, L. O., & Ruane, A. C. (2017). Representing agriculture in Earth System Models: Approaches and priorities for development. Journal of Advances in Modeling Earth Systems, 9(5), 2230–2265. https://doi.org/10.1002/2016MS000749
McKee TB, Doesken NJ, Kleist J (1993) The relationship of drought frequency and duration ot time scales. Eighth conference on applied climatology, American Meteorological Society, Jan 17–23, 1993, Anaheim CA, pp 179–186
McKenna, O.P., Mushet, D.M., Rosenberry, D.O. and LaBaugh, J.W., 2017. Evidence for a climate-induced ecohydrological state shift in wetland ecosystems of the southern Prairie Pothole Region. Climatic Change, 145(3-4), pp.273-287.
Meehl GA, Tebaldi C (2004) More intense, more frequent, and longer lasting heat waves in the 21st century. Science 305(5686):994–997. https://doi.org/10.1126/science.1098704
Meixner, T., Manning, A. H., Stonestrom, D. A., Allen, D. M., Ajami, H., Blasch, K. W., Brookfield, A. E., Castro, C. L., Clark, J. F., Gochis, D. J., Flint, A. L., Neff, K. L., Niraula, R., Rodell, M., Scanlon, B. R., Singha, K. and Walvoord, M. A.: Implications of projected climate change for groundwater recharge in the western United States, J. Hydrol., 534, 124–138, doi:10.1016/j.jhydrol.2015.12.027, 2016.
Mekonnen, M. A., Wheater, H. S., Ireson, A. M., Spence, C., Davison, B., & Pietroniro, A. (2014). Towards an improved land surface scheme for prairie landscapes. Journal of Hydrology, 511, 105–116. https://doi.org/10.1016/j.jhydrol.2014.01.020
Melton, J. R., Wania, R., Hodson, E. L., Poulter, B., Ringeval, B., Spahni, R., et al. (2013). Present state of global wetland extent and wetland methane modelling: conclusions from a model inter-comparison project (WETCHIMP). Biogeosciences, 10(2), 753–788. https://doi.org/10.5194/bg-10-753-2013
Meng L, Shen Y (2014) On the relationship of soil moisture and extreme temperatures in East China. Earth Interact. https://doi.org/10.1175/2013EI000551.1
Menne MJ, Durre I, Vose RS, Gleason BE, Houston TG (2012) An overview of the global historical climatology network-daily database. J Atmos Ocean Technol 29(7):897–910. https://doi.org/10.1175/JTECH-D-11-00103.1
Miguez-Macho, G., Fan, Y., Weaver, C. P., Walko, R., & Robock, A. (2007). Incorporating water table dynamics in climate modeling: 2. Formulation, validation, and soil moisture simulation. Journal of Geophysical Research Atmospheres, 112(13), 1–16. https://doi.org/10.1029/2006JD008112
Miguez-Macho, G. and Fan, Y.: The role of groundwater in the Amazon water cycle: 1. Influence on seasonal streamflow, flooding and wetlands, J. Geophys. Res. Atmos., 117(15), 1–30, doi:10.1029/2012JD017539, 2012.
Miralles DG, Teuling AJ, van Heerwaarden CC, Vilà-Guerau de Arellano J (2014) Mega-heatwave temperatures due to combined soil desiccation and atmospheric heat accumulation. Nat Geosci 7(5):345–349. https://doi.org/10.1038/ngeo2141
Mitra, S., Wassmann, R., Vlek, P. L. G. (2005) An appraisal of global wetland area and its organic carbon stock. Curr Sci 88:25–35
Mitsch WJ, Gosselink JG (2007) Wetlands, 4th edn. Wiley, Hoboken

Moeck, C., Brunner, P. and Hunkeler, D.: The influence of model structure on groundwater recharge rates in climate-change impact studies, Hydrogeol. J., 24(5), 1171–1184, doi:10.1007/s10040-016-1367-1, 2016.

Mohammed, A. A., Kurylyk, B. L., Cey, E. E. and Hayashi, M.: Snowmelt Infiltration and Macropore Flow in Frozen Soils: Overview, Knowledge Gaps, and a Conceptual Framework, Vadose Zo. J., 17(1), doi:10.2136/vzj2018.04.0084, 2018.

Moomaw, W. R., Chmura, G. L., Davies, G. T., Finlayson, C. M., Middleton, B. A., Natali, S. M., Perry, J. E., Roulet, N. and Sutton-Grier, A. E.: Wetlands In a Changing Climate: Science, Policy and Management, Wetlands, 38(2), 183–205, doi:10.1007/s13157-018-1023-8, 2018.

Mueller B, Seneviratne SI (2012) Hot days induced by precipitation defcits at the global scale. Proc Natl Acad of Sci 109(31):12398–12403. https://doi.org/10.1073/pnas.1204330109

Musselman KN, Clark MP, Liu CH, Ikeda K, Rasmussen R (2017) Slower snowmelt in a warmer world. Nat Clim Change 7(February):214–220. https://doi.org/10.1038/NCLIMATE3225

National Research Council: Groundwater fluxes across inter- faces. The National Academy Press, 85 pp, 2003

National Research Council. (2011). Climate Stabilization Targets: Emissions, Concentrations, and Impacts over Decades to Millennia Committee on Stabilization Targets for Atmospheric Greenhouse Gas Concentrations. Retrieved from http://www.nap.edu/catalog.php?record_id=12877

National Wetlands Working Group. 1997. The Canadian Wetland Classification System, 2nd Edtion. Warner, G.g. and C.D.A. Rubec (Eds). Wetlands Research Centre, University of Waterloo, On, Canada.

Newman AJ et al (2015) Gridded ensemble precipitation and temperature estimates for the contiguous United States. J Hydrometeorol 16(6):2481–2500. https://doi.org/10.1175/JHM-D-15-0026.1

Niemuth, N.D., Solberg, J.W., & Shaffer, T.L. (2008). Influence of moisture on density and distribution of grassland birds in North Dakota. Condor 110:211–22.

Niemuth, N.D., Wangler, B. and Reynolds, R.E., 2010. Spatial and temporal variation in wet area of wetlands in the Prairie Pothole Region of North Dakota and South Dakota. Wetlands, 30(6), pp.1053-1064.

Niemuth, N. D., Fleming, K. K., & Reynolds, R. E. (2014). Waterfowl conservation in the US prairie pothole region: Confronting the complexities of climate change. PLoS ONE, 9(6). https://doi.org/10.1371/journal.pone.0100034

Niraula R, Meixner T, Dominguez F, et al (2017) How Might Recharge Change Under Projected Climate Change in the Western U.S.? Geophys Res Lett 44:10,407-10,418. doi: 10.1002/2017GL075421

Niu, G.-Y., Yang, Z.-L., Dickinson, R. E., & Gulden, L. E. (2005). A simple TOPMODEL-based runoff parameterization (SIMTOP) for use in global climate models. Journal of Geophysical Research, 110(D21), D21106. https://doi.org/10.1029/2005JD006111

Niu, G.-Y., & Yang, Z.-L. (2006). Effects of Frozen Soil on Snowmelt Runoff and Soil Water Storage at a Continental Scale. Journal of Hydrometeorology, 7(5), 937–952. https://doi.org/10.1175/JHM538.1

Niu G, Yang Z, Dickinson RE, Gulden LE (2007) Development of a simple groundwater model for use in climate models and evaluation with Gravity Recovery and Climate Experiment data. 112:1–14. doi: 10.1029/2006JD007522

Niu, G. Y., Yang, Z. L., Mitchell, K. E., Chen, F., Ek, M. B., Barlage, M., et al. (2011). The community Noah land surface model with multiparameterization options (Noah-MP): 1. Model description and evaluation with local-scale measurements. Journal of Geophysical Research Atmospheres, 116(12), 1–19. https://doi.org/10.1029/2010JD015139

Niu G-Y, Zeng X (2012) Earth System Model, Modeling the Land Component of. In: Climate Change Modeling Methodology. Springer New York, New York, NY, pp 139–168

Oleson, K. W., Niu, G.-Y., Yang, Z.-L., Lawrence, D. M., Thornton, P. E., Lawrence, P. J., Stöckli, R., Dickinson, R. E., Bonan, G. B., Levis, S., Dai, A. and Qian, T.: Improvements to the Community Land Model and their impact on the hydrological cycle, J. Geophys. Res. Biogeosciences, 113(G1), n/a-n/a, doi:10.1029/2007JG000563, 2008.

Oleson, K. W., et al. (2013), Technical Description of version 4.5 of the Community Land Model (CLM), NCAR Tech. Note NCAR/TN-503+STR, 422 pp., Natl. Cent. for Atmos. Res., Boulder, Colo., doi:10.5065/D6RR1W7M. [Available at http://www.cesm.ucar.edu/models/cesm1.2/ clm/CLM45_Tech_Note.pdf.]

Orlowsky B, Seneviratne SI (2013) Elusive drought: uncertainty in observed trends and short-and long-term CMIP5 projections. Hydrol Earth Syst Sci 17(5):1765–1781. https://doi.org/10.5194/hess-17-1765-2013

Ozdogan, M., & Gutman, G. (2008). A new methodology to map irrigated areas using multi-temporal MODIS and ancillary data: An application example in the continental US. Remote Sensing of Environment, 112(9), 3520-3537. https://doi.org/10.1016/j.rse.2008.04.010

Pattison-Williams, J. K., Pomeroy, J. W., Badiou, P., & Gabor, S. (2018). Wetlands, Flood Control and Ecosystem Services in the Smith Creek Drainage Basin: A Case Study in Saskatchewan, Canada. Ecological Economics, 147, 36–47. https://doi.org/10.1016/j.ecolecon.2017.12.026

Perkins SE, Alexander LV (2013) On the measurement of heat waves. J Clim 26(13):4500–4517. https://doi.org/10.1175/JCLID-12-00383.1

Perkins SE (2015) A review on the scientifc understanding of heatwaves—their measurement, driving mechanisms, and changes at the global scale. Atmos Res 164–165:242–267. https://doi.org/10.1016/j.atmosres.2015.05.014

Pielke, R. A., Adegoke, J., BeltraáN-Przekurat, A., Hiemstra, C. A., Lin, J., Nair, U. S., et al. (2007). An overview of regional land-use and land-cover impacts on rainfall. Tellus B: Chemical and Physical Meteorology, 59(3), 587–601. https://doi.org/10.1111/j.1600-0889.2007.00251.x

Pitman, A. (1991). A simple parameterization of sub-grid scale open water for climate models. Climate Dynamics, 6(2), 99–112. https://doi.org/10.1007/BF00209983

Pokhrel, Y. N., Fan, Y. and Miguez-Macho, G.: Potential hydrologic changes in the Amazon by the end of the 21st century and the groundwater buffer, Environ. Res. Lett., 9(8), doi:10.1088/1748-9326/9/8/084004, 2014.

Pokhrel, Y. N., Fan, Y., Miguez-Macho, G., Yeh, P. J. F. and Han, S. C.: The role of groundwater in the Amazon water cycle: 3. Influence on terrestrial water storage computations and comparison with GRACE, J. Geophys. Res. Atmos., 118(8), 3233–3244, doi:10.1002/jgrd.50335, 2013.

Pomeroy, J. W., Stewart, R. E. and Whitfield, P. H.: The 2013 flood event in the South Saskatchewan and Elk River basins: Causes, assessment and damages, Can. Water Resour. J. / Rev. Can. des ressources hydriques, 41(1–2), 105–117, doi:10.1080/07011784.2015.1089190, 2016.

Pomeroy, J. W.: The cold regions hydrological model: a platform for basing process representation and model structure on physical evidence, Hydrol. Process., 21, 2650–2667, doi:10.1002/hyp, 2007.
Prairie Habitat Joint Venture. 2014. Prairie Habitat Joint Venture Implementation Plan 2013-2020: The Prairie Parklands.Report of the Prairie Habitat Joint Venture. Environment Canada, Edmonton, AB
Prairie Pothole Joint Venture. (2017). Prairie Pothole Joint Venture Implementation Plan. S. P. Fields, editor. U.S. Fish and Wildlife Service, Denver, Colorado.
Prein AF, Gobiet A, Suklitsch M, Truhetz H, Awan N, Keuler K, Georgievski G (2013a) Added value of convection permitting seasonal simulations. Clim Dyn 41(9–10):2655–2677
Prein AF, Holland GJ, Rasmussen RM, Done J, Ikeda K, Clark MP, Liu CH (2013b) Importance of regional climate model grid spacing for the simulation of heavy precipitation in the Colorado headwaters. J Clim 26(13):4848–4857
Prein, A. F., Langhans, W., Fosser, G., Ferrone, A., Ban, N., Goergen, K., et al. (2015). A review on regional convection-permitting climate modeling: Demonstrations, prospects, and challenges. Reviews of Geophysics, 53(2), 323–361. https://doi.org/10.1002/2014RG000475
Prein, A. F., Rasmussen, R. M., Ikeda, K., Liu, C., Clark, M. P., & Holland, G. J. (2016). The future intensification of hourly precipitation extremes. Nature Climate Change, 7(1), 48–52. https://doi.org/10.1038/nclimate3168
Prigent, C., Matthews, E., Aires, F., and Rossow, W. B. (2001). Remote sensing of global wetland dynamics with multiple satellite data sets, Geo. Res. Lett., 28 , 4631-4634
Prigent, C., Papa, F., Aires, F., Jimenez, C., Rossow, W. B., & Matthews, E. (2012). Changes in land surface water dynamics since the 1990s and relation to population pressure. Geophysical Research Letters, 39(8), n/a-n/a. https://doi.org/10.1029/2012GL051276
Prigent, C., Papa, F., Aires, F., Rossow, W. B., & Matthews, E. (2007). Global inundation dynamics inferred from multiple satellite observations, 1993–2000. Journal of Geophysical Research, 112(D12), D12107. https://doi.org/10.1029/2006JD007847
Quesada B, Vautard R, Yiou P, Hirschi M, Seneviratne SI (2012) Asymmetric European summer heat predictability fom wet and dry southern winters and springs. Nat Clim Change 2(10):736–741. https://doi.org/10.1038/nclimate1536
Quiring SM, Kluver DB (2009) Relationship between winter/spring snowfall and summer precipitation in the Northern Great Plains of North America. J Hydrometeorol 10(5):1203–1217. https://doi.org/10.1175/2009JHM1089.1
R Core Team (2020). R: A language and environment for statistical computing. R Foundation for Statistical Computing, Vienna, Austria. https://www.R-project.org/.
Rasmussen, R., Liu, C., Ikeda, K., Gochis, D., Yates, D., Chen, F., Tewari, M., Barlage, M., Dudhia, J., Yu, W., Miller, K., Arsenault, K., Grubišić, V., Thompson, G., & Gutmann, E. (2011). High-resolution coupled climate runoff simulations of seasonal snowfall over Colorado: A process study of current and warmer climate. Journal of Climate, 24(12), 3015–3048. https://doi.org/10.1175/2010JCLI3985.1
Rasmussen KL, Prein AF, Rasmussen RM, Ikeda K, Liu C (2017) Changes in the convective population and thermodynamic environments in convection-permitting regional climate simulations over the United States. Clim Dyn. https://doi.org/10.1007/s00382-017-4000-7
Ray, D. K., Gerber, J. S., Macdonald, G. K., & West, P. C. (2015). Climate variation explains a third of global crop yield variability. Nature Communications, 6, 1–9. https://doi.org/10.1038/ncomms6989

Ray, D. K., West, P. C., Clark, M., Gerber, J. S., Prishchepov, A. V., & Chatterjee, S. (2019). Climate change already affects global food production, 1–18.

Remenda VH, van der Kamp G, Cherry JA (1996) Use of vertical profiles of • 180 to constrain estimates of hydraulic conductivity in a thick, unfractured aquitard. 32:2979–2987

Rich, T.C., Beardmore, C.J., Berlanga, H., Blancher, P.J., Bradstreet, M.S.W., Butcher, G.S., Demarest, D.W., Dunn, E.H., Hunter, W.C., Inigo-Elias, E.E., Kennedy, J.A., Martell, A.M., Panjabi, A.O., Pashley, D.N., Rosenberg, K.V., Rustay, C.M., Wendt, J.S., & Will, T.C. (2004). Partners in flight North American landbird conservation plan. Cornell Lab of Ornithology, Ithaca, NY.

Roberts, D.A., Gardner, M., Church, R., Ustin, S., Scheer, G., Green, R.O. (1998). Mapping Chaparral in the Santa Monica Mountains Using Multiple Endmember Spectral Mixture Models, Remote Sensing of Environment, 65(3), 267–279.

Schaefer GL, Cosh MH, Jackson TJ (2007) The USDA natural resources conservation service soil climate analysis network (SCAN). J Atmos Ocean Technol 24(12):2073–2077. https://doi.org/10.1175/2007JTECHA930.1

Schär, C., Frei, C., Lüthi, D., & Davies, H. C. (1996). Surrogate climate-change scenarios for regional climate models. Geophysical Research Letters, 23(6), 669–672. https://doi.org/10.1029/96GL00265

Schwingshackl C, Hirschi M, Seneviratne SI (2017) Quantifying spatiotemporal variations of soil moisture control on surface energy balance and near-surface air temperature. J Clim 30(18):7105–7124. https://doi.org/10.1175/JCLI-D-16-0727.1

Sellers, P. J., Mintz, Y., Sud, Y. C., & Dalcher, A. (1986). A Simple Biosphere Model (SIB) for Use within General Circulation Models. *Journal of the Atmospheric Sciences*, *43*(6), 505–531. https://doi.org/10.1175/1520-0469(1986)043<0505:ASBMFU>2.0.CO;2

Sellers, P. J., D. A. Randall, G. J. Collatz, J. A. Berry, C. B. Field, D. A. Dazlich, C. Zhang, G. D. Collelo, and L. Bounoua (1996a), A revised land surface parameterization (SiB2) for atmospheric GCMs. Part I: Model formulation, J. Clim., 9, 676–705, doi:10.1175/1520-0442(1996)009<0676:ARLSPF>2.0.CO;2.

Sellers, P. J., S. O. Los, C. J. Tucker, C. O. Justice, D. A. Dazlich, G. J. Collatz, and D. A. Randall (1996b), A revised land surface parameteriza- tion (SiB2) for atmospheric GCMs. Part II: The generation of global fields of terrestrial biophysical parameters from satellite data, J. Clim., 9, 706–737, doi:10.1175/1520-0442(1996)009<0706:ARLSPF>2.0. CO;2.

Seneviratne SI, Lüthi D, Litschi M, Schär C (2006) Land–atmosphere coupling and climate change in Europe. Nature (443(7108):205–209. https://doi.org/10.1038/nature05095

Seneviratne, S. I., Corti, T., Davin, E. L., Hirschi, M., Jaeger, E. B., Lehner, I., Orlowsky, B., & Teuling, A. J. (2010). Investigating soil moisture-climate interactions in a changing climate: A review. *Earth-Science Reviews*, *99*(3–4), 125–161. https://doi.org/10.1016/j.earscirev.2010.02.004

Shangguan W, Dai Y, Duan Q, et al (2014) Journal of Advances in Modeling Earth Systems. J Adv Model Earth Syst 6:249–263. doi: 10.1002/2013MS000293.Received

Shaw, D. A., Pietroniro, A., & Martz, L. W. (2012). Topographic analysis for the prairie pothole region of Western Canada. Hydrological Processes, n/a-n/a. https://doi.org/10.1002/hyp.9409

Sherwood, S. C., Bony, S. and Dufresne, J.: Spread in model climate sensitivity traced to atmospheric convective mixing, doi:10.1038/nature12829, 2014.

Siebert, S., & Döll, P. (2010). Quantifying blue and green water uses and virtual water contents in global crop production as well as potential production losses without irrigation. Journal of Hydrology, 384(3-4), 198-217. https://doi.org/10.1016/j.jhydrol.2009.07.031Skamarock, W. C., Klemp, J. B., Dudhia, J., Gill, D. O., Barker, D., Duda, M. G., … Powers, J. G. (2008). A Description of the Advanced Research WRF Version 3 (No. NCAR/TN-475+STR). University Corporation for Atmospheric Research. doi:10.5065/D68S4MVH

Sivapalan, M., Beven, K., & Wood, E. F. (1987). On hydrologic similarity: 2. A scaled model of storm runoff production. Water Resources Research, 23(12), 2266–2278. https://doi.org/10.1029/WR023i012p02266

Skamarock, W., Klemp, J., Dudhia, J., Gill, D., Barker, M., Huang, X.-Y., Wang, W., & Powers, J. (2008). *A Description of the Advanced Research WRF Version 3* (Vol. 49, Issue 2). https://doi.org/http://dx.doi.org/10.5065/D68S4MVH

Skamarock, W. C., Klemp, J. B., Dudhia, J., Gill, D. O., Liu, Z., Berner, J., … Huang, X. -yu. (2019). A Description of the Advanced Research WRF Model Version 4 (No. NCAR/TN-556+STR). doi:10.5065/1dfh-6p97

Smerdon, B. D.: A synopsis of climate change effects on groundwater recharge, J. Hydrol., 555, 125–128, doi:10.1016/j.jhydrol.2017.09.047, 2017.

Sofaer, H. R., Skagen, S. K., Barsugli, J. J., Rashford, B. S., Reese, G. C., Hoeting, J. A., et al. (2016). Projected wetland densities under climate change: habitat loss but little geographic shift in conservation strategy. Ecological Applications, 26(6), 1677–1692. https://doi.org/10.1890/15-0750.1

St. Jacques, J. M., Huang, Y. A., Zhao, Y., Lapp, S. L., & Sauchyn, D. J. (2014). Detection and attribution of variability and trends in streamflow records from the Canadian Prairie Provinces. Canadian Water Resources Journal, 39(3), 270–284. https://doi.org/10.1080/07011784.2014.942575

St. Jacques, J. M., Lapp, S. L., Zhao, Y., Barrow, E. M., & Sauchyn, D. J. (2013). Twenty-first century central Rocky Mountain river discharge scenarios undergreenhouse forcing. Quaternary International, 310, 34–46. https://doi.org/10.1016/j.quaint.2012.06.023

Statistics Canada: Quarterly Estimates of the Population of Canada, the Provinces and the Territories, 11-3, Catalogue 91-001, Ottawa, 1996

Statistics Canada. Ecological Land Classification, 2017. https://www.statcan.gc.ca/eng/subjects/standard/environment/elc/2017-1

Stieglitz, M., Rind, D., Famiglietti, J., & Rosenzweig, C. (1997). An Efficient Approach to Modeling the Topographic Control of Surface Hydrology for Regional and Global Climate Modeling. *Journal of Climate*, *10*(1), 118–137. https://doi.org/10.1175/1520-0442(1997)010<0118:AEATMT>2.0.CO;2

Sun Q, Miao C, AghaKouchak A, Duan Q (2017) Unraveling anthropogenic infuence on the changing risk of heat waves in China. Geophys Res Lett 44(10):5078–5085. https://doi.org/10.1002/2017GL073531

Taylor, R. G.: Ground water and climate change, 3(November 2012), doi:10.1038/NCLIMATE1744, 2013.

Thiery, W., Davin, E. L., Lawrence, D. M., Hirsch, A. L., Hauser, M., & Seneviratne, S. I. (2017). Present - day irrigation mitigates heat extremes. Journal of Geophysical Research: Atmospheres, 122(3), 1403–1422. https://doi.org/10.1002/2016JD025740

Thompson G, Eidhammer T (2014) A study of aerosol impacts on clouds and precipitation development in a large winter cyclone. J Atmos Sci 71:3636–3658

Thornthwaite CW (1948) An approach toward a rational classification of climate. Geogr Rev 38(1):55–94. https://doi.org/10.1016/0022-3115(71)90076-6

Tremblay, L., Larocque, M., Anctil, F. and Rivard, C.: Teleconnections and interannual variability in Canadian groundwater levels, J. Hydrol., 410(3–4), 178–188, doi:10.1016/j.jhydrol.2011.09.013, 2011.

Trier, S. B., Chen, F., Manning, K. W., LeMone, M. A., & Davis, C. A. (2008). Sensitivity of the PBL and Precipitation in 12-Day Simulations of Warm-Season Convection Using Different Land Surface Models and Soil Wetness Conditions. *Monthly Weather Review*, *136*(7), 2321–2343. https://doi.org/10.1175/2007MWR2289.1

UNESCO: Groundwater Resources of the Wrold and Their Use, edited by I. Zektser and L. Everett, Paris., 2004.

van Der Kamp G, Hayashi M (2009) Groundwater-wetland ecosystem interaction in the semiarid glaciated plains of North America. Hydrogeol J 17:203–214. doi: 10.1007/s10040-008-0367-1

van der Kamp, G., & Hayashi, M. (2009). Groundwater-wetland ecosystem interaction in the semiarid glaciated plains of North America. Hydrogeology Journal, 17(1), 203–214. https://doi.org/10.1007/s10040-008-0367-1

van der Kamp, G., Hayashi, M., Bedard-Haughn, A., & Pennock, D. (2016). Prairie Pothole Wetlands – Suggestions for Practical and Objective Definitions and Terminology. Wetlands, 36, 229–235. https://doi.org/10.1007/s13157-016-0809-9

Van Hoy, D. F., Mahmood, T. H., Todhunter, P. E., & Jeannotte, T. L. (2020). Mechanisms of Cold Region Hydrologic Change to Recent Wetting in a Northern Glaciated Landscape. Water Resources Research, 56(7). https://doi.org/10.1029/2019WR026932

Vanderhoof, M. K., Lane, C. R., McManus, M. G., Alexander, L. C., & Christensen, J. R. (2018). Wetlands inform how climate extremes influence surface water expansion and contraction. Hydrology and Earth System Sciences, 22(3), 1851–1873. https://doi.org/10.5194/hess-22-1851-2018

Vanderhoof, M.K. and Alexander, L.C., 2016. The role of lake expansion in altering the wetland landscape of the Prairie Pothole Region, United States. Wetlands, 36(2), pp.309-321

Verseghy, D. L. (1991). Class-A Canadian land surface scheme for GCMS. I. Soil model. International Journal of Climatology, 11(2), 111–133. https://doi.org/10.1002/joc.3370110202

Vicente-Serrano SM, Beguería S, López-Moreno JI (2009) A multiscalar drought index sensitive to global warming: the standardized precipitation evapotranspiration index. J Clim. https://doi.org/10.1175/2009JCLI2909.1

Vorosmarty, C. J. (2000). Global Water Resources: Vulnerability from Climate Change and Population Growth. Science, 289(5477), 284–288. https://doi.org/10.1126/science.289.5477.284

Wania, R., Melton, J. R., Hodson, E. L., Poulter, B., Ringeval, B., Spahni, R., et al. (2013). Present state of global wetland extent and wetland methane modelling: methodology of a model inter-comparison project (WETCHIMP). Geoscientific Model Development, 6(3), 617–641. https://doi.org/10.5194/gmd-6-617-2013

Watmough, M.D., & Schmoll M.J. (2007). Environment Canada's Prairie & Northern Region Habitat Monitoring Program Phase II: Recent habitat trends in the Prairie Habitat Joint Venture. Technical Report Series No. 493. Environment Canada, Canadian Wildlife Service, Edmonton, Canada.

Weisman, M. L., Skamarock, W. C., & Klemp, J. B. (1997). The Resolution Dependence of Explicitly Modeled Convective Systems. *Monthly Weather Review*, *125*(4), 527–548. https://doi.org/10.1175/1520-0493(1997)125<0527:TRDOEM>2.0.CO;2

Whan K et al (2015) Impact of soil moisture on extreme maximum temperatures in Europe. Weather Clim Extremes 9:57–67. https://doi.org/10.1016/j.wace.2015.05.001

Whan K, Zwiers F (2016) Evaluation of extreme rainfall and temperature over North America in CanRCM4 and CRCM5. Clim Dyn 46(11–12):3821–3843. https://doi.org/10.1007/s00382-015-2807-7

Wood, S.N. (2011) Fast stable restricted maximum likelihood and marginal likelihood estimation of semiparametric generalized linear models. Journal of the Royal Statistical Society (B) 73:3-36.

Xia, Y., Mitchell, K., Ek, M., Cosgrove, B., Sheffield, J., Luo, L., Alonge, C., Wei, H., Meng, J., Livneh, B., Duan, Q., & Lohmann, D. (2012). Continental-scale water and energy flux analysis and validation for North American Land Data Assimilation System project phase 2 (NLDAS-2): 2. Validation of model-simulated streamflow. *Journal of Geophysical Research: Atmospheres*, *117*(D3), n/a-n/a. https://doi.org/10.1029/2011JD016051

Xu, X., F. Chen, M. Barlage, D. Gochis, S. Miao, and S. Shen, 2019: Lessons learned from modeling irrigation from field to regional scales. J. Adv. Model. Earth Syst., DOI:10.1029/2018MS001595

Xue Y, Sellers PJ, Kinter JL, Shukla J (1991) A Simplified Biosphere Model for Global Climate Studies. J Clim 4:345–364. doi: 10.1175/1520-0442(1991)004<0345:ASBMFG>2.0.CO;2

Yang, H. S., A. Dobermann, J. L. Lindquist, D. T. Walters, T. J. Arkebauer, and K. G. Cassman (2004), Hybrid - maize — A maize simulation model that combines two crop modeling approaches, Field Crops Res., 87, 131– 154.

Yang, Z. L. (2004). Modeling land surface processes in short-term weather and climate studies (pp. 288–313). https://doi.org/10.1142/9789812791139_0014

Yang, Z. L., Niu, G. Y., Mitchell, K. E., Chen, F., Ek, M. B., Barlage, M., et al. (2011). The community Noah land surface model with multiparameterization options (Noah-MP): 2. Evaluation over global river basins. Journal of Geophysical Research Atmospheres, 116(12). https://doi.org/10.1029/2010JD015140

Zhang, Z., Li, Y., Chen, F., Barlage, M., & Li, Z. (2018). Evaluation of convection-permitting WRF CONUS simulation on the relationship between soil moisture and heatwaves. Climate Dynamics. https://doi.org/10.1007/s00382-018-4508-5

Zhang, Z., Li, Y., Barlage, M., Chen, F., Miguez-Macho, G., Ireson, A., & Li, Z. (2020). Modeling groundwater responses to climate change in the Prairie Pothole Region. Hydrology and Earth System Sciences, 24(2), 655–672. https://doi.org/10.5194/hess-24-655-2020

Zhang, Z., Barlage, M., Chen, F., Li, Y., Helgason, W., Xu, X., et al. (2020). Joint modeling of crop and irrigation in the Central United States using the Noah-MP land surface model. Journal of Advances in Modeling Earth Systems. https://doi.org/10.1029/2020MS002159

Zhang, Z., Bortolotti, L. E., Li, Z., Armstrong, L. M., Bell, T. W., & Li, Y. (2021). Heterogeneous Changes to Wetlands in the Canadian Prairies Under Future Climate. Water Resources Research, 57(7), 1–16. https://doi.org/10.1029/2020WR028727

Zheng, Y., Kumar, A., & Niyogi, D. (2015). Impacts of land-atmosphere coupling on regional rainfall and convection. *Climate Dynamics*, *44*(9–10), 2383–2409. https://doi.org/10.1007/s00382-014-2442-8

Appendix A

This appendix is part of chapter 1 for introducing the convection-permitting regional climate model in CONtiguous U.S. (CONUS WRF I) simulations.

Procedure of dynamical downscaling of regional climate simulations in the CONtiguous U.S. (CONUS) using the Pseudo global warming method.

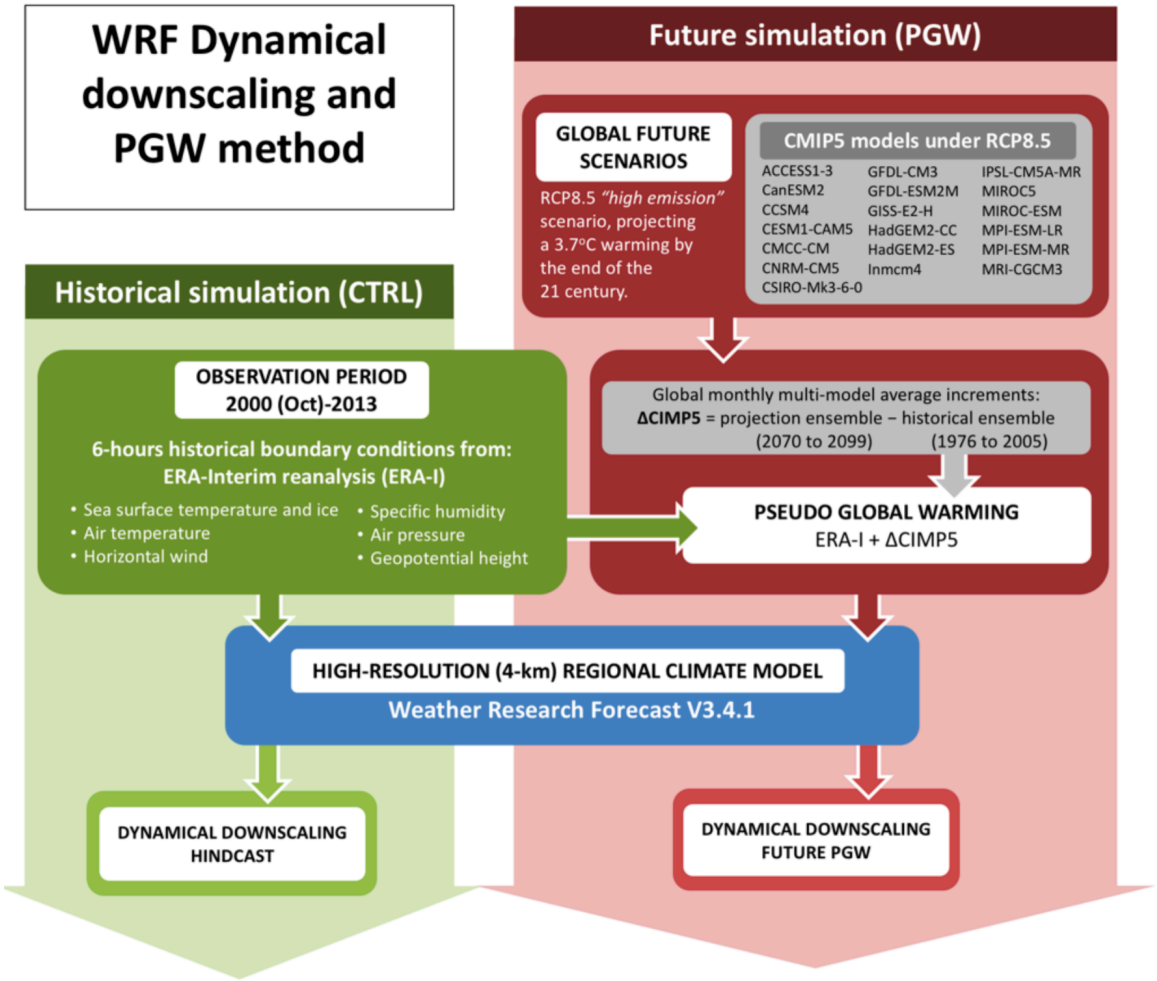

Figure A1. Methodology of the CONUS WRF simulations. Historical simulation is in the green column and the future climate simulation is presented in the red column.

Appendix B

This appendix is part of the chapter 3, introducing the parameters used in the Noah-MP crop model regarding planting and harvesting date and photosynthesis processes.

Table B1. Field Crops Usual Planting and Harvesting Dates (October 2010)
USDA, National Agricultural Statistics Service
https://usda.library.cornell.edu/concern/publications/vm40xr56k

Corn for Grain Usual Planting and Harvesting Dates – States

State	code	Usual planting dates				Usual harvesting date			
		Begin	Most active	End	Middle day	Begin	Most active	End	Middle day
Illinois	IL	Apr14	Apr21-May23	Jun 5	127	Sep 14	Sep 23-Nov 5	Nov 20	288
Indiana	IN	Apr20	May1-Jun1	Jun 10	137	Sep 15	Oct 1-Nov 10	Nov 25	294
Iowa	IO	Apr19	Apr25-May18	May26	127	Sep 21	Oct 5-Nov 9	Nov 21	296
Michigan	MI	Apr21	May1- May27	Jun 6	134	Sep 5	Oct10-Nov25	Dec 10	306
Minnesota	MN	Apr22	Apr26-May19	May29	128	Sep 27	Oct 8- Nov 8	Nov 23	297
Missouri	MO	Apr 3	Apr11- May27	Jun 12	124	Aug 29	Sep 8-Nov 3	Dec 22	279
Nebraska	NE	Apr19	Apr27-May15	May21	126	Sep 18	Oct 4 -Nov10	Nov 20	296
Ohio	OH	Apr18	Apr 24-May24	May30	129	Spe27	Oct11-Nov20	Dec 1	304
South Dakota	SD	Apr26	May2-May27	Jun 10	135	Sep24	Oct 6-Nov 16	Dec 3	300
Wisconsin	WI	Apr26	May -May27	Jun 6	135	Oct 2	Oct14-Nov17	Nov 28	304

Soybean Usual Planting and Harvesting Dates - States

State	code	Usual planting dates				Usual harvesting date			
		Begin	Most active	End	Middle day	Begin	Most active	End	Middle day
Arkansas	AR	Apr19	May5-Jun22	Jun5	149	Sep 10	Sep29-Nov13	Nov 26	294
Illinois	IL	May2	May8-Jun12	Jun24	145	Sep 19	Sep26-Oct26	Nov 7	284
Indiana	IN	May1	May5-Jun10	Jun25	143	Sep 20	Oct1-Nov1	Nov 10	289
Iowa	IO	May2	May8-Jun2	Jun16	140	Sep 21	Sep28-Oct20	Oct 31	282
Michigan	MI	May2	May11-Jun9	Jun18	145	Sep 25	Oct3-Nov3	Nov 13	291
Minnesota	MN	May2	May8-Jun2	Jun13	140	Sep 20	Sep27-Oct20	Oct 31	281
Missouri	MO	May2	May13-Jun24	Jul4	154	Sep25	Oct3-Nov8	Nov 23	294
Mississippi	MS	Apr19	Apr26-May31	Jun17	133	Sep10	Sep13-Oct31	Nov 9	280
Nebraska	NE	May5	May11-May31	Jun8	141	Sep23	Sep29-Oct24	Nov 2	284
Ohio	OH	Apr26	May3-May30	Jun10	136	Spe17	Sep24-Oct21	Nov 5	288
South Dakota	SD	May8	May15-Jun11	Jun21	148	Sep22	Sep28-Oct24	Nov 3	284
Tennessee	TN	May5	May15-Jun25	Jul5	155	Spe25	Oct5-Nov20	Nov 30	301

Table B2. A synthesis of photosynthesis parameters used for C4 corn. In this study, we used the Adjust parameters for C4 corn parameters are the same as in the Noah-MP (2011).

Reference	K_p	V_{cmx25} ($\mu molm^{-2}s^{-1}$)	$QE25$ (α	m	b ($\mu molm^{-2}s^{-1}$	R_d ($\mu molm^{-2}s^{-1}$)
Noah-MP (2011)	$4000 * V_{cmx}$	80	0.06	9	2000	1.0 (carbon)
Collatz (1992)	0.7, 18000* V_{cmx}	39	0.04	3	80000	0.8, 0.021 * V_{cmx}
Bonan (1996)	$4000 * V_{cmx}$	33 (C4 grass)	0.04	5	2000	0.82 (C4 grass, carbon)
Sellers (1996)	20000* V_{cmx}	30 (C4 grass)	0.05	4	40000	0.025 * V_{cmx} (PSN)
CLM4	$4000 * V_{cmx}$	52 (C4 grass)	0.04	4	40000	-
Bonan (2011)	20000* V_{cmx}	52 (C4 grass; CLM4) 57 (crop; CLM4) 78 (C4 grass; Kattge2009) 101 (C3 crop; Kattge2009)	0.05	4	40000	0.025 * V_{cmx} (PSN)
CLM4.5	20000* V_{cmx}	52 (C4 grass) 101 (corn)	0.05	4	40000	0.025 * V_{cmx} (PSN)
Adjust	20000* V_{cmx}	60 (corn)	0.05	4	40000	0.8 (carbon)

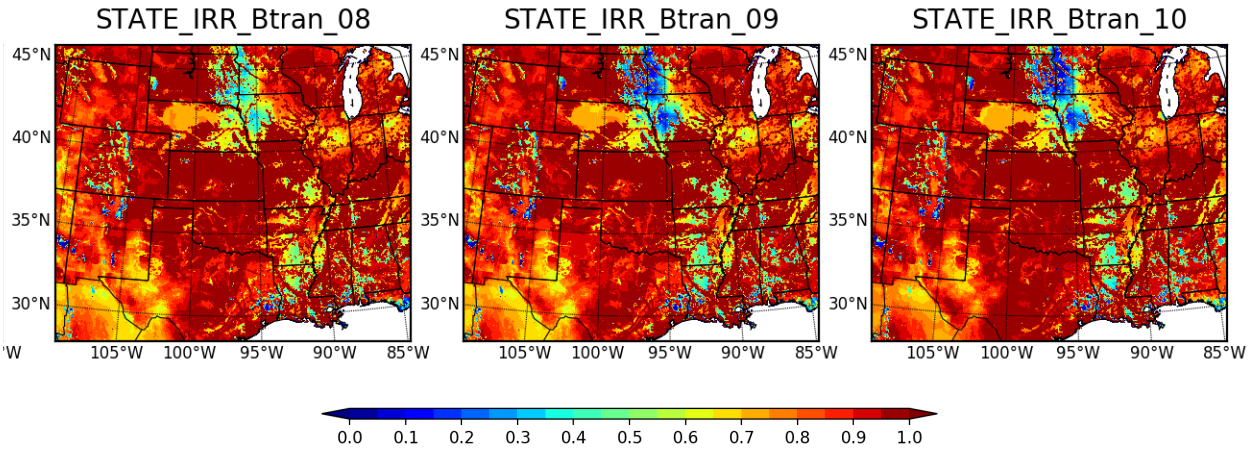

Figure B1. Monthly-averaged water stress factor, β_t, from STATE_IRR simulation from August to October. The blue regions show that the western Iowa, southwest Minnesota and eastern South Dakota are under water stress while the irrigation fraction (Figure 3a) in these regions are small. These suggest that while irrigation and rainfall are not significant water source, the water input from perched shallow water table might be the neglected component for the crop model.

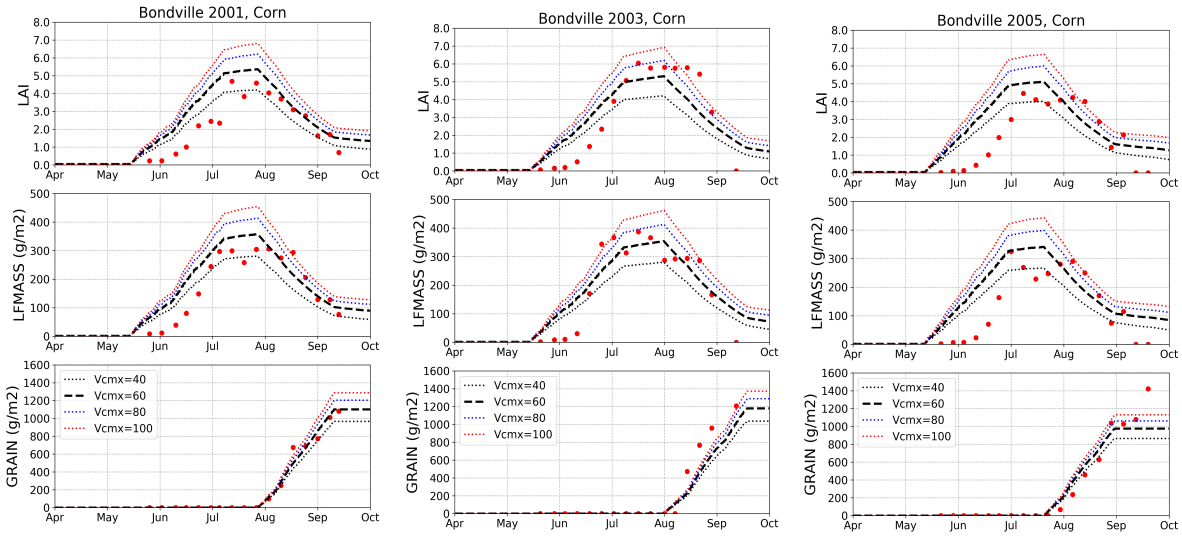

Figure B2. Calibration results for corn rubisco capacity V_{cmx25}, ranging from 40 to 100 $\mu molm^{-2}s^{-1}$, using the Ameriflux site Bo1 biomass data in 2001, 2003, and 2005. The $V_{cmx25} = 60\ \mu molm^{-2}s^{-1}$ (black dashed line) is the parameter value used in our regional simulations.

Appendix C

This appendix is a part of the chapter 4, including water table depth timeseries from 33 groundwater wells in the Prairie Pothole Region.

WTD dynamics from observational wells and CTRL model with default soil (DEF, blue lines) and replacing default soil with sandy soil (REP, red lines) for the 33 sites in the PPR.

Alberta Environment and Parks

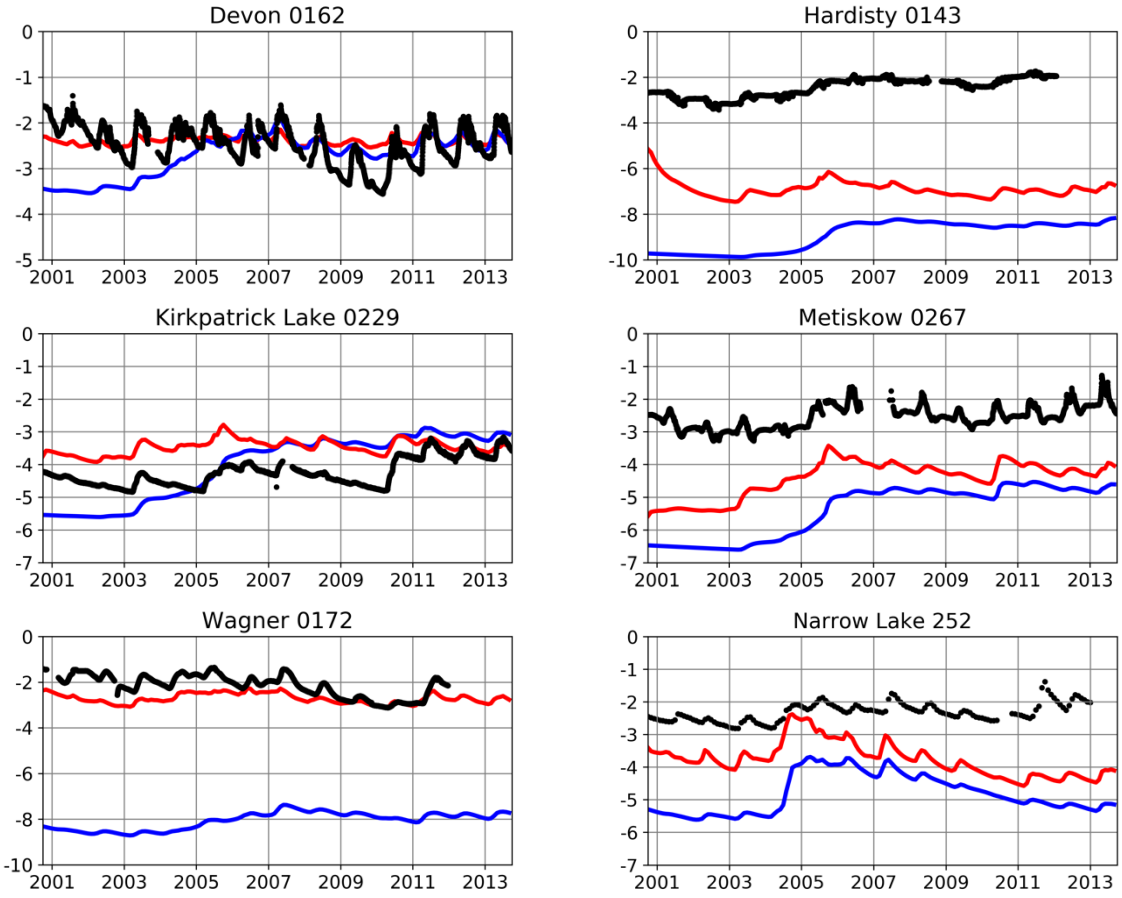

Saskatchewan Water Securtiy Agency

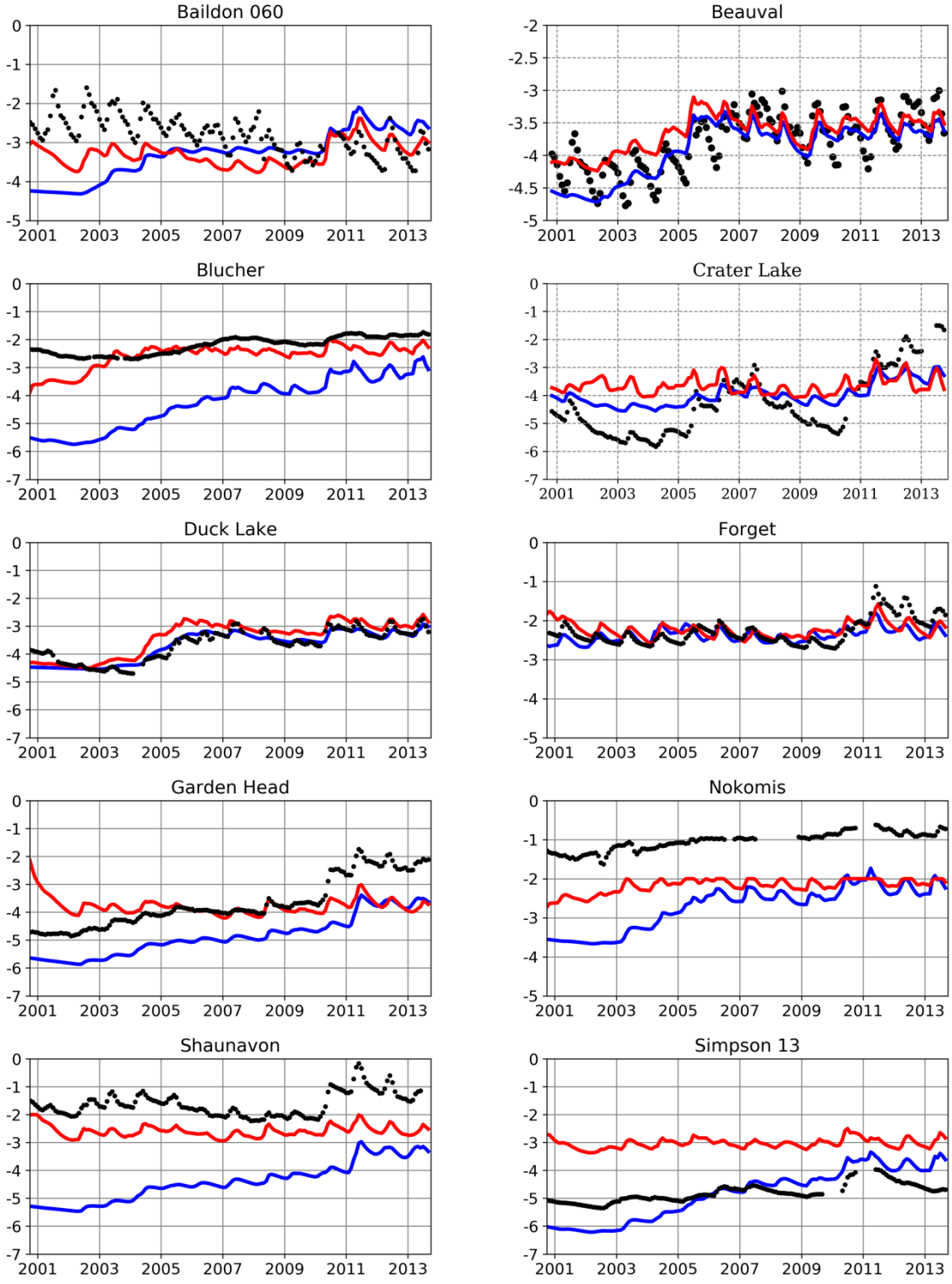

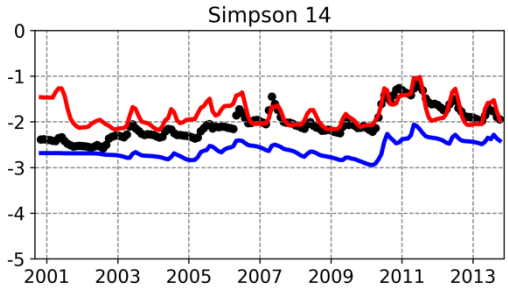
Simpson 14
0
-1
-2
-3
-4
-5
2001
2003
2005
2007
2009
2011
2013

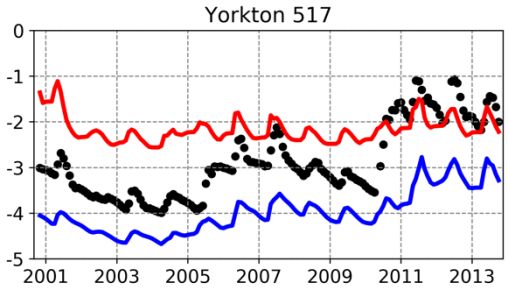
Yorkton 517
0
-1
-2
-3
-4
-5
2001
2003
2005
2007
2009
2011
2013

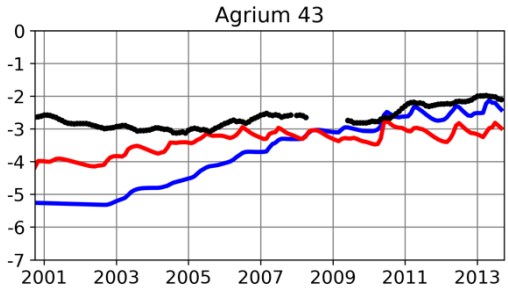
Agrium 43
0
-1
-2
-3
-4
-5
-6
-7
2001
2003
2005
2007
2009
2011
2013

USGS

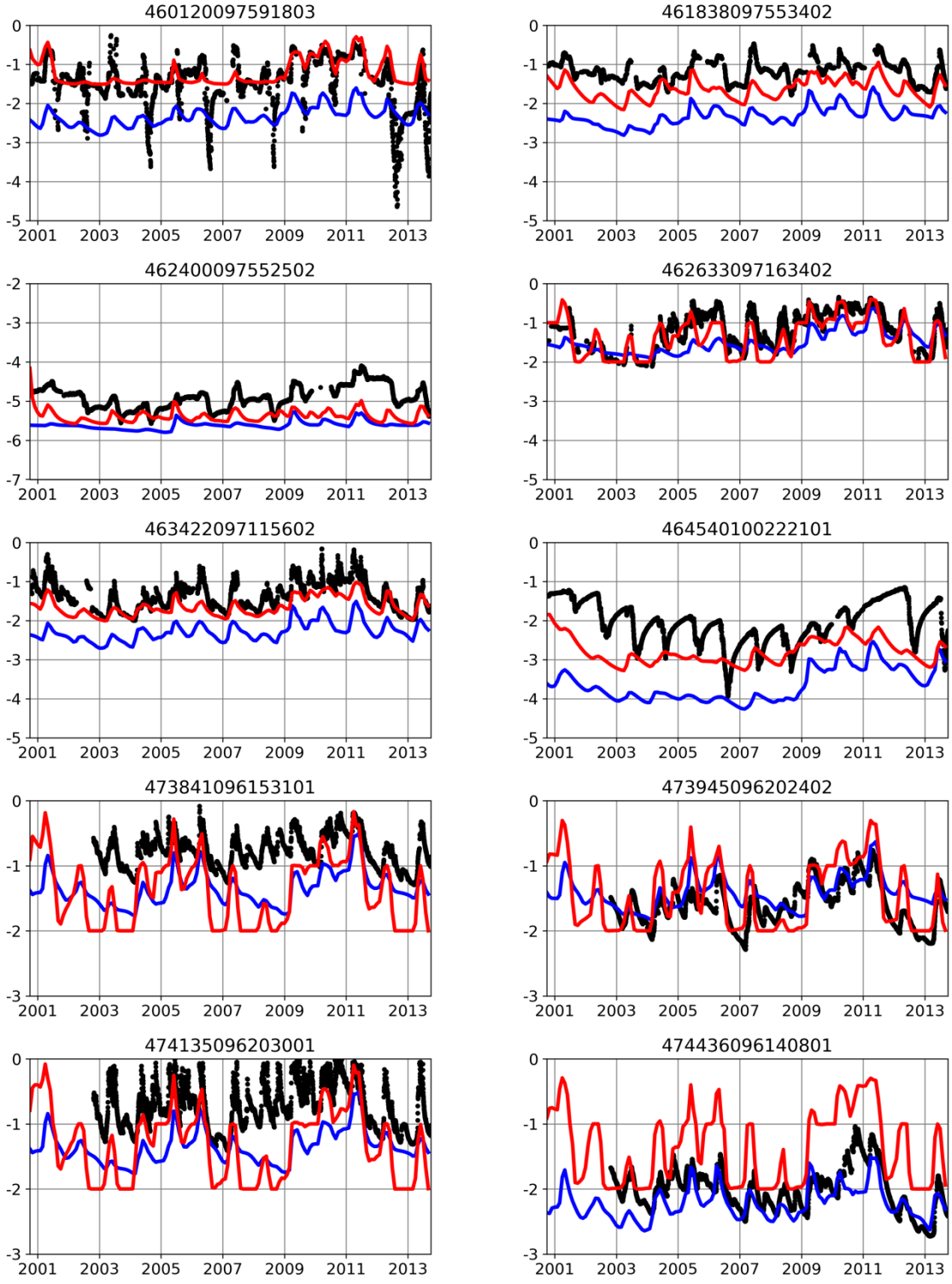
460120097591803
461838097553402
462400097552502
462633097163402
463422097115602
464540100222101
473841096153101
473945096202402
474135096203001
474436096140801
2001
2003
2005
2007
2009
2011
2013

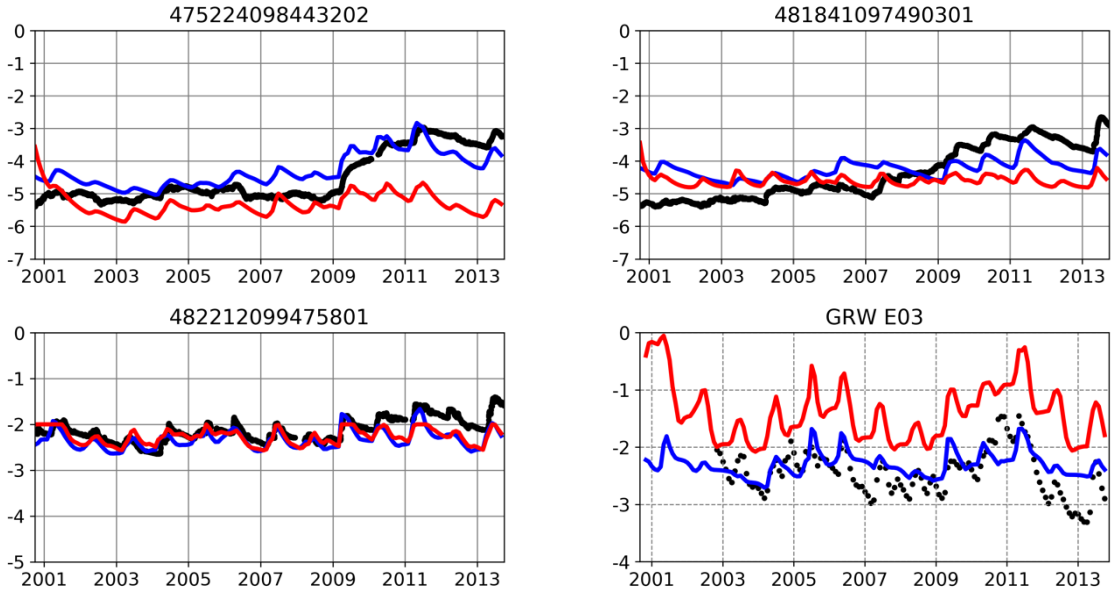
475224098443202
481841097490301
482212099475801
GRW E03
0
-1
-2
-3
-4
-5
-6
-7
2001
2003
2005
2007
2009
2011
2013

Appendix D

This appendix is a part of the chapter 5, including supporting information for the description of the MESMA method, GAM model, Noah-MP evaluation on snow water equivalent, and water balance in the eight ecoregions.

Text D1. An introduction to the MESMA method

Three Landsat satellite sensors (Landsat 5 Thematic Mapper [1984 – 2011], Landsat 7 Enhanced Thematic Mapper + [1999 – 2019], and Landsat 8 Operation Land Imager [2013 – 2019]) imaged the Smith Creek watershed over the study period at a 30 m pixel resolution with a repeat interval of 16 days (8 days if two sensors were active). We used Multiple Endmember Spectral Mixture Analysis (MESMA) to estimate the proportion of open water cover in each pixel through time. The MESMA process allows endmembers to vary on a per pixel basis by selecting from multiple endmembers for one or more cover types enabling spectral variability of cover types to vary in space and time. In order to estimate the fractional water cover, MESMA iteratively models each pixel's reflectance spectrum as linear combinations of three 'open water' and three 'dry vegetation' spectral endmembers, for a total of nine different combinations. The best model is selected based on minimizing the root mean squared error between the actual and modelled spectrum. 'Open water' and 'dry vegetation' spectral endmembers were selected as pixels from Landsat images with low probabilities of habitat mixing. These represent spectrally 'pure' pixels containing different 'open water' (clear, turbid, and water with sun glint) and 'dry vegetation' (live and dry vegetation, forest) types commonly seen in the imagery. We used six spectral bands spanning the visible to short wave infrared regions of the reflectance spectrum in the MESMA analysis corresponding to bands 1 - 5 and 7 for Landsat 5 and 7, and bands 2 – 7 for Landsat 8. The summed fractional cover estimates of 'open water' and 'dry vegetation' were constrained to equal one to remove the effect of shade. All cloud contaminated pixels were removed from each image using the quality assessment band supplied with each Landsat image.

To focus our analysis on wetland areas within the Smith Creek watershed and exclude the effects of anthropogenic water features in agricultural fields, we employed a two-step classification process. All atmospherically corrected Landsat Level 2 Surface Reflectance image products acquired between April and September from 1984 – 2019 were collected from the United States Geological Survey Earth Explorer website (earthexplorer.usgs.gov). We then calculated the normalized difference vegetation index (NDVI) for all pixels across all images and a produced histogram of NDVI for each pixel. One thousand pixels of each class ('wetland' and 'dry vegetation/agriculture') were randomly selected from the study area and class type was confirmed using high resolution imagery in Google Earth. A random forest classifier was then trained (Matlab function 'treebagger') and each NDVI pixel time histogram was then classified as either 'wetland' or 'dry vegetation/agriculture'. Pixel classifications were then compared to a DUC CWI-standard wetland layer and correctly classified 'wetland area' with 88% accuracy and 'dry vegetation/agriculture' with 77% accuracy. Because there was an order of magnitude greater 'dry vegetation/agriculture' pixels within the Smith Creek watershed versus 'wetland' pixels we employed a secondary classification step to further exclude agricultural pixels. Since we would expect 'wetland' areas to be completely inundated at various points in the time series, we excluded pixels where the MESMA 'open water' fraction never exceeded 0.7. The overall accuracy of the model was similar with 'wetland area' classified with 77% accuracy and 'dry vegetation/agriculture' with 87% accuracy, however many additional 'dry vegetation/agriculture' pixels were excluded from further analysis. The fractional cover of 'open water' within each pixel was assessed for all images using MESMA and the 90th percentile 'open water' fractional value was recorded for each pixel across each year. Total wetland area was then calculated by summing the 'open water' area for all 'wetland' pixels within the Smith Creek watershed for each year from 1984 to 2019.

Text D2. Additional details about the Generalized Additive Model of wetland fraction as a function of soil water content and ecoregion.

In this study, we fit the following statistical model: $g(E(Fwet)) = s(SWC) + ER$. We used a binomial distribution and logistic link of wetland fraction (i.e., $g(p)$ = ln(p/(1-p)), a smooth function of soil water content ($s(SWC)$) and included ecoregion (ER) as a factor predictor variable in the model to allow for different baseline wetland fractions (or intercepts) among the eight ecoregions. The smooth function of soil water content ($s(SWC)$) had 4.89 effective degrees of freedom, which remained stable with increasing basis dimensions (k), and the effect was significant (chi-squared value = 16.36 and p = 0.014). Table S1 provides the parameter estimates and standard errors for the different ecoregions. Figure S2 plots predicted values of wetland fraction over the full range of SWC for each ecoregion, including 95% confidence intervals.

Table D1. Parameter estimates (and standard errors) for the effect of different ecoregions in a General Additive Model of wetland fraction as a function of ecoregion and soil water content. The Aspen Parkland ecoregion is the reference category in the model and so has no associated parameter estimate.

Ecoregion	β (Standard error)
Boreal Transition	0.20 (0.15)
Fescue Grassland	-1.14 (0.32)
Mid-Boreal Uplands	0.24 (0.34)
Mixed Grassland	-0.17 (0.12)
Moist Mixed Grassland	0.085 (0.090)
Southwest Manitoba Uplands	0.64 (0.36)
Western Alberta Uplands	-2.88 (2.74)

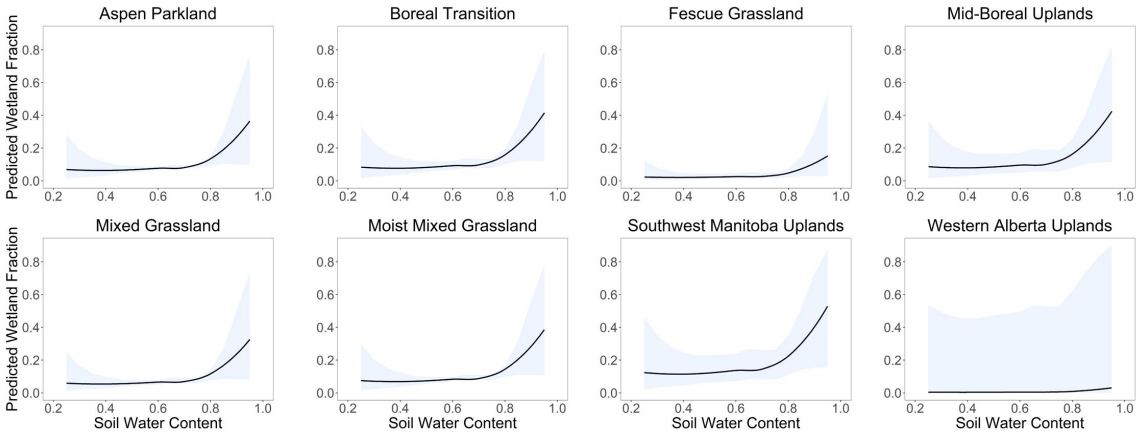

Figure D1. Predicted values of wetland fraction, from a General Additive Model, over a range of soil water content for eight Canadian ecoregions.

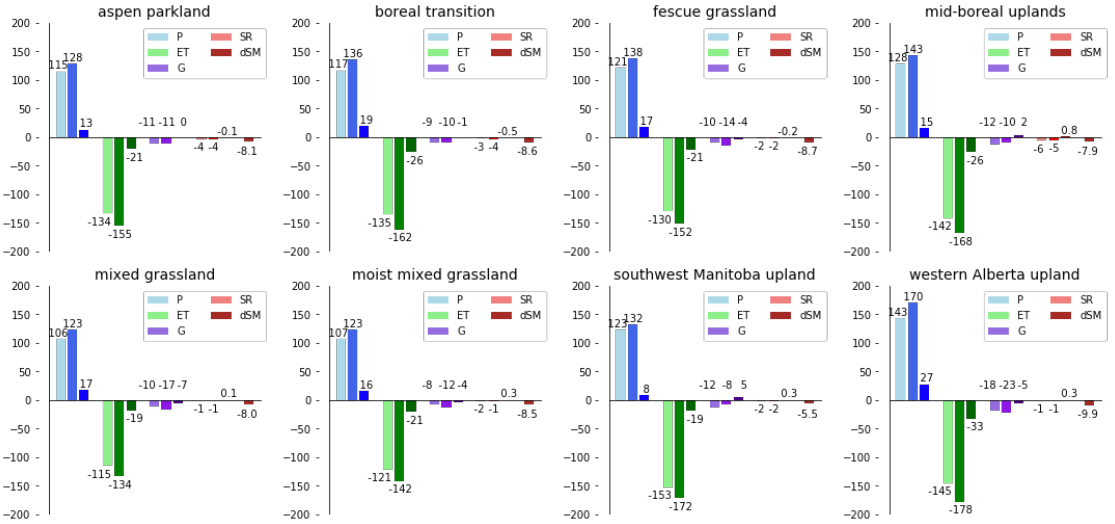

Figure D2. Water balance components (mm) for eight ecoregions in the Canadian Prairies for spring and summer (from MAM to JJA). Three columns in each term are for CTRL, PGW, and their change (PGW-CTRL). *P* is precipitation, *ET* is evapotranspiration, *SR* is surface runoff, *G* is groundwater recharge, and *dSM* is the net change of soil moisture.

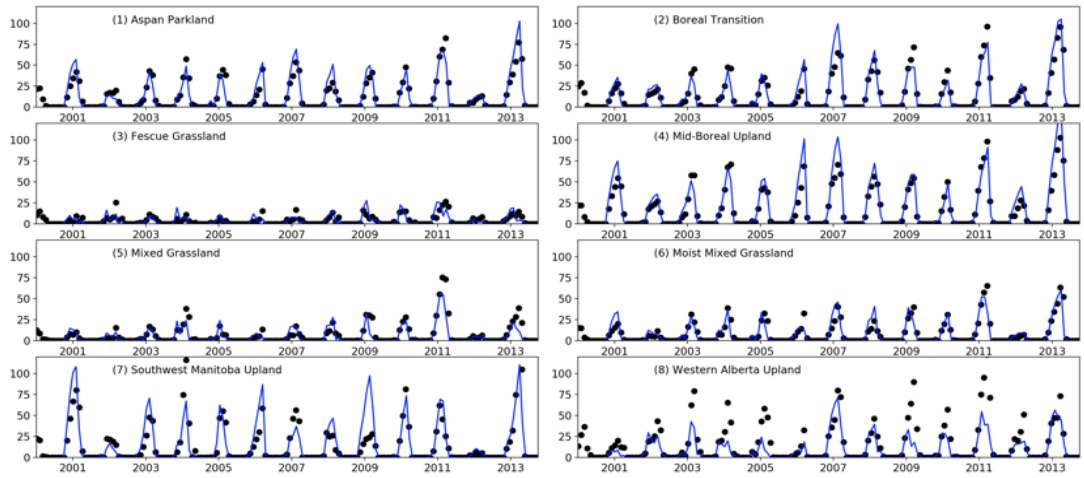

Figure D3. Monthly snow water equivalent (mm/month) from CMC snow data (black dots) and Noah-MP simulation (blue lines) from 2000 winter to 2013 summer, averaged over eight ecoregions in the study domain (ecoregions as in Figure 2) in the manuscript.

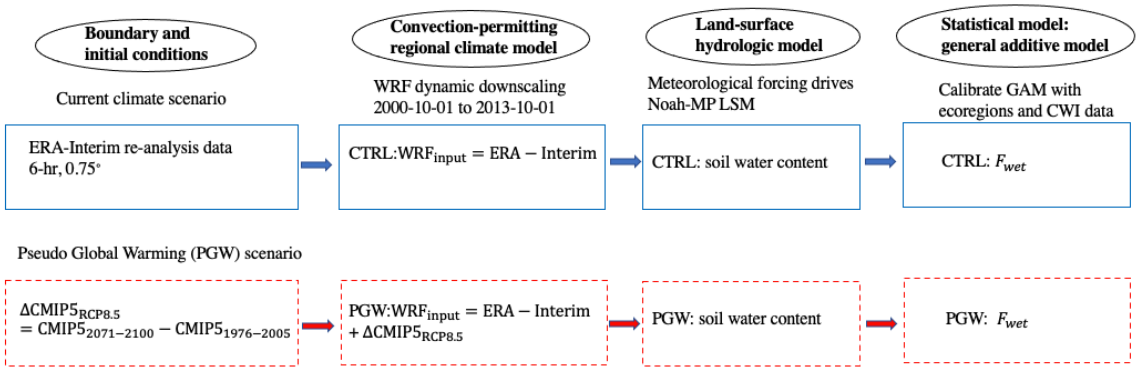

Figure D4. Flowchart of the method and models used in this study. Two rows represent two paralleled climate scenarios, CTRL and PGW. Four columns represent the boundary and initial conditions for WRF, dynamical downscaling on convection permitting scale using WRF, land-surface hydrology model Noah-MP, and the statistical GAM model.

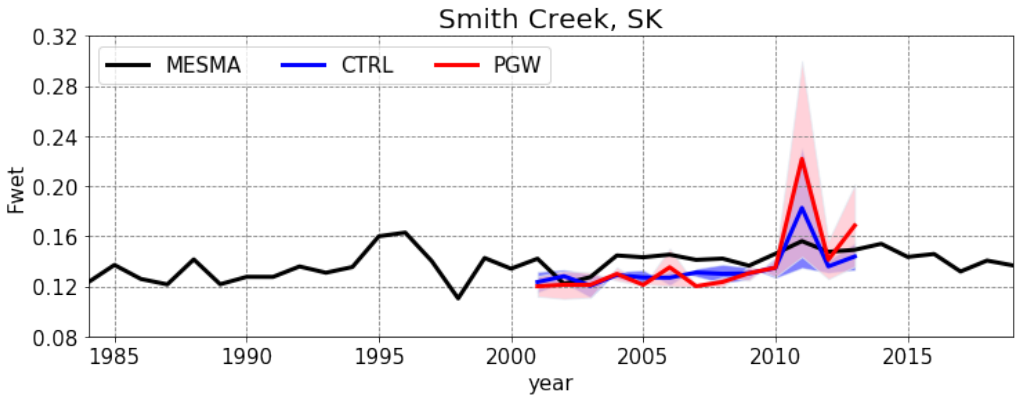

Figure D5. F_{wet} timeseries in current (CTRL) and future (PGW) climate in the Smith Creek watershed, Saskatchewan. The MESMA method represents annual wetland fraction from April to September. The red and blue shading represent the seasonal range of F_{wet} within the spring (MAM) and summer (JJA) for CTRL and PGW climate.

Text D3 Additional analysis for the Smith Creek watershed, comparing the GAM model F_{wet} results with the MESMA method.

Figure D5 shows the annual timeseries of F_{wet} in the Smith Creek watershed, in southeast Saskatchewan. The average values for F_{wet} from April to September are shown for MESMA and model-simulated F_{wet} under CTRL and PGW climate (mean plus seasonal range for spring and summer). The PGW simulation, which represents the pseudo global warming scenario by the end of 21st century, is plotted upon the simulation period from 2001-2013 for direct comparison with CTRL. The MESMA timeseries from 1984 to 2019 reflects the fluctuations in F_{wet} through wet-dry cycles, showing that wetland fraction in the watershed has fluctuated by more than 5% over the past 36 years (equivalent to wetland area varying by 21.7 km^2 between the wettest and driest years). The modeled F_{wet} from CTRL often underestimates the MESMA F_{wet} , but generally matches the increasing trend observed from the MESMA method for the 13-year period. The underestimate of CTRL is less than 0.01 (F_{wet}_CTRL- F_{wet}_$MESMA$) of the 4-km grid cell and could be due to differences in resolutions and methods. MESMA detects the fractional open water portion within 30-m pixels, whereas the GAM-derived F_{wet} from CTRL climate is a function of soil moisture content at the 4-km grid scale, reflecting the original CWI depressions. The trend of increasing wetland extent observed in both datasets (MESMA and CTRL) from 2001 to 2013 is confirmed by field observations of increasing pond (wetland) counts by the Waterfowl Breeding Population and Habitat Survey (Ballard et al., 2014).

The seasonal variation in F_{wet} is represented by the blue and red shading for CTRL and PGW climate, respectively. The range of F_{wet} is driven by the snowmelt infiltration to the soil moisture and filling of the surface water storage in spring and the drying in summer due to evapotranspiration, indicating strong intra-annual variation. Therefore, it is important to investigate F_{wet} at the seasonal scale. This is especially evident in the spring of 2011, when a record-breaking intensive precipitation event occurred and induced flooding (Dumanski et al., 2015; Pattison-Williams et al., 2018). This results in the highest F_{wet} value since 1996 and is well captured by CTRL. The F_{wet} peak in 2011 in PGW is even larger than in current climate, indicating the potential intensification of the hydrological cycle in these wetlands.

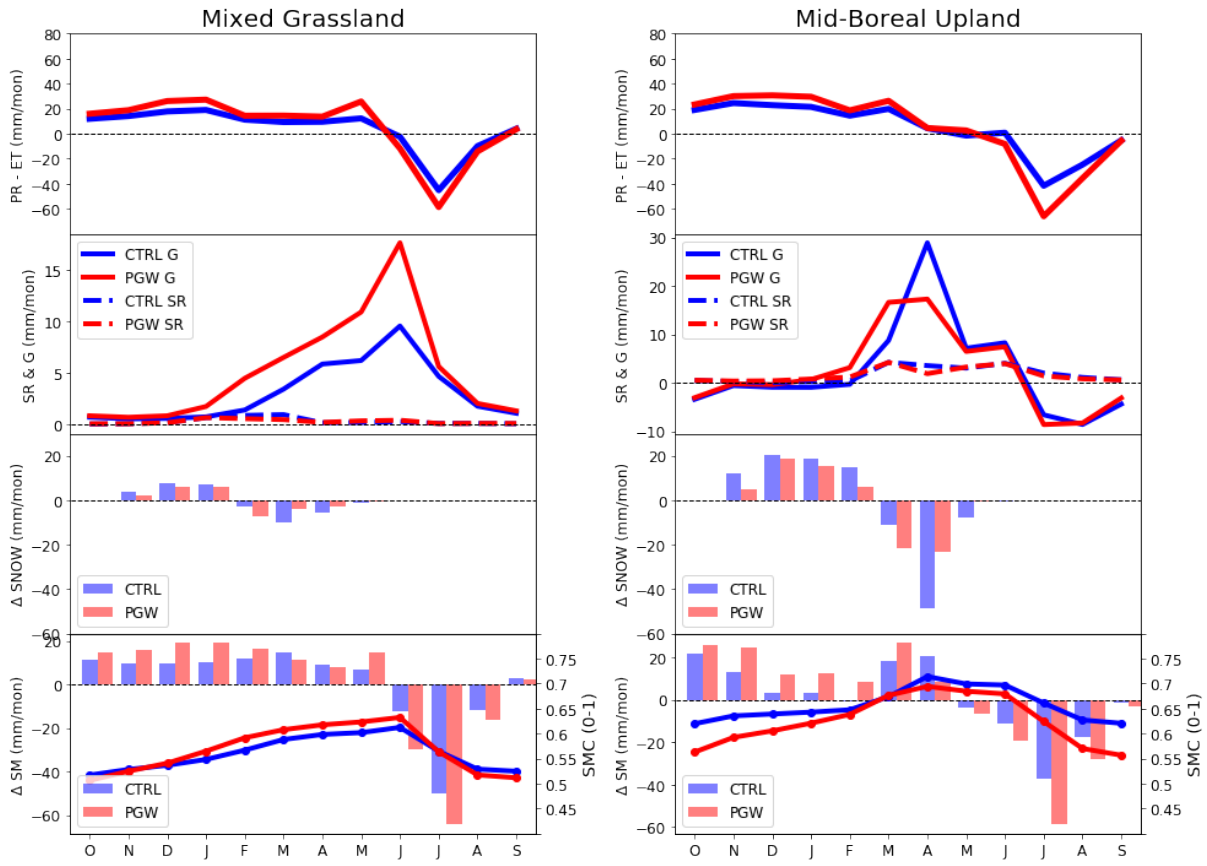

Figure D6. Water balance analysis for the mixed grassland and the mid-boreal upland region, including precipitation – evapotranspiration (first row), groundwater and surface runoff (second row), change of snow by month (third row), and change of soil moisture (bars, left axis) and SMC (lines, right axis) (fourth row). Blue and red correspond to the CTRL and PGW simulation. The increase of SMC over winter can be explained by the net results of precipitation – ET – G – SR - ΔSNOW. Possible snowmelt events through winter contribute to soil moisture increase.

Addendum for Chapter 6 – Evident wetland cooling effects to temperature relieves heat stress and mitigates climate change

This **addendum** is the revision of the original manuscript submitted to *Water Resources Research* in 2021 and Chapter 6. Several modifications have been made, including:

- Evaluation of single-point simulation at the fen site and regional simulation against MODIS satellite data;
- Investigation of wetlands' climate interactions with cloud formation as well as boundary layer dynamics;
- Explore the uncertainties between GIEMS-2 25-km data with a high-resolution (30-m) Global Surface Water Explorer (GSWE) dataset.

The original submission to *Water Resources Research* is as follow:

Zhang, Z., Chen, F., Barlage, M., Bortolotti, E. L., Famiglietti, J., Ma, X., Li, Z., Li, Y. Evident cooling effects of surface wetlands to mitigate climate change – a study of North America Prairie Pothole Region. (2021). Water Resources Research.

Abstract

Wetlands are important ecosystems – they provide vital hydrological and ecological services such as regulating floods, storing carbon, and providing wildlife habitat. The ability to simulate their spatial extents and hydrological processes is important for valuing wetlands' function. The purpose of this study is to dynamically represent the spatial extents and hydrological processes of wetlands and investigate their feedback to regional climate in the Prairie Pothole Region (PPR) of North America, where a large number of wetlands exist. In this study, we incorporated a wetland scheme into the Noah-MP Land Surface Model with two major modifications: (1) modifying the sub-grid saturation fraction for spatial wetland extent; (2) incorporating a dynamic wetland storage to simulate hydrological processes. This scheme was evaluated at a fen site in central Saskatchewan, Canada and applied regionally in the PPR with 13-year climate forcing produced by a high-resolution convection-permitting model. The differences between wetland and no-wetland simulations are significant, with increasing latent heat and evapotranspiration while suppressing sensible heat and runoff in the wetland scheme. Finally, the dynamic wetland scheme was applied in the Weather Research & Forecasting model (WRF). The wetlands scheme not only modifies the surface energy balance but also interacts with the lower atmosphere, shallowing the planetary boundary layer height and promoting cloud formation. A cooling effect of 1~3℃ in summer temperature is evident where wetlands are abundant. In particular, the wetland simulation shows reduction in the number of hot days for more than 10 days over the summer of 2006, when a long-lasting heatwave occurred. This research has great implications for land surface/regional climate modeling and wetland conservation, especially in mitigating extreme heatwaves under climate change.

Keywords

Wetland, Hydrology, Land surface model, Land-atmosphere interaction, Convection-permitting model, Climate change mitigation

1 Introduction

Wetlands are important and unique ecosystems that play vital roles in Earth's ecosystem balance and biodiversity. Although wetlands occupy a small portion of the global land surface (~6%), they store about one third of terrestrial carbon (Lehner and Döll, 2004; Mitra et al., 2005; Mitsch and Gosselink, 2007). Their unique productivity supports a wide variety of plants, birds, and amphibians (The Ramsar Convention, 2007). Wetlands are natural reservoirs to prevent flooding, especially in high latitude and mountainous regions (Hayashi et al., 2016; Pattison-Williams et al., 2018). After springtime snowmelt or heavy rainfall, surface runoff can be stored in wetlands, effectively reducing the peak flow and delaying the peak time of flooding, hence, mitigating flooding impacts.

In particular, wetlands may influence the regional climate through changing the partition of turbulent energy fluxes of sensible and latent heat. These land-atmosphere interactions are analogous to soil moisture-temperature and the soil moisture-precipitation feedbacks (Seneviratnes et al., 2010). Greater partitioning of latent heat flux over sensible heat flux in wetlands has been shown to induce a cooling effect on summer temperature (Bonan, 1995) and reduce daily air temperature variability (Hostetler et al. 1993; Houspanossian et al., 2018). Wetlands also provide a moisture source for the formation of clouds, reducing solar radiation and atmospheric upwards motion, and thus resulting in a shallower planetary boundary layer height (PBLH) (Pal, et al., 2020). In African wetlands, wetland inundation may suppress local rainfall over wetlands, but increase the initiation of convective storms in the upwind direction (the "wetland breeze" effect; Taylor, 2010; Taylor et al., 2018). This suppression of precipitation has also been demonstrated in a model sensitivity study over the Canadian Prairies, where the accumulated and peak precipitation amount decreased with an increase in open water bodies (Joshi et al., 2017).

Given their importance to global and regional environments, the need to represent wetland spatial extents and hydrological processes in earth system models (ESMs) and land surface models (LSMs) has emerged in recent decades. From a modeling perspective, wetlands are defined as grid cells, or fractions, where the land surface is inundated or saturated. These are usually associated with a shallow water table depth. Previous studies have used prescribed wetland maps from remote sensing products, for example the Global Inudation Extent from Multiple Satellite (GIEMS, Prigent et al., 2007), or land survey data, such as Mathews and Fung (1987) and the Global Lake and Wetland Database (GLWD, Lehner and Doll, 2004). Other modeling studies applied parameterization schemes to estimate wetland extents. For example, in the Community Land Model (Oleson et al., 2008) and Noah-MP LSM (Niu et al., 2011; Yang et al., 2011), grid cell saturated fraction was determined by the depth of groundwater, based on the TOPMODEL hydrological model (Beven and Kirkby, 1979) and its application in LSMs (Famiglietti and Wood, 1991, 1994a). In Fan and Miguez-Macho (2012), the authors used a threshold 0.25 m of groundwater depth to determine the spatial extent of wetlands.

On the other hand, large-scale hydrological models and ESMs have incorporated surface water inundation schemes to represent the dynamics of lakes, wetlands, and floodplains to investigate their impacts on the water cycle and climate system. For example, Yamazaki et al. (2011) developed a new global river routing model, CaMa-Flood, to explicitly represent floodplain inundation dynamics, based on subgrid topographic parameters. Dadson et al. (2010) employed an overbank flow parameterization to the Joint UK Land-Environment Simulator (JULES) LSM to simulate wetland inundation dynamics and evaporation loss from the Niger inland delta. The model reproduces spatial and seasonal wetland inundation dynamics and river flow and shows the

inundation scheme doubling the water vapor fluxes to the atmosphere. The Variable Infiltration Capacity model (VIC, Liang et al., 1994) has a dynamic lake and wetland scheme to study the impacts of surface water heterogeneity on energy and water balance (Bowling and Lettenmaier, 2010). Results show that incorporating wetlands increases the annual ET and latent heat fluxes while decreasing runoff and sensible heat fluxes in the U.S. Pitman (1991) incorporated a sub-grid scheme for water surfaces and their contribution to latent and sensible heat as the weighted average over the fraction of water, vegetated and bare ground surface in a coarse resolution (~2°) GCM.

Despite progress in developing wetland schemes in LSMs, the wetland physics in the Noah-MP LSM and its coupled regional climate model, Weather Research & Forecasting (WRF, Skamarock, et al., 2008), are still crude. As in many regional climate models (RCMs) and operational weather models, wetlands are treated as a land cover type with static parameters in WRF. Moreover, there is no wetland storage in Noah-MP, so that the simulated surface runoff will leave the model grid instantly. In reality, wetland depressions actively collect surface runoff from snowmelt/rainfall and allow interaction with the atmosphere. Therefore, a dynamic wetland scheme, incorporating both sub-grid energy and water balance, is needed to represent the complex hydrological processes in prairie wetlands and their potential feedback to the atmosphere.

This study was conducted over the Prairie Pothole Region (PPR) in North America where numerous small wetlands exist over a large spatial extent and play important roles in regional hydrology, ecology and climate. There were two objectives: (1) improve the representation of wetland extents and hydrological processes in the Noah-MP LSM and (2) explore the impacts of wetlands on the regional climate, especially the wetland-temperature feedback, in a high-resolution convection-permitting regional climate model (CPRCM, Prein et al., 2015). For the above purposes, this paper is organized into the following sections: The study region, data materials, and newly proposed wetland scheme are introduced in section 2, Materials and Methods. Three sets of simulations are conducted with the new wetland schemes in Noah-MP, including single-point simulations at a fen site, regional offline simulations, and coupled WRF (Skamarock et al., 2008) simulations in the PPR, and their results are shown in section 3 Results. Then, these results are discussed with other similar model studies in section 4 Discussion, focusing on the cooling effect of wetlands. The section 5 Conclusion provides a summary of the study and ending remarks.

2 Data and Methods

2.1 Study region – Prairie Pothole Region

The Prairie Pothole Region (PPR) is in the center of North America, covering about 770,000 km^2 across Canada and the U.S. Figure 1 presents the topography of the PPR, whose boundary is outlined by a solid black line. Millions of small wetland depressions, also known as "potholes", exist in the PPR, as a result of continental ice sheets retreating over 11,000 years ago, which left behind uneven glacial deposition upon the landscape (La Baugh et al., 1998; Pomeroy et al., 2005). These depressions are isolated from large river networks and are poorly hydraulically connected (Pomeroy et al., 2010). The cold winters allow snow to accumulate over cold seasons, accounting for about one third of annual precipitation, and snowmelt runoff is a major water input to these wetlands (Dumanski et al., 2015). Over the warm season, evaporation exceeds precipitation, drying surface water and exposing the underlying soils. The persistence and storage of wetland ponds depend on receiving seasonal rainfall and connection with shallow groundwater (Hayashi et al., 2016). Under extremely wet conditions, surface runoff by strong rainfall or sudden snowmelt exceeds the maximum capacity, spilling water to other surrounding wetlands, and form a largely connected wetland complex through the "fill-and-spill" process (van der Kamp and Hayashi, 2009; Mekonnen et al., 2014; Vanderhoof et al., 2018).

A fen site (53.802°N, 104.618°W; red triangle in Figure 1) from the Boreal Ecosystem Research and Monitoring Sites (BERMS) is selected to test the new wetland scheme in this study. Observation measurements of wind, temperature, humidity, pressure, precipitation, solar and longwave radiation were used as meteorological forcing to drive the Noah-MP model in a single-point simulation. Latent (LH) and sensible (SH) heat fluxes measured by eddy covariance system are used to evaluate single-point model results. Moreover, to evaluate the wetlands' impacts on regional climate, in-situ station measurements of daily tempature and precipitation data, in total 3095 stations, from the Global Historical Climate Network (GHCN) have been obtained. Their locations are shown in black dots in Figure 1.

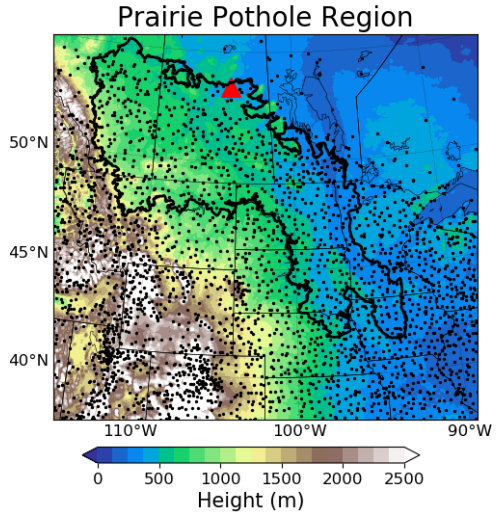

Figure 1. Topography of the Prairie Pothole Region (PPR) in North America. The black line shows the boundary of the PPR. The red triangle in Central Saskatchewan represents the location of the fen validation site. Black dots show the locations of 3095 stations from the Global Historical Climate Network (GHCN).

2.2 Data

In this study, the Global Inundation Extent from Multiple Satellites-2 (GIEMS-2, Prigent et al., 2019) dataset is used to prescibe the wetland spatial extents and seasonal dynamics in the PPR. The GIEMS-2 dataset is an extension of the unique GIEMS dataset which uses a collection of satellite sensors to provide estimates of surface water extent and dynamics at the global scale (Prigent et al., 2007; 2012). Such estimates use both passive and active microwave measurements, along with visible and near-infrared reflectance to capitalize on their complementary strengths, to extract maximum information about inundation characteristics, and to minimize problems related to one instrument only. The GIEMS-2 data provide monthly-mean inundated fractions of equal-area grid cells (0.25°x0.25° at the equator) from 1992 to 2015, covering 24 years of global inundation dynamics. The GIEMS and GIEMS-2 remote sensing product have been evaluated extensively over the globe (Papa et al., 2010) and used to evaluate simulated wetland fraction in ESM intercomparison studies (Ringeval et al., 2011; Melton et al., 2012). Figure 2 presents the maximum inundation extent, seasonality (month of inundation), and month of maximum inundation from GIEMS-2 in PPR.

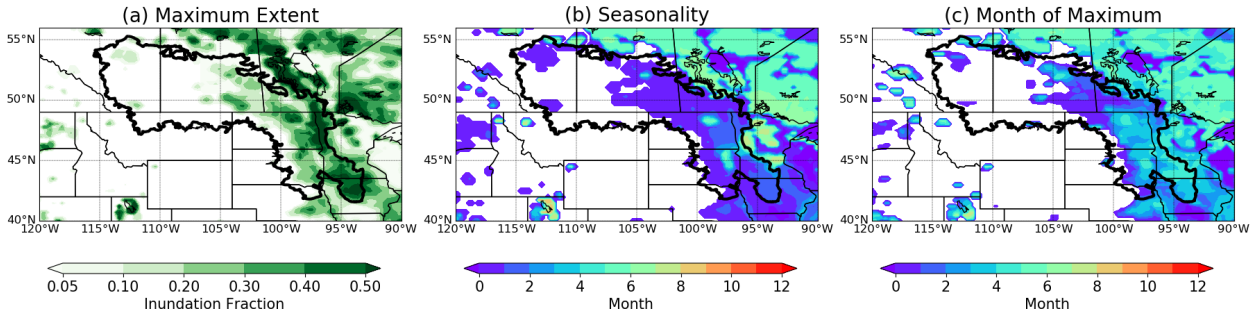

Figure 2. Spatial distribution of (a) the maximum inundation extent, (b) seasonality (month of inundation) and (c) month of maximum inundation in the PPR (black outline) from the GIEMS-2 data.

A CPRCM simulation over the Contiguous U.S. (CONUS WRF, Liu et al., 2017) is used to provide long-term (13-year) high-resolution (4-km) meteorological forcing for regional offline simulations. Convection-permitting models (CPMs) are atmospheric models whose grid spacing is fine enough (usually < 5-km) to permit convection and resolve mesoscale orography (Rasmussen et al., 2011; Prein et al., 2015; Liu et al., 2017). Long-term high-resolution climate downscaling using CPMs provides important added value to improve precipitation forecasts, which is critical to surface wetland hydrology, as well as for resolving fine-scale land surface heterogeneity (Kenden et al., 2017).The CONUS WRF data has been extensively evaluated and applied in multiple climate, hydrology, and land surface studies (Zhang et al., 2018, 2020; Fang et al., 2021).

To evaluate the offline Noah-MP simulation at the regional scale, two remote sensing datasets from MODIS Terra satellite are used, including land surface temperature (LST, MOD11) and evapotransporation (ET, MOD16). The Terra satellite passes above the PPR twice a day at about 4 and 18 hour UTC, representing the LST for nightime and daytime respectively. The MODIS satellite datasets were obtained from NASA Earthdata Search Engine (https://search.earthdata.nasa.gov/search).The Gravity Recovery And Climate Experiment (GRACE) satellite provides Terrestrial Water Storage (TWS) for global coverage from 2002 to

2017, at monthly interval for 1° x 1° resolution. The GRACE TWS data were used to evaluate the Noah-MP-simulated water storage for the whole wetland-soil-groundwater column in the PPR.

2.3 Surface water and energy partition scheme in Noah-MP LSM

The Noah-MP LSM adopts a runoff scheme to estimate a subgrid saturated fraction and surface water partition based on the TOPMODEL (TOPography based hydrological MODEL, Beven and Kirkby, 1979; Beven et al., 2020). This method assumes the sub-grid representation of grid cell saturation, F_{sat}, is based on a redistribution of water table depth, given the topographic variations in the grid cell. The F_{sat} fraction is an important parameter in partitioning surface water using the saturation runoff mechanism and was first integrated into a Soil-Vegetation-Atmosphere Transfer Scheme (SVATS) at local-, catchment-, and large-scale model by Famiglietti and Wood (1994a&b). In Noah-MP, the F_{sat} portion of the available surface water from rainfall and snowmelt (Q_{insurf}) becomes surface runoff (R_{srf}), which is a loss term leaving the grid cell, and the remaining (1-F_{sat}) portion becomes infiltration (Q_{infil}). In Niu and Yang (2005), F_{sat} is estimated by an exponential function of the water table depth (Z_{∇}, equation (3)) and has been utilized in the Noah-MP LSM (Niu et al., 2011; Yang et al., 2011). F_{satmx} is the maximum saturated fraction in a grid cell derived from digital elevation model (DEM).

$$R_{srf} = Q_{insurf} * F_{sat} \quad (1)$$

$$Q_{infil} = Q_{insurf} * (1 - F_{sat}) \quad (2)$$

$$F_{sat} = F_{satmx} * exp\,(-0.5 * f * (Z_{\nabla} - 2)) \quad (3)$$

This TOPMODEL-based F_{sat} framework is also widely used in the NASA GISS land surface model (Stieglitz et al., 1997) and the NASA Catchment Land Surface Model (CLSM, Koster et al., 2000; Bechtold et al., 2018).

The energy balance in Noah-MP is calculated separately for two sub-grid semitiles: a fractional vegetated area (F_{veg}) and a fraction bare ground area (1-F_{veg}). In this semitile scheme, shortwave radiation transfer is computed over the entire grid, while longwave radiation, sensible and latent heat flux, and ground heat flux are computed separately over these two tiles. As such, these two tiles in a Noah-MP grid neglect the large extent and seasonal variability of open-water wetlands. The total LH and SH of these two semitiles are aggregated in a weighted function:

$$LH = F_{veg}\left(LE_{gv} + LE_{v}\right) + (1 - F_{veg})LE_{gb} \quad (4)$$

$$SH = F_{veg}\left(SH_{gv} + SH_{v}\right) + (1 - F_{veg})SH_{gb} \quad (5)$$

Where the subscript *v* represents the vegetation canopy, *gv* is ground under canopy and *gb* is the bare-ground flux.

However, the above water and energy balance setting does not reflect dynamic water movement in prairie wetlands. These wetland depressions actively receive surface water from snowmelt and rainfall, but there is no surface water storage process in Noah-MP, so that the simulated surface runoff component will leave the model grid. Additionally, this setting further neglects the latent heat flux/evaporation contribution from the wetland surface to the atmosphere. Therefore, the

deficiency of current TOPMODEL-based F_{sat} parameterization in estimating surface saturation extents will be demonstrated and an updated method will be proposed in the next section.

2.4 Modifying F_{sat} fraction to represent wetlands

The original TOPMODEL-based F_{sat}, based on an exponential function of water table depth, does not reasonably reflect the magnitude and seasonal variation of wetland extent in the Prairies. Figure 3 shows the temporal evolution of the inundation fraction from GIEMS and Noah-MP simulated F_{sat} fraction in the PPR from 2000 to 2014. It is clear that the modeled F_{sat} has underestimated the maximum extent while overestimating the minimum extent. This is for two reasons: (1) the parameter F_{satmx} is a fixed value (0.38) for the global mean; and, (2) the seasonally frozen soil and glacial till with low hydraulic conductivity prevent direct groundwater connection with surface water, hence the water table dynamic is not a good indicator of surface water extent in the PPR. Detailed reasons for this discrepancy are provided in the discussion section.

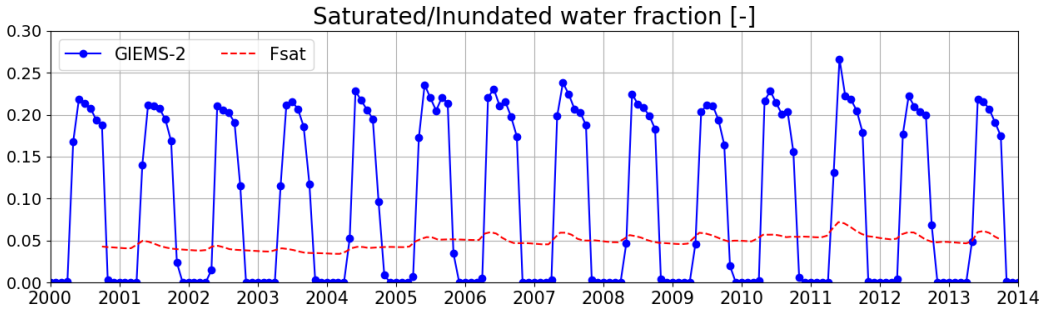

Figure 3. Temporal evolution of the inundation fraction from GIEMS and Noah-MP modelled F_{sat} in the PPR (regional average for $F_{satmx} > 0.1$).

Therefore, we propose a new formula for the saturated fraction F_{sat}, based on the first layer soil saturation, instead of water table depth:

$$F_{sat} = F_{satmx} * \left(\frac{SH_2O - SM_{wlt}}{SM_{ref} - SM_{wlt}}\right) \quad (6)$$

The first layer soil moisture (SH_2O) responds more rapidly to surface hydrological processes, such as snowmelt infiltration and evapotranspiration, than groundwater level. F_{sat} is determined by the maximum saturated fraction (F_{satmx}) and a relative soil moisture saturation condition, normalized by the soil moisture wilting point (SM_{wlt}) and field capacity (SM_{ref}). This method assumes the mean soil moisture saturation in the first layer soil can empirically represent spatial heterogeneity of soil saturation at the sub-grid scale.

2.5 Implementing the surface wetland storage scheme

In this study, we incorporate a sub-grid bucket-style surface water storage scheme to represent three important hydrological processes in Prairie Pothole wetlands: (1) The surface runoff from snowmelt and rainfall becomes the inflow to surface water storage (Q_{inflow}). The water in surface wetlands evaporates to the atmosphere at the potential rate, calculated by the Priestley-Tayer equation (9). The outflow is a result of total water exceeding the maximum water storage (W_{cap}), representing the "fill-and-spill" process. Note this wetland storage scheme is not connected to other wetland storage or a river network, so that the outflow term will leave the grid point and is lost to the water balance, similar to the runoff term in the default Noah-MP. The change of surface water storage (ΔW_{surf}) is calculated by the net balance of inflow, evaporation, and outflow in equation (11). The contribution to the latent heat flux is calculated as a weighted average over all three sub-grid types in equation (12), similar to the treatment in Pitman (1991). The sensible heat flux is calculated as the residual term from the energy balance equation.

$$Q_{insur} = Q_{snowmelt} + Q_{rain} \quad (7)$$

$$Q_{inflow} = Q_{insur} * F_{sat} \quad (8)$$

$$Q_{evap} = \alpha \frac{m(R_n - G)}{\lambda_v (m+\gamma)} \quad (9)$$

$$Q_{outflow} = max(Q_{inflow} - W_{cap}, 0) \quad (10)$$

$$\Delta W_{surf} = Q_{inflow} - Q_{evap} * F_{sat} - Q_{outflow} \quad (11)$$

$$LH_{all} = (1 - F_{sat})(F_{veg}(LE_{g,v} + LE_v) + (1 - F_{veg})LE_{g,b}) + F_{sat} * Q_{evap}\lambda_v \quad (12)$$

Figure 4 illustrates the difference between the default Noah-MP and the new surface wetland scheme in this study. The left-hand side shows the default Noah-MP surface runoff scheme based on the TOPMODEL saturation-excess concept. The inflow from rain and snowmelt (Q_{insur}) will be partitioned into infiltration (in the 1-F_{sat} portion), which enters soil moisture, and to surface runoff (in the F_{sat} portion), which eventually leaves the grid cell. The right-hand side shows the two modifications in our study: (1) the modified F_{sat} parameterization based on first layer soil saturation; (2) creating a surface water storage W_{cap} representing surface wetland dynamics. The F_{sat} portion of the inflow will now be collected within the W_{cap} storage and evaporate to the atmosphere with a weighted function. The water amount exceeding the maximum capacity will become the outflow from the wetland (also referred to as the new runoff term, R_{srf}).

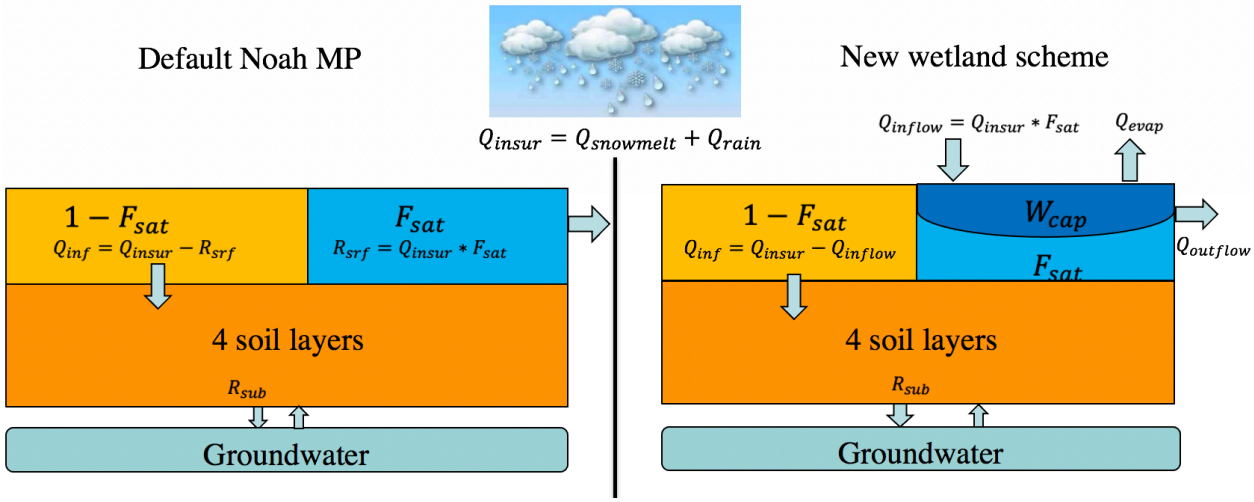

Figure 4. Simple diagram demonstrating the modifications in this study, which includes the modification of surface saturated fraction and incorporating a surface wetland storage scheme in the Noah-MP Land Surface Model.

2.6 Simulation design

Three sets of numerical simulations are conducted to study the impacts of representing wetlands on the simulated energy and water balance in the Noah-MP LSM, as well as feedback to the regional climate in the coupled WRF model. A summary of these three simulations is in Table 1.

The first set of simulations was conducted at the fen site in central Saskatchewan. The meteorological forcings were wind, temperature, humidity, pressure, precipitation, solar and longwave radiation from a tower measurement. The purpose of this simulation was to evaluate the improved estimation on the F_{sat} fraction and ET and explore the sensitivity of maximum storage (W_{cap}) in the wetland scheme. A variety of W_{cap} levels were selected to demonstrate the impacts of different wetland capacity on simulated energy/water balance at the fen site.

The second set of simulations was at the regional scale in the PPR, driven by the 4-km WRF regional climate simulation (CONUS WRF, Liu et al., 2017). The purpose of this offline simulation was to investigate the wetland scheme over the PPR, focusing on its impacts on energy and water balance at a regional scale. In this regional simulation, we constrain the maximum F_{satmx} by the GIEMS-2 data and the maximum surface water storage capacity W_{cap} by the 90-m DEM (MERIT, Yamazaki et al., 2017, http://hydro.iis.utokyo.ac.jp/~yamadai/MERIT_DEM/). Figure 5 presents the spatial map of F_{satmx} from GIEMS-2 data and W_{cap} derived from the MERIT 90-m DEM and aggregated to a 4-km resolution grid:

$$W_{cap} = \sum_{i=1}^{n} min\left((H_i - \bar{H}), 0\right) \quad (13)$$

H_i represents the 90-m elevation and $\bar{H}$ is the mean elevation for a 4-km grid, such that W_{cap} represents the collective topographical variation in the depressional area from 90-m DEM and aggregated into the 4-km grid. The high F_{satmx} regions are located in the Northeast part of the domain, near Lake Winnipeg in Manitoba and the Red River Valley. These regions also correspond with the low W_{cap} regions.

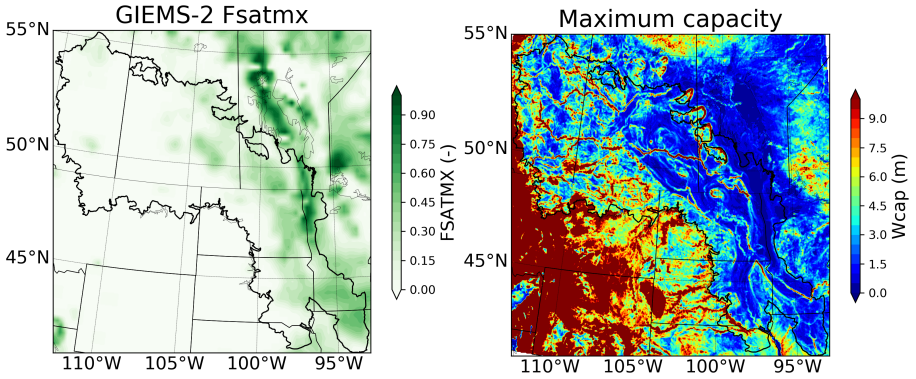

Figure 5. Map of maximum saturation (F_{satmx}) and wetland storage capacity (W_{cap}) in the Prairie Pothole Region, derived from the Global Inundation Extent from Multiple Satellites (GIEMS-2) product and MERIT 90-m DEM, respectively.

The third set of simulations was the coupled WRF regional climate simulation for the summer of 2006. This was to investigate the impacts of wetland dynamics on regional climate, in particular under a high-resolution convection-permitting configuration. It is noteworthy that in the summer of 2006, an intense and prolonged heatwave occurred in the Central U.S. and Southern Canada from mid-July to early August. Two simulations were conducted: the default simulation (DEF) uses the TOPMODEL-based runoff scheme (Niu et al., 2005) and the wetland simulation (WS) uses the updated wetland scheme in this study. Moreover, the model sensitivity to two groundwater schemes was also investigated for the Simple Groundwater Scheme (SIMGW, Niu et al., 2007) and the shallow groundwater scheme from Miguze-Macho and Fan (MMF-GW, Miguze-Macho et al., 2007). Please see Supporting Information for detailed results for these two GW schemes.

Table 1. Summary of the three sets of simulations conducted in this study.

Simulation design	**Location**	**Period**	**Purpose**
Single-point Noah-MP	Fen site, SK	2003/01/01-2010/12/31	Examine the sensitivity of F_{sat} formula and different levels of storage
Offline regional Noah-MP	PPR region	2000/10/01-2013/10/01	Incorporate spatially varied F_{satmx} and W_{cap} parameters in the PPR
Coupled regional WRF	PPR region	2006, summer from Apr to Aug	Conduct coupled WRF-NoahMP-Wetland simulation and study the feedback to temperature

3 Results

3.1 Implementation and sensitivity tests on a single-point LSM

We first performed a single-point LSM simulation at the fen site in Central Saskatchewan. A sensitivity test was performed with the updated wetland scheme with various storage capacities (W_{cap}=0, 5, 50, 500 mm). Figure 5 shows the sub-grid F_{sat} fraction, energy and water balance at the fen site simulated by Noah-MP, evaluated against the GIEMS-2 timeseries and in-situ measurement. Due to the scale difference between GIEMS-2 data and the fen site observations, we selected the closest grid point from the GIEMS-2 data and surrounding eight grid points to the fen site for this comparison. In Figure 6a, the default F_{sat} formula using the exponential function of the water table depth fails to represent the large magnitude and strong seasonal variation, as shown by the GIEMS-2 data. The modified formula using the first layer of soil moisture improves both the magnitude and seasonal cycle of the F_{sat}, while different capacity levels have little influence on the F_{sat}. By increasing the F_{sat} fraction and incorporating different storage capacity, the modeled ET increases, accounting for the evaporation contribution from wetland surface water (Figure 6c). Correspondingly, the modeled sensible heat fluxes decrease as water storage capacity increases (Figure 6d). As a result, the modeled Bowen ratio (SH/LH) also decreases, as more energy was partitioned into latent heat fluxes over sensible heat fluxes (Figure 6b).

Given different capacity levels, WS=0 demonstrates the driest case with the smallest ET, highest SH, and largest Bowen ratio. This is because even with the F_{sat} increasing, a larger amount of surface water is partitioned into runoff, but not collected by the wetland (WS=0), neglecting the surface water evaporation. By increasing the storage capacity, ET and latent heat fluxes are enhanced while sensible heat fluxes are suppressed (WS=5 and WS=50). With large storage capacities (WS=50 and WS=500), the summer evaporation demand cannot sufficiently dry out all water from the wetland, so the contribution to ET was the same for these two storage levels. Compared to the observations from the fen site, the WS=5 simulation provided the best estimate of ET, and although slightly underestimating SH, had the best estimation of Bowen ratio for partitioning surface energy at the wetland surface.

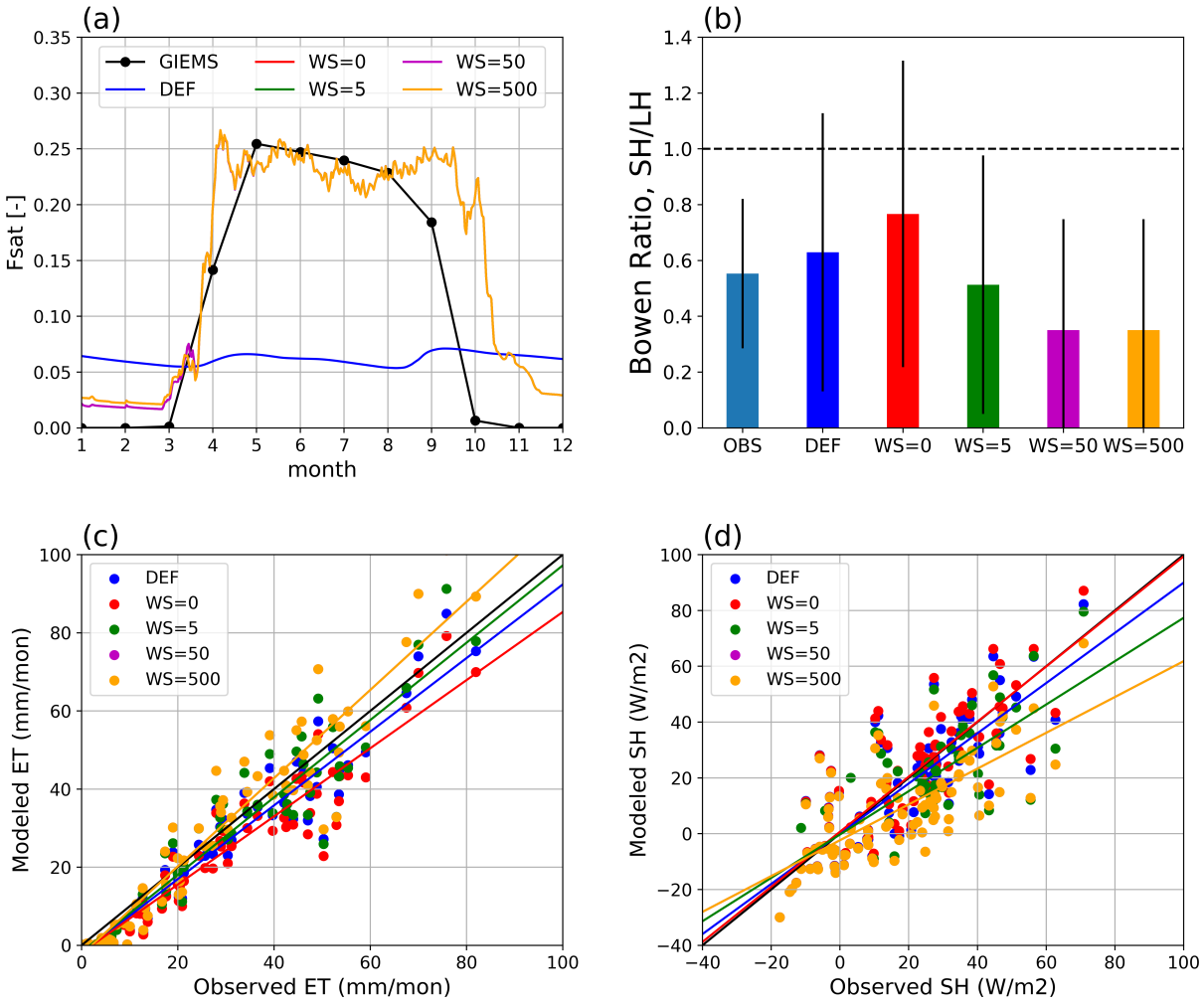

Figure 6. Single-point simulation at the fen site. (a) surface saturated fraction from default (DEF) and wetland scheme with different capacities (WS=0, 5, 50, 500 mm) and GIEMS-2 inundation extent, (b) Mean Bowen ratio from observation, default model and different WS simulations with one standard deviation error bar (c) scatter plot of monthly ET from DEF and WS models against observation; (d) same as (c) but for SH. A black 1:1 line is shown in both (c) & (d) for reference.

3.2 Offline simulation over the PPR

Two 13-year offline Noah-MP simulations were conducted: one with the default setting and one with the new wetland scheme. Three aspects of the model simulations were evaluated, including the terrestrial water storage (TWS) against the GRACE satellite data, the land surface temperature (LST) and evapotransporation (ET) against the MODIS Terra satellite data. Figure 7 shows the TWS trend from the GRACE satellite and Noah-MP model in the PPR. Over the 15-year GRACE period, the south PPR has experienced an increasing trend of around 15~30 mm/year (Figure 7a). This increasing trend is also shown by the timeseries in Figure 7b, together with results from two Noah-MP simulations. The annual cycle of the TWS anomalies are shown in Figure 7c. Both Noah-MP simulations reasonably capture the increasing trend and annual cycle of the TWS. However, the DEF simulation shows smaller seasonal variation than GRACE TWS. On the other hand, the WS simulation produces higher TWS from spring to summer than DEF, which matches better with

the GRACE data. This increase in TWS can be attributed to the implementation of the wetland scheme, which collects inflow from snowmelt and rainfall, increasing the surface water storage, while decreasing surface runoff.

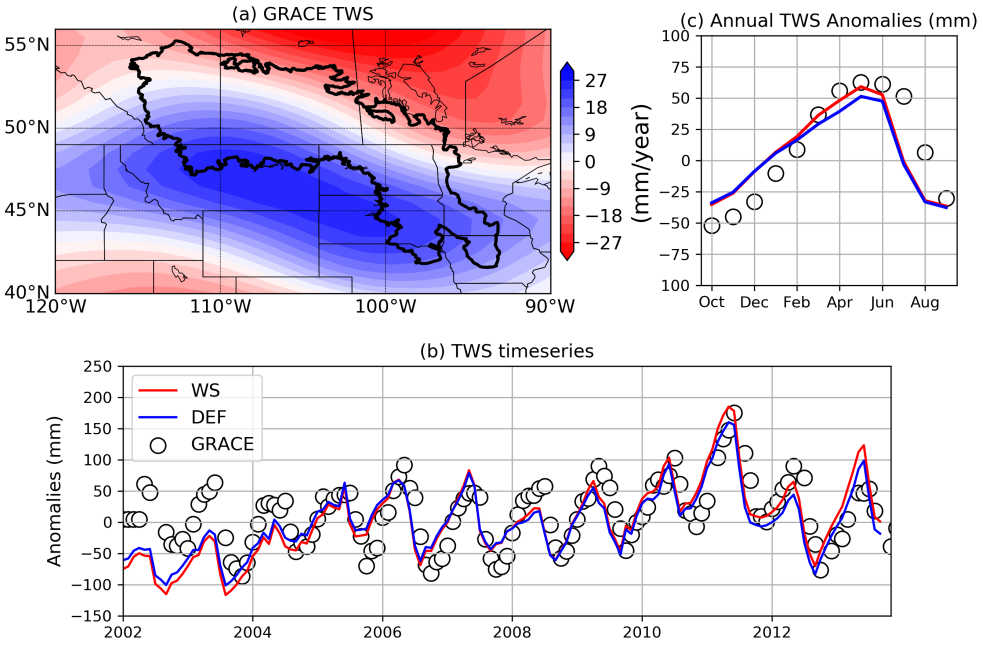

Figure 7. (a) spatial distribution of the anomaly trend for GRACE Terrestrial Water Storage (TWS) in the Prairie Pothole Region; (b) timeseries of TWS anomalies from GRACE, default (DEF) and wetland scheme (WS) simulations; (c) annual cycle of TWS anomalies.

Figure 8 demonstrates the effect of the wetland scheme on monthly ET compared to DEF and their evaluation against the MODIS Terra satellite over the PPR. The domain spatial plots are 13-year averages for May, June, July and August. The scatter plot is for the spring and summer months for the whole 13-year period (78 months). The increased ET from WS simulation mostly concentrates on the northeast domain, where F_{satmx} are the highest (Figure 5), by about 20~40 mm/mon. As compared to the MODIS ET data, both DEF and WS simulations present overestimation in spring months (MAM) and underestimation in summer months (JJA). The increased ET in WS simulation improves the underestimation of ET in summer months compared to DEF, while also contributes to much overestimation in spring months. Overall, the WS simulation is more comparable to (77.12 mm/mon) the MODIS ET data (80.01 mm/mon) than the DEF simulation (72.17 mm/mon).

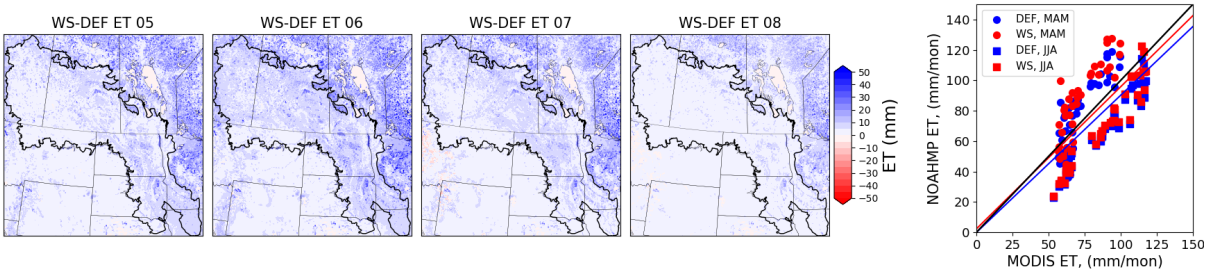

Figure 8. Differences in ET from wetland scheme (WS) and default (DEF) simulations (WS-DEF) from May to August (13-year average) and their scatter plot against the MODIS ET data in spring

and summer months. Two linear regression lines are fitted for the DEF (blue) and WS (red) simulation and a 1:1 line (black).

Figure 9 shows the bar plot for regional average LST at daytime and nighttime from May to August in the PPR. The DEF simulation shows substantially warmer LST than the MODIS data, especially in July by more than 6 ℃ in the daytime. The enhanced ET and suppressed SH effect from the wetland scheme creates a cooling effect on LST for both daytime and nighttime in all months compared to DEF. The cooling effect is stronger in the daytime (~3℃) than the nighttime (~1℃), contributing to reduced warm biases in the WS simulation (Day: 0.78℃; Night: 2.16℃) than in DEF simulation (Day: 3.57℃; Night: 2.69℃) relative to MODIS.

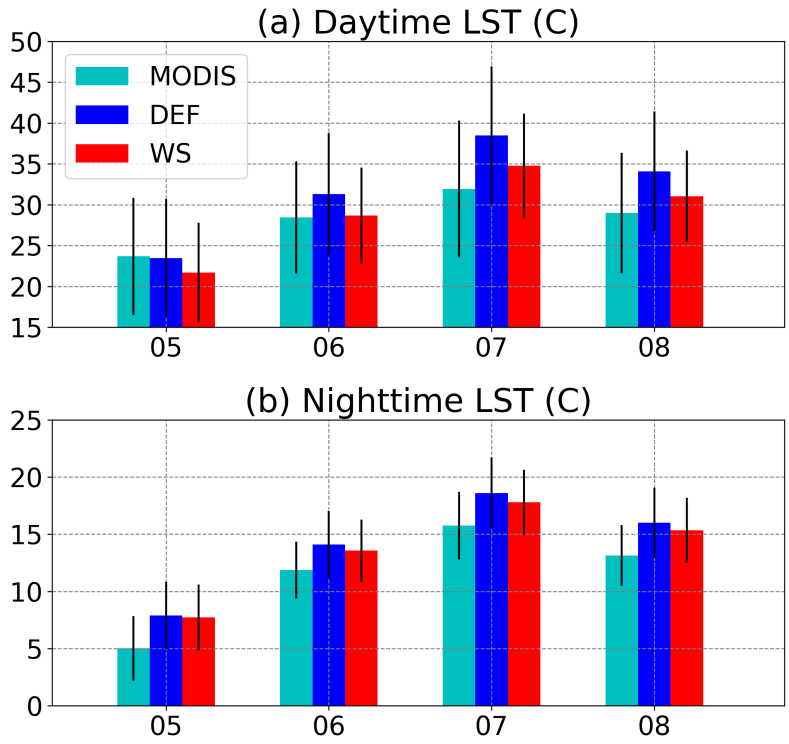

Figure 9. Barplot of land surface temperature (LST) from MODIS data, default (DEF), and wetland scheme (WS) simulations from May to August in (a) daytime and (b) nighttime.

3.3 Regional climate simulation with coupled wetland dynamics

To study the feedback from wetlands to regional climate, we performed two coupled WRF-wetland simulations for the summer of 2006. Our analysis focused on wetlands' cooling effect on temperature from May to August, especially in 2006 when an intense summer heatwave occurred from mid-July to early August in the Central U.S. and Southern Canada.

Figure 9 shows the monthly temperature biases from two simulations, and the cooling effect induced by the WS scheme in 2006. In the DEF simulation, it is clear that a warm bias exists in the southern part of the domain, ranging from more than 4°C in the Central U.S. to 1°C in the Western Canadian Prairies. This warm bias is stronger in July and August. The WS simulation shows a significant cooling effect in the Northeast portion of the domain, where the saturated fraction is high. The cooling in temperature ranges from less than 1°C in May to about 1~2°C in July. This cooling signal is evident in high-F_{sat} regions from May to August.

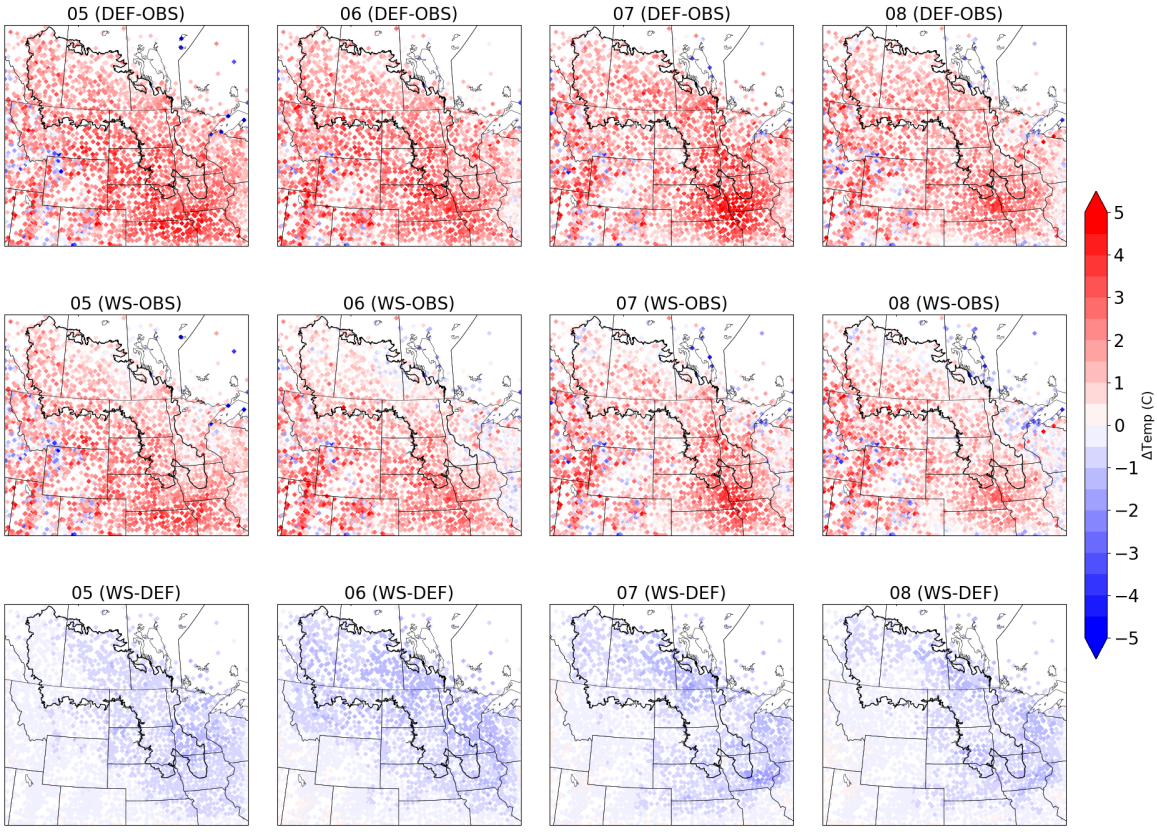

Figure 10. Monthly temperature biases from default (DEF) and wetland scheme (WS) simulations agasint GHCN station observation, and the cooling effect (WS-DEF) in the summer (May-August) of 2006.

In the summer of 2006, a record-breaking heatwave hit much of the U.S. and Southern Canada. The extreme heat conditions can be represented by the number of "hot days" during the summer, with the daily maximum temperature (Tmax) exceeding the 90th percentile (TX90) of the 30-year climatology. We calculated the number of hot days from May to August in 2006 from station observations and two simulations and the results are presented in Figure 11. Through these four months, the hottest region is in the southeast of the domain in South Dakota, Nebraska, and

Wyoming – with more than 30 hot days – while in the Canadian Prairies, there are about 10~20 hot days. The DEF simulation demonstrates significant overestimation of hot days in the U.S. Midwest and Southeast PPR, with 8~30 days more than in observation data. The WS simulation shows that wetlands could effectively reduce the hot days by about 10~15 days in the entire domain, and it reduces the overestimation of hot days in the southern domain while overcooling in the Canadian Prairies. Two regions, including southern Manitoba and the area between Nebraska and Iowa, receive greater impacts from wetlands. The timeseries of regional average Tmax also shows a consistent cooling of 1~2 ℃ through the summer period. These results demonstrate the important role of wetlands in mitigating climate change, especially in extreme heat events.

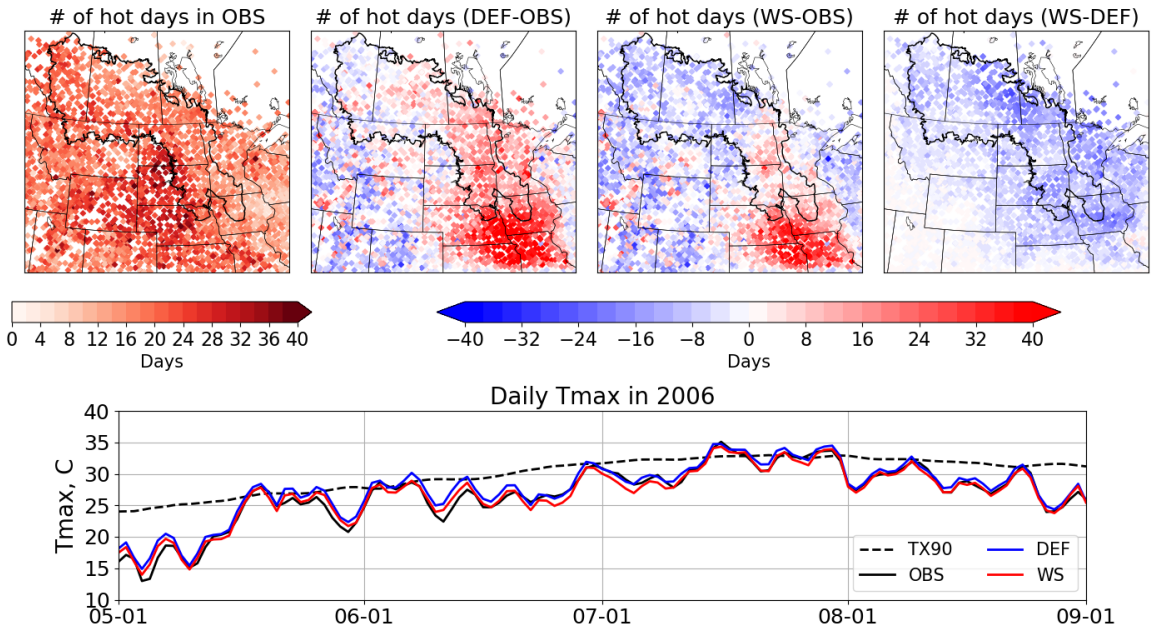

Figure 11. Number of hot days in default (DEF), wetland scheme (WS) simulations, and the reduction in hot days from WS to DEF, as well as the timeseries of Tmax in the summer of 2006 from these two simulations and observation data. OBS is from the station temperature from GHCN network and TX90 represents the 90th percentile threshold to define extreme hot days.

Figure 12 shows the differences in model-simulated clould fraction (WS-DEF) for 2006, two cross-sections are also provided at 52°N and -95°W. Through the summer of 2006, increased cloud fraction by the wetland scheme is evident for up to 0.1 in the Northeast of the PPR domain and is strongest in May. Vertically, this enhanced cloud fraction emerged below 1000 m in the lower troposphere. Conversely, the wetland scheme produces less cloud in the middle troposphere, roughly 7000 m in height. These results suggest that incorporating wetland storage in the WS simulation not only modifies surface energy and water balance, but also impacts cloud formation in the lower troposphere.

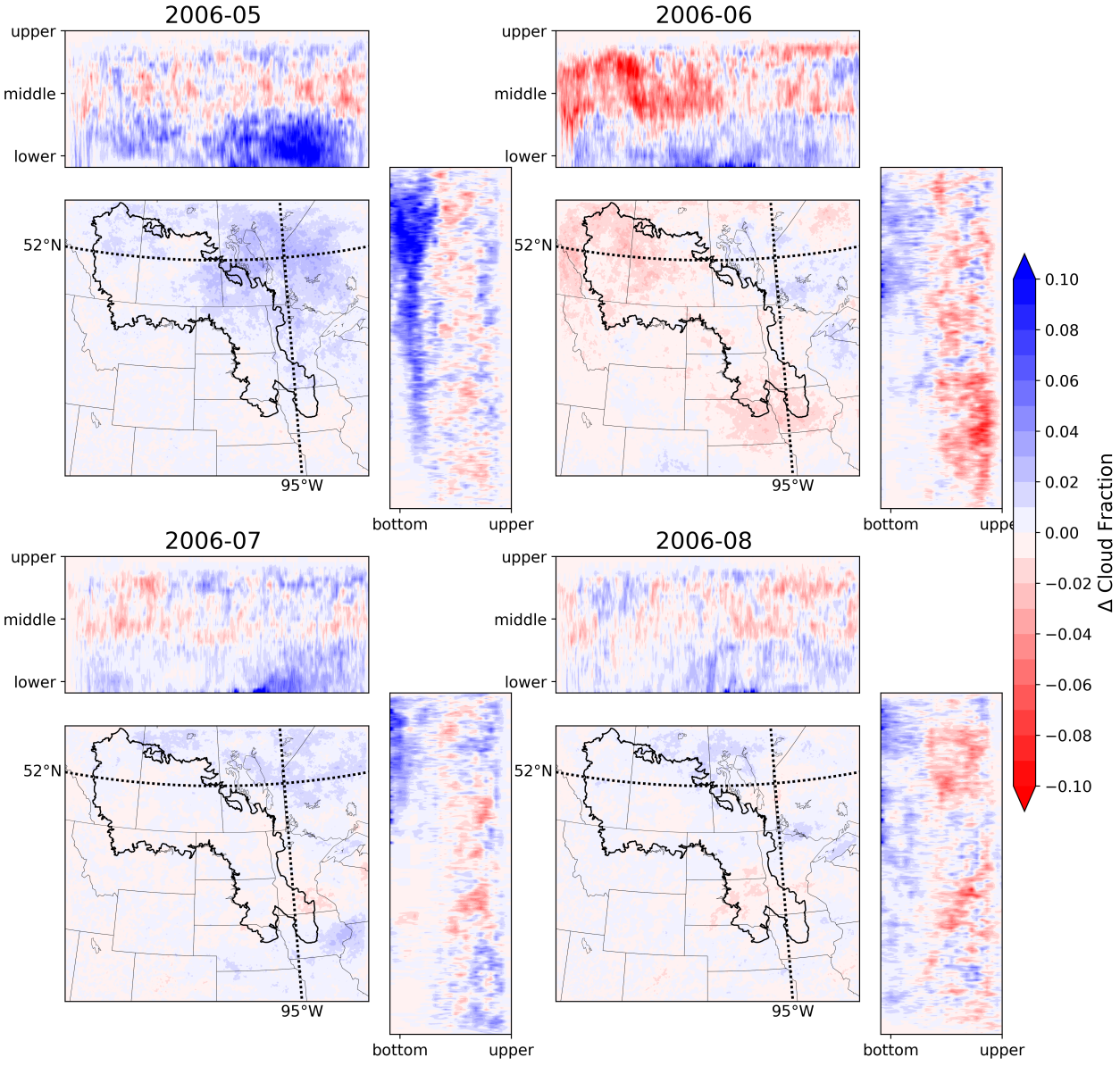

Figure 12. Differences in cloud fraction from wetland scheme-default in May, June, July and August in 2006. Two vertical cross-sections of cloud fraction are shown at 52°N and -95°W. Upper, middle and lower roughly correspond to 15000, 7000, and 1000 m in height.

Figure 13 shows the differences in midday boundary layer height (ΔPBLH) and soil moisture (ΔSM) from the two simulations (WS-DEF). There is a significant negative correlation between ΔPBLH and ΔSM that is more evident in July and August. The WS simulation clearly reduces the midday PBLH occuring in these four months in 2006, ranging up to 800 m shallower than the DEF simulation. The greater reductions in PBLH are associated with wetter conditions in SM. This analysis further adds evidence to the wetland scheme modifying surface energy partitioning, suppressing boundary layer height at midday. On the other hand, the differences in ΔSM between the two simulations are not as obvious as the differences in ΔPBLH. Our study also found that precipitation differences in these two simulations are spatially heterogenous, with ~ 2 mm/mon more precipitation in the WS regional average. This change is not large enough to conclude there is a positive SM-precipitation feedback for the region due to high variability of precipitation (See supporting information).

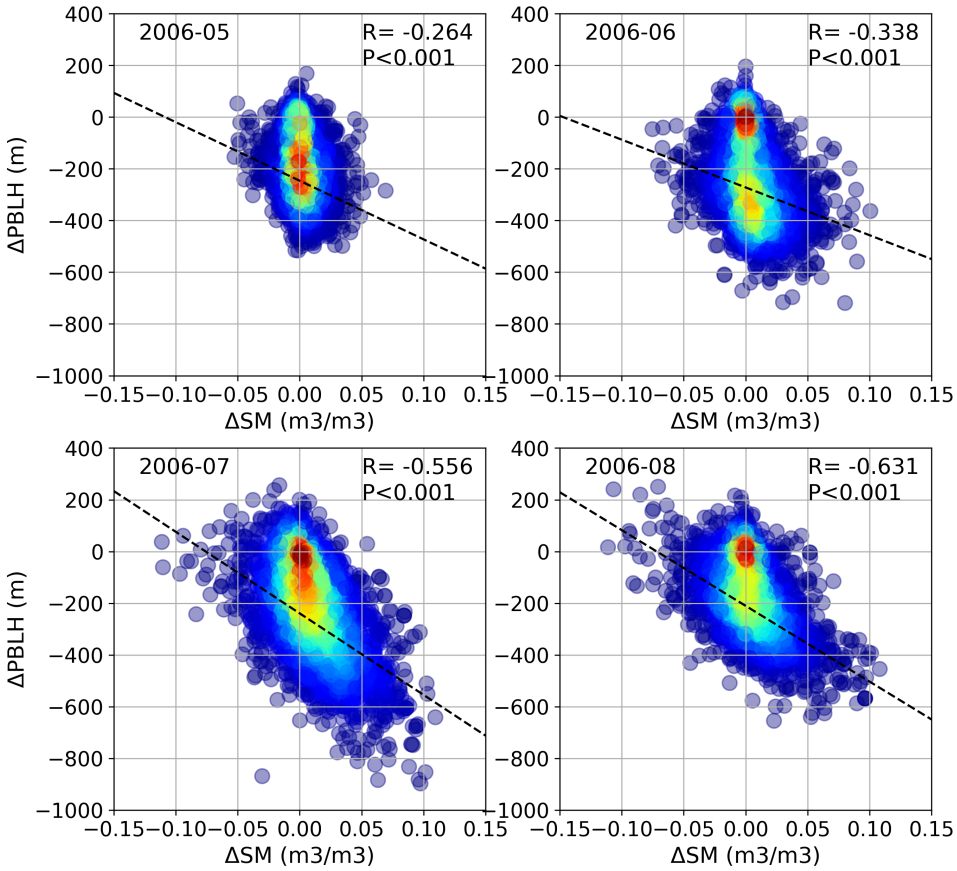

Figure 13. Scatter plot of ΔPBLH and ΔSM are shown from the differences between WS and DEF simulation for May, June, July and August in 2006. Color represents the density of samples, red means data samples are more converged and blue means data samples are sparse. Linear repressions were performed with Pearson's correlation coefficient and Student's t-test P-value in the top right corner for each month.

4 Discussion

Reasonable representations of sub-grid saturated fraction for wetland spatial extents and runoff generation processes for dynamic water storage are challenging in light of data scarcity, coarse model resolution, and insufficient understanding of the physical processes (Ringeval et al., 2012). Traditional TOPMODEL-based parameterization fails to represent highly variable Fsat seasonal cycles, as we showed in Section 2.2. Here we provide three possible reasons for the discrepancy between TOPMODEL F_{sat} and the inundation dynamics from GIEMS-2 data. (1) The underlying assumption of the TOPMODEL method requires "steady state" precipitation and soil moisture heterogeneity, which is more likely in wet, relatively shallow soils on moderate slopes (Beven and Kirkby, 1979; Kirkby et al., 2021). However, this is not the case in the Prairie Pothole Region, where the climate is usually semi-arid and the large-scale topography is flat with small-scale variation. (2) Another possible reason for this discrepancy is that the TOPMODEL method calculates a critical topographic index value when the local water table is at the surface. However, in the PPR, frozen soils in wintertime prevent interaction between the soil moisture and groundwater (Ireson et al., 2013). (3) The inadequency stems from the scale differences between regional-scale land surface simulation and the catchment-scale hydrological study, where TOPMODEL was originally developed.

In our modification of the F_{sat} formulation, we used the first layer of soil saturation to indicate the sub-grid saturation fraction. This method assumes the grid cell mean soil moisture saturation can be translated into a spatial fraction for surface saturation, which further plays an important role in the saturation runoff mechanism. This positive correlation between soil moisture and surface runoff is highlighted in Ghajarnia et al. (2020) and Ghajarnia et al. (2021, under review), in which the authors studied this close covariation from multi-catchment data across Europe and the globe, repectively. In these studies, the authors found that there is a strong correlation between soil moisture and runoff exihibited in independent observations and re-analysis data, but that fails to manifest in ESM data. Moreover, we also incorporate a spatially varied maximum F_{satmx} map from the GIEMS-2 product to replace the default global mean value (0.38) in Noah-MP and WRF. Both modifications improve the spatial heterogeneity and the temporal dynamics of wetland extents in the PPR.

The wetland scheme in this study sufficiently modified the surface energy and water partition in prairie wetlands, showing increased ET with decreased surface runoff and an increase in LH with decreased SH. This finding aligns with our expectations, as well as with previous VIC model wetland and lake simulations in the U.S. Midwest region (Mishra and Cherkauer et al., 2010) and a floodplain modeling study in the Niger river delta (Dadson et al., 2010).

One highlight of this study is the wetland cooling effect on atmospheric temperature. Previous studies have documented this effect in detail, specific to different wetland characteristics and dominant vegetation types (Pitman, 1991; Bonan, 1995). The cooling effect shown in the wetland simulation is not only due to modified surface energy partition, enhancing latent heat while suppressing sensible heat, but also the result of land-atmosphere interactions, involving boundary layer dynamics and cloud formation, which is analogous to the soil moisture-temperature feedback (Seneviratne et al., 2010). That inundated conditions are associated with shallow boundary layer height and smaller daily temperature range has been also demonstrated in an observational study in Mississippi and Missouri River flooding (Pal et al., 2019) and the long-lasting floods in the

Pampas (Houspanossian et al., 2018). A previous study using WRF with a prescribed soil moisture threshold to indicate wetlands in the Great Plains at coarser resolution (12-km) also showed a temperature cooling effect, but the precipitation effect was negligible (Capehart et al., 2012). The wetland cooling effect, especially during extreme heatwave events, echoes a previous study in the Central U.S. where antecedent soil moisture could effectively reduce the frequency, intensity, and duration of extreme heatwaves (Zhang et al., 2018).

The simulated warm temperature biases associated with dry soil moisture conditions is a long-standing issue in modeling the summer climate in Central U.S. (Cheruy et al., 2014; Klein et al., 2006; Liu et al., 2017; Mueller & Senevirnatne 2014). Efforts have been dedicated to improve the representation of shallow groundwater in the MMF-GW scheme (Miguez-Macho et al., 2007), in which groundwater closely connects with soil moisture and provides a moisture source to ET and precipitation recycling, hence cooling the atmosphere (Barlage et al., 2021). Our study presents an alternative solution to mitigate the warm biases in the PPR, where surface wetland contribution to ET is non-negligible. However, the combined cooling effect of the MMF-GW scheme and the WS scheme is too strong, inducing cool biases in the Canadian Prairies (See Supporting Information). Moreover, the wetlands' impacts on regional precipitation in the PPR (~ 2 mm/mon increase) is not as strong as the precipitation recycling shown in applying the MMF-GW scheme in the Central U.S. (~10 mm/mon). This may be because the PPR is further north than the Central U.S., which is characterized as one of the coupling "hot spots" for soil moisture-precipitation feedback (Koster et al., 2004).

This study approach has some limitations. For example, there is uncertainty in prescribed wetland maximum extents from GIEMS-2 data. Aires et al. (2018) compared three high-resolution global inundation datasets, including two from visible satellites at 30-m, Global Surface Water Explorer, (GSWE) and Global 3 arc-second Water Body Map (G3WBM), and one downscaled product from GIEMS (GIEMS-D3) at 90-m. The advantages of the GIEMS method is that the multi-sensor technique minimizes limitations from single instruments, for example under vegetation canopy and cloudy conditions. The disadvantages of the GIEMS dataset is its low original resolution (25-km) which may underperform at detecting small water bodies. Although it has been widely used in prescribing wetland extents (Ringeval et al., 2012) and analysis of wetland-precipitation feedbacks (Taylor et al., 2018) at regional and global scales, it was challenging to apply at the single-point fen site. We compared the discrepancies between inundation fraction from GIEMS-2 and GSWE (aggregated to different resolution) and showed that GIEMS-2 data may overestimate surface water extent on water-saturated soils compared to GSWE data, while their seasonality are similar (see Supporting information). Although uncertainties exist for using different remote sensing product to prescribe maximum wetland extents, it would not change the main conclusions from this study. A final notable limitation is that different types of wetlands have distinct characteristics due to their soil composition and dominant vegetation and, hence, exihibit a large range in partitioning of surface energy (e.g., drier in bogs and wetter in fens). However, in this study, wetlands are only represented as open-water storage to capture their contribution to evaporation, neglecting these detailed classifications. Future studies are encouraged to include sophisiticated biogeophysical and biogeochemical processes to characterize different wetland types, yet scarcity in spatial data and uncertainties in model parameters may further emerge.

5 Conclusions

Wetlands play a crucial role in Earth systems for their climatic and hydrological functions. However, reasonably representing the spatial extents and dynamics of small-scale wetlands has been challenging to LSMs and coupled ESMs. This is particularly important and urgent in the PPR as the wetlands are critical to the region's ecology and the hydrological conditions are complex. In this research, we developed a wetland scheme with two modifications to represent wetland dynamics in the Noah-MP LSM: (1) modification of the sub-grid saturation fraction to represent spatial wetland extents based on grid cell soil moisture; (2) incorporation of a dynamic surface water storage scheme to represent the hydrological processes in wetlands. The new wetland scheme was incorporated in a single-point, offline regional simulation, and coupled WRF simulation in the PPR. The main findings are as follow:

The single-point simulation at the fen site showed that the modified sub-grid F_{sat} reasonably reproduces the magnitude and seasonality of surface inundation dynamics from the GIEMS-2 data, compared to the default TOPMODEL-based method. Incorporating the wetland scheme effectively modified the surface energy and water balance, enhancing latent heat fluxes and ET while suppressing sensible heat fluxes and surface runoff. This results in improved estimate of ET and the Bowen ratio but a slight underestimation of sensible heat fluxes. The modeled wetland's impacts on surface energy and water balance also depend on its maximum capacity, W_{cap}, a parameter related to the shape of the wetland and its surrounding topography.

Incorporating the wetland scheme in the PPR demonstrates three improvements: (1) the simulated terrestrial water storage increases from March to June, matching better results from the GRACE satellite. (2) the simulated ET also increases compared to the default simulation, reducing the underestimation of ET in summer months while overestimating ET in spring months. (3) These increases in ET and latent heat fluxes contribute to a cooling effect, reducing the warm biases in land surface temperature ~3°C in the daytime and 1°C at nighttime.

Finally, the wetlands' feedback to regional climate was explored in the coupled WRF-NoahMP-Wetland model. The cooling effect induced by wetlands was evident in summer for about 2~3°C from May to August, significantly reducing warm biases from the default simulation. This cooling is the result of wetlands altering energy balance partitioning as well as interactions with atmosphere, shallowing the boundary layer height and promoting cloud formation. In the summer of 2006, when an extreme heatwave hit the Central U.S. and Southern Canada, the presence of wetlands could profoundly reduce the number of extreme hot days by more than 10 during the summer period, effectively relieving the heat stress to human comfort.

In recent years, the tradeoffs between agriculture and wetland conservation has been a serious topic of discussion among the public, universities, and government agencies. Agricultural land expansion at the cost of wetland drainage increases the risk of emerging flooding in springtime (Dumanski et al., 2015; Pattison-Williams et al., 2018). Wetland drainage also results in increased nutrient export (Badiou et al., 2018; Wilson et al., 2019) and carbon release to the atmosphere (Badiou et al., 2011), reducing resilience to drought and high temperature, which leads to crop failures (Hatifield, 2016). However, the loss of wetlands to agricultural, industrial and residential land development is not confined to the PPR but rather is a common problem worldwide and

requires greater attention (The Rasmar Convention 2007; Nature Geoscience, 2021). Our results show that the presence of wetlands could be beneficial to many sectors by cooling atmospheric temperatures during heatwaves. These highlights should inspire future studies to understand wetlands' value in regional environments and the Earth system, especially those that have been neglected at the cost of human expansion.

Acknowledgments

Z. Zhang, Z. Li and Y. Li acknowledge the financial support from the Natural Sciences and Engineering Research Council of Canada (NSERC) Discovery Grant, and Global Water Futures Program, Canada First Research Excellence Fund and Global Institute for Water Security (GIWS). Z. Zhang was funded by a Mitacs Accelerate Fellowship funded by Ducks Unlimited Canada's Institute for Wetland and Waterfowl Research. This project was supported by grants from Wildlife Habitat Canada, Bass Pro Shops Cabela's Outdoor Fund, and the Alberta NAWMP Partnership.

References

Badiou, P., McDougal, R., Pennock, D., & Clark, B. (2011). Greenhouse gas emissions and carbon sequestration potential in restored wetlands of the Canadian prairie pothole region. Wetlands Ecology and Management, 19(3), 237–256. https://doi.org/10.1007/s11273-011-9214-6

Badiou, P., Page, B., & Akinremi, W. (2018). Phosphorus Retention in Intact and Drained Prairie Wetland Basins: Implications for Nutrient Export. Journal of Environmental Quality, 47(4), 902–913. https://doi.org/10.2134/jeq2017.08.0336

Barlage, M., Tewari, M., Chen, F., Miguez-Macho, G., Yang, Z. L., & Niu, G. Y. (2015). The effect of groundwater interaction in North American regional climate simulations with WRF/Noah-MP. Climatic Change, 129(3–4), 485–498. https://doi.org/10.1007/s10584-014-1308-8

Barlage, M., Chen, F., Rasmussen, R., Zhang, Z. & Miguez-Macho, G. The importance of scale-dependent groundwater processes in land-atmosphere interactions over the central United States. Geophys. Res. Lett. (2021) doi:10.1029/2020GL092171.

Bechtold, M., De Lannoy, G. J. M., Koster, R. D., Reichle, R. H., Mahanama, S. P., Bleuten, W., Bourgault, M. A., Brümmer, C., Burdun, I., Desai, A. R., Devito, K., Grünwald, T., Grygoruk, M., Humphreys, E. R., Klatt, J., Kurbatova, J., Lohila, A., Munir, T. M., Nilsson, M. B., … Tiemeyer, B. (2019). PEAT-CLSM: A Specific Treatment of Peatland Hydrology in the NASA Catchment Land Surface Model. Journal of Advances in Modeling Earth Systems, 11(7), 2130–2162. https://doi.org/10.1029/2018MS001574

Beven, K. J., & Kirkby, M. J. (1979). A physically based, variable contributing area model of basin hydrology / Un modèle à base physique de zone d'appel variable de l'hydrologie du bassin versant. Hydrological Sciences Bulletin, 24(1), 43–69. https://doi.org/10.1080/02626667909491834

Beven, K. (1997). TOPMODEL: A critique. Hydrological Processes, 11(9), 1069–1085. https://doi.org/10.1002/(SICI)1099-1085(199707)11:9<1069::AID-HYP545>3.0.CO;2-O

Beven, K. J., Kirkby, M. J., Freer, J. E. & Lamb, R. A history of TOPMODEL. Hydrol. Earth Syst. Sci. 25, 527–549 (2021).

Bonan, G. B. (1995). Sensitivity of a GCM Simulation to Inclusion of Inland Water Surfaces. Journal of Climate, 8(11), 2691–2704. https://doi.org/10.1175/1520-0442(1995)008<2691:SOAGST>2.0.CO;2

Bowling, L. C., & Lettenmaier, D. P. (2010). Modeling the effects of lakes and wetlands on the water balance of arctic environments. Journal of Hydrometeorology, 11(2), 276–295. https://doi.org/10.1175/2009JHM1084.1

Dadson, S. J., Ashpole, I., Harris, P., Davies, H. N., Clark, D. B., Blyth, E., & Taylor, C. M. (2010). Wetland inundation dynamics in a model of land surface climate: Evaluation in the Niger inland delta region. Journal of Geophysical Research Atmospheres, 115(23), 1–7. https://doi.org/10.1029/2010JD014474

Dee, D. P., Uppala, S. M., Simmons, A. J., Berrisford, P., Poli, P., Kobayashi, S., Andrae, U., Balmaseda, M. A., Balsamo, G., Bauer, P., Bechtold, P., Beljaars, A. C. M., van de Berg, L., Bidlot, J., Bormann, N., Delsol, C., Dragani, R., Fuentes, M., Geer, A. J., … Vitart, F. (2011). The ERA-Interim reanalysis: configuration and performance of the data assimilation system. Quarterly Journal of the Royal Meteorological Society, 137(656), 553–597. https://doi.org/10.1002/qj.828

Dumanski, S., Pomeroy, J. W., & Westbrook, C. J. (2015). Hydrological regime changes in a Canadian Prairie basin. Hydrological Processes, 29(18), 3893–3904. https://doi.org/10.1002/hyp.10567

Fan, Y., & Miguez-Macho, G. (2011). A simple hydrologic framework for simulating wetlands in climate and earth system models. Climate Dynamics, 37(1), 253–278. https://doi.org/10.1007/s00382-010-0829-8

Fang, X., & Pomeroy, J. (2020). Diagnosis of future changes in hydrology for a Canadian Rocky Mountain headwater basin. Hydrology and Earth System Sciences Discussions, 1–40. https://doi.org/10.5194/hess-2019-640

Famiglietti, J. S. & Wood, E. F. (1991). Evapotranspiration and Runoff from Large Land Areas: Land Surface Hydrology for Atmospheric General Circulation Models, Surveys in Geophysics, 12, 179-204.

Famiglietti, J. S. & Wood, E. F. Multiscale modeling of spatially variable water and energy balance processes. Water Resour. Res. 30, 3061–3078 (1994a).

Famiglietti, J. S. & Wood, E. F. Application of multiscale water and energy balance models on a tallgrass prairie. Water Resour. Res. 30, 3079–3093 (1994b).

Gardner, Royal C. and Connolly, Kim Diana, The Ramsar Convention on Wetlands: Assessment of International Designations Within the United States (2007). Enviromental Law Review, 37, 1089, Available at SSRN: https://ssrn.com/abstract=983546

Gedney, N., & Cox, P. M. (2003). The Sensitivity of Global Climate Model Simulations to the Representation of Soil Moisture Heterogeneity. Journal of Hydrometeorology, 4(6), 1265–1275. https://doi.org/10.1175/1525-7541(2003)004<1265:TSOGCM>2.0.CO;2

Ghajarnia, N., Kalantari, Z., Orth, R., & Destouni, G. (2020). Close co-variation between soil moisture and runoff emerging from multi-catchment data across Europe. Scientific Reports, 10(1), 4817. https://doi.org/10.1038/s41598-020-61621-y

Hatfield, J. L. (2016). Increased Temperatures Have Dramatic Effects on Growth and Grain Yield of Three Maize Hybrids. Agricultural & Environmental Letters, 1(1), 150006. https://doi.org/10.2134/ael2015.10.0006

Hayashi, M., van der Kamp, G., & Rosenberry, D. O. (2016). Hydrology of Prairie Wetlands: Understanding the Integrated Surface-Water and Groundwater Processes. Wetlands, 36, 237–254. https://doi.org/10.1007/s13157-016-0797-9

Hostetler, S. W., Bates, G. T., & Giorgi, F. (1993). Interactive coupling of a lake thermal model with a regional climate model. Journal of Geophysical Research: Atmospheres, 98(D3), 5045–5057. https://doi.org/10.1029/92JD02843

Houspanossian, J., Kuppel, S., Nosetto, M., Di Bella, C., Oricchio, P., Barrucand, M., Rusticucci, M., & Jobbágy, E. (2018). Long-lasting floods buffer the thermal regime of the Pampas. Theoretical and Applied Climatology, 131(1–2), 111–120. https://doi.org/10.1007/s00704-016-1959-7

Ireson, A. M., van der Kamp, G., Ferguson, G., Nachshon, U. & Wheater, H. S. Hydrogeological processes in seasonally frozen northern latitudes: understanding, gaps and challenges. Hydrogeol. J. 21, 53–66 (2013).

Ireson, A. M. et al. The changing water cycle: the Boreal Plains ecozone of Western Canada. Wiley Interdiscip. Rev. Water 2, 505–521 (2015).

Joshi, D., Carrera, M., Bélair, S., & Leroyer, S. (2017). Influence of Open Water Bodies on the Modeling of Summertime Convection over the Canadian Prairies. Journal of Hydrometeorology, 18(6), 1583–1594. https://doi.org/10.1175/JHM-D-15-0225.1

Koster, R. D., Suarez, M. J., Ducharne, A., Stieglitz, M., & Kumar, P. (2000). A catchment-based approach to modeling land surface processes in a general circulation model: 1. Model structure. Journal of Geophysical Research: Atmospheres, 105(D20), 24809–24822. https://doi.org/10.1029/2000JD900327

Randal D. Koster, P. A. D., Zhichang Guo, Gordon Bonan, Edmond Chan, Peter Cox, C. T. Gordon, Shinjiro Kanae, Eva Kowalczyk, David Lawrence, Ping Liu, Cheng-Hsuan Lu, Sergey Malyshev, Bryant McAvaney, Ken Mitchell, D. M., & Taikan Oki, Keith Oleson, Andrew Pitman, Y. C. Sud, Christopher M. Taylor, Diana Verseghy, Ratko Vasic, Yongkang Xue, T. Y. (2004). Regions of Strong Coupling Between Soil Moisture and Precipitation. Science, 1138(2004), 10–13. https://doi.org/10.1126/science.1100217

Lehner, B., & Döll, P. (2004). Development and validation of a global database of lakes, reservoirs and wetlands. Journal of Hydrology, 296(1–4), 1–22. https://doi.org/10.1016/j.jhydrol.2004.03.028

Liang, X., Lettenmaier, D. P., Wood, E. F., & Burges, S. J. (1994). A simple hydrologically based model of land surface water and energy fluxes for general circulation models. Journal of Geophysical Research, 99(D7), 14415. https://doi.org/10.1029/94JD00483

Liu, C. et al. Continental-scale convection-permitting modeling of the current and future climate of North America. Clim. Dyn. 49, 71–95 (2017).

Melton, J. R., Wania, R., Hodson, E. L., Poulter, B., Ringeval, B., Spahni, R., et al. (2013). Present state of global wetland extent and wetland methane modelling: conclusions from a model inter-comparison project (WETCHIMP). Biogeosciences, 10(2), 753–788. https://doi.org/10.5194/bg-10-753-2013

Miguez-Macho, G., Fan, Y., Weaver, C. P., Walko, R. & Robock, A. Incorporating water table dynamics in climate modeling: 2. Formulation, validation, and soil moisture simulation. J. Geophys. Res. Atmos. 112, 1–16 (2007).

Mishra, V., Cherkauer, K. A., & Bowling, L. C. (2010). Parameterization of lakes and wetlands for energy and water balance studies in the great lakes region. Journal of Hydrometeorology, 11(5), 1057–1082. https://doi.org/10.1175/2010JHM1207.1

Mitra, S., Wassmann, R., Vlek, P. L. G. (2005) An appraisal of global wetland area and its organic carbon stock. Curr Sci 88:25–35

Mitsch WJ, Gosselink JG (2007) Wetlands, 4th edn. Wiley, Hoboken

Valuing wetlands. (2021). Nature Geoscience, 14(3), 111–111. https://doi.org/10.1038/s41561-021-00713-4

Niu, G.-Y., Yang, Z.-L., Dickinson, R. E., & Gulden, L. E. (2005). A simple TOPMODEL-based runoff parameterization (SIMTOP) for use in global climate models. Journal of Geophysical Research, 110(D21), D21106. https://doi.org/10.1029/2005JD006111

Niu, G.-Y., Yang, Z.-L., Dickinson, R. E., Gulden, L. E., & Su, H. (2007). Development of a simple groundwater model for use in climate models and evaluation with Gravity Recovery and Climate Experiment data. Journal of Geophysical Research, 112(D7), D07103. https://doi.org/10.1029/2006JD007522

Niu, G.-Y., Yang, Z.-L., Mitchell, K. E., Chen, F., Ek, M. B., Barlage, M., et al. (2011). The community Noah land surface model with multiparameterization options (Noah-MP): 1. Model description and evaluation with local-scale measurements. Journal of Geophysical Research, 116(D12), D12109. https://doi.org/10.1029/2010JD015139

Oleson, K. W., Niu, G.-Y., Yang, Z.-L., Lawrence, D. M., Thornton, P. E., Lawrence, P. J., Stöckli, R., Dickinson, R. E., Bonan, G. B., Levis, S., Dai, A., & Qian, T. (2008). Improvements to the

Community Land Model and their impact on the hydrological cycle. Journal of Geophysical Research: Biogeosciences, 113(G1), n/a-n/a. https://doi.org/10.1029/2007JG000563

Pattison-Williams, J. K., Pomeroy, J. W., Badiou, P., & Gabor, S. (2018). Wetlands, Flood Control and Ecosystem Services in the Smith Creek Drainage Basin: A Case Study in Saskatchewan, Canada. Ecological Economics, 147, 36–47. https://doi.org/10.1016/j.ecolecon.2017.12.026

Perkins, S. E. (2015). A review on the scientific understanding of heatwaves-Their measurement, driving mechanisms, and changes at the global scale. Atmospheric Research, 164–165, 242–267. https://doi.org/10.1016/j.atmosres.2015.05.014

Pitman, A. (1991). A simple parameterization of sub-grid scale open water for climate models. Climate Dynamics, 6(2), 99–112. https://doi.org/10.1007/BF00209983

Prigent, C., Matthews, E., Aires, F., and Rossow, W. B. (2001). Remote sensing of global wetland dynamics with multiple satellite data sets, Geo. Res. Lett., 28 , 4631-4634

Prigent, C., Papa, F., Aires, F., Rossow, W. B., & Matthews, E. (2007). Global inundation dynamics inferred from multiple satellite observations, 1993–2000. Journal of Geophysical Research, 112(D12), D12107. https://doi.org/10.1029/2006JD007847

Prigent, C., Papa, F., Aires, F., Jimenez, C., Rossow, W. B., & Matthews, E. (2012). Changes in land surface water dynamics since the 1990s and relation to population pressure. Geophysical Research Letters, 39(8), n/a-n/a. https://doi.org/10.1029/2012GL051276

Ringeval, B., Decharme, B., Piao, S. L., Ciais, P., Papa, F., de Noblet-Ducoudré, N., Prigent, C., Friedlingstein, P., Gouttevin, I., Koven, C., & Ducharne, A. (2012). Modelling sub-grid wetland in the ORCHIDEE global land surface model: evaluation against river discharges and remotely sensed data. Geoscientific Model Development, 5(4), 941–962. https://doi.org/10.5194/gmd-5-941-2012

Sivapalan, M., Beven, K., & Wood, E. F. (1987). On hydrologic similarity: 2. A scaled model of storm runoff production. Water Resources Research, 23(12), 2266–2278. https://doi.org/10.1029/WR023i012p02266

Stieglitz, M., D. Rind, J. Famiglietti & C. Rosenzweig (1997), An Efficient Approach to Modeling the Topographic Control of Surface Hydrology for Regional and Global Climate Modeling, J. Clim., 10, 118-137.

Taylor, C. M. (2010). Feedbacks on convection from an African wetland. Geophysical Research Letters, 37(5), n/a-n/a. https://doi.org/10.1029/2009GL041652

Taylor, C. M., Prigent, C., & Dadson, S. J. (2018). Mesoscale rainfall patterns observed around wetlands in sub-Saharan Africa. Quarterly Journal of the Royal Meteorological Society, 144(716), 2118–2132. https://doi.org/10.1002/qj.3311

van der Kamp, G., & Hayashi, M. (2009). Groundwater-wetland ecosystem interaction in the semiarid glaciated plains of North America. Hydrogeology Journal, 17(1), 203–214. https://doi.org/10.1007/s10040-008-0367-1

Wania, R., Melton, J. R., Hodson, E. L., Poulter, B., Ringeval, B., Spahni, R., et al. (2013). Present state of global wetland extent and wetland methane modelling: methodology of a model inter-comparison project (WETCHIMP). Geoscientific Model Development, 6(3), 617–641. https://doi.org/10.5194/gmd-6-617-2013

Yamazaki, D., Kanae, S., Kim, H., & Oki, T. (2011). A physically based description of floodplain inundation dynamics in a global river routing model. Water Resources Research, 47(4). https://doi.org/10.1029/2010WR009726

Yamazaki, D., Ikeshima, D., Tawatari, R., Yamaguchi, T., O'Loughlin, F., Neal, J. C., Sampson, C. C., Kanae, S., & Bates, P. D. (2017). A high-accuracy map of global terrain elevations. Geophysical Research Letters, 44(11), 5844–5853. https://doi.org/10.1002/2017GL072874

Zhang, Z., Li, Y., Chen, F., Barlage, M. & Li, Z. Evaluation of convection-permitting WRF CONUS simulation on the relationship between soil moisture and heatwaves. Clim. Dyn. (2018) doi:10.1007/s00382-018-4508-5.

Zhang, Z., Li, Y., Barlage, M., Chen, F., Miguez-Macho, G., Ireson, A., & Li, Z. (2020). Modeling groundwater responses to climate change in the Prairie Pothole Region. Hydrology and Earth System Sciences, 24(2), 655–672. https://doi.org/10.5194/hess-24-655-2020